Author:
Drizou, Despoina

Title:
Characterising Red Cell-Derived Vesicles in Sickle Cell Disease and Investigating Potential to Induce Tolerance to Human Red Cell Antigens

Characterising Red Cell-Derived Vesicles in Sickle Cell Disease and Investigating Potential to Induce Tolerance to Human Red Cell Antigens

Despoina Drizou

A dissertation submitted to the University of Bristol in accordance with the requirements for award of the degree of Doctor of Philosophy in the Faculty of Biomedical Sciences

School of Cellular and Molecular Medicine

August 2020

Word count: 47,960

Abstract

Patients with sickle cell disease (SCD) receive regular blood transfusions, which can lead to alloimmunisation due to exposure to different red blood cell (RBC) antigens. The spleen is frequently damaged in these patients, resulting in higher numbers of red cell-derived particles (RCDP) and autophagic vesicles (AV). Most RCDP, produced through membrane budding, are right-side out and expose the external domains of RBC proteins, whereas AV are inside-out, exposing cytoplasmic domains. Since SCD patients have higher numbers of RCDP and AV, we aimed to characterise these particles and compare with healthy donor plasma and with storage vesicles (SV) from outdated blood. We also investigated the use of these particles to induce tolerance to RBC antigens, in a murine model. RCDP and AV from SCD and healthy plasma were isolated using immunomagnetic separation. Results using imaging flow cytometry (IS) showed that RBC markers like glycophorins A and C, band 3, glucose transporter1 and phosphatidylserine, were detected in all particles, confirming they originated from RBC. RCDP were more prevalent and generally larger than AV but both particle types were more abundant in SCD than healthy plasma. IS was more sensitive for small particle detection than flow cytometry. The latter detected large ghost membranes. All particle types were detected by transmission electron microscopy (TEM) and immunogold staining against extracellular or cytoplasmic GPA domains further confirmed their RBC origin. TEM, IS and dynamic light scattering showed that RCDP were larger than AV. A model system was developed to investigate tolerance induction in vivo and indicated that both SV and ghosts could be used to prime host animals. In conclusion, small RCDP and AV from SCD and healthy plasma have been characterised for first time, using IS. It may be possible to use particles from blood cells induce tolerance to RBC antigens and thereby reduce alloimmunisation.

Abstract word count: 299

Dedication and Acknowledgements

I have always wanted to pursue a PhD after finishing my undergraduate studies. However, it took several years to find (or to be found by!) the best project I could ever imagine. On top of that, I had the greatest opportunity to work alongside with not only lovely people but also top experts in the field of transfusion and red blood cell biology.

I would like to deeply thank my supervisor Dr Allison Blair for all her support, guidance, kindness, invaluable help and for making this 4-year journey easier for me. I am also grateful to my second supervisor, Professor Dave Anstee, for trusting me with his great idea of inducing tolerance in young patients with sickle cell disease, with the aim of improving the quality of their adult life. This thought kept me focused on my work throughout the last and most challenging years. The Ethos and Values of both my supervisors, so different to what I had encountered thus far in the pharmaceutical industry, inspired me to do science to make a difference. It's good to know there are still researchers that are human first and scientists second.

Special thanks go to Dr Tosti Mankelow for his instrumental advice, patience and for always being available for me. Many thanks to Dr Rachel Smith for all her help, especially during my first steps in this PhD. This project could not have taken place without the kind contribution of Drs. Tom Latham, Sara Trompeter and their patients; I could not thank them enough. Sincere thanks should also go to Mr Shane Grimsley and Dr Nicole Thorton, as well as all the staff in the Red Cell Reference Lab in IBGRL, Filton. Without their valuable help I would not have managed to perform serology. Special thanks to Professor Lindsay Nicholson for his precious advice to the immunological part of the project.

I would also like to thank all the people in the IBGRL in Filton for their help and support, as well as people in C72 office at Bristol University. Many thanks to my Progression Panel members, Professor Jan Frayne and Dr David Morgan for all their advice and guidance. Special thanks to our group members, Dr Ben Ede and particularly Dr Vivian Diamanti for their suggestions on my work. Vivian's gorgeous smile and positive energy have been an energetic boost the past few years.

I will be always grateful to Professor Athanasios Koutinas, who saw my passion for research and advised me to do a PhD. I cannot thank enough my parents and my sister Dimitra for everything they have done for me so far. Last but not least, many thanks to my partner Zisimos for his patience, amazing cooking skills and for helping me to deal with stress and anxiety through the sleepless PhD nights.

Author’s declaration

I declare that the work in this dissertation was carried out in accordance with the requirements of the University's *Regulations and Code of Practice for Research Degree Programmes* and that it has not been submitted for any other academic award. Except where indicated by specific reference in the text, the work is the candidate's own work. Work done in collaboration with, or with the assistance of, others, is indicated as such. Any views expressed in the dissertation are those of the author.

SIGNED: Despoina Drizou DATE: 31/08/2020

Table of Contents

Abstract....1
Dedication and Acknowledgements 2
Author's Declaration 3
Table of Contents....4
List of Figures....8
List of Tables....10
Abbreviations....11

CHAPTER 1 Introduction....14
1.1 HAEMOPOIESIS....14
1.1.1 Production of haemopoietic stem cells....14
1.1.2 Haemopoietic Hierarchy....15
1.1.3 Transcription factors....16
1.1.4 Haemopoietic stem cell regulation by other cells....16
1.2 THE RED BLOOD CELL....17
1.2.1 Function and characteristics....17
1.2.2 Formation and maturation....17
1.2.3 Metabolic pathways in red cells....18
1.2.4 Red cell components....19
1.2.4.1 Haemoglobin....19
1.2.4.2 Red cell membrane composition....21
1.2.4.3 Phospholipids....22
1.2.4.4 Red blood cell antigens....23
1.2.5 *Ex vivo* generation of red cells....24
1.2.6 Animal models of erythropoiesis....25
1.2.7 Material exported by red cells....26
1.3 CELLULAR MICROPARTICLES....26
1.3.1 Circulating microparticles in plasma....26
1.3.2 Red cell-derived particles and clinical significance....288
1.3.3 Autophagic vesicles....29
1.3.4 Storage vesicles....30
1.3.4.1 Formation of storage vesicles....30
1.3.4.2 Storage vesicle characteristics....30
1.3.4.3 Storage effect on red cell proteins....31
1.3.4.4 Storage vesicle analysis methods....32
1.3.4.5 Clinical significance of storage vesicles....33
1.4 RED CELL DISORDERS....34
1.4.1 Haemoglobinopathies....34
1.4.2 B-thalassaemia....34
1.4.3 Sickle cell disease....35
1.4.3.1 Formation of sickle cells....35
1.4.3.2 Mechanisms of coagulation....36
1.4.3.3 Complications caused by coagulation in sickle cell disease....37

1.4.3.4 Sickle cell disease management 38

1.5 IMMUNOLOGY OF BLOOD TRANSFUSIONS 40

1.5.1 Overview of the immune system 40
1.5.2 Blood transfusions and the immune system 41
1.5.3 Alloimmunisation 42

1.6 AIMS 403

CHAPTER 2 Materials and methods 44

2.1 SAMPLES 44

2.1.1 Patient Samples 44
2.1.2 Normal Blood Samples 44

2.2 SAMPLE PROCESSING 44

2.2.1 Plasma and red cells 44
2.2.2 Red cell ghost membrane preparation 45
2.2.3 Storage vesicle isolation 45

2.3 MONOCLONAL ANTIBODIES 46

2.4 PRODUCTION OF RED CELL-DERIVED PARTICLES FROM CULTURED RETICULOCYTES 48

2.4.1 $CD34^+$ progenitor cell isolation 48
2.4.2 *Ex vivo* generation of reticulocytes from $CD34^+$ cells 48
2.4.3 Red cell-derived particle collection from cultured reticulocytes 49

2.5 ISOLATION METHODS OF RED CELL PARTICLES AND AUTOPHAGIC VESICLES FROM PLASMA 50

2.5.1 Centrifugation 50
2.5.2 Immunomagnetic enrichment 50

2.6 FLOW CYTOMETRY 51

2.6.1 Negative control for flow cytometry 52

2.7 IMAGING FLOW CYTOMETRY (IMAGESTREAM) 53

2.8 FLUORESCENCE ACTIVATED CELL SORTING (FACS) 55

2.9 MICROSCOPY TECHNIQUES 55

2.9.1 Confocal microscopy 55
2.9.2 Spinning-disk confocal microscopy 55
2.9.3 Transmission electron microscopy and immunolabelling 56
2.9.4 Super-resolution microscopy 57

2.10 DYNAMIC LIGHT SCATTERING 57

2.11 PROTEIN DETERMINATION OF ENRICHED RED CELL PARTICLES AND AUTOPHAGIC VESICLES 57

2.11.1 Protein lysate preparation 57
2.11.2 Bradford assay 57
2.11.3 Bicinchoninic acid assay 58
2.11.4 Protein precipitation 58
2.11.5 SDS-PAGE and protein staining 58
2.11.6 SDS-PAGE and immunoblotting 59

2.12 MASS SPECTROMETRY 59

2.12.1 Mass spectrometry of proteins from gel bands 59
2.12.2 Nano- Liquid Chromatography Mass Spectrometry 60
2.12.3 Data Analysis 61

2.13 *IN VIVO* STUDIES 61
2.13.1 Animals and study protocol 61
2.13.2 Processing mouse cardiac blood 62
2.13.3 Mononuclear cell isolation from spleens 63
2.13.4 Assessment of immune reactions 63
2.13.5 Cytokine assay 64
2.14 STATISTICAL ANALYSES 64

CHAPTER 3 Identification of red cell-derived particles and autophagic vesicles 65
3.1 INTRODUCTION 65
3.2 ASSESSMENT OF RETICULOCYTE MORPHOLOGY 66
3.3 IDENTIFICATION OF RED CELL-DERIVED PARTICLES AND AUTOPHAGIC VESICLES 67
3.3.1 Optimising flow cytometry analysis 67
3.3.1.1 Antibody titration 67
3.3.1.2 Investigation of platelets and HLA cells in plasma 70
3.3.2 Abundance of red cell proteins 71
3.3.3 Size estimation 73
3.3.3.1 Use of known size storage vesicles 73
3.3.3.2 Size beads 73
3.4 EXAMINATION OF HIGHLY IMMUNOGENIC PROTEINS ON SICKLE CELLS 75
3.5 ISOLATION OF RED CELL-DERIVED PARTICLES AND AUTOPHAGIC VESICLES USING FACS 75
3.5.1 Optimisation of red cell-derived particle isolation using FACS 75
3.5.1.1 Sample dilution 75
3.5.1.2 Antibody dilution 75
3.5.1.3 Pelleting samples 76
3.5.1.4 Refining plasma pelleting and antibody titrations 77
3.5.1.5 Determination of size limit detection by FACS compared to flow cytometry 78
3.5.2 Yields of sorted red cell-derived particles 79
3.6 PROTEIN DETERMINATION ON SORTED RED CELL-DERIVED PARTICLES BY BRADFORD ASSAY 80
3.7 SIZE ESTIMATION OF SORTED RED CELL-DERIVED PARTICLES USING DLS 80
3.8 SIZE ESTIMATION OF LARGE SORTED PARTICLES USING MICROSCOPY 81
3.9 ANALYSIS USING IMAGING FLOW CYTOMETRY (IMAGESTREAM) 84
3.9.1 ImageStream analysis of GPA^+ sorted particles from plasma 84
3.9.2 Comparison of imaging flow cytometry with conventional flow cytometry 86
3.9.3 Summary of populations identified using different methods 87
3.10 DISCUSSION 89

CHAPTER 4 Characterisation of red cell-derived, autophagic and storage vesicles 93
4.1 INTRODUCTION 93
4.2 RED CELL-DERIVED PARTICLE, AUTOPHAGIC AND STORAGE VESICLE ISOLATION AND CHARACTERISATION 94
4.2.1 Optimisation of particle enrichment in plasma using immunomagnetic beads 94
4.2.1.1 Comparison of isolation methods and morphology examination 94

4.2.1.2 Examination of macrovesicles present in enriched particles from filtered plasma ... 96
4.2.1.3 Antibody contribution to the total protein. ... 98
4.2.1.4 Extent of antibody contribution to protein content. ... 99
4.2.1.5 Bead concentration optimisation for red cell-derived particle and autophagic vesicle isolation ... 101

4.3 MORPHOLOGY OF ENRICHED POPULATIONS IN HEALTH AND SICKLE CELL DISEASE ... 103

4.3.1 Red cell-derived particles and autophagic vesicles ... 103
4.3.2 Storage vesicles and storage effects ... 105
4.3.3 Imaging storage vesicles by super resolution microscopy ... 106

4.4 SIZE DETERMINATION OF ENRICHED RED CELL PARTICLES, AUTOPHAGIC AND STORAGE VESICLES BY DLS ... 106

4.5 DETECTION OF RED CELL PROTEINS, CALCEIN AND PS ON ENRICHED AND STORAGE VESICLES ... 108

4.6 OPTIMISING A PROTEIN QUANTIFICATION PROTOCOL ON ENRICHED VESICLES ... 110

4.7 DISCUSSION ... 113

CHAPTER 5 Inducing tolerance to red cell antigens in a murine model ... 117

5.1 INTRODUCTION ... 117

5.2 EXPERIMENTAL DESIGN ... 118

5.2.1 Developing an appropriate haemagglutination test for mouse plasma ... 118
5.2.2 Setting up an appropriate experimental model ... 120

5.3 INVESTIGATING IMMUNE RESPONSES INDUCED BY GHOST PREPARATIONS ... 122

5.4 ASSESSING EFFECTS OF EXPOSURE TO RED CELL ANTIGENS ... 125

5.5 COMPARISONS OF RESPONSES TO O AND A BLOOD GROUPS ... 127

5.6 SEQUENTIAL CHALLENGE WITH RED CELLS ... 129

5.7 EXAMINATION OF SICKLE CELL GHOST IMMUNOGENICITY ... 132

5.8 DISCUSSION ... 134

Chapter 6 Discussion ... 138

6.1 SUMMARY OF THE KEY FINDINGS IN THE THESIS AND SUGGESTIONS TO TAKE THE PROJECT FORWARD. ... 138

6.2 FURTHER WORK ... 143

6.3 CONCLUSION ... 144

References ... 145

List of Figures

Figure 1.1 Models of haemopoiesis..... 15
Figure 1.2 The maturation stages of erythrocytes. 18
Figure 1.3 Structure of haemoglobin. 20
Figure 1.4 Red cell major membrane proteins and their connection to the cytoskeleton..... 22
Figure 1.5 Secretion of microparticles 27
Figure 1.6 Suggested mechanisms of particle formation in erythrocytes 29
Figure 1.7 Sickle haemoglobin polymerisation. 35
Figure 1.8 Red cell agglutination. 41
Figure 2.1 Schematic representation of red cell vesicle isolation. 51
Figure 2.2 Flow cytometry gating strategy. 52
Figure 2.3 ImageStream gating strategy. 54
Figure 2.4 Detecting circular objects using spinning disk confocal. 56
Figure 2.5 Schematic representation of immunotolerance experiments. 62
Figure 2.6 Mouse antibody screen test using a gel card..... 64
Figure 3.1 Schematic of the analytical methods for vesicle characterisation in CR media and plasma. 65
Figure 3.2 Morphology of reticulocytes during their maturation……..66
Figure 3.3 Antibody titration in plasma 68
Figure 3.4 Use of mouse plasma as an alternative control in antibody titration, in SCD plasma. ... 69
Figure 3.5 Platelet and HLA detection in plasma by flow cytometry 71
Figure 3.6 Proteins detected in plasma and CR media by flow cytometry. 72
Figure 3.7 GPA^+ red cell vesicle size estimation using size beads. 74
Figure 3.8 Sorting strategy for GPA^+ vesicles from plasma. 76
Figure 3.9 Comparison of methods of vesicle sedimentation for isolation by FACS. 77
Figure 3.10 Size estimation of sorted GPA^+ events using DLS..... 81
Figure 3.11 Confocal analysis of sorted GPA^+ events from plasma. 82
Figure 3.12 Spinning-disk confocal analyses 83
Figure 3.13 Morphology of objects detected by imaging flow cytometry. 85

Figure 3.14 Comparison of imaging flow cytometry and conventional flow cytometry..... 87

Figure 3.15 Schematic of populations detected by different methods..... 88

Figure 4.1 Hypothetical mechanism of autophagic vesicle and red cell-derived particle formation..93

Figure 4.2 Morphology examination of enriched red cell-derived particles by two different methods on TEM. 95

Figure 4.3 Examination of enriched red cell particles from 3μm filtered plasma 96

Figure 4.4 Examination of different filters in macrovesicle removal from enriched particles…….99

Figure 4.5 Comparison of total protein in samples enriched by FACS and magnetic beads. 99

Figure 4.6 Assessment of beads contribution to the total protein 100

Figure 4.7 Examination of bead saturation by TEM. 102

Figure 4.8 TEM of enriched red cell-derived particles and autophagic vesicles. 104

Figure 4.9 TEM of storage vesicles. 105

Figure 4.10 Protein detection in storage vesicles 106

Figure 4.11 Size estimation of enriched plasma vesicles and storage vesicles by DLS. 107

Figure 4.12 Protein abundance of enriched plasma and storage vesicles 108

Figure 4.13 Investigation of band 3 and stomatin on SDS-PAGE gels and blots 112

Figure 5.1 Assessment of mouse anti-human antibody production using a gel card. 118

Figure 5.2 Detected results on a gel card..... 119

Figure 5.3 Examination of red cell ghost preparations. 120

Figure 5.4 Assessing the gel card sensitivity by antibody titres. 121

Figure 5.5 Syringe position for cardiac puncture. 122

Figure 5.6 Responses following inoculation of ghosts. 123

Figure 5.7 Assessing immune responses after a boost of red cell ghosts 124

Figure 5.8 Examination of immune responses post red cell challenge. 126

Figure 5.9 Comparison of immune responses post A^+ and O^+ red cell challenge 128

Figure 5.10 Investigation of tolerance induction 132

Figure 5.11 Comparison of ghosts from sickle cell patients and healthy donors 133

List of Tables

Table 2.1 Antibodies used..... 47

Table 3.1 Optimum antibody concentration calculated from two dilution methods..... 70

Table 3.2 Statistical comparison of proteins detected in SCD plasma..... 73

Table 3.3 Assessment of sorting potential using the proportions of GPA^+ events in pelleted plasma, by two centrifugation methods..... 78

Table 3.4 Event number of small and large GPA^+ particles in pelleted and non pelleted plasma... 79

Table 4.1 Purity calculation before and after vesicle enrichment from plasma using 4% beads…102

Table 4.2 Absolute protein counts in particles detected by imaging flow cytometry..... 109

Table 4.3. Protein assays and conditions tested for RBC ghosts, storage and enriched vesicles.110

Table 4.4 Protein detected in controls and lysates using Nanodrop. 112

Table 5.1 Antibody titres in plasma. 130

Table 5.2 Plasma dilution factors detecting mixed agglutination..... 131

Table 6.1 Summary of the key findings in the thesis and suggestions to take the project forward. 138

Abbreviations

Abbreviation	Meaning
ACD	acid citrate dextrose
ADP	adenosine diphosphate
AF	AlexaFluor
APC	antigen presentation cell
ATP	adenosine triphosphate
AV	autophagic vesicles
BFU-e	burst-forming unit-erythroid cells
BM	bone marrow
2,3-BPG	2,3-bisphosphoglycerate
Bregs	B regulatory cells
BSA	serum bovine albumin
C5/C5a	complement component 5a
cDC	conventional dendritic cells
CFA	complete Freund's adjuvant
CFU-e	colony-forming unit-erythroid cells
CFU-f	colony-forming unit fibroblasts
CLP	common lymphoid progenitors
CMP	common myeloid progenitor
CO_2	carbon dioxide
CPD	citrate-phosphate-dextrose
CPDA	citrate-phosphate-dextrose-adenine
CR media	cultured reticulocytes media
CXCL	CXC chemokine ligand of CXC family
CXCL12 or SDF-1	stromal cell-derived factor 1
CXCL13 or BLC	B lymphocyte chemoattractant
Cyt.	cytoplasmic
DC	dendritic cells
DLS	dynamic light scattering
DMSO	dimethyl sulfoxide
DNA	deoxyribonucleic acid
DTT	diothiothreitol
EDTA	ethylenediaminetetraacetic acid
EMP	erythroid-myeloid progenitors
EPO	erythropoietin
Ex.	extracellular
FACS	fluorescence-activated cell sorting
FBS	foetal bovine serum
FSC	forward-scatter
FSC A	FSC area
FSC H	FSC height
GAPDH	glyceraldehyde-3-phosphate dehydrogenase
GLUT1	glucose transporter1

GM-CSF	granulocyte-macrophage colony-stimulating factor
GMP	granulocyte- macrophage progenitors
GPA	glycophorin A
GPB	glycophorin B
GPC	glycophorin C
GSH	glutathione
H	healthy samples
Hb	haemoglobin
HbA	haemoglobin A
HbF	haemoglobin F
HbS	sickle haemoglobin
HBSS	Hanks buffered salt solution
HLA	human leukocyte antigen
Hp	haptoglobin
HRP	horseradish peroxidase conjugate
HSA	human serum albumin
HSC	haematopoietic stem cells
HSCT	haematopoietic stem cells transplantation
Hx	haemopexin
ICAM-1	inter-cellular adhesion molecule-1
IFN-γ	interferon-γ
Ig	immunoglobulin
IL	interleukin
IMDM	Iscove's Modified Dulbecco's Medium
IS	imaging flow cytometry (ImageStream)
K (KEL1)	antigen from the Kell system K
k (KEL2)	antigen from the Kell system k
LISS	low ionic strength saline
Lu	Lutheran blood group
MaV	macrovesicles
M-CSF	macrophage colony-stimulating factor
MEP	megakaryocyte- erythrocyte progenitors
MHC	major histocompatibility complex
MNC	mononuclear cells
MP	microparticles
m-RBC	murine red blood cells
MSC	mesenchymal stem cells
NADH	nicotinamide adenine dinucleotide (reduced)
NADPH	nicotinamide adenine dinucleotide phosphate
NK	Natural Killer cells
NO	nitric oxide
NSG	NOD scid gamma immunodeficient transgenic mouse model
NTA	nanoparticle tracking analysis
O_2	oxygen
PBS	phosphate buffered saline
PFP	platelet free plasma

PK	peak
PMSF	phenylmethylsulfonyl fluoride
PS	phosphatidylserine
R state	relaxed state of haemoglobin
RBC	red blood cells
RCDP	red cell-derived particles
RhAG	Rh-associated protein
RIPA	radioimmunoprecipitation assay
ROS	reactive oxygen species
SAGM	saline-adenine-glucose and mannitol
SC	sickle cell
SCD	sickle cell disease
SCF	stem cell factor
scid	severe combined immunodeficiency mutation
SD	standard deviation
SDS	sodium dodecyl sulfate
sICAM-1	soluble intercellular adhesion molecule-1
SSC	side-scatter
SV	storage vesicles
T state	tense state of haemoglobin
TCR	T-cell receptor
TEM	transmission electron microscopy
TF	tissue factor
Th	T helper cell
TIMP-1	tissue inhibitor of metalloproteinase-1
TNF-α	tumour necrosis factor alpha
Tregs	regulatory T cells
UK	United Kingdom
USFDA	United States Food and Drug Administration
VCAM-1	vascular cell adhesion molecule-1
VOC	vaso-occlusive crisis
WHO	World health Organisation

Chapter 1 Introduction

1.1 Haemopoiesis

1.1.1 Production of haemopoietic stem cells

Haemopoiesis (from Ancient Greek haema (αἷμα) "blood" and poiein (ποιεῖν) "to make") is the process by which blood cells are formed. It starts in the embryo of mammalian and non-mammalian vertebrates and occurs throughout life. Blood components are synthesised by two different pathways: the primitive wave and the definitive wave (1). The primitive wave leads to macrophages and erythrocytes (from Ancient Greek erythrós (ἐρυθρός), “red” and kytos, cell) or red blood cell (RBC) formation through blood islands (2). It occurs in the embryonic yolk sac in early development (3, 4). Blood production is similar for mammals and zebrafish: early in the development during the primitive wave, the embryo differentiates from a single layer of epithelial cells called the blastula to form the multi-layered gastrula, composed of ectoderm, mesoderm and endoderm, which differentiate to form other tissues (5). One of these is the intermediate cell mass, which originates from the ventral mesoderm and from which the primitive erythroid progenitors arise. These progenitors contain foetal haemoglobin (Hb) and facilitate the oxygen transport during the rapid development of the embryo. Macrophage and megakaryocyte progenitors are formed as well (6, 7). Blood islands are also derived from the mesoderm and lead to the production of erythroid-myeloid progenitors (EMP) in the yolk sac, through a temporary wave of the definitive pathway, resulting in the production of myeloid lineage progenitors (8-11).

Definitive haemopoiesis begins later through the precursors of other blood cells, called pluripotent haemopoietic stem cells (HSC) (7). HSC have self renewal and differentiation capacity. In contrast, proliferation and differentiation of progenitor cells derived from HSC, is more strictly controlled (12). HSC in humans and other vertebrates rise in the aorta-gonad-mesonephros area of the mid-gestation embryo (13, 14), then relocate to the foetal liver to expand and finally colonise the bone marrow (BM) and thymus (15). Definitive erythroid progenitors containing adult Hb are produced in the foetal liver and give rise to enucleated foetal red cells, which are then released in the circulation (16). The micro-environment of the BM where HSC are renewed and maintained in an undifferentiated state is known as the niche (17). From there, HSC produce cells from all blood lineages throughout adulthood (10).

1.1.2 Haemopoietic Hierarchy

Original perceptions of the haemopoiesis were usually depicted as a hierarchical pyramid or a branching tree (Figure 1.1 left). At the top were multipotent HSC, which were losing their self-renewal ability while differentiating into multipotent, oligopotent and finally unipotent progenitors of blood lineages. Oligopotent common myeloid progenitors were thought to give rise to bipotent granulocyte-monocyte progenitors and megakaryocyte-erythroid progenitors, which further gave rise to granulocytes, monocytes, platelets and RBC respectively. Common lymphoid progenitors were thought to differentiate to T, B and Natural Killer (NK) cells (18-20) .

Advances in genomics and single-cell transcriptomic analysis revealed a new haemopoietic model, in which HSC pool showed to consist of molecularly heterogenous populations, rather than homogenous (Figure 1.1 right). HSC continually differentiate through multiple branches, to give distinct cell types which can “omit” intermediate subcategories (21-26). For example, it was shown that unipotent progenitors can arise directly from HSC, skipping differentiation to oligopotent progenitors (22). Stem and progenitor cells cannot be easily distinguished and progenitors are not strictly unipotent or oligopotent during their maturation to distinct cells (27, 28). Additionally, despite the existence of multipotent HSC, most progenitors seem to be unipotent (29, 30). The new model suggests that cell differentiation is difficult to represent by a diagram such as those preferred in the past publications, showing HSC differentiation in multiple stages (Figure 1.1). Instead, cell localisation throughout the HSC development is suggested and new approaches need to be investigated (27).

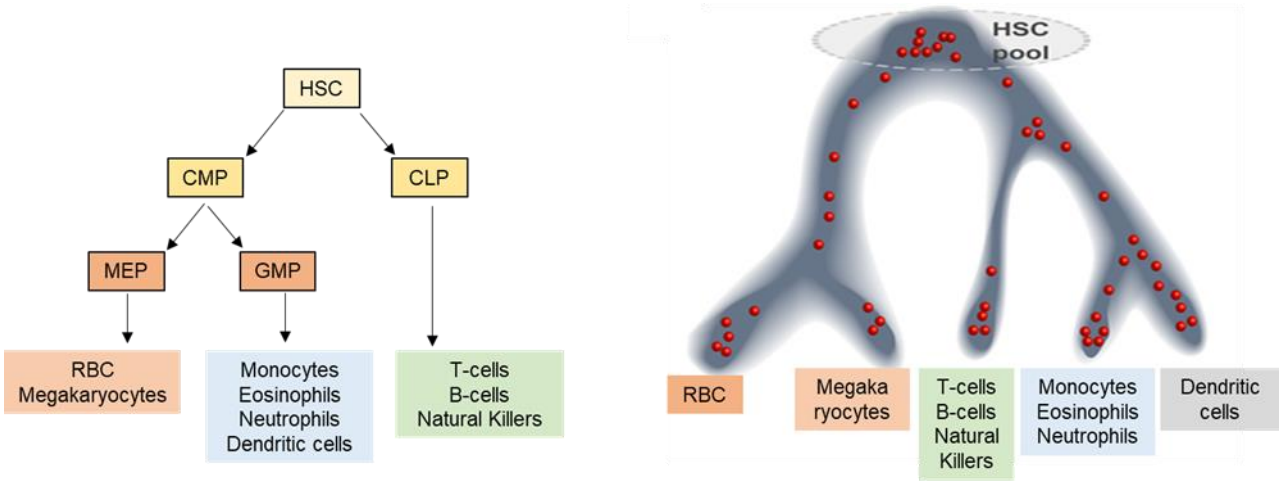

Figure 1.1 Models of haemopoiesis. Older (left) and a newer (right) models of haemopoiesis. In the old model, multipotent HSC gave rise to oligopotent common myeloid progenitor (CMP), which then differentiated to bipotent megakaryocyte/ erythrocyte progenitors (MEP) or to granulocyte/ macrophage progenitors (GMP). Oligopotent common lymphoid progenitors (CLP) were thought to produce T, B and Natural Killer cells directly. One of the newest models is based on transcriptomics analyses and suggests that the HSC pool is highly heterogenous and cell location represents continuous cell differentiation. Image modified from Laurenti 2018 (27).

1.1.3 Transcription factors

Two transcription factors mainly regulate the primitive wave of haemopoiesis; Gata1 and Pu.1 that cross-inhibit each other's function to regulate primitive erythroid and myeloid fates, respectively. For instance, pro-erythroblasts in mice lacking Gata1 (*Gata1*$^{-/-}$) could not mature into RBC during gestation and mice fail to survive *in utero*. Gata1-expressing cells in zebrafish are thought to encode alpha and beta embryonic globin, synthesising erythrocyte specific Hb (6). On the other hand, Pu.1 is a major regulator for the myeloid lineage giving rise to macrophages and granulocytes (31). This is believed to occur through the direct competition of the transcription factors, regulators for the target genes (32). In definitive wave of haemopoiesis, Runx1 is a transcription factor which greatly affects erythroid, myeloid and lymphoid lineages, as its absence can diminish or even eliminate the corresponding cells (3). Primitive erythroid progenitors originate from the hemangioblast, which in development is regulated by a panel of transcription factors (6, 33, 34).

Some other important transcription factors for haemopoiesis include Gata2, Tal1, Lmo2, Etspr and Fli1, which were found to support HSC differentiation (34-38). Gata2 is involved in maintenance and proliferation of haemopoietic progenitors, since absence of Gata2 (*Gata2*$^{-/-}$) is fatal for the embryo, which dies from severe anaemia (39). Tal1 affects endothelial differentiation, as *tal1* knock down in zebrafish and mice inhibits the primitive erythropoiesis and myelopoiesis (40). In addition, *Lmo2*$^{-/-}$ mice lack erythropoiesis in the yolk sac and die, while Fli1 has been suggested to support Tal1 and Lmo2 activation through enhancer *Flil+12* (41). Etsrp is important for the vascular endothelial and primitive myeloid cells in zebrafish (42), as it has been shown that knockout of *Etsrp* in mice eliminates endothelium and blood cells, suggesting that it is involved in the stimulation of progenitors. These progenitors co-express *etsrp, gata2, tal1, lmo2* and *fli1* and can develop into either HSC or endothelial progenitors called angioblasts (43).

1.1.4 Haemopoietic stem cell regulation by other cells

Different BM stromal cells and other cells are involved in the HSC regulation. Some of them are osteolineage cells, which were the first cells reported to be implicated in the regulation of HSC activity, as their depletion affects haemopoiesis by decrease of erythroid, lymphoid and myeloid progenitors (44). Mesenchymal stem cells (MSCs) are stromal cells that assist haemopoiesis in the BM. They have self-renewal ability and are pluripotent, giving rise to fibroblasts, fat, bone and cartilage. MSC form colony-forming unit fibroblasts (CFU-F) and are involved in the organisation of niche, as well as generation of other BM stromal cells like osteoblasts, chondrocytes, myocytes and adipocytes (45). Adipocytes are involved in BM aging, in which active haemopoietic areas are substituted by adipose (yellow marrow) with limited cell differentiation ability in long bones (46).

Endothelial cells express several ligands in the BM such as Notch ligands and CXC chemokine ligand (CXCL) 12 and produce stem cell factor (SCF) and pleiotrophin. Notch receptors on HSC interact with ligands on BM stromal cells to control haemopoiesis (47, 48).

1.2 The red blood cell

1.2.1 Function and characteristics

Human erythrocytes are one of the most well characterised cells. Their main function is to transfer oxygen to tissues by the protein Hb. It is estimated that a human adult produces 2-3x10^{11} RBC every day, comprising almost 70% of the total cells (49). RBC are approximately 7–8μm in size and their life span is around 120 days (50). In contrast to leukocytes that can leave the blood to contribute to organism's immune defence, RBC remain in the blood stream. Their shape is biconcave which results in a greater membrane surface than being spherical, enabling efficient gas exchange. Additionally, the RBC high surface-to-volume ratio allows reversible deformation during repeated passage through the narrow capillaries of the microcirculation. RBC can pass through sections as small as one third of the cell diameter. RBC deformability is crucial for gas transportation. The greatest alteration of RBC shape is during its passage from the splenic cords to the splenic sinus. Abnormal RBC shapes with decreased deformability were reported in different haemolytic disorders even back in the 1940s, to lead to splenic sequestration (51). Such a disorder is sickle cell disease (SCD), in which discoid RBC turn to sickle shape, which will be further discussed in section 1.4.3. In the microvasculature, narrow capillaries allow RBC to pass slowly, so that gas exchange can take place efficiently. RBC are surprisingly flexible; they can fold and bend themselves in order to pass through very narrow capillaries. Bending and unfolding is facilitated by structural proteins, such as spectrin, actin, protein 4.1R and ankyrin (51).

1.2.2 Formation and maturation

RBC originate from multipotent HSC in BM that follow the erythroid lineage and give rise to committed erythroid precursors, such as proerythroblasts. Then, they further develop into polychromatic and orthochromatic normoblasts (erythroblasts, Figure 1.2) (52). Macrophages participate in the regulation of RBC generation at different stages; initially they retain HSCs in the hematopoietic niche, then, granulocyte-macrophage colony-stimulating factor (GM-CSF) along with other growth factors and cytokines such as interleukin (IL) 3, stimulate the differentiation into early erythroid progenitor cells, called burst-forming unit-erythroid cells (BFU-e) (53). Erythropoietin (EPO), produced in the kidney, induces the differentiation into rapidly dividing colony-forming unit-erythroid cells (CFU-e) (54), which then further differentiate in erythroblastic islands. In them, a

central macrophage can interface with up to 30 erythroblasts by using adhesion molecules present on both types of cells and assists in increasing the number or proerythroblasts up to three times (55, 56).

During later stages of RBC maturation, resulting normoblasts expel their nuclei and other organelles, like mitochondria, ribosomes and endoplasmic reticula, to form multi-lobular reticulocytes (Figure 1.2). The nuclei and organelles are phagocytosed by macrophages. Newly formed R1 reticulocytes are motile and normally remain in the BM 24 hours after enucleation. R2 reticulocytes are formed after maturation is complete, whereby approximately 20% of the surface area is removed along with unwanted organelles in red cell derived particles (RCDP). R2 are less motile, more mechanically stable and are found in the circulation. They need approximately 24 hours to mature to RBC (57, 58). Reticulocytes comprise 1-2% of the total erythrocyte number. Membrane remodelling can last 2-3 days, resulting in non-adherent, flexible and biconcave RBC which can circulate in the bloodstream. Senescent and deformed RBC, as well us unwanted organelles, are cleared by macrophages in the spleen and liver (52, 56).

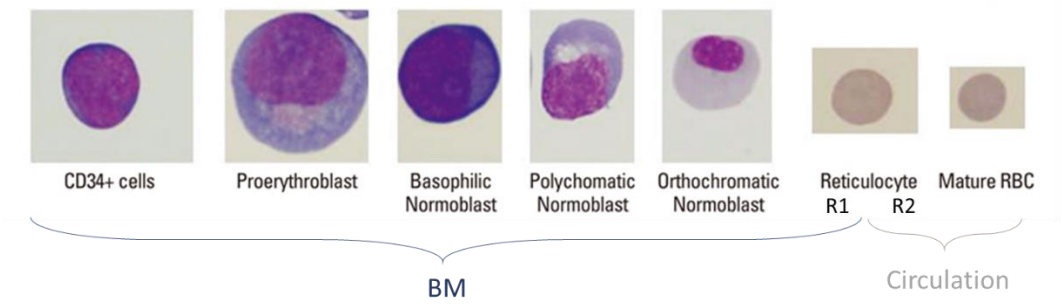

Figure 1.2 The maturation stages of erythrocytes. In the bone marrow haemopoietic stem cells differentiate to proerythroblasts, which further develop into basophilic, polychromatic and orthochromatic normoblasts (erythroblasts). After enucleation immature reticulocytes R1 in the bone marrow are released in the blood stream (R2) and mature to red cells. Image was modified from Kim 2014 (59).

1.2.3 Metabolic pathways in red cells

Mature RBC have reduced metabolic ability in contrast to other human cells. However, it is adequate for their function, including oxygen binding and transport by Hb (60). The main metabolic pathways in RBC are the anaerobic glycolysis (Embden–Meyerhof pathway), the pentose phosphate pathway and nucleotide metabolic pathways (61, 62). The anaerobic glycolysis pathway provides energy to the cell, through adenosine triphosphate (ATP) production by conversion of intracellular glucose into pyruvate or lactate. Among other functions, ATP is a major contributor in crucial functions of the cell, like its integrity and deformability through protein phosphorylation via kinases in the cytoskeleton

(63) and in membrane phospholipid asymmetry through ATP- dependant phospholipid transporters (64). Apart from ATP, reduced nicotinamide adenine dinucleotide (NADH) that facilitates the reduction of methaemoglobin to Hb is also produced by the anaerobic glycolysis pathway. Furthermore, this pathway plays an important role during oxygen delivery to the tissues by producing a shunt called Rapoport - Luebering shunt (65). This generates the production of 2,3-bisphosphoglycerate (2,3-BPG), which decreases the Hb affinity for O_2 by binding to Hb, enabling oxygen delivery to the tissues (66).

Membrane lipids, cytoskeletal proteins and other important cell components are produced by oxidation. A contributor to this is nicotinamide adenine dinucleotide phosphate (NADPH), which converts oxidised glutathione to its reduced form (GSH) that is important for combating oxidative stress. In physiology, NADPH is produced by glucose through the hexose monophosphate pathway. During oxidative stress, NADPH levels are maintained through additional consumption of glycose by the pentose phosphate pathway (67). Activation of the pathway takes place through the enzyme glucose-6-phosphate dehydrogenase. Its deficiency along with pyruvate kinase, which catalyses the transfer of a phosphoryl group to adenosine diphosphate (ADP) to generate ATP at the anaerobic pathway, are amongst the most common hereditary enzymopathies (65). On the other hand, nucleotide metabolic pathways recycle the existing adenine nucleotides required for the ATP production in mature RBC, since they lack the machinery for de novo synthesis. Therefore, although reduced, metabolic pathways are crucial for erythrocyte survival (60).

1.2.4 Red cell components

1.2.4.1 Haemoglobin

In adults, Hb is a globular protein that forms a tetramer consisting of two pairs of alpha (α1, α2) and two beta (β1, β2) globin chains, known as HbA (α_2/β_2). Each globin binds a heme molecule which contains an iron complex called porphyrin. The iron ion (Fe^{2+}) allows the reversible binding to one molecule of oxygen (O_2) or carbon dioxide (CO_2). Thus, one Hb molecule can transport four gas molecules (Figure 1.3) (52, 68). In the foetus, gamma chains substitute the two beta chains resulting in a stronger bond between oxygen and Hb than that in the adults. This allows efficient oxygen transfer to the developing foetus. Foetal Hb (HbF, α_2/γ_2) is replaced by HbA three to six months after birth (69). A single erythrocyte may contain about $3x10^6$ Hb molecules that allow the transfer of approximately $1.2\ x10^9$ O_2 molecules (70).

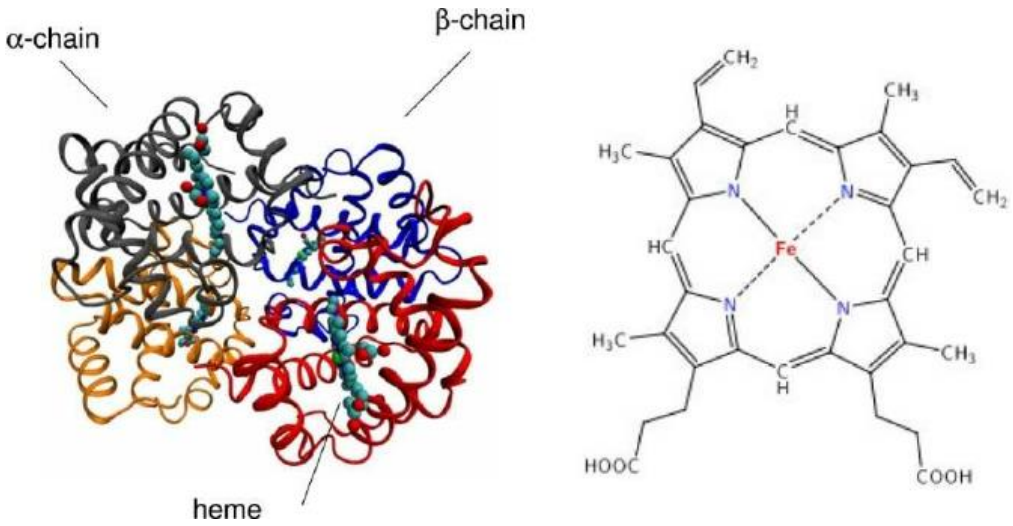

Figure 1.3 Structure of haemoglobin. Left: The tetramer of haemoglobin consisting of four globins (in grey, blue, yellow and red ribbons). Subunits of haemoglobin interact cooperatively; once a heme binds an oxygen molecule (red spheres) then all other hemes bind oxygen too. Right: Bond-line structure of heme. Oxygen binds to the ferrous in the centre of heme. Image was reproduced from Wu *et. al*, 2010 (71).

Oxygen collected in the lungs is insoluble in water and it is transported to the tissues by Hb, which forms red oxyhaemoglobin upon the binding to O_2. Hb adopts two states, the tense (T) and the relaxed (R) state. In the absence of O_2, the T state is more stable than the R. O_2 binds to the exposed binding sites of the R state (72). Factors that affect O_2 binding are the pH, temperature and Hb allostery. Carbon compounds affect the pH; CO_2 in the respiratory system decreases the pH in the blood ($CO_2 + H_2O \rightleftharpoons H_2CO_3 \rightarrow HCO_3^- + H^+$) and decreases O_2 binding affinity (73). Furthermore, the allosteric inhibitor 2,3-BPG is absent in the tissues, therefore O_2 binding affinity is high, preventing its release (66). Upon O_2 release to the tissues, oxygenated Hb turns to darker red deoxyhaemoglobin (71).

Production of Hb depends on the plasma proteins hephaestin and ceruloplasmin; iron absorption from the intestine is enabled by hephaestin and ceruloplasmin, a copper transport protein. Both catalyse iron oxidation from Fe^2 to Fe^{3+}, a form that allows transferrin to bind iron. Unbound iron in tissues can lead to organ damage (74). Both heme and vitamin B_{12} (cobalamin) derive from a common pyrrole precursor and their synthesis is facilitated using zinc as a co-enzyme. Vitamin B_{12} and the B vitamin folate function as co-enzymes in DNA synthesis by the class II ribonuceotide reductase enzymes, thus, they are very important for cell generation, including RBC. Porphyrin is produced in the cytoplasm and mitochondria of RBC (74).

Components of Hb are recycled once RBC are phagocytosed. Globin, the protein part of Hb, is degraded into amino acids that can be transported to the BM for RBC synthesis. Globin chain

remnants are degraded in the circulation and removed by the kidneys. Almost $2x10^6$ RBC, with $2.7x10^{11}$ Hb molecules in each RBC, are recycled every second (75). Heme is transported to the cytosol to be metabolised to biliverdin, free iron, and CO by heme-oxygenase using NADPH and oxygen as catalysts (76). Iron is stored as either ferritin or hemosiderin in the spleen or liver, or it is transported by transferrin to the BM for RBC generation. Biliverdin is converted to bilirubin by biliverdin reductase (77).

Removal of excess Hb and its constituents from the circulation is facilitated by the serum proteins haptoglobin (Hp) and hemopexin (Hx), which are both induced in inflammation. Hp has high affinity for free Hb, while Hx scavenges free heme. In pathological conditions where extended haemolysis is triggered, such as SCD, increased Hb levels cannot all be cleared by Hp and therefore released Hb is oxidised. This occurs either by O_2 in the circulation to produce methaemoglobin (Fe^{3+}) or by reactive oxygen species (ROS) producing ferryl Hb (Fe^{4+}) (78), which is unstainable and is further degraded to methemoglobin. Hb oxidisation along with metabolic products from pathogens, as well as pro-inflammatory cytokines produced, disrupt the oxidative-reductive balance of RBC and oxidation of intracellular Hb to methaemoglobin is induced, increasing the ROS levels and leading to lysis of proximate RBC (79, 80).

1.2.4.2 Red cell membrane composition

The RBC membrane is comprised of phospholipids, cholesterol, and more than 100 proteins with red cell antigens, which contribute to its elasticity (81). Membrane proteins facilitate important functions such as nutrients transportation, cytoskeleton support and communication with other cells like neutrophils and platelets (81). The cytoskeleton is mainly comprised of α- and β-spectrin, protein 4.1R, actin and actin binding proteins α-adducin, dematin, tropomyocin and tropomodulin (Figure 1.4). The major structure of the cytoskeleton is a tetramer consisting of triple helical repeats of α- and β-spectrin placed antiparallelly to form a heterodimer. The resulting tetramer is bound together by the side interaction of two spectrin dimers with the N-terminal domain of α-spectrin of one dimer with the C-terminus of β-spectrin of the second dimer (82). The other end of the dimer forms a complex with actin and with protein 4.1R to facilitate connection between the cytoskeleton and the membrane (83, 84). The ankyrin complex consists of ankyrin, band 3 tetramer, glycophorins A and B (GPA and GPB), Rh proteins, Rh-associated protein (RhAG), CD47, glycoprotein LW and protein 4.2. The protein 4.1R complex contains 4.1R, band 3 dimer, glycophorins C and D (GPC and GPD), as well as glycoproteins Kell, XK and Duffy. These protein complexes penetrate the membrane lipid bilayer and link it with the spectrin-based skeleton through interactions of their cytoplasmic domains (85, 86). Skeletal proteins interact with anionic phospholipids to further support the connection between skeleton and the lipid bilayer (51).

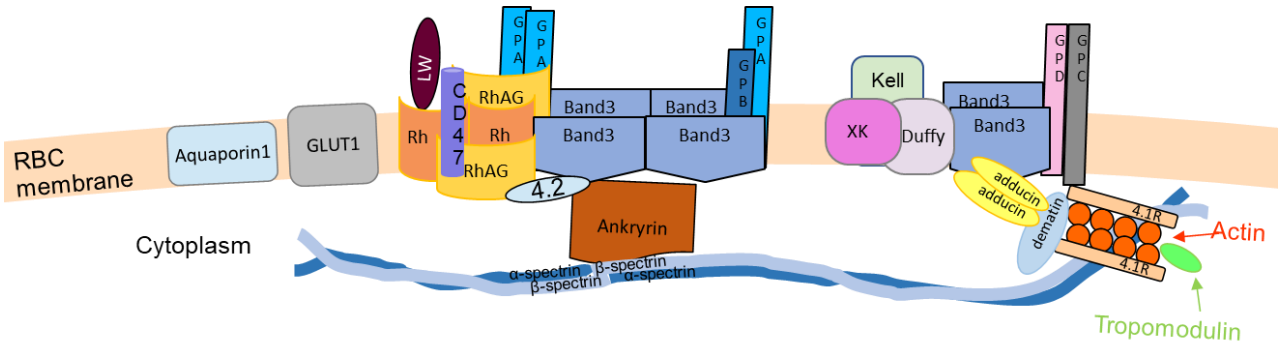

<u>Figure 1.4</u> Red cell major membrane proteins and their connection to the cytoskeleton. Transporters aquaporin1 and GLUT1 are depicted on the left. The ankyrin complex (proteins Rh, RhAG, LW, CD47, band 3, 4.2, GPA, GPB and ankyrin) is presented in the middle and complex 4.1R (glycoproteins XK, Kell, Duffy along with band 3, GPC and GPD) is on the right. These complexes link the membrane with cytoskeleton (α- and β-spectrin dimers, actin, protein 4.1R, dematin, α-adducin and tropomodulin). Image was modified from Anstee 2010 (87).

RBC membranes contain ion channels that control cell hydration and proteins such as glucose transporter 1 (GLUT1) and aquaporin-1 that transport glucose and water, respectively (88). Band 3 serves as a chloride/bicarbonate anion exchanger, Kidd protein transports urea and RhAG is a gas transporter (51) (89). Band 3 is an integral protein and it is the most abundant protein on RBC along with the major sialoglycoprotein GPA, present at approximately 10^6 copies per cell (90). Both carry blood group antigens (see section 1.2.4.4), are highly polymorphic and apart from RBC, they are also found on the kidney cells (91). GPA acts as a chaperone for band 3 transport to the membrane and prevents RBC aggregation in the circulation. It also contributes to the negative charge on the RBC membrane preventing potential binding between RBC or other cells (92).

1.2.4.3 <u>Phospholipids</u>

Phospholipids penetrate the RBC membrane asymmetrically; neutral phospholipids comprised of choline, such as phosphatidylcholine and sphingomyelin, are located on the external part of the membrane, while charged amino-containing phospholipids, such as phosphatidylserine (PS), phosphatidylinosirol and phosphatidyl-ethanolamine, can be found in the inside leaflet of the membrane (93). PS exposure on the outer side of the membrane attracts phagocytic cells, as it is a known apoptotic signal (94). Three enzymes control the distribution of the phospholipids in the membrane; an amino phospholipid translocase, called ATP dependent flippase, transfers (flips) amino-containing phospholipids from the external part of the membrane to the inside. The ATP-

dependent floppase controls the transfer of the choline-containing phospholipids from the inner leaflet of the membrane to the outside, a slower process compared to flippases. Finally, a bivalent-cation activated scramblase facilitates the distribution of the phospholipids, as it bidirectionally transfers (scrambles) them according to their concentration gradient, to achieve a symmetrical membrane (95). PS translocation on the external leaflet of the membrane has been reported to take place through vesicles by bidirectional trafficking between cytoplasm and plasma membrane (96).

Disturbances in membrane asymmetry and exposure of PS can not only trigger phagocytosis but they are also critical points in RCDP formation (95). Such a disturbance takes place when the intracellular calcium concentration increases. This results in flippase inhibition and scramblase activation which leads to further disturbance of the membrane asymmetry and PS exposure (95, 97). The role of floppase in membrane asymmetry disturbance is not clear yet (98). Low levels of Ca^{2+} (1μM) are enough to inhibit the flippase, whereas the scramblase needs much higher concentrations for its activation (approximately 100μM) (99-101). Physiologically, this is avoided by the plasma membrane Ca^{2+} pump, which is the only active Ca^{2+} transporter. However, high PS exposure in blood disorders, such as SCD, is thought to be associated with an increased electrogenic cation permeability induced by deoxygenation, in coordination with decreased Ca^{2+} pump activity leading to increased Ca^{2+} levels (102-104). High levels of calcium also activate proteolytic enzymes, e.g. calpain, which disrupt the binding between the cytoskeleton and plasma membrane, leading to the formation of vesicles (105). Intracellular Ca^{2+} levels and extracellular PS exposure have been reported in higher levels during RBC aging (106, 107).

1.2.4.4 Red blood cell antigens

RBC antigens are carried on proteins or sugars exposed on the erythrocyte membrane. They can elicit an immune response and are detected by specific alloantibodies. The ABO glycosyltransferase was the first blood group discovered by Landsteiner in 1901 (108), demonstrating that matching blood groups between patient and donor is vital for a successful blood transfusion. This was done through observation of RBC clumping (agglutination) when mixing RBC and plasma from different people (108). The precursors for ABO are H antigens. Rare individuals lacking H are consequently A and B negative and were first reported in Bombay (Bombay phenotype) (109).

The Rh antigens, which were discovered 40 years later than ABO, consist of proteins. Rh was originally named after the Rhesus monkey, as it was mistakenly thought to be similar to the antigens produced by these monkeys (110). The RhD antigen, a large protein encoded by the *RHD* gene, together with the ABO blood group antigens, are of major clinical significance, as they must be matched before a blood transfusion takes place to prevent haemolysis. This is attributed to the immune system defence, which produces antibodies against foreign proteins (111). Additionally, ABO group antigens are naturally found in food and some microorganisms, hence it was thought

that antibody production was stimulated by the environment (112, 113). Interestingly however, the presence of anti-A and -B antibodies in the blood of people lacking the corresponding blood group antigens has been reported, e.g. individuals with A or B blood group produce anti-B and anti-A respectively, even in infants and new-borns. Such antibodies were not derived from the mother, showing that these antibodies are naturally produced (114, 115). On the other hand, anti-RhD production by a RhD-negative person is only stimulated after exposure to the RhD antigen. Anti-RhD are mostly small immunoglobulins (Ig) consisting of IgG monomer and can cross the placenta easier compared to the larger pentameric IgM, anti-A and anti-B. If the mother is D-negative, fatal haemolysis can be caused via the haemolytic disease of the foetus and newborn (116).

There are 38 formally registered blood groups at present, encoded by 45 genes (117). Some of these clinically important blood group antigens are RhC/c and RhE/e in the Rh system, K/k in Kell, Fy^a/Fy^b in Duffy, Jk^a/Jk^b in Kidd, as well as M/N and S/s in the MNS system (116). The naming of the antigens was often haphazard. Kell, Duffy and Kidd systems were named by the original patients in which the antibody was initially found (118). M and N for MNS were taken from the word “immune” and S from Sydney, as a place where anti-S was first described (89). The majority of the blood antigens are carried by RBC proteins; MNS antigens are carried by GPA and GPB, whereas band 3 carries the antigens of the ABO (119) and the Diego systems (91). The Diego blood group was also named after the first patient in which it was described (118). RBC antigens exhibit high polymorphism caused by single-nucleotide substitutions, single nucleotide insertions or deletions and gene rearrangements (116). For patients who require frequent blood transfusions, like those with SCD, blood screening of not only the ABO and Rh, but the minor blood groups must be taken into consideration. This is needed because RBC antigen prevalence differs greatly between patients with African ancestry and mostly Caucasian donors who represent the majority of donating population. Some antigens are commonly present in white but rarely in black populations, such as RhC, RhE, Kell, Duffy, Kidd and MNS. Minor blood groups can be highly immunogenic after a blood transfusion, leading to haemolytic reactions and alloimmunisation (120), which are further discussed in section 1.5.3.

1.2.5 *Ex vivo* generation of red cells

RBC generation in culture is of scientific interest for many laboratories around the world, as it may increase the blood bank supplies for blood transfusion, especially for patients with rare blood groups. A pool of cultured reticulocytes expressing or lacking particular blood groups, could also contribute to prevent mismatched blood and decrease alloimmunisation (section 1.5.3) (121). A source material for erythroid cell cultures can be human embryonic stem cells or stem cells from adult peripheral blood, cord blood and bone marrow (122-124). An alternative source is using immortalised cell lines, which can proliferate continuously preserving their phenotype, through transformation of haemopoietic progenitor with transcription factors by using viral vectors. However, attempts to

generate mature RBC at large scale have been challenging and not feasible for the time being (125). To date the highest amplification achieved is >10^5-fold from 10^6 $CD34^+$ from cord blood and peripheral blood. The reticulocytes were generated using a well-established protocol according to a good manufacturing practice compliant procedure, comprised of three stages using different supplemented media (126). Cultured cells were found to be similar to the donor cells in terms of deformability, oxygen-binding capacity and immunogenicity using serology (123, 127). Interestingly, significantly higher levels of cultured cells remained in the circulation of a mouse transfusion model, compared to RBC from a donor. This demonstrated the feasibility of using cultured reticulocytes, which represent a homogenous population of young red cells, *in vivo.* Additionally, cells from both sources did not exhibit toxicity when introduced in a mouse model (126). Blood transfusions are further discussed in section 1.5.2.

1.2.6 Animal models of erythropoiesis

Despite the fact that *in vitro* RBC cultures have enhanced our knowledge about cell cycle and function, the information provided is limited. This is mainly due to lack of other cells in the culture system producing natural signals like cytokines that can affect RBC fate in a living organism. Another limiting factor is the limited two-dimensional environment in culture plates, in contrast to 3-D structures found in an organism (128, 129). Immune deficient mice are commonly used as study models of haematopoiesis, due to the absence of immune cells such as T, B, and NK, as their presence would cause graft rejection (130). Although the engraftment of human peripheral blood mononuclear cells (131) or HSC (132) in humanised animal models was achieved by the discovery of the severe combined immunodeficiency mutation (scid) (133), there are limitations. These concern the restricted engraftment of multiple hematopoietic lineages, which fail to generate a functional immune system in xenograft models (134, 135). While human myeloid lineage and erythropoiesis can arise from human HSC in the BM of immunodeficient mice, they cannot differentiate into mature RBC and the presence of megakaryocytes is limited (129, 130). Hence, studies in diseases with impaired erythropoiesis like SCD are difficult to be performed.

Elimination of murine macrophages using liposomal clodronate was shown to allow short-term (up to 7 days) RBC detection in the circulation (136). However, murine macrophages recover quickly and destroy the transfused human cells. RBC from a donor along with cultured reticulocytes generated from $CD34^+$ cells, isolated from cord and peripheral blood, were introduced in a NOD/LtSz-scid IL-2Rγ_c null (NSG) mouse model (126). These mice are immune deficient, lacking T, B and NK cells and can be used for the engraftment of normal and malignant human blood cells (137, 138). The use of liposomal clodronate allowed the expansion of the grafted cells. Cultured reticulocytes could differentiate into mature RBC in the animal model, indicating that macrophages were not involved in the formation of the biconcave shape but they may participate in removing unwanted

material (see sections 1.3.2 and 1.3.3). This showed that the selected animal model closely imitated a blood transfusion (126).

Animal models can be genetically modified using gene-targeted knockout techniques, knock-in mutations and random mutagenesis methods to provide a good framework for *in vivo* studies (128, 129). Synthetic peptides exhibiting the K immunogenic antigen of the Kell brood group were shown capable to induce tolerance in HLA-transgenic mice, by suppressing responses of T helper (Th) subsets (139). In addition, KEL1 and KEL2 transgenic mice, that express the human immunogenic antigens from the Kell system K and k, respectively, were generated by vectors (140). These systems were used to examine the effects of IgG subclasses in alloantibody production during alloimmunisation (section 1.5.3) (141). Lately, SCD and normal mouse models having both human α-globin and healthy or sickle β-globin genes, knocked into the mouse locus, were used to investigate the effect of SC in coagulation. The results suggested that retention of SC in clots occurs not only due to their shape but also through thrombin production (142).

1.2.7 Material exported by red cells

Mature RBC still contain a few cellular components, such as structural proteins like spectrin, which supports cell formation and allow RBC to move into small capillaries. Interestingly, mammals are the only organisms with enucleated RBC. Mitochondria, ribosomes and endoplasmic reticula are lost during the enucleation stage (143). It was suggested that enucleation and organelle extrusion through RCDP increased the ratio of cell surface area to volume, leading to better gas exchange as well as leaving more space for Hb (144, 145). However, ejection of endoplasmic reticulum deprives RBC of protein synthesis and export of mitochondria prevents oxygen consumption by the cell, maximising the amount transported to the tissues (58). In addition, since RBC produce a high number of free radicals, mitochondria exported by mammalian RBC may decrease harmful ROS, which reduce Hb oxygenation (146, 147) and consequently damage the membrane deformability (148, 149). This theory is in contrast to avian RBC, which preserve mitochondria and nuclei but have lower levels of oxidative stress and similar levels of Hb (144). The mechanisms by which organelles are removed in RCDP are discussed in sections 1.3.2 and 1.3.3.

1.3 Cellular microparticles

1.3.1 Circulating microparticles in plasma

RBC-derived particles are referred to in this dissertation as RCDP and belong to a larger group of extracellular vesicles or microparticles (MP) which are secreted from most cells, if not all (150). They are comprised of membrane lipid bilayers and they differ in composition and physicochemical proteins. In 1967, MP were thought to be cellular dust or to originate from platelet membrane

splintering (151). They have been implicated in intracellular communication in health and pathology by transferring cargo between cells (152). MP were showed to trigger and/or modulate immune responses in cells which take them up. They have even been reported to alter cell migration in cancer cells. For these properties, MP are studied to be used as therapeutic targets, diagnostic aids and prognosis predictors, like biomarkers, e.g. in lung disease (153, 154). MP can be formed as membrane blebs in the extracellular space, known as microvesicles or ectosomes (Figure 1.5). They can also be formed as exosomes, by membrane endocytosis and development of multi-vesicular bodies, which subsequently fuse with the membrane and are then exported extracellularly (155). Microvesicle sizes vary between 100–1,000nm in diameter, whereas exosomes are smaller, ranging from 40–150nm in diameter. A third category of MP is apoptotic bodies (Figure 1.5), resulting from fragments of old cells, ranging from 50–5,000nm in diameter. Microvesicles and apoptotic bodies expose PS on their membrane surface (155, 156), while most exosomes expose cytoplasmic proteins like actin, tetraspanins, heat shock proteins, such as Hsp70 and Hsp90 and biogenesis-associated proteins like Alix and Tsg101 (157-160).

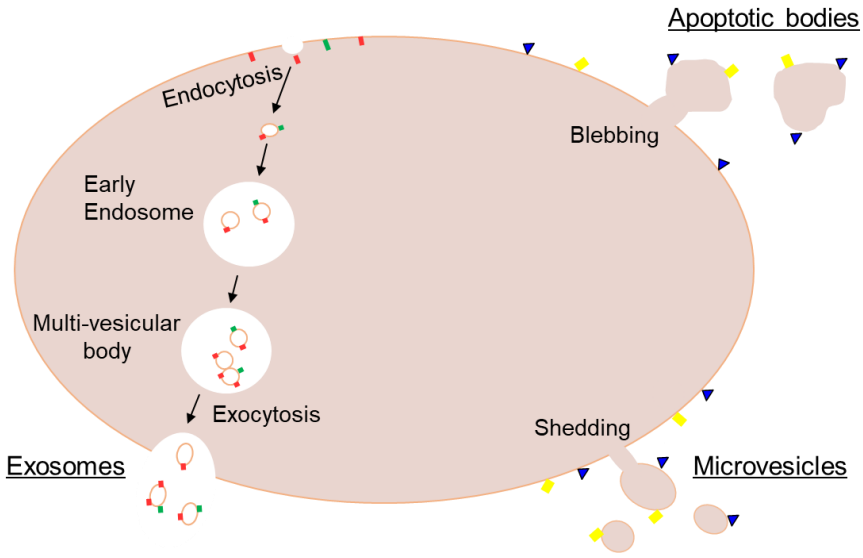

Figure 1.5 Secretion of microparticles. MP are formed as apoptotic bodies (top right), exosomes (bottom left) and microvesicles (bottom right). Apoptotic bodies are membrane blebs and fragments from senescent cells, whereas microvesicles are formed by membrane shedding. Both expose extracellular membrane components (in blue and yellow). Exosomes form multi-vesicular bodies by membrane endocytosis, which then fuse with the membrane and are exported outside the cell. They expose cytoplasmic membrane components (depicted by red and green on the image). Image was modified from Gustafson *et. al*, 2017 (161).

1.3.2 Red cell-derived particles and clinical significance

In healthy people, the majority of MP come from platelets and RBC (151). Two different studies in 1983 showed the export of RCDP, as well as exosomes, from immature reticulocytes (162, 163). RCDP are formed by shedding of the lipid bilayer of the RBC membrane which is rich in phospholipids and proteins (164), therefore they have a right-side out membrane orientation. RCDP are naturally shed during RBC aging due to membrane disturbance and collapse of cytoskeleton network. It was suggested that disturbance of the band 3-ankyrin anchoring complex increased the compression and generated a bud of the RBC membrane bilayer, forming RCDP (165).

RCDP may also be involved in inflammation and immunomodulation. It is suspected that RCDP down-regulate macrophage activity whilst being phagocytosed when inhibiting the production of tumour necrosis factor α (TNF-α) and IL-8. This was reported in macrophages that had cleared up RCDP after exposure to known macrophage stimulators like zymosan A and lipopolysaccharide (166). Furthermore, phospholipids on the RCDP membrane are substrates of the phospholipase A2 enzyme, which may lead to lysophosphatidic acid production, known to participate in inflammation, cell proliferation and migration (167). RCDP are also involved in nitric oxide (NO) availability. NO is a major contributor to vasodilation (168-170) but it can be efficiently scavenged by RCDP (168). This should be taken into consideration before using stored blood for transfusion, as RCDP numbers increase rapidly during storage and can thus decrease NO availability (171).

In haemolytic anaemias such as β-thalassaemia and SCD, RBC are more fragile due to defective mechanisms in membrane integrity, enzymes or Hb. In such conditions, RCDP levels were found to be significantly increased (172-175). PS abundance on RCDP triggers phagocytosis by macrophages and promotes coagulation since it catalyses the conversion of prothrombin into thrombin, which is involved in coagulation (176). Another initiator of coagulation is tissue factor (CD142) which has been reported to be found on RCDP membranes (177). It has also been shown that RCDP participate in the initiation of vaso-occlusive crises in SCD (178). Recently, we have shown that removal of large RCDP exposing PS and prothrombotic factors from SCD plasma has led to decreased plasma clotting times. This suggests that removing this population from patients' plasma may alleviate any symptoms caused by hypercoagulation in these individuals (Smith *et. al*, manuscript submitted).

1.3.3 Autophagic vesicles

Apart from RCDP formation by membrane shedding, reticulocyte membrane fragments were also thought to be exported through membrane endocytosis by the endosome-exosome pathway and formation of multivesicular particles. These fuse with the plasma membrane and are exported extracellularly as exosomes (Figure 1.6) (179, 180). Removal of excess organelles is thought to occur by autophagy, in which organelles are encapsulated in the double membrane forming autophagosomes, transferred to lysosomes and then exported outside the cell (180). There is evidence that endocytosis and autophagy may merge, leading to the formation of autophagic vesicles (AV) (181). This term is used in this dissertation to describe inside-out membrane AV secreted by RBC, where their orientation is different to RCDP, which are the right-side out (Figure 1.6).

Using an *in vitro* culture system, our colleagues suggested that reticulocyte maturation and AV formation takes place in two phases; one in the BM where excess membrane is removed by the endosomal-exosome pathway and the other occurring later in the circulation, where large membrane particles are endocytosed and fused with autophagosomes forming AV. Then, AV are exported outside of the cell, probably during passage through the spleen. Interestingly, both were found to take place in the absence of lysosomes (123, 182). Our colleagues also showed that in SCD patients, and in individuals splenectomised due to other haemoglobinopathies, PS was expressed on the surface of RBC in similar levels to that of the AV from cultured reticulocytes (127). The properties of AV and RCDP generated by SCD patients and cultured reticulocytes were further investigated in this dissertation.

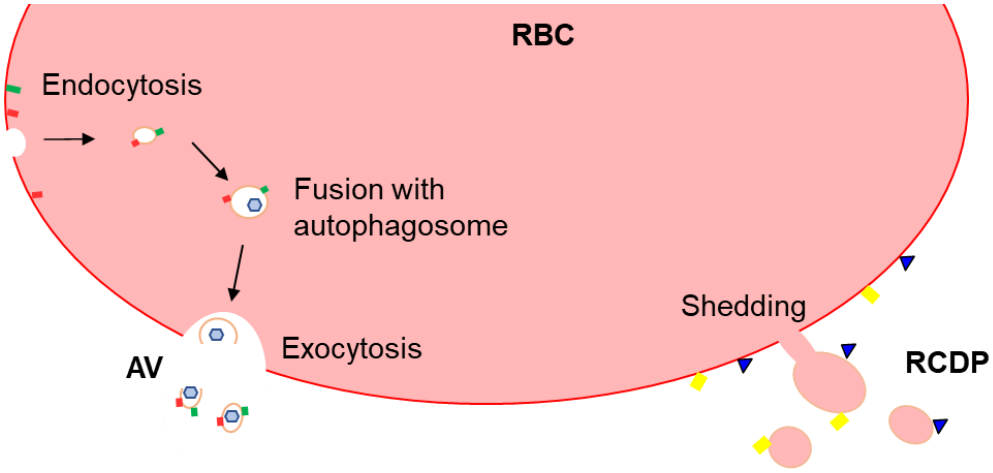

Figure 1.6 Suggested mechanisms of particle formation in erythrocytes. On the left, the red cell membrane is internalised by endocytosis to form a microparticle that fuses with an autophagosome to form a large vesicle, which is expelled and released extracellularly. The resulting AV expose the cytoplasmic components of the maternal cell on their membrane. RCDP are formed by membrane budding and instead expose the extracellular components.

1.3.4 Storage vesicles

RBC units for transfusion contain storage vesicles (SV), the levels of which increase exponentially during storage (183, 184). RBC are isolated from whole blood by plasma separation after centrifugation and RBC units are then leukofiltered prior to storage, to prevent alloimmunisation by human leukocyte antigen (HLA) antigens (185). In continental Europe, the United States, Canada and other countries, RBC units are kept for up to 42 days (186), whereas in the United Kingdom (UK) they are kept for up to 35 days, at 2–6°C (187).

1.3.4.1 Formation of storage vesicles

SV are a heterogenous population of vesicles forming round or rod structures (188). Generation of SV is stimulated by several events taking place during RBC storage. RBC undergo biochemical, mechanical and immunological changes with time spent in storage, for instance changes in ATP and NO levels (189-191). ATP levels decrease while oxidative conditions promoted by depletion of glutathione and its associated enzymes, such as glutathione peroxidase and glutathione reductase, harm membrane lipids and proteins. This leads to transformations in membrane structure and morphology, known as storage lesions (192). Changes caused by storage lesions can be restored *in vivo* after transfusion, in contrast to other changes, e.g. membrane remodelling (190, 191). Reduction in ATP is thought to cause vesiculation. In parallel, this leads to further vesiculation by increasing intracellular calcium (193, 194). In addition, oxyhaemoglobin is released extracellularly, either free or within RCDP, and both forms may scavenge NO and decrease vasodilation (see section 1.2.4.1). *In vivo*, rats inoculated with plasma from stored blood units were found to show increased haemolysis and significant vasoconstriction, potentially caused by NO elimination (168).

1.3.4.2 Storage vesicle characteristics

The number of SV and haemolysis levels amongst different blood units is primarily linked to various features of the donor RBC, such as membrane fragility, levels of Hb and intracellular calcium (195, 196). Different levels of uric acid could be another factor in vesiculation, as it acts as an antioxidant and could reduce oxidative stress reactions (197). SV characteristics have been reported to depend on the leukoreduction method and the additives in RBC concentrates (198). Two different methods of leukoreduction using whole blood and buffy coat filtration were compared to assess potential effects on SV size (199). The SV population was initially 100nm size and reached up to 200nm during storage in both methods. However, SV from units prepared by whole blood filtration were always smaller in size than those prepared from buffy coats, throughout the whole storage period (199). Interestingly, the number of SV generated by whole blood filtration was higher than that from buffy

coats (200). This is of great importance, as SV size and absolute number may affect their bioactivity, as well as their coagulation activity (201). Furthermore, stored RBC from buffy coat leukofiltration had higher ATP levels and were less affected by storage osmotic changes, than from non-leukofiltered units (202). The above differences in SV size and cellular components when generated by different RBC isolation methods could affect SV composition and bioactivity, thus further research on this is required (186).

Additives in storage RBC bags, used to preserve cells for up to 6 weeks by providing nutrients, can also affect SV characteristics (203). SAGM is a popular additive solution, named according to its constituents, saline-adenine-glucose and mannitol, which scavenges free radicals and stabilises the cell membranes (204). While SAGM is widely used in Europe, it is not approved by the United States Food and Drug Administration (USFDA) and instead the citrate–phosphate-dextrose-adenine (CPDA) based additives are used in the USA (205). Comparisons of RBC stored in SAGM or CPDA showed that SV numbers were reduced in SAGM, potentially because of a lower oxidation status (198, 206). Newly developed additives like alkaline preservatives such as ATP 2,3-BPG seem to maintain higher levels of important metabolites, as well as lower haemolysis levels when compared to SAGM-stored RBC (207, 208). Further research is required to investigate and/or develop new additives (186).

1.3.4.3 Storage effect on red cell proteins

RBC storage temperature can also affect vesiculation. The RBC membrane permeability decreases at 4°C, triggering an increase of intracellular calcium, therefore promoting vesiculation (209). Permeability is further decreased by inhibition of the ATP-dependent Na^+/K^+ cationic pumps at this temperature, resulting in increased intracellular Na^+, which stimulates further transport of calcium into the cell (193, 194). Oxidative stress reactions occurring in RBC during storage are enhanced by a reduction in endogenous antioxidants, such as glutathione and peroxiredoxin-2, which protect the cell from hydrogen peroxide (191, 210, 211). The most affected proteins by oxidative stress are band 3, spectrin, β-actin, glyceraldehyde-3-phosphate dehydrogenase (GAPDH), band 4.1, band 4.2, band 4.9 and ankyrin (210, 212). ROS can cause vesiculation by interference with cytoskeletal proteins such as β-actin, spectrin and band 4.1, or with proteins involved in membrane formation and stability, such as ankyrin, band 3, band 4.2 and band 4.9 (210, 211). These proteins can also react with GAPDH and Hb and subsequently affect RBC metabolism. GAPDH is found in two forms; an active cytosolic and an inactive membrane bound to band 3, where both are essential for glycolysis. During ROS reactions, reversible oxidation of GAPDH switches glycolysis to a pentose phosphate pathway and NADPH production, which facilitates redox reactions compensating the oxidation and preserving Hb, as well as cell integrity (213). Two GAPDH oxidative mechanisms have

been reported for RBC stored in SAGM. One is a reversible oxidation of the enzyme, resulting in NADPH production to preserve stored RBC (214). The second is an irreversible oxidation of membrane bound GAPDH that reduces its activity. It occurs through continuous enzyme oxidation during storage, which results in export of excess oxidised enzyme through SV, suggesting that vesiculation is facilitated to remove unused material from the cell (215). Oxidation has been reported to affect functional parts of the β chain of Hb, such us the proximal cysteine 94 that is implicated in NO scavenging and histidine 144, which is involved in the maintenance of the stability of the deoxygenated form (216).

With the use of proteomics, SV have been reported to contain the apoptosis stimulating fragment proteins called Fas, their related Fas-associated death domain proteins and caspases 3.8 (206), as well as ubiquitinated proteins (198). They are also rich in Hb and raft proteins acetylcholinesterase, flotillin-2 and stomatin (183, 216). The levels of the last two were two-fold higher when compared to RCDP produced *in vivo* (217). Flotillin-2 is a cytoskeleton protein that anchors band 3 complexes during storage and both proteins were found highly associated (218). Stomatin is a membrane, cytoplasmic protein and acetylcholinesterase is an extracellular enzyme anchored to the membrane (219, 220). PS has been reported not only on SV but also in RCDP and stored RBC (183, 217), which could result from the decreased flippase activity triggered by ATP elimination and the pH changes during storage (183, 205, 221).

1.3.4.4 Storage vesicle analysis methods

The International Society for Extracellular Vesicles has published protocols for microparticle isolation in plasma. In terms of SV, however, several isolation methods have been described (reviewed by Wannez *et. al*, 2019). Double centrifugation is a feature of most of them, starting from 400g and reaching 12,500g at 4°C (186). SV size is usually calculated by dynamic light scattering (DLS), nanoparticle tracking analysis (NTA), atomic force microscopy and tunable resistive pulse sensing (199, 219, 222). DLS and NTA use the Brownian motion of microparticles in suspension and the laser light scattered allows measurement of the average size and the zeta potential, using the Stokes-Einstein relationship (222). DLS is effective for monodispersed samples but less accurate for polydisperse samples. NTA on the other hand uses a camera and allows particle visualisation (223). Tunable resistive pulse sensing uses voltage change readings caused by particle passage through a pore. It allows concentration of particles of a specific size range (224). Atomic force microscopy can generate precise, versatile data on three-dimensional characteristics, such as size, as well as protein abundance simultaneously. However, despite the detailed results, the method is not often chosen due to the object immobilisation required during analysis (225).

SV morphology can be examined by transmission electron microscopy (TEM) or cryo TEM (226), while usually flow cytometry is used to determine the SV phenotype, including PS exposure (183,

199, 200, 227). For this, beads are commonly used for instrument calibration, which help in gating populations with different size and scatter characteristics (228, 229). However, most flow cytometers are not sensitive enough to detect SV smaller than 300nm (230) and consequently NTA is the most popular method used for characterisation of small SV (231). Imaging flow cytometry is a new method which combines flow cytometry with microscopy, allowing visualisation of individual objectives. This technique was proven to be sensitive for populations above 200nm (232, 233) and can be optimised for even smaller populations close to 100nm (234).

1.3.4.5 Clinical significance of storage vesicles

It is suspected that SV could have clinical applications because of their constituents (186). An increase in the coagulation properties of stored RBC, which is linked to the exposure of tissue factor (TF) has been previously described (235-237). The effects of SV in stored RBC after blood transfusion were examined by spiking blood from healthy donors with SV from expired RBC units, which lead to a significantly decreased clotting time from 194 to 161 seconds (237). Plasma and monocytes showed increased TF levels, while TF messenger RNA expression was found to increase with time and SV concentration. Levels of proinflammatory cytokines, IL-1β and -6, and activated platelets were significantly increased. It was also suggested that platelet interactions with neutrophils and monocytes were promoted, indicating that SV may trigger inflammation after blood transfusion (237). In other studies, proinflammatory cytokines IL-2, -7 and -15 and TNF-α were produced by macrophages post stimulation by SV. It was also shown that SV, up to 200nm, activated $CD4^+$ and $CD8^+$ T-cells through antigen presentation and led to their proliferation (237). Furthermore, since phospholipids are converted to arachidonic acid and lysophospholipids by phospholipase A2, it is possible that lysophosphatidylcholine exposed on senescent RBC and SV results from consumption of high phospholipid levels by phospholipase A2. As these lysophospholipids have a contiguous structure to platelet activating factor, they could be involved in neutrophil activation or priming. Furthermore, CD11b, which is a marker of neutrophil priming, has been found to be increased upon stimulation with SV (238-240). It was also shown that neutrophils could produce superoxide and undergo phagocytosis, after interactions with SV (240). Results from all of the above studies suggest that SV may be involved in immune responses, however further investigation on this should be carried out (186).

1.4 Red cell disorders

1.4.1 Haemoglobinopathies

In pathological conditions, differences in RBC numbers or levels of free Hb and oxyhaemoglobin, result in different types of anaemias (from Greek *anaimia*, from *an-* un, 'without' and *haima* 'blood'). Anaemia particularly affects pregnant women and young children; the World Health Organisation (WHO) estimates that 40% of pregnant women and 42% of children less than 5 years old suffer from anaemia, usually due to dietary deficiencies (241). Haemoglobinopathies and infectious diseases are other causes of anaemia. HbA is the major type of Hb in adults, comprising 95% of the total Hb. HbA2, with two delta chains instead of beta (2α/2δ), comprises less than 3.5%, while HbF accounts for <1% of the total Hb in adults. Abnormalities in Hb genes' expression lead to inherited anaemias, i.e. haemoglobinopathies, which is a greater burden for health care systems worldwide, including the UK. There are two main categories of haemoglobinopathies; (i) thalassaemias, where mutations in the genes for α or β globin chains cause reduced or inadequate synthesis of normal α- or β-globin chains leading to decreased levels of HbA and (ii) structural abnormalities in HbA, such as sickle Hb (HbS), resulting from the mutations in the genes for α or β globin chains (242). As stated previously, RCDP levels are significantly increased in β-thalassaemia and SCD patients (172-175).

1.4.2 B-thalassaemia

One of the main categories of thalassaemia is β-thalassaemia major, caused by absence of β-globin chains due to mutations of the beta-globin gene on chromosome 11. More than 200 mutations are reported to cause β-thalassaemias (243). Most patients originate from the Mediterranean (thalassaemia from Greek word *Thalassa* for sea), Middle East, South Asia or the Far East. In the UK, there are more than 1000 patients with β-thalassaemia, most of them relying on frequent blood transfusions, usually every 3-4 weeks. Most patients require life-long transfusion regime, since they may suffer from life-threatening anaemia from an early age of one year old (242). The anaemia occurs because HbF would normally be replaced by HbA (α_2,β_2) in adults, but as HbA is absent in these patients, the HbF (α_2,γ_2) levels remain increased. This causes unpaired α chains to precipitate on the RBC membrane as hemichromes, which can lead to further RBC membrane oxidation and cell damage (243). Treating children with β-thalassaemia using HSC transplantation is the only curative procedure. It is possible but finding suitably matched donors is usually problematic. Inadequately treated anaemia can lead to bone marrow enlargement, splenomegaly and skeletal deformities (244).

1.4.3 Sickle cell disease

SCD is a hereditary disorder caused by a single base mutation at codon 6 in the β-globin gene, replacing glutamic acid to valine (245). It is estimated that over 300,000 babies are born every year suffering from SCD, most in sub-Saharan Africa (246). In 2018, it was estimated that there are approximately 14,000 SCD patients in the UK; that is one patient in 4,600 people (247). Most heterozygous patients, who have one HbS gene, are asymptomatic (known as sickle cell trait). In contrast, homozygous patients suffer from sickle cell anaemia (245).

1.4.3.1 Formation of sickle cells

The sickle cell shape forms after RBC deoxygenation in the circulation. In normal conditions, Hb undergoes changes during oxygen binding. Atoms of heme in the deoxygenated Hb (T state Hb), are bound to hydrogen and electrostatic bonds. Binding of oxygen forms oxygenated Hb in the R-state and leads to disruption of these bonds and formation of the new ones. Thus, the binding of only one molecule of oxygen to the tetramer dramatically changes the tetramer conformation (248, 249). Replacement of the polar glutamic acid with hydrophobic valine disrupts the bond formation and alters Hb structure. Instead, the formation of new hydrophobic bonds between valine residues on the β-globin chain of one HbS and alanine, phenylalanine and leucine of another HbS molecule on a different β-globin chain, is forming double strands. This can occur only in the T-state Hb when hydrophobic areas are exposed to form the new bonds. At low oxygen concentrations, increased strand numbers result in formation of long fibres and HbS polymerisation, disrupting the RBC membrane deformability and leading the biconcave cells that transform into the sickle cell shape (Figure 1.7) (248-252).

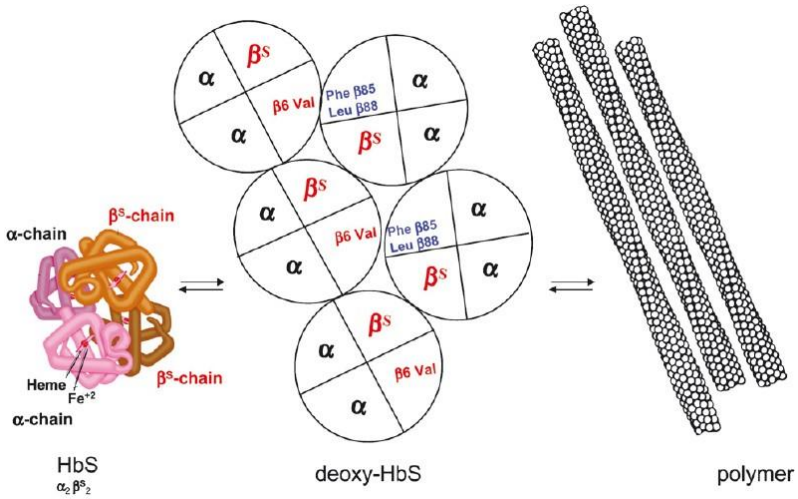

Figure 1.7 Sickle haemoglobin polymerisation. Hydrophobic valine (Val) forms bonds with phenylalanine (Phe) and leucine (Leu) residues. At low oxygen levels, deoxy-HbS polymerises and gives long fibres that alter RBC shape from biconcave to sickle. Image was reproduced from Odièvre *et. al*, 2011 (253).

In contrast to healthy RBC, sickle cells (SC) flow slower in the circulation and can adhere to the endothelium. The inflexible SC membrane prevents cell passage through the microvasculature and eventually, they block the capillaries (245, 252, 254). Furthermore, repeated reversible HbS polymerisation result in haemolysis, followed by increased free Hb and RCDP levels in the circulation (255). RCDP levels were found to be up to 3- to 4-fold higher than in healthy individuals and along with SC, they contribute to vaso-occlusion. This can lead to further complications, such as organ damage, severe anaemia, stroke and infections (252, 255), discussed in section 1.4.3.3.

In the early stages of RBC deformability disruption, polymerisation of Hb affects other cellular functions and ion channels such as the K-Cl transport system and the Ca-dependent K-channel (Gardos channel), which decrease the intake of potassium and water molecules (256).This results in increased intracellular Hb levels which further contribute to HbS polymerisation and make cells irreversibly sickled (253). Additionally, cytoskeletal proteins, particularly band 3 are released as hemichromes, which are defective Hb aggregates in the internal leaflet of the membrane (257, 258). In parallel, heme decreases and Fe^{3+} is released, leading to oxidising conditions. PS levels on the cell membrane increase, disrupting the phospholipid asymmetry on the membrane. Anti-band 3 IgG target band 3 clusters and phagocytosis by macrophages is triggered, leading to haemolysis (257). All of the above processes trigger RCDP formation (259).

1.4.3.2 Mechanisms of coagulation

SC adhesion to the endothelium was shown to result from immature reticulocytes, called stress reticulocytes, which are released into the blood stream too early. This is due to their increased production by the bone marrow in response to anaemia, attempting to maintain the oxygen levels (259). Adhesion of the stress reticulocytes to the endothelium decreases the blood flow rate and supports the accumulation of SC, leading to blockage of the blood vessels (259). Adhesion is facilitated by a number of molecules on the RBC surface and on the endothelium. They include α4β1 integrin or very late antigen-4 binding to the vascular cell adhesion molecule-1 (VCAM-1), CD36 on RBC binding to CD36 on endothelial cells via plasma thrombospondin, Lutheran blood group Lu/ basal cell adhesion molecule isoform antigen binding to laminin and CD44 on the RBC membrane binding VCAM-1 through fibronectin (260, 261).

Stress reticulocyte levels are increased within hours of blood loss, which has also been shown in other types of anaemia, i.e. pyruvate kinase deficiency. However, acute painful episodes (crises) caused by vaso-occlusion (vaso-occlusive crisis, VOC) have not been reported in other haemolytic diseases and are associated with HbS (253). Along with stress reticulocytes and endothelial cells, activated platelets, leukocytes and plasma components also contribute to VOC. PS exposure on RBC and TF expressed by endothelial cells trigger thrombin production that leads to coagulation (253). Even low thrombin concentrations combined with ischaemia-reperfusion injury (damaged

tissue due to interrupted oxygen supply) can contribute to hypercoagulation and inflammation by stimulating proinflammatory cytokines (262, 263). Furthermore, oxidative stress leads to haemolysis and release of iron inducing the production of endothelial molecules, which are involved in the adhesion of stress reticulocytes and leukocytes activation. Two of these molecules are nuclear factor-kappa β and activating protein-1, which are implicated in VCAM-1, inter-cellular adhesion molecule-1 and E-selectin production in the endothelium (264). Additionally, NO bioavailability is limited, as release of Hb leads to NO scavenge and decreases vasodilation and free erythroid arginase, produced by haemolysis, degrades L-arginine, the precursor for NO synthesis (265). NO decomposition produces free radicals one thousand times more quickly than in RBC (265). All the above, along with clearance of deformed SC by macrophages in the spleen and subsequent release of heme and SC products, exacerbate existing haemolysis (266).

RCDP and MP are produced from cells participating in the inflammation response, such as endothelial cells, platelets and leukocytes (267). However, the majority are RBC-derived (267-269). Elevated RCDP numbers in SCD have been reported, due to the lack of a functional spleen. Initially, these RCDP were found by Allan *et. al* in 1982 to be HbS loaded and lacking spectrin (255). RCDP were found to contribute to coagulation as well as vaso-occlusion and were found at increased levels during VOC (267). Because of their altered components, due to RBC transformation to SC, they are considered to have clinical implications (253). Recently, it was shown that removal of large PS exposing RCDP from patient plasma may alleviate any symptoms caused by hypercoagulation in these patients (Smith *et. al*, manuscript submitted).

1.4.3.3 Complications caused by coagulation in sickle cell disease

Pain and life-threating conditions

Microvascular occlusion and tissue ischaemia caused by SC are characteristic features of the disease. Acute pain, which is related to SCD severity, is caused by blood flow blockage in capillaries and small vessels and it is the most common reason for hospital admission (266). Acute pain is also associated with acute chest syndrome, caused by several respiratory features like chest pain and tachypnoea, which can be life-threatening for many patients (270). Painful VOC are related to cellular interactions in the vascular endothelium and the inflammation (253, 271). VOC can lead to cerebrovascular accidents like stroke, affecting 11% of 20 years old patients and 24% of 45 year olds (272). The abnormal SC shape, combined with VOC and inflammation, can also cause organ damage, particularly the spleen, liver, bone, lungs, brain and kidney. Another serious complication can be acute splenic sequestration crisis, which can be lethal, especially for children under two years of age. It is caused by increased SC numbers in the spleen, resulting in splenomegaly and can also lead to severe anaemia or circulatory shock (273, 274).

Infections

Patients with SCD are susceptible to infections, probably due to splenic dysfunction caused by repeated sickling in the spleen, damaging its filtration capability, as well as impaired opsonisation of encapsulated pathogens, which is essential for phagocytosis (275-277). Such infections can be bacterial, mycobacterial, viral or parasitical (278). In malnourished children, further deficiencies in innate and humoral immunity are caused by lack of nutrients, low immunoglobulin levels and zinc deficiency (279).

The main function of the spleen is to filter and destroy circulating pathogenic organisms captured by macrophages. Opsonisation mediated phagocytosis is mainly facilitated by macrophages and neutrophils. It is dependent on complement cascade activation through three major pathways: classical, lectin and alternative. Tagging the pathogen surface with different complement opsonins mediates its uptake by phagocytic cells (280). If mechanisms using antibodies and/ or complement are defective during opsonisation, macrophages cannot effectively kill pathogens (275, 276). Splenic hypofunction is characterised by defective filtration and RBC shunting. It usually starts in early life and can be identified by circulating Howell-Jolly bodies (281). These are found as spots on RBC comprised of packed DNA, which was not exported during reticulocyte enucleation in the BM and are usually cleared by a healthy spleen (282). Ischaemia and chronic vaso-occlusion injure the spleen and result in its dysfunction in early life, usually leading to splenectomy around 3-5 years of age (283).

Defective B- and T-cell functions in children with SCD lead to susceptibility to bacterial and viral infections, due to low memory B-cells and limited antibody production by T-cells (277). For example, impaired immunity can cause B-cells to produce only very low IgM antibody levels in response to influenza vaccine (284). $CD4^+$ and $CD8^+$ T cells are also decreased in SCD. $CD4^+$ T-cells can kill infected cells, while $CD8^+$ assist in antibody production. Both can trigger macrophage and neutrophil recruitment to the infected site (111). In SCD patients, these populations cannot mature properly (285), leading to a reduced number of T helper cell subpopulations, Th1 and Th2. The humoral immune response is facilitated by Th2 and Th1 cells that are responsible for cell mediated immune responses. It is thought that lack of $CD4^+$ cell mediated immunity may be the reason for the severe influenza infections in children suffering from SCD (286).

1.4.3.4 Sickle cell disease management

Early prognosis of SCD not only assists in alleviating the symptoms but also prevents early death due to sepsis or acute splenic sequestration crisis (281, 287). Various treatments including natural approaches such as heat, oral hydration and massage can relieve pain (288). On the other hand, non-opioid analgesics and anti-inflammatory drugs like ibuprofen can help patients to control pain (289). When hospitalised, due to acute and aggressive pain, management by intravenous opioids is

used (290). Blood transfusions, including simple transfusion of packed RBC and exchange transfusions, are often used to alleviate symptoms and anaemia from early in childhood, whereas regular transfusions given on a monthly basis can be used to prevent stroke episodes. Blood transfusion increases oxygen-carrying capacity by providing the patient with healthy RBC. However, complications such as alloimmunisation - an immune response to antigens from genetically different donors, iron overload and cost should be taken into account (291).

Hydroxyurea is a myelosuppressive agent that was shown to reduce painful episodes, potentially by increasing HbF levels (292). Although the exact mechanism is unknown, hydroxyurea was shown to inhibit deoxyribonucleic acid (DNA) synthesis and potentially cytotoxicity by inhibiting the enzyme ribonucleotide reductase, which is involved in ribonucleoside conversion to deoxyribonucleosides. In this way, hydroxyurea inhibits DNA synthesis and any cytotoxic events by increasing erythropoiesis via HbF promotion. Furthermore, hydroxyurea seems to be beneficial by decreasing the production of cells involved in inflammation and vaso-occlusion, such as neutrophils and reticulocytes (292, 293).

HSC transplantation using mobilised peripheral blood or BM cells, is the only cure for SCD. For this, normal HSC from an HLA-matched healthy donor can be transplanted into patients. However, graft (donated cells) *versus* host disease can occur, where donor leukocytes present in the transplant attack recipient cells. This can last for several months and can be life threatening. Graft rejection can also occur. Gene therapy is promising but it is only in early stage clinical trials (294). In the UK, all above treatments are available to patients (295). The USFDA has also approved L-glutamine, Crizanlizumab and recently voxelotor (296). L-glutamine improves RBC flexibility and circulation, allowing improved oxygen transport to the tissues (297). Crizanlizumab targets P-selectin which is involved in SC adhesion to the endothelium and thrombin activation (298), assisting smooth flow of SC and preventing their adhesion to blood vessels (299). Voxelotor binds Hb increasing its affinity for oxygen, promoting oxyHb. Therefore, deoxygenated sickle Hb polymerisation is inhibited and SC adherence is avoided (300)

Most treatment options mentioned above are used to alleviate SCD symptoms, as drugs can decrease VOC painful crisis episodes (292, 293, 297, 299, 300). Blood transfusions are widely used but complications such as alloimmunisation are common (discussed in section 1.5.3) (291). Likewise, haematopoietic stem cells transplantation (HSCT) are not without risk and HSCT are restricted by a lack of HLA-matched donors. While gene therapy may benefit the patients in future, there remains an unmet need for effective therapy for these patients (294).

1.5 Immunology of blood transfusions

1.5.1 Overview of the immune system

As was previously discussed in section 1.1, the BM gives rise to lymphoid progenitors, which can differentiate to leukocytes that comprise the organisms defence against foreign antigens. Some of the most important immune cells are neutrophils, which respond early and perform phagocytosis, T- and B- lymphocytes that are involved with adaptive immunity and monocytes that are early responders, carry out antigen presentation and mature to macrophages. Basophils and eosinophils are rarely found in the circulation. They can bind IgE, destroy parasites and are present during allergic reactions (111). When an antigen enters the organism, the innate immune system responds with neutrophils and macrophages that act first by secreting proteolytic enzymes and phagocytosing pathogens. Surviving invaders are confronted by lymphocytes; T-cells produce specific antibodies or kill specific cells, while B-cells remember specific features of the antigens and so generate antibodies faster in the event of future exposure (111, 301).

Antibodies are Ig consisting of light and heavy chains and are divided into several isotype groups. The main isotypes are: IgD that is a B-cell receptor; IgG, a monomer carrying out opsonisation and complement activation; IgM, a pentamer found on B-cells that activates complement; IgE, found in allergic reactions and IgA, which is responsible for mucosal immunity (111). If an antigen enters the organism for first time, several days are needed for an IgM antibody to be generated and then IgG production follows. IgM has a weak affinity for the antigen whereas IgG binds strongly and kills it effectively. If the antigen has been exposed to immune cells in the past, circulating memory B-cells will quickly scale up IgG production. This is known as a secondary immune response (302).

Antibody production is stimulated by antigen presenting cells (APC) and T-cells, via the T-cell receptor (TCR) that recognises the antigen on the APC. Lymphocytes can identify specific groups of molecules on cells known as major histocompatibility complex (MHC) molecules. HLA are the human equivalent of MHC (303, 304). MHC molecules are mainly comprised of peptides of the digested antigen exposed in a way that lymphocytes can recognise them. HLA molecules are divided into different groups, with class I and II being the best characterised. All human nucleated cells, except RBC produce HLA-I, while HLA-II proteins are only expressed on immune APC, specialised in antigen identification and digestion. These APC are B- cells, activated granulocytes and T-cells, monocytes and dendritic cells (DC) (303, 305). The human immune system diversity arises due to approximately 9 HLA molecules inherited randomly from one’s parents (306). The HLA-I and -II define the tissue type and HLA matching is vital for a successful HSC or organ transplant. HLA variability in humans is vast; amongst 20 million donors there will not be an exact match but for 2–5% of patients. This is the reason that compatible donors are usually close relatives who share common genes (111, 303).

1.5.2 Blood transfusions and the immune system

The immune response can be humoral, using antibodies, and cellular involving immune cells. Antibodies already found in plasma or produced against foreign blood cell antigens, known as alloantibodies, can destroy incompatible donor RBC after a blood transfusion. These cells express ABO group antigens and/or RhD that are absent from patient RBC. RBC lysis occurs either by binding to and coating the foreign RBC, or activating the complement cascade, or even causing RBC to adhere and clump together, known as agglutination (Figure 1.8). Agglutinated RBC may survive or are removed by macrophages in the spleen or liver, which also phagocytose donor RBC coated with antibodies (302).

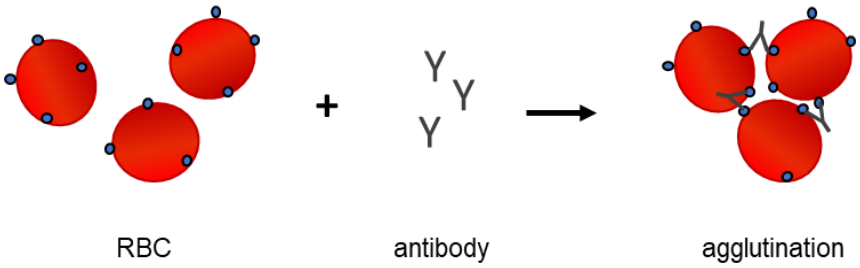

Figure 1.8 Red cell agglutination. Antibodies bind to foreign RBC antigens resulting in agglutination (clumping). Image modified from Parslow *et. al*, 2004 (307).

During an incompatible blood transfusion, mainly macrophages, monocytes and to a smaller extent DC and granulocytes will engulf antigens and then load the antigen peptides on MHCII. A Th1 cell recognises the MHCII / antigenic peptides, binds to them and gets activated by APC through cytokine secretion. The Th1 cell produces cytokines to induce production of cytotoxic T-cells (308). Eventually, the activated Th cells are released and bind to B-cells, which in turn will proliferate to produce antibodies specific for the antigen or memory B cells which will circulate for many years and will recognise the antigen (302).

For a blood transfusion, matched ABO blood group and RhD status of donor and recipient are crucial. However, there may be other blood group antigens on donor cells, which can be attacked by the recipient's antigens. Thus, a "type and cross match" test is carried out, in which recipient's plasma is mixed with donor RBC. If agglutination is observed by microscopy, the RBC are incompatible and transfusion cannot take place. An incompatible transfusion causes haemolytic reactions, in which the donor RBC are destroyed by the recipient alloantibodies (302). For patients who require frequent blood transfusions, matching should take into account minor blood group antigens such as RhC/c, RhE/e, K/k in Kell, Fy^a/Fy^b in Duffy, Jk^a/Jk^b in Kidd, M/N and S/s in the MNS system, which can cause alloimmunisation (116, 120).

1.5.3 Alloimmunisation

Multiple blood transfusions can cause alloimmunisation, an immune response to antigens from genetically different donors. Alloimmunisation can also occur naturally during pregnancy (309). It can be dangerous as it can lead to acute and delayed haemolytic transfusion reactions. In SCD, haemolytic transfusion reactions can result in hyperhaemolysis, a life-threating condition in which RBC from both donor and patient are destroyed (120, 310, 311). Whereas the alloimmunisation rate for most individuals is generally low (2-5%) following transfusion, around 30-40% of transfused SCD patients are affected (312). This is mainly caused by genetic and racial differences between patients of African ancestry and mostly Caucasian white donors that represent the majority of donors, due to blood group antigen disparity between these ethnic groups (313). The most common highly immunogenic antigens that have been reported are C, D and E in the Rh group, K in the Kell system, Jk^b in Kidd system, S in the MNS system and Fy^a and Fy^b in Duffy system (120, 312). Even phenotypically matched blood cannot prevent alloimmunisation due to notable diversity of the *RH* genes among patients of African origin (314).

RhC, Fy^a, Fy^b, Jk^b and S antigens are significantly less common in the majority of black SCD patients than in most white donors (315). Consequently, alloantibodies against these antigens are found more frequently in SCD patients (120, 312). The exact mechanism of alloimmunisation is unknown (316). A small study of multiply transfused patients with SCD showed that $CD4^+$ regulatory T cells (Tregs) which control the proliferation of cells like DC, T- and B-cells during an immune response, were suppressed in alloantibody responders when compared to non-responders. In addition, responders showed lower IL-10 and higher levels of IFN-γ which is a Th1 cytokine, along with altered Th2, humoral immune response subpopulation (317). These results are in line with a SCD model in which underlying inflammation could disturb the equilibrium between Tregs and Th cells (318). It was suggested that since Tregs can either suppress B cell function directly (319, 320), or decrease IgG production through Th suppression (321), their low levels detected in non-responders can explain antibody generation in responders (316, 317).

Alloimmunisation has been found to be dependent on the patient's immune system, since a weak or immature immune system will not develop antibodies efficiently. The age of first blood transfusion was also shown to play an important role, as infants who received their first transfusion before age of three had significantly lower rates of alloimmunisation compared to children transfused after this age. This is thought to be due to their undeveloped immune system (322-326). It was also reported that a subpopulation of splenic conventional DC (cDC) was involved in alloimmunisation in a mouse model. Deletion of cDC2 diminished alloimmunisation, in contrast to deletion of cDC1 which had no effect on alloantibody production (327). As cDC2 are absent from neonatal mice until week 3, this could indicate that these cells are actively involved in alloantibody induction. However, further research on human cDC1 and cDC2 is needed, in order to identify if these populations can affect alloimmunisation in humans in a similar manner to that in mice (328, 329).

Alloimmunisation prevention by RBC antigen matching is challenging due to the limited availability of rare blood groups units (314). However, since SV have been previously shown to expose RBC proteins (183, 216) they could be considered a suitable source of RBC antigens to investigate tolerance induction.

1.6 Aims

Extracellular vesicles have been identified in RBC from healthy donors and patients with SCD. The reasons for the increased levels of RDCP, in particular circulating in SCD patients, is not known and their effects have not been fully elucidated. Therefore, the main goal for this body of work was to investigate potential differences in RCDP and AV from SCD patients and healthy individuals and determine their potential to induce tolerance to RBC antigens.

The aims were as follows:

1. Identification and isolation of RCDP and AV from SCD patients and healthy donors.

2. Extensive characterisation of RCDP and AV from SCD patients and healthy donors.

3. Comparison of RCDP characteristics to *ex vivo* generated reticulocytes and SV from outdated blood.

4. Investigation whether SV can be used to induce tolerance to human RBC antigens in a murine model.

Chapter 2 Materials and methods

2.1 Samples

2.1.1 Patient Samples

For all experiments, apart from the mass spectrometry proteome analysis, blood samples from anonymised SCD patients, presenting at University Hospitals Bristol Trust for clinical haematological analysis, were used. These patients were classed as 'steady state', defined by the hospital as "attending the clinic for a routine red cell exchange transfusion and not having had a transfusion in the previous 4 weeks". Patients were also characterised as "functionally asplenic" although there may be a few who still had some splenic function. The patients were not on regular transfusion, most will be transfused rarely but were likely to have received a transfusion sometime in the past.

For the proteomic analysis: blood samples were obtained from SCD patients attending University College London Hospitals (UCLH) in a steady state. Blood samples were collected immediately, prior to any transfusion procedure and anonymised. Patients from both hospitals gave informed written consent and the study was approved by NRES Committee London (Harrow).

2.1.2 Normal Blood Samples

For all experiments, blood units (ABO type A RhD positive or O RhD negative or positive) were obtained from routine blood donations at NHS Blood and Transplant (NSBT), Filton in Bristol and processed identically to the patients' blood. However, the normal samples were processed 48 hours after collection, which was the effective time of release.

2.2 Sample processing

2.2.1 Plasma and red cells

SCD blood samples from UCLH were centrifuged at 2,000g for 15 minutes, at room temperature with no brake, within 1 hour of collection. Plasma was separated from RBC and as soon as it arrived in Bristol, it was centrifuged twice at 2500g for 20 minutes at room temperature. The pellet, composed mainly of platelets, was discarded after each spin. The resulting platelet free plasma (PFP) was aliquoted and stored at -80°C until analysis, when it was thawed at room temperature and used immediately. Repeat freeze-thaw cycles were avoided. SCD samples from UHBT were processed in the same way once clinical haematological analysis had been completed, which was after 72 hours.

RBC used for the *in vivo* studies: blood units (ABO type O or A RhD positive) from healthy donors were collected between 2-14 days from the day of bleeding. To isolate RBC, 10ml of whole blood

was centrifuged at 400g for 10 minutes and the supernatant was discarded. RBC pellets were dissolved in Alsever's (Lorne Laboratories, Berkshire, UK) medium and were either stored at 4˚C for up to 3 weeks, or snap-frozen as droplets in liquid nitrogen. Prior to use, cryopreserved RBC were thawed at 37˚C in Alsever's and kept at 4˚C up to a week. The remaining whole blood was stored at 4˚C up to 22 days from day of donation, for RBC ghost membrane preparations, or for 35 days for SV isolation.

2.2.2 Red cell ghost membrane preparation

Reagents and centrifuges were chilled to 4˚C to prevent protein degradation and locking of haemoglobin inside the membrane during production of the red cell ghosts. Packed RBC from healthy donors (22 days after donation) were washed twice in PBS at 1,660g for 10 minutes, at 4˚C then 1ml of RBC was added per Nalgene™ Oak Ridge tube (Thermo Fisher Scientific) on ice, topped up with RBC lysis buffer (5mM Na_2HPO_4 and 0.2M NaH_2PO_4 (both Sigma Aldrich, pH 7.4) and left for 5 minutes. Tubes were centrifuged at 15,000g for 10 minutes, at 4˚C and pellets were washed in RBC lysis buffer supplemented with 100mM protease inhibitor phenylmethylsulfonyl fluoride (PMSF, Sigma-Aldrich), until the haemoglobin (red colour) in the pellets was washed off. Ghost membranes were aliquoted (100µl) and stored at -80˚C.

2.2.3 Storage vesicle isolation

Blood from healthy donors was centrifuged twice at 2,500g for 20 minutes at room temperature, then pelleted RBC were removed. Plasma was filtered through a 1.2µm filter, to remove RBC ghosts and large particles, and then it was centrifuged at 20,000g for 30 minutes at 4˚C. Pellets were rinsed in HBSS supplemented with a complete protease inhibitor cocktail (Roche , Welwyn Garden City, UK) and PMSF at a final concentration of 1X and 0.2mM, respectively.

2.3 Monoclonal Antibodies

Most monoclonal antibodies used in this study came from the Protein Development and Production Unit (PDPU) at NHSBT, unless otherwise indicated. All antibodies and suppliers can be found in Table 2.1. Unconjugated antibodies were conjugated to fluorescent dyes using the Alexa Fluor™ 488, or Alexa Fluor™ 647 Antibody labelling Kit, or EZ-Link Micro Sulfo-NHS-Biotinylation Kit, (Thermo Fisher Scientific, Paisley, UK) according to the manufacturer's protocol. In brief, antibodies were washed 3 times in phosphate buffered saline (PBS, Sigma-Aldrich, Poole, UK) to remove any residual solvent of ammonium ions or primary amines that would compete with the amine groups of the reactive dye. Then, they were diluted in PBS and mixed with 1 M solution of sodium bicarbonate buffer, provided in the kit, at a 9:1 ratio. One ml of this solution was added to a vial containing Alexa Fluor® dye, optimized for labelling 100µg of protein, and incubated for 1 hour at room temperature. In order to purify the labelled antibody from the unbound dye molecules, a purification column was saturated with purification resin, both provided in the kit and centrifuged at 1,100g for 3 minutes. The labelled antibody mix was loaded onto the column and centrifuged at 1,100g for 5 minutes. The concentration of the labelled antibody was determined by Nanodrop Gene Flow P3 (Geneflow Ltd, Lichfield UK). The concentration of the directly conjugated Abs was provided by the specified manufacturers.

Table 2.1 Antibodies used.

Antigen	Supplier	Clone	Immunoglobulin Class
CD235/ GPA (extracellular domain)	PDPU[1]	BRIC256	Mouse IgG1
CD235/ GPA (extracellular domain)	PDPU	R10	Mouse IgG1
CD235/ GPA (cytoplasmic domain)	PDPU	BRIC163	Mouse IgG2a
CD233 / Band 3 (extracellular domain)	PDPU	BRIC200	Mouse IgG1
CD233 / Band 3 (cytoplasmic domain)	PDPU	BRIC132	Mouse IgG1
CD233 / Band 3 (cytoplasmic domain)	PDPU	BRIC155	Mouse IgG2b
CD233 / Band 3 (N-terminal cytoplasmic domain)	PDPU	BRIC170	Mouse IgG1
CD233/ Band 3 (extracellular domain)	PDPU	BRAC18	Rat IgG2a
CD233/ Band 3 (N-terminal cytoplasmic domain)	PDPU	BRAC66	Rat IgG2a
CD236R/ GPC (cytoplasmic domain)	PDPU	BGRL100	Mouse IgG1
GLUT1	PDPU	BRAC67	Rat IgG2c
Anti-HLA Class I antibody	Abcam[2]	W6/32	Mouse IgG2a
CD41/ CD61	PDPU	PAB1	Mouse IgG1
CD238/ Kell	PDPU	BRIC68	Mouse IgG2a
SLC14A1 (contains an epitope identified as Kidd)	R&D Systems[3]	888418	Mouse IgG2b
Streptavidin-horseradish peroxidase conjugate (HRP)	Sigma-Aldrich	-	Polyclonal
Stomatin	In house[4]	anti-STOM	Rabbit IgG
Anti-rabbit HRP	Agilent Dako[5]	-	Goat polyclonal
Lu^b blood group CD239	PDPU	BRIC108	Mouse IgG2b

[1]Protein Development and Production Unit (PDPU) of the International Blood Group Reference Laboratory, NHS Blood and Transplant, Filton, UK,

[2]Cambridge, UK

[3]Abingdon, UK

[4]Dr Lesley Bruce, NIHR Blood and Transplant Research Unit, University of Bristol, UK

[5]Glostrup, Denmark

2.4 Production of red cell-derived particles from cultured reticulocytes

2.4.1 $CD34^+$ progenitor cell isolation

RCDP are produced from the maturation of the reticulocytes into RBC. To culture RCDP *in vitro*, $CD34^+$ progenitor cells were isolated from whole blood and differentiated down the red cell lineage (see Fig. 1.2 from Introduction). Cells from apheresis cone filters or buffy coat packs were left to drain into a tube and then were diluted 1:1 in Hanks buffered salt solution (HBSS, Sigma-Aldrich) containing 0.6% (v/v) acid citrate dextrose (ACD, Sigma-Aldrich). The mononuclear cell (MNC) fraction was enriched using Ficoll-Hypaque (Sigma-Aldrich). Cells were re-suspended in 5ml red cell lysis buffer (RCLB, pH 7.5, containing 150mM ammonium chloride (Sigma-Aldrich), 1mM $K_2EDTA.2H_2O$ (Sigma-Aldrich), 10mM $KHCO_3$ (Sigma-Aldrich)) and incubated at room temperature for 10 minutes. HBSS/ACD was added up to 50ml and the cells washed twice at 200g for 10 minutes. Cells were re-suspended in 20ml of cold PBS buffer (1% (v/v) with 0.5% (w/v) human serum albumin (HSA, FUJIFILM Irvine Scientific, Newtownmountkennedy, Ireland) and 0.6% (v/v) citrate-phosphate-dextrose (CPD, Sigma-Aldrich), counted using a haemocytometer and centrifuged at 400g for 5 minutes. PBS buffer (500µl per maximum $1x10^9$ cells) was added together with 75µl Fc blocking agent and 75µl MACS-$CD34^+$ magnetic beads (both Miltenyi Biotec Ltd). Cells were mixed and incubated at 4°C for 30 minutes with gentle rotation on mixer, at an angle of approximately 30°. Afterwards, cells were washed in 5ml of cold PBS buffer/$1x10^9$ cells and centrifuged at 400g, for 5 minutes. The supernatant, containing unbound beads, was discarded and the cell pellet was re-suspended in 8ml of cold PBS buffer.

To enrich for $CD34^+$ cells, an LS MACS® column was placed in a magnet and washed in cold PBS buffer. Cells were applied to the LS column and washed in 8ml cold PBS buffer three times to remove the non-magnetically stained cells. The column was removed from the magnet and the retained $CD34^+$ cells were flushed out using PBS buffer. In order to remove any smaller cells and particles, which potentially had not been washed off and remained adherent to the $CD34^+$ cells, enriched cells were applied to an MS MACS® column, prepared as in LS column above. $CD34^+$ cells were eluted and washed as described above for LS column and centrifuged at 400g, for 5 minutes.

2.4.2 *Ex vivo* generation of reticulocytes from $CD34^+$ cells

$CD34^+$ cells were resuspended at $12x10^5$ per ml in Iscoves basal medium (Source BioScience, UK) containing 3% human serum from male AB Plasma (Sigma-Aldrich), 2mg/ml HSA, 10µg/ml Insulin (Sigma-Aldrich), 3U/ml heparin sodium salt (Sigma-Aldrich), 3U/ml EPO (Roche) and 500µg/ml Iron saturated human transferrin (R&D Systems). Cells were incubated at 37°C with 5%CO_2. For days 0-5, cells were maintained at a density of $2x10^5$ cells/ml in the basal medium along with 10ng/ml recombinant human stem cell factor (SCF, Medsafe, Sweden) and 1ng/ml recombinant human IL-3

(R&D Systems) to expand the cells. Every day, cells were counted using a haemocytometer and sufficient media was added in order to gradually expand cells to $40x10^5$ cells/ml up to day 20, when cells have usually enucleated. Cytospin preparations were used to check the morphology of the cells (see below paragraph), in order to ensure that reticulocytes had grown normally and that they have enucleated. Enucleated reticulocytes were leukofiltered using a leucoflex LXT filter (Macopharma, Twickenham, UK) and centrifuged at 600g for 5 minutes. The supernatant was discarded and the cell pellet was resuspended in HBSS and cells counted. Cells were then centrifuged at 600g for 5 minutes and cultured for RCDP production.

In order to assess reticulocyte morphology throughout maturation, the cells were suspended in 200µl HBSS at a concentration of 10^5cells/ml, loaded in a cytopsin funnel and centrifuged onto a slide at 218g for 5 minutes. The slide was left to dry, then 90µl Leishman's Staining Solution (VWR International, Lutterworth, UK) was added to the cell disc for 2 minutes, to stain the cells. Afterwards, 180µl of 1x Sorenson's buffer (dilution 1:20 of a 20x stock pH 6.8, 508ml 9.1g/l of KH_2PO_4 and 492ml 9.5g/l of Na_2HPO_4) was added, mixed with the remaining Leishman's buffer and left for 7 minutes. Slides were rinsed with 1x Sorenson's buffer then immersed in 1x Sorenson's buffer for 2 minutes, before being left to air dry. Images were taken using a Leica DM750 (Leica Microsystems, Milton Keynes, UK) and a Pixera Penguin 600CL camera (Digital Imaging Systems, Bourne End, UK), at 20x magnification.

2.4.3 Red cell-derived particle collection from cultured reticulocytes

For the RCDP production, the media had to be cleared of all extracellular MP before the reticulocytes were suspended into it. Thus, 25ml Iscoves media were ultra-centrifuged at 200,000g for 2 hours at 4ºC and then filtered through a 0.2µm filter and stored at 4ºC. Foetal bovine serum (FBS) has been found to contain MP and so was not used further in the cell expansion protocol (330). Reticulocytes were cultured at $5x10^6$ cells/ml in ultra-centrifuged media at 37ºC with 5% CO_2 for 96 hours. After this, the cells were counted and centrifuged twice at 400g for 5 minutes, the supernatant was collected and centrifuged, as above to remove any remaining cells. An Amicon filter (Sigma-Aldrich) was used to concentrate the vesicle media 10-fold, by centrifugation at 2,100g for 7 minutes. Vesicles were stored at -20ºC in 60µl aliquots. Repeat freeze-thaw cycles were avoided.

2.5 Isolation methods of red cell particles and autophagic vesicles from plasma

2.5.1 Centrifugation

Ultra-centrifugation

One to two millilitres of plasma samples were diluted to 11.2ml with PBS supplemented with PMSF at a final concentration of 2mM. PBS/PMSF was previously filtered through a 3µm filter (Whatman International Ltd, Dassel, Germany). The diluted plasma was transferred into 11.2ml Optiseal tubes (Beckman Coulter, London, UK) and ultra-centrifuged in a fixed angle NVT65 rotor (Beckman Coulter) at 100,000g for 2h, at 4˚C. The pellet was resuspended in 100µl of filtered PBS/PMSF and stored at −80°C until further analysis. Repeat freeze-thaw cycles were avoided.

High-speed centrifugation

One millilitre of previously separated PFP (see section 2.2) was centrifuged at 20,000g for 30 minutes at 4˚C. Pellets were diluted in 100µl PBS with 0.2mM PMSF and stored at −80°C until further analysis. Repeat freeze-thaw cycles were avoided.

2.5.2 Immunomagnetic enrichment

PFP was filtered through a 1.2µm polyethersulfone acrodisc filter (PALL Life Sciences, Farlinton, UK) to remove RBC ghosts and large particles. RCDP were enriched from SCD or healthy donor PFP using anti-CD235a (extracellular GPA) MicroBeads (Miltenyi Biotec Ltd) and AV were enriched using anti-Cy5/Alexa Fluor-647 MicroBeads (Miltenyi Biotec Ltd) in conjunction with BRIC155, BRIC163 or BRIC132 (see Table 2.1 and Fig. 2.1). Antibodies were filtered through a 15nm filter (Whatman International Ltd, Allington, UK) to remove aggregates. Microbeads (10µl) and, if appropriate, 5µg BRIC155, BRIC163 or BRIC132 were added to 500µl of PFP and incubated with rotation at 4˚C for 30 minutes. PFP and beads were passed through MS MACS® column, in a magnetic field, under gravity and collected in PBS buffer containing 0.5% (v/v) HSA and 0.6% (v/v) CPD (Sigma-Aldrich). For protein analysis (section 2.11), HSA was not added to the PBS buffer.

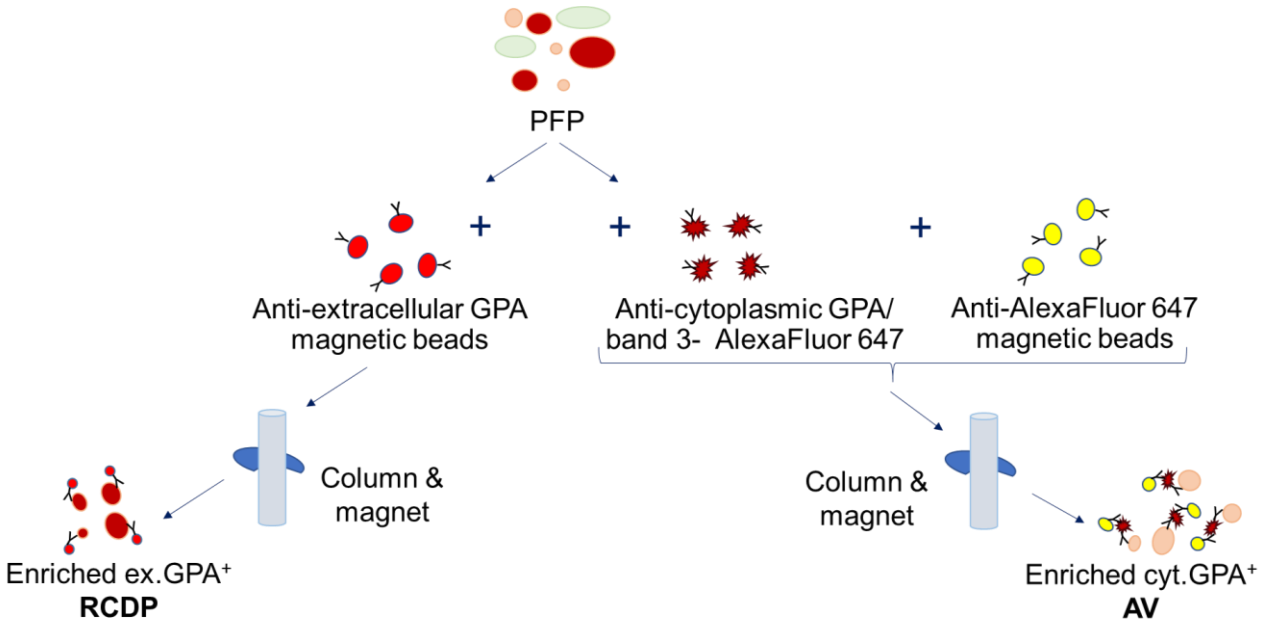

Figure 2.1 Schematic representation of red cell vesicle isolation. PFP was incubated with either anti-extracellular GPA MicroBeads for RCDP (left) or with antibodies detecting cytoplasmic domains of either band 3 (BRIC155, BRIC132) or GPA (BRIC163) conjugated to Alexa Fluor-647, along with anti- Alexa Fluor-647 MicroBeads for the AV enrichment (right).

2.6 Flow cytometry

In order to identify RCDP in plasma samples, several antibodies against abundant RBC proteins were used (Table 2.1) or 80µl of 0.22µm filtered annexin V binding buffer containing fluorescent annexin V (annexin-V-FLUOS Staining Kit, Sigma-Aldrich) detecting PS, or calcein AM (Tocris Bioscience, Abingdon, UK), a marker for intact cells. Twenty microlitre aliquots of plasma samples diluted in PBS buffer (1:5), containing 1% serum bovine albumin (BSA, Sigma-Aldrich) and 0.05% sodium azide (Sigma-Aldrich), were mixed with 20µl of antibody and incubated for 30 minutes in ice. For RBC, 1µl of packed RBC was diluted to 100µl in HBSS, then 20µl were stained with 20µl of antibody and incubated for 30 minutes at room temperature. RBC were washed in 1ml HBSS by centrifugation at 400g for 5 minutes, at room temperature, three times. The pellet was dissolved in 100µl PBS buffer. The optimum concentration of the antibodies (Table 2.1) was initially identified by titration at a range of concentrations (0.156µg/ml - 10µg/ml) and the one giving the best staining without shifting the negative population into the positive range, as this indicates non-specific staining.

PFP and RBC samples were then diluted to a final volume of 400µl in PBS buffer and analysed using a MACSQuant 10 flow cytometer (Miltenyi Biotec Ltd, Bisley UK). Data were analysed using FlowJo V10 software (BD Biosciences, Wokingham, UK). Plasma samples were plotted in forward-scatter

(FSC) vs side-scatter (SSC), in order to detect small RCDP, which have a similar size to instrument noise (Fig. 2.2A). FSC area (FSC A) that represents area vs FSC height (FSC H) maximum signal plot was used to separate individual events (singlets) from doublets (two stacked events that instrument records as one, Fig. 2.2B). An unlabelled sample, gated on singlets, was used to set the quadrants on the negative populations (Fig. 2.2C). These quadrants were applied to gated singlets of stained sample to determine the positive populations (Fig. 2.2D). The sensitivity was set based on diluent (PBS flow buffer) by acquiring some events, excluding the instrument noise and allowing small microparticles to be detected. Size estimation was carried out using commercially available size beads (Flow Cytometry Sub-micron Particle Size Reference Kit, Thermo Fisher Scientific).

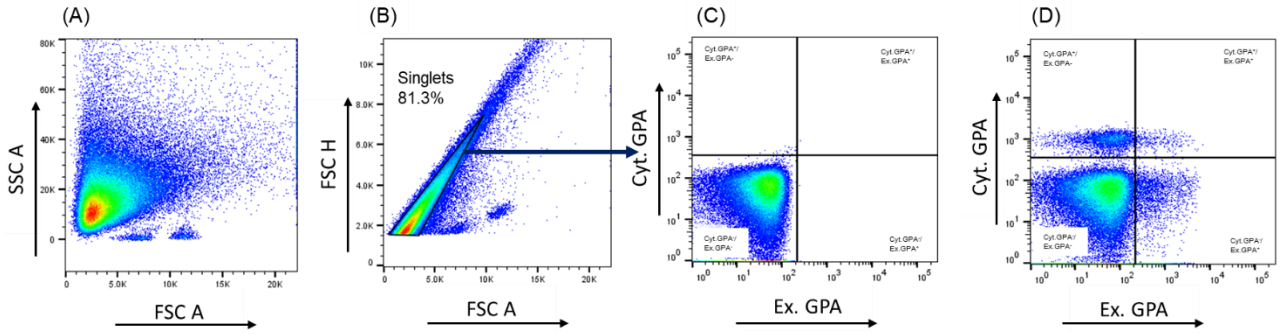

Figure 2.2 Flow cytometry gating strategy. PFP stained for extracellular (ex.) and cytoplasmic (cyt.) GPA. Plasma sample plotted **(A)** in FSC area (FSC A) vs SSC A of all events. **(B)** in FSC A vs FSC height (FSC H) in order to determine the singlet gate. **(C)** The gated singlets of unlabelled samples were used to set the quadrants on the unstained population (cyt.GPA$^-$ / ex.GPA$^-$), which defined where the quadrants for the stained populations should be (cyt.GPA$^+$ / ex.GPA$^-$, cyt.GPA$^-$ / ex.GPA$^+$, cyt.GPA$^+$ / ex.GPA$^+$). **(D)** Ex. and/or cyt. GPA populations on a stained sample.

2.6.1 Negative control for flow cytometry

HL-60 cells (ATCC® CCL-240™), human myeloblastic cells derived from a patient with acute promyelocytic leukaemia (331), were used as a negative control for the flow cytometry experiments, as they do not extrude reticulocytes-derived vesicles. HL-60 cells were suspended in Iscove's basal medium with 10% FBS at 3 x 10^6 cells in 10ml, at 37ºC and 5% CO_2. Cell numbers and viability were checked every 2-3 days and media was toped up until cells had expanded to a total of 12 x 10^6 cells/ml.

2.7 Imaging flow cytometry (ImageStream)

PFP, RCDP and AV, enriched using immunomagnetic separation (described in section 2.5.2), were also analysed on Amnis ImageStream® X Mark II (Merck Millipore, Hertfordshire, UK), at Cardiff University. Twenty microlitres of sample were mixed with antibodies (Table 2.1) at optimum concentration or 80µl of 0.22µm filtered annexin V binding buffer containing fluorescent annexin V, or 50µM calcein AM and placed on ice. The samples were analysed upon arrival in Cardiff. Data were analysed using Ideas software (Merck Millipore). The calibration programme of the ImageSteam uses “speed beads” that scatter the signal to monitor the samples during acquisition. These were excluded from analysis by creating a plot of scatter intensity vs scatter max pixel, since the speed beads had a higher scatter than other particles detected (Fig. 2.3A). The resulting population was split on the basis of size on SSC scatter into low scatter for small RCDP (Fig. 2.3B) and high scatter for large particles (Fig. 2.3C). Histograms of brightfield area of the respective RCDP were set up using normalised frequency vs area scatter plot, to exclude large area events and small area events from the “low scatter” and “high scatter” populations, respectively. This is because the smallest particle that can be confidently measured on brightfield at 60x magnification is 0.5µm, so it was used to remove large aggregates that may have a low scatter. Scatter plots were created using the “low scatter-low area” gate, showing low scatter events (Fig. 2.3D) and the “high scatter-high area” gate, representing high scatter events (Fig. 2.3E). Similarly to flow cytometric analyses, gates were set on Alexa Fluor 488 versus Alexa Fluor 647 based on unstained samples (Fig. 2.3 Di & Ei), to identify populations on stained samples (Fig. 2.3 Dii & Eii). Random individual events from the gated populations in each quadrant were observed in the image gallery of the software to confirm that the gates were placed accordingly. Counts were used from the stained samples (Fig. 2.3 Dii & Eii) to obtain the absolute number of “high scatter” and “low scatter” events/ml that were positive for the antibodies (conjugated to Alexa Fluor-488 or Alexa Fluor-647) or annexin V or calcein AM.

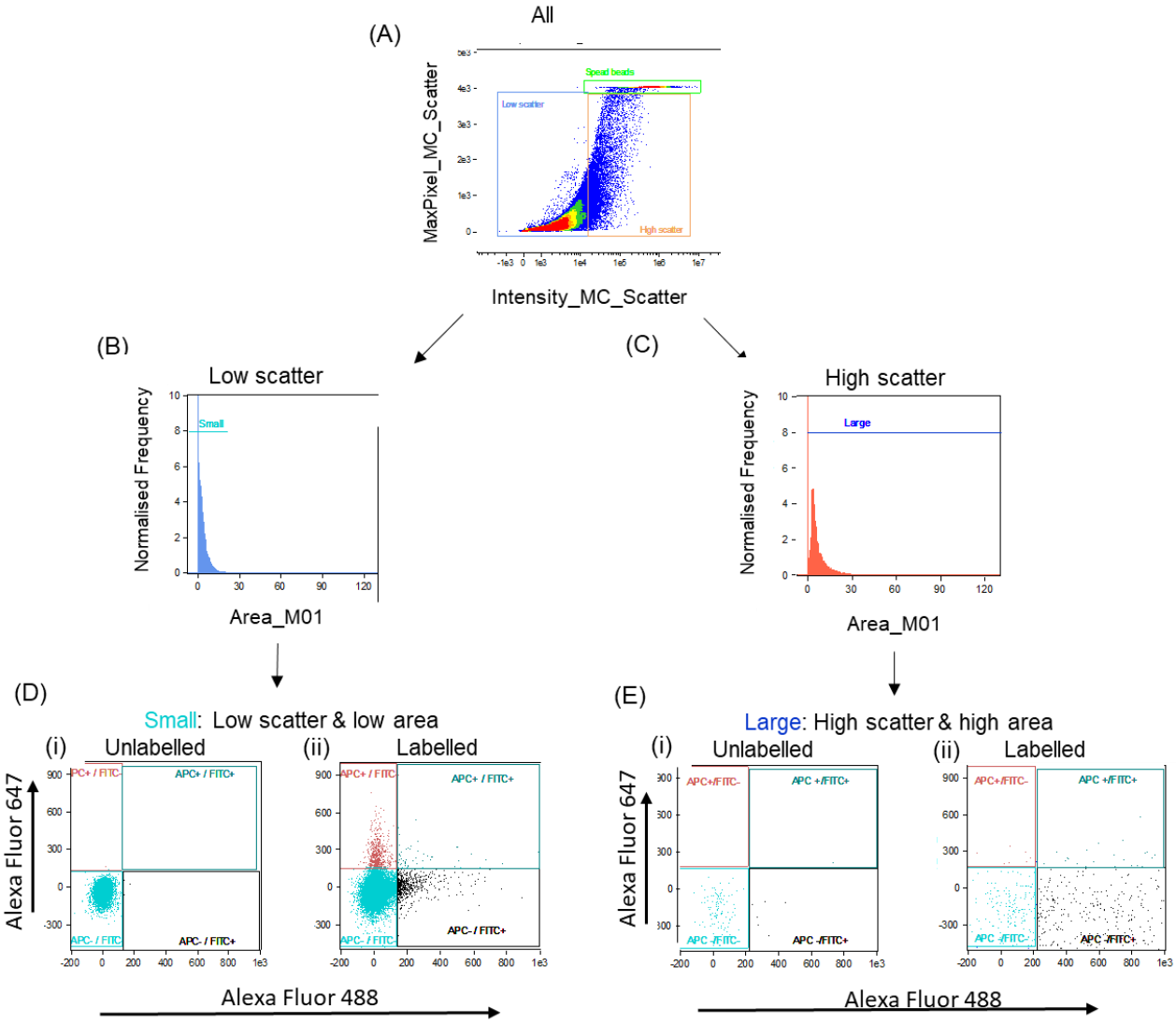

<u>Figure 2.3</u> ImageStream gating strategy. PFP was stained with fluorescent antibodies. **(A)** Scatter intensity was plotted against Scatter Max Pixel and gates were drawn to exclude speed beads (green) and select low scatter (blue) and high scatter (yellow) events. Low scatter events **(B)** and high scatter events **(C)** were plotted in a histogram of brightfield area. Scatter plots of Alexa Fluor 488 and Alexa Fluor 647 intensity were created for low scatter and low area events- small **(D)** and high scatter & high area events- large **(E)**. Unlabelled samples (Di & Ei) were used to set the gates for the labelled samples (Dii & Eii).

2.8 Fluorescence activated cell sorting (FACS)

In order to isolate RCDP, 100µl PFP were stained with anti-extracellular GPA and sorted using a BD Influx high speed fluorescence activated cell sorter (BD Biosciences). Gates for GPA^+ populations (Fig. 2.4) were set based on the unstained population of the whole sample, as it was previously shown for flow cytometry (see section 2.6, Fig. 2.2). The GPA^+ RCDP were gated and collected in 50µl PBS. Excess sorted RCDP were stored at -80ºC in 500µl aliquots.

2.9 Microscopy techniques

2.9.1 Confocal microscopy

Two hundred microlitres of poly-L-lysine 0.1% (Sigma-Aldrich) was used to keep sorted GPA^+ RCDP immotile on the microscopy slides. Three conditions were tested: prior to addition of 20µl RCDP, poly-L-lysine was left to settle (i) 30 minutes, (ii) overnight at 4˚C or (iii) poly-L-lysine along with RCDP were left overnight at 4˚C to settle. Non adherent poly-L-lysine was washed off the slides with 200µl PBS, twice. Samples were imaged either on a Leica DMI 6000 inverted microscope with phase contrast connected to a Leica TCS SP5 confocal imaging system, or on a Leica SP8 Inverted Confocal Microscope System with a LAS X 3D Visualisation operating system. Images were obtained using Leica LAS AF software and subsequently processed using Adobe Photoshop (Adobe).

2.9.2 Spinning-disk confocal microscopy

Twenty microlitres of poly-L-lysine 0.1% (Sigma-Aldrich) was used in each well of a 96well plate (Greiner Bio-One Ltd, Stonehouse, UK), to keep sorted RCDP or GPA stained RBC (as described in section 2.6) as immotile as possible. The plate was centrifuged at 2,500g for 10 minutes to assist the poly-L-lysine adherence, it was washed twice in PBS buffer and 20µl of sorted RCDP were added. The plate was centrifuged again, to ensure RCDP adhered. RCDP were examined using an Opera LX HCS spinning-disk confocal system (Perkin Elmer) with a 60x (NA 1.2) water-immersion lens and Acapella analysis software. The digital images were visualised by ImageJ. The size and shape of RCDP were analysed using a custom MATLAB script developed by the Wolfson Bioimaging Facility, University of Bristol. The script uses a built-in circular Hough transform in XY axes to detect particles. The 3D shape was determined by fitting an active contour to the radial average of the image, centred on Z-axis of each particle. The Hough transform tool is selective for objects with a high degree of radial symmetry and will ignore ellipses (Fig. 2.4).

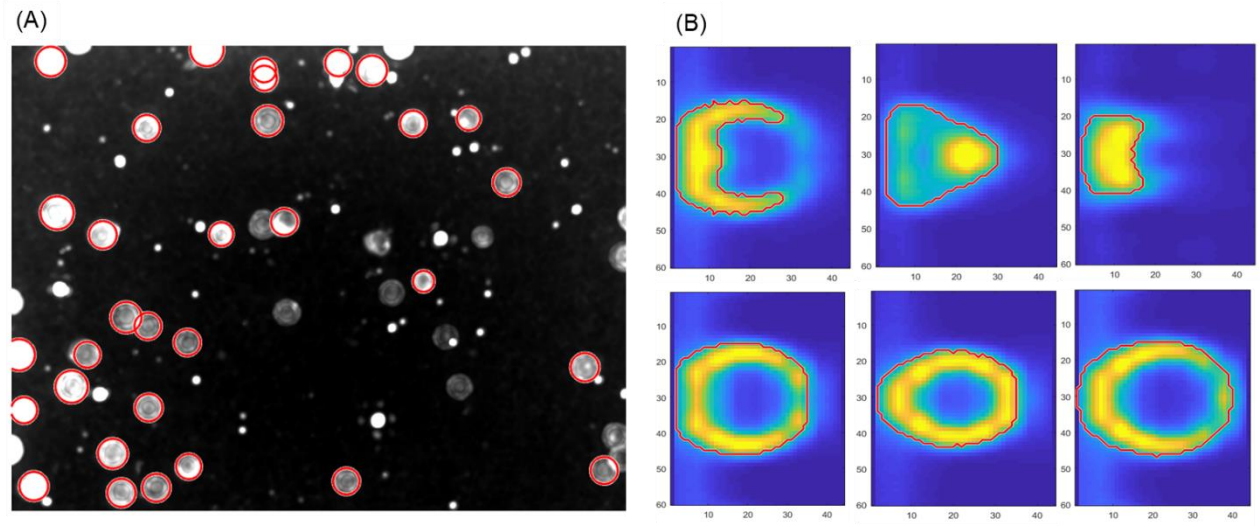

Figure 2.4 Detecting circular objects using spinning disk confocal. (A) Digital image of the detected particles, the approved round ones are circled in red. (B) Individual images of selected detected particles. Particles on the upper panel were found to be non-circular and were excluded from diameter measurement. The lower images were confirmed to be circular and were included in the measurement. Image was obtained using a 60x water-immersion lens.

2.9.3 Transmission electron microscopy and immunolabelling

Three microlitres of enriched right-side RCDP or inside-out AV were placed on a carbon coated copper grid, left to dry, then fixed in 4% (v/v) paraformaldehyde (Sigma-Aldrich) with 0.05% (v/v) glutaraldehyde (Agar Scientific, London, UK) at room temperature for 30 minutes. RCDP or AV were washed in PBS, quenched in 20mM glycine (Thermo Fisher Scientific) for 10 minutes and incubated with 1% acetylated BSA (Aurion, Wageningen, The Netherlands) in PBS for 10 minutes to block non-specific binding. Grids containing RCDP were placed in R10, which detects extracellular GPA and those containing AV were stained with BRAC66 to cytoplasmic band 3, for 1 hour at room temperature, then washed in 0.1% BSA/PBS. Aurion conventional gold reagents (particle size 10 nm) were added to the grids. Anti-mouse gold particles detecting the mouse antibody (R10) were used for right side-out RCDP and anti-rat gold particles against the rat antibody (BRAC66) were used for inside-out AV. Unbound gold was removed by washing in 0.1% BSA/PBS. Grids were counterstained with a solution of 0.3% (w/v) uranyl acetate (Electron Microscopy Sciences, Hatfield, UK) in 1.8% methylcellulose (Sigma-Aldrich) for 10 minutes on ice then air-dried using the wire loop method. Grids were examined on a Tecnai12 120 kV BioTwin Spirit transmission electron microscope (FEI Company, Eindhoven, The Netherlands) and visualised using a FEI CETA camera and TIA software.

2.9.4 Super-resolution microscopy

One hundred microlitres of poly-L-lysine 0.1% were added to a slide and left overnight at 4˚C. Then, excess poly-L-lysine was washed off using HBSS, twice. Twenty microlitres of SV (section 2.2.3) were incubated with 1µl of neat antibody against the extracellular domain of GPA (BRIC256- Alexa Fluor 647) and band 3 (BRIC200- Alexa Fluor 488) for 30 minutes at room temperature. Unbound antibody was removed by washing in HBSS with 0.5% (w/v) HAS, twice and SV were added to the slide and left for 4 hours to settle. Samples were imaged on a Zeiss LSM 800 Airyscan (Zeiss, Cambridge, UK) compact confocal laser scanning microscope. Images were processed using ZEN Blue (Zeiss).

2.10 Dynamic Light Scattering

Particle size measurements of enriched RCDP, AV and SV were carried out by dynamic light scattering (DLS) using a Malvern Nano ZSP Zetasizer (Malvern Instruments Ltd, Worcestershire UK). Samples were diluted 1:1 in PBS and size was defined at 10°C with minimum equilibration time of 5 minutes. Measurements on each sample were carried out 15 times comprising a set.

2.11 Protein determination of enriched red cell particles and autophagic vesicles

2.11.1 Protein lysate preparation

RCDP and AV were put on ice and ice-cold 10X radioimmunoprecipitation assay (RIPA) buffer (Abcam), protease inhibitor (1X) and PMSF (2mM) were added then left for 15 minutes. Lysates were mechanically forced using a 1ml syringe, or sonicated for 3 seconds at 60% power, 3 times, in order to break any protein interactions. Then, they were centrifuged for 5 minutes at 17,000g at 4°C to pellet cell debris and insoluble proteins. Supernatants were transferred into new tubes on ice in preparation for protein assay and precipitation.

2.11.2 Bradford assay

One hundred microlitres RCDP or RBC ghost preparations were added to 400µl PBS, then made up to 1ml with Bradford reagent. Seven BSA standards (Sigma-Aldrich) were prepared in Bradford reagent (Sigma-Aldrich) in concentrations between 0-0.015mg/ml. Standards and samples were kept in the dark and on ice during the preparation and incubated at room temperature for 5 minutes before the measurement. Triplicate measurements of each standard/ sample were taken using a Benchmark Plus Microplate Spectrophotometer (Biorad Laboratories Ltd, Watford, UK) at 595 nm.

The absorbance values of the BSA standards were plotted and the concentration of the samples were calculated from the resulting equation.

2.11.3 Bicinchoninic acid assay

Pierce™ BCA Protein Assay Kit -Reducing Agent Compatible kit was used (Thermo Fisher Scientific) and the manufacturer's protocol was followed. In brief, 25µl of the lysates and protein BSA standards (provided in the kit) were mixed with equal volumes of Compatibility Reagent Stock Solution (provided in the kit) and incubated at 37°C for 15 minutes in a water bath. One millilitre of the working agent (provided in the kit) was added to each sample/standard and they were incubated for 30 minutes at 37°C. Samples and standards were let to cool down and triplicate measurements using a Benchmark Plus Microplate Spectrophotometer at 562 nm were taken, as mentioned in the Bradford assay method above.

2.11.4 Protein precipitation

Six volumes of chilled acetone (-20°C) were added to one volume of lysates. Samples were left overnight at -20°C to precipitate protein then centrifuged for 10 minutes 8,000g at 4°C. Supernatants were removed and the precipitant protein was air dried for 20 minutes at room temperature. Dry pellets were dissolved in 20µl of 200nM triethyl ammonium bicarbonate (TEAB, Thermo Fisher Scientific). Protein concentrations were determined with a Nanodrop Lite spectrophotometer (Thermo Fisher Scientific), using 200nM TEAB as a blank. Lysates were stored at -80˚C for subsequent analysis by immunoblotting or mass spectrometry.

2.11.5 SDS-PAGE and protein staining

In order to visualise the total amount of protein in enriched RCDP in early experiments, NuPAGE 4-12% Bis-Tris Protein Gel (Biorad Laboratories Ltd) was used and covered in 1x running buffer, which was made by diluting a 10x running buffer [25mM Tris base (Sigma-Aldrich), 192mM glycine (Severn Biotech Ltd), 0.1% Sodium dodecyl sulfate (SDS, Thermo Fischer Scientific), pH 8.3] to 1x with water. Lysates were prepared by diluting different volumes of enriched RCDP (1-10µl) and immunomagnetic beads were used for the RCDP isolation with equal volume of 2x SDS sample buffer [125mM Tris-HCl, 20% (v/v) glycerol (Thermo Fischer Scientific), 4% (w/v) SDS], 2mM ethylenediaminetetraacetic acid (EDTA, Sigma-Aldrich), bromophenol blue 0.1mg/ml and 0.1mg/ml xylene cyanol, along with 2mM PMSF and 50mM diothiothreitol (DTT, Sigma-Aldrich). Samples were boiled for 45 seconds to fully denaturate the proteins and break the disulphide bonds. SDS was used to unfold the proteins and ensure all proteins are negatively charged and so will be separated

according to their molecular weight. DTT is a reducing agent that eliminates disulphide bridges. The protein markers used were Prosieve Pres ladder (Thermo Fisher Scientific) or MagicMarker™ WesternSure Pre-stained (Life Technologies, Warrington, UK). After electrophoresis, the gel was stained with 35ml of GelCode™ Blue Stain Reagent (Thermo Fisher Scientific) for 20 minutes at room temperature. This is a Coomassie-based stain, which binds only to proteins and stains them blue. Then, the gel was washed three times with distilled water at room temperature and digital images were captured using an Odyssey® Fc (LI-COR Biosciences UK Ltd, Cambridge, UK). The band of interest was cut and sent for protein identification by mass spectrometry (section 2.12.1).

2.11.6 SDS-PAGE and immunoblotting

In order to detect band 3 (90-100,000kDa) and GPA (43,000kDa) from precipitated lysates on the same gel, a commercial 10% Mini-PROTEAN® TGX Stain-Free™ Protein Gel (Biorad Laboratories Ltd) was used. Samples were prepared by mixing 20µg protein with equal volume of 2x SDS sample buffer and the gel was run under the same conditions as described in 2.11.5. When electrophoresis finished, samples were transferred in a semi-dry transfer system using blotting apparatus on a PVDF membrane (Merck Millipore), pre-soaked in methanol (Fisher Scientific), to activate the PVDF. The membrane was then blocked in 5% (w/v) BSA in PBS (blocking buffer) overnight, to block non-specific protein binding sites. After incubation for 1 hour at room temperature with the biotinylated primary antibody (anti-GPA or anti-band 3 or anti-stomatin, see Table 2.1) diluted in blocking buffer, the membrane was washed in PBS-Tween 20 [0.05% Tween 20 (Sigma-Aldrich) in PBS]. Then, the membrane was incubated with the respective secondary antibody (see Table 2.1) diluted in blocking buffer for 1 hour at room temperature, then was washed in PBS Tween. Chemiluminescent detection was carried out using ECL Plus reagent (Western Lightning; PerkinElmer, Beaconsfield, UK) and visualised in Odyssey® Fc.

2.12 Mass spectrometry

2.12.1 Mass spectrometry of proteins from gel bands

The gel band of interest (section 2.11.5) was subjected to in-gel tryptic digestion using a DigestPro automated digestion unit (INTAVIS Bioanalytical Instruments AG, Cologne Germany). The resulting peptides were fractionated using an Ultimate 3000 nano-LC system in line with an LTQ-Orbitrap Velos mass spectrometer (Thermo Fisher Scientific). In brief, peptides in 1% (vol/vol) formic acid were injected onto an Acclaim PepMap C18 nano-trap column (Thermo Fisher Scientific). After washing with 0.5% (vol/vol) acetonitrile 0.1% (vol/vol) formic acid peptides were resolved on a 250mm x 75µm Acclaim PepMap C18 reverse phase analytical column (Thermo Fisher Scientific) over an 80 minutes organic gradient, (1-50% solvent B over 55 minutes, 50-90% B over 0.5 minutes,

held at 90% B for 5 minutes and then reduced to 1% B over 0.5 minutes) with a flow rate of 300nl min^{-1}. Solvent A was 0.1% formic acid and Solvent B was aqueous 80% acetonitrile in 0.1% formic acid. Peptides were ionized by nano-electrospray ionization at 2.1kV using a stainless-steel emitter with an internal diameter of 30µm (Thermo Fisher Scientific) and a capillary temperature of 250°C. Tandem mass spectra were acquired using an LTQ- Orbitrap Velos mass spectrometer controlled by Xcalibur 2.1 software (Thermo Fisher Scientific) and operated in data-dependent acquisition mode. The Orbitrap was set to analyze the survey scans at 60,000 resolution (at m/z 400) in the mass range m/z 300 to 2,000 and the top twenty multiply charged ions in each duty cycle selected for MS/MS in the LTQ linear ion trap. Charge state filtering, where unassigned precursor ions were not selected for fragmentation, and dynamic exclusion (repeat count, 1; repeat duration, 30seconds; exclusion list size, 500) were used. Fragmentation conditions in the LTQ were as follows: normalized collision energy, 40%; activation q, 0.25; activation time 10 minutes; and minimum ion selection intensity, 500 counts.

The raw data files were processed and quantified using Proteome Discoverer software v1.4 (Thermo Fisher Scientific) and searched against the UniProt Human database (downloaded September 2017: 140000 sequences) using the SEQUEST algorithm. Peptide precursor mass tolerance was set at 10ppm, and MS/MS tolerance was set at 0.8Da. Search criteria included carbamidomethylation of cysteine (+57.0214) as a fixed modification and oxidation of methionine (+15.9949) as a variable modification. Searches were performed with full tryptic digestion and a maximum of 2 missed cleavage sites were allowed. The reverse database search option was enabled and all peptide data was filtered to satisfy a false discovery rate (FDR) of 1%.

2.12.2 Nano- Liquid Chromatography Mass Spectrometry

Precipitated lysates (100µg, section 2.11.4) were resuspended into 100 mM TEAB and digested with 2.5µg trypsin (Thermo Fisher Scientific) at 37°C overnight. Samples were desalted using a SepPak cartridge, according to the manufacturer's instructions (Waters, Milford, Massachusetts, USA). Eluate from the SepPak cartridge was evaporated to dryness and resuspended in 1% formic acid prior to analysis by nano-LC MSMS using an Orbitrap Fusion Tribrid mass spectrometer (Thermo Fisher Scientific). For total proteome analysis, peptides were fractionated using an Ultimate 3000 nano-LC system in line with an Orbitrap Fusion Tribrid mass spectrometer (Thermo Fisher Scientific). In brief, peptides in 1% (vol/vol) formic acid were injected onto an Acclaim PepMap C18 nano-trap column (Thermo Fisher Scientific). After washing with 0.5% (vol/vol) acetonitrile 0.1% (vol/vol) formic acid peptides were resolved on a 250mm × 75µm Acclaim PepMap C18 reverse phase analytical column (Thermo Fisher Scientific) over an organic gradient for 150 minutes, using 7 gradient segments (1-6% solvent B over 1 minute, 6-15% B over 58 minutes, 15-32%B over 58 minutes, 32-40%B over 5 minutes, 40-90%B over 1 minute, held at 90%B for 6 minutes and then reduced to

1%B over 1 minute) with a flow rate of 300nl minutes^{-1}. Solvent A was 0.1% formic acid and Solvent B was aqueous 80% acetonitrile in 0.1% formic acid. Peptides were ionized by nano-electrospray ionization at 2.2 kV using a stainless-steel emitter with an internal diameter of 30µm (Thermo Fisher Scientific) and a capillary temperature of 250°C.

All spectra were acquired using an Orbitrap Fusion Tribrid mass spectrometer controlled by Xcalibur 2.1 software (Thermo Fisher Scientific) and operated in data-dependent acquisition mode. FTMS1 spectra were collected at a resolution of 120,000 over a scan range (m/z) of 350-1,550, with an automatic gain control (AGC) target of 400,000 and a max injection time of 100ms. Precursors were filtered according to charge state (to include charge states 2-7), with monoisotopic peak determination set to peptide and using an intensity range from 5E3 to 1E20. Previously, interrogated precursors were excluded using a dynamic window (40s +/-10ppm). The MS2 precursors were isolated with a quadrupole mass filter set to a width of 1.6m/z. ITMS2 spectra were collected with an AGC target of 5000, max injection time of 50ms and HCD collision energy of 35%.

2.12.3 Data Analysis

The raw data files were processed and quantified using Proteome Discoverer software v2.1 (Thermo Fisher Scientific) and searched against the UniProt Human database using the SEQUEST HT algorithm. Peptide precursor mass tolerance was set at 10ppm, and MS/MS tolerance was set at 0.6Da. Search criteria included oxidation of methionine (+15.995Da), acetylation of the protein N-terminus (+42.011Da) and Methionine loss plus acetylation of the protein N-terminus (-89.03Da). Searches were performed with full tryptic digestion and a maximum of 2 missed cleavage sites were allowed. The reverse database search option was enabled and all data was filtered to satisfy a false discovery rate (FDR) of 5%.

2.13 *In vivo* studies

2.13.1 Animals and study protocol

Six week old Balb/c mice were purchased from Charles River and maintained in conventional open cages at ambient temperature, at the University of Bristol, Animal Services Unit. On day 0 separate groups of mice were primed subcutaneously either with 10^4-10^6 RBC ghost membranes or 10^6 SV and HBSS (control mice) 1:1 in Complete Freund's adjuvant (CFA, BD Difco- Fisher Scientific) subcutaneously (Fig. 2.5A). Five to ten microlitres of peripheral blood were aspirated from the lateral tail vein every 7 days to assess immune response by serology (see section 2.13.4). Fourteen days (d14) after the first inoculation, if no immune response was detected, mice were given a boost of ghost membranes or SV, at the same dose as the initial inoculum and left for two weeks (Fig. 2.5B above), whereas if mice showed an immune response, they were left for 1 week (Fig. 2.5B below).

Then, test animals and controls were challenged with human RBC (day 28 for mice given a boost and day 21 for those that did not), at the same dose as the initial inoculum (Fig. 2.5C). These RBC were from the same donor used to prime the animals. Later in the experiments, mice were challenged again 2 weeks later (Fig. 2.5D), terminated 2 weeks after the final RBC challenge and exsanguinated, by cardiac puncture under anaesthesia with isoflurane (Fig 2.5.E). Cardiac blood and spleens were collected for further analyses.

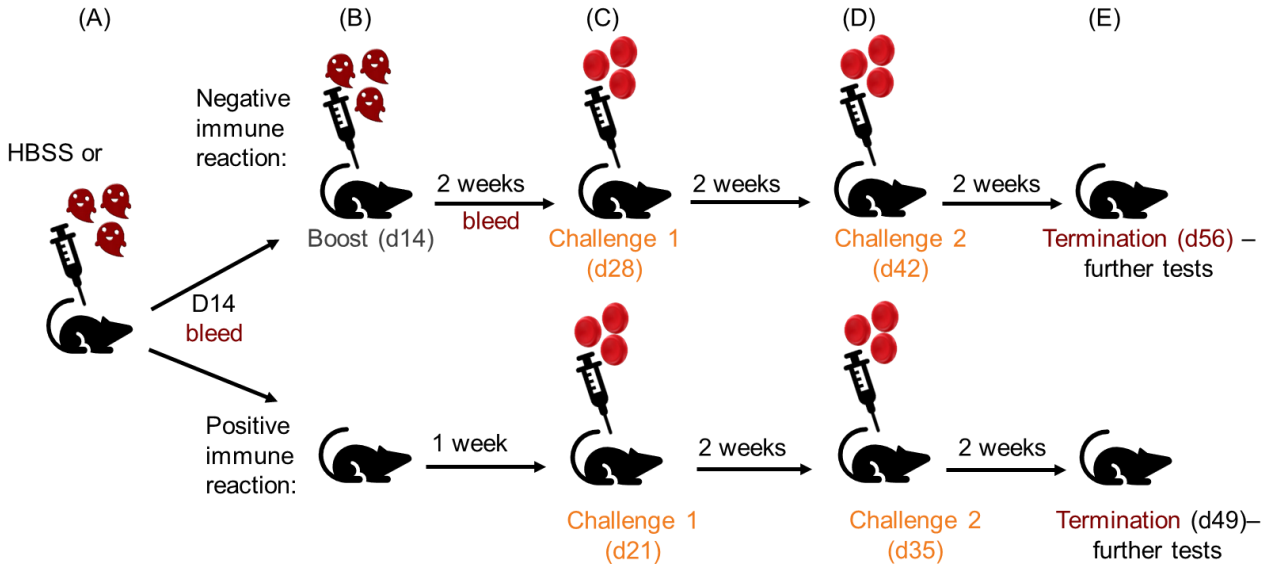

Figure 2.5 Schematic representation of immunotolerance experiments. (A) Mice were inoculated with HBSS (control) or RBC ghosts or SV and left to develop an immune response until day 14. **(B)** If no immune response was detected (above), mice were given a boost of the same source used to prime the mice and left for 2 weeks. If an immune response was observed, mice were left for 1 week (below). **(C)** Mice that had developed an immune response along with control mice were challenged with human RBC, from the same donor as the initial inoculum on day 21 (below) or on day 28 if they were given a boost (above). **(D)** Two weeks later, mice were challenged again with the same RBC. (E) Mice were culled 2 weeks later.

2.13.2 Processing mouse cardiac blood

Cardiac blood from mice was centrifuged at 2,000g for 15 minutes and pelleted RBC and plasma from the top layer of the supernatant were separated. Plasma was either assayed immediately for cytokine content and serology or stored at -20˚C. RBC were added to Alsever's in the same volume as the plasma that was removed and stored at 4˚C for 3 weeks.

2.13.3 Mononuclear cell isolation from spleens

Spleens were excised and kept in Iscove's Modified Dulbecco's Medium (IMDM, Invitrogen, Thermo Fisher Scientific) with 50% FBS (Thermo Fisher Scientific) at 4˚C for a maximum of 24 hours. Spleens were ground by using a syringe plunger on a 70μm filter (Miltenyi Biotec Ltd) and cells were washed in 10ml IMDM, then centrifuged at 350g for 5 minutes. Pellets were dissolved in 1ml of HBSS buffer and MNC were separated *via* density gradient centrifugation using Ficoll-Hypaque at 450g for 20 minutes. The MNC layer was collected in 1ml HBSS and centrifuged at 1,000g for 5 minutes. Pellets were suspended in 90% FBS and 10% dimethyl sulfoxide (DMSO, Origen Biomedical, Solihull, UK) and stored in liquid nitrogen prior to use.

2.13.4 Assessment of immune reactions

To assess immune reactions generated by the mice, a gel agglutination assay was used (Bio-Rad Laboratories). The gel card is designed for identification of paroxysmal nocturnal haemoglobinuria, however, the gel contains rabbit antiserum against mouse immunoglobulins which will bind mouse antibodies. Gel in the microtubes acts as a filter and retains any agglutinated cells carrying mouse antibodies in the upper part of the microtube (positive result, Fig. 2.6 right), while cells that do not express mouse proteins will settle to the bottom of the tube (Fig. 2.6 left). Three human reference RBC (cell screens in Alsever's, NHSBT) ABO O RhD positive, designed for identification of minor antigens, such as Lu^b, Fy and Jk, were used as reference controls and added to the first three tubes. Human RBC were the actual test (4^{th} tube), investigating whether ghost membranes or SV from the same donor generated an immune response and murine packed RBC (m-RBC) were used as a negative control (5^{th} tube). One hundred microlitres of murine and donor RBC were washed 5 times in PBS at 1,000g for 45 seconds and 3 human reference RBC were washed once, as they were cleaner due to storage in Alsever's. All cells were then washed once in modified low ionic strength saline (LISS, Source BioScience, Nottingham, UK) followed by 1 wash in ID- Diluent 2 (Biorad Laboratories Ltd) and a red cell solution (0.8%) was prepared for human and murine red cells. Then, 50μl of 0.8% RBC were added to each microtube of the gel card, along with 25μl of mouse antibody against human Lu^b (positive control, see BRIC108 on Table 1), or mouse plasma previously centrifuged at 1,660g for 45 seconds. When assessing aspirates at days 14-21, half the volumes were used: 25μl of 0.8% RBC with 12.5μl antibody or plasma. Samples were incubated for 15 minutes at 37˚C to assist antibody binding and the gel card was centrifuged for 10 minutes in an ID-centrifuge (Biorad Laboratories Ltd). To compare antibody levels between different groups of animals, serial plasma dilutions were carried out.

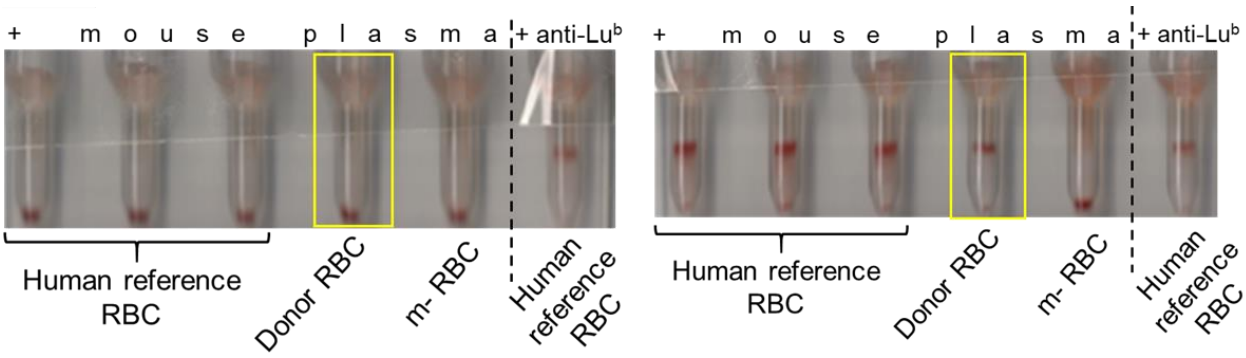

Figure 2.6 Mouse antibody screen test using a gel card. RBC (0.8%) from human standards, human donor and mouse RBC were added along with mouse plasma (first 5 tubes) or anti- mouse Lu^b (tube 6). (Left: No agglutination - negative test representation; all human RBC sink to the bottom apart from the positive control (tube 6). Right: RBC agglutination of all human RBC -positive test demonstrating reaction of murine plasma to human RBC. No reaction was observed against murine RBC (m-RBC).

2.13.5 Cytokine assay

The Proteome Profiler Mouse Cytokine Array Kit, Panel A (R&D Systems) was used to identify selected cytokine and chemokine responses to SV and ghosts preparations. Cardiac mouse blood was centrifuged at 2,000g for 15 minutes within 2 hours of collection. One hundred microlitres of plasma was added to 500µm Array buffer 4, topped up to 1.5 ml with Array buffer 6, which is a blocking buffer, and then 15µl of reconstituted Mouse Cytokine Array Panel A Detection Antibody Cocktail (all provided in the kit) was added and incubated for an hour at room temperature. Plasma and Antibody Cocktail mix were added to a provided membrane, which was pre-soaked in Array buffer 6, and incubated on a rotor overnight at 4˚C. Then the membrane was washed, probed with HRP streptavidin, provided in the kit and then exposed on X-ray film.

2.14 Statistical analyses

Data represent results from at least 3 independent experiments, unless otherwise stated. Statistical analyses were performed using nonparametric ANOVA using Kruskal-Wallis test for groups>3, whereas 2 groups were compared using non parametric t-test in Prism 8 (Graphpad, San Diego, USA), unless otherwise stated. P values < 0.05 were considered significant. Results are reported as mean ± standard deviation (SD) unless otherwise stated. Significant results are designated by asterisks on graphs.

Chapter 3 Identification of red cell-derived particles and autophagic vesicles

3.1 Introduction

In patients with SCD, deformed cells can block blood vessels and cause vaso-occlusion, severe pain, known as crisis, infections, anaemia and stroke. The spleen, which clears senescent cells and extracellular vesicles, is frequently damaged in SCD patients, resulting in significantly higher numbers of RCDP in the plasma. These RCDP expose PS and were originally reported using flow cytometric analyses (255, 269, 332). PS is well known to cause hypercoagulation in SCD (333). RCDP in SCD are thought to be produced through membrane budding as a result of repeated erythrocyte sickling. In physiological conditions, RCDP are produced by membrane budding when reticulocytes form mature RBC. Thus, they are right-side out and expose the extracellular domains of the proteins present on the RBC membrane. Our colleagues identified a type of autophagic exosome in SCD and in media from cultured reticulocytes (CR media) using confocal microscopy. These AV exposed PS and cytoplasmic protein domains, therefore, they have an inside-out orientation (123, 127, 334) (see Chapter 1, Fig. 1.6).

The different characteristics and role of RCDP and AV in normal and pathological conditions have not been fully investigated. PS exposure on RCDP and AV in SCD suggests potential contributions to hypercoagulation. In addition, the fact that higher levels of RCDP have been reported in SCD patients, could be an indicator of the severity of the disease. SCD plasma was used in order to detect and isolate these populations using several methods. Additionally, CR media from cultured reticulocytes, using a well-established protocol (123, 334), was assessed for RCDP and AV using flow cytometry and different microscopy methods. This would potentially enhance our knowledge of reticulocyte maturation in culture. RCDP from SCD PFP and CR media were characterised by flow cytometry and then isolated by FACS. Confocal microscopy, DLS and imaging flow cytometry were used to assess morphology of sorted and unsorted populations, while protein content was assessed by Bradford assay. SV of predetermined size were used as controls (Fig. 3.1).

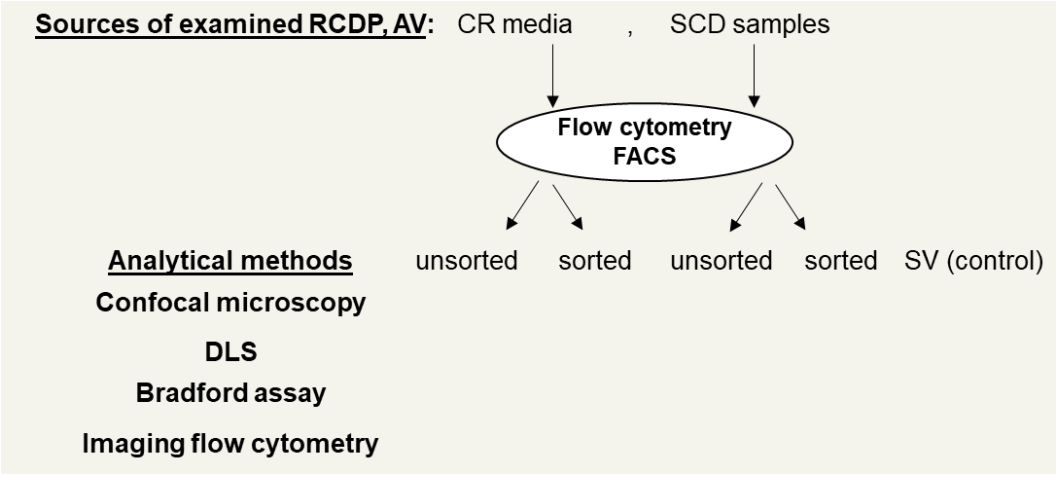

Figure 3.1 Schematic of the analytical methods for vesicle characterisation in CR media and plasma. SV (0.2μm) were used as a control.

Results

3.2 Assessment of reticulocyte morphology

In order to characterise RCDP from *ex vivo* expanded reticulocytes, $CD34^+$ cells were isolated and grown under appropriate conditions to produce enucleated reticulocytes (123, 334). The morphology of the cultured cells was checked frequently throughout the maturation of the polychromatic (day 11-16) to orthochromatic blasts (day 15-19). When most reticulocytes were enucleated (day 20), leukocyte filtration was used to isolate enucleated reticulocytes from free nuclei and immature reticulocytes (Fig. 3.2). Mature reticulocytes were cultured for a further 96h and RCDP produced were isolated and analysed for RBC protein content.

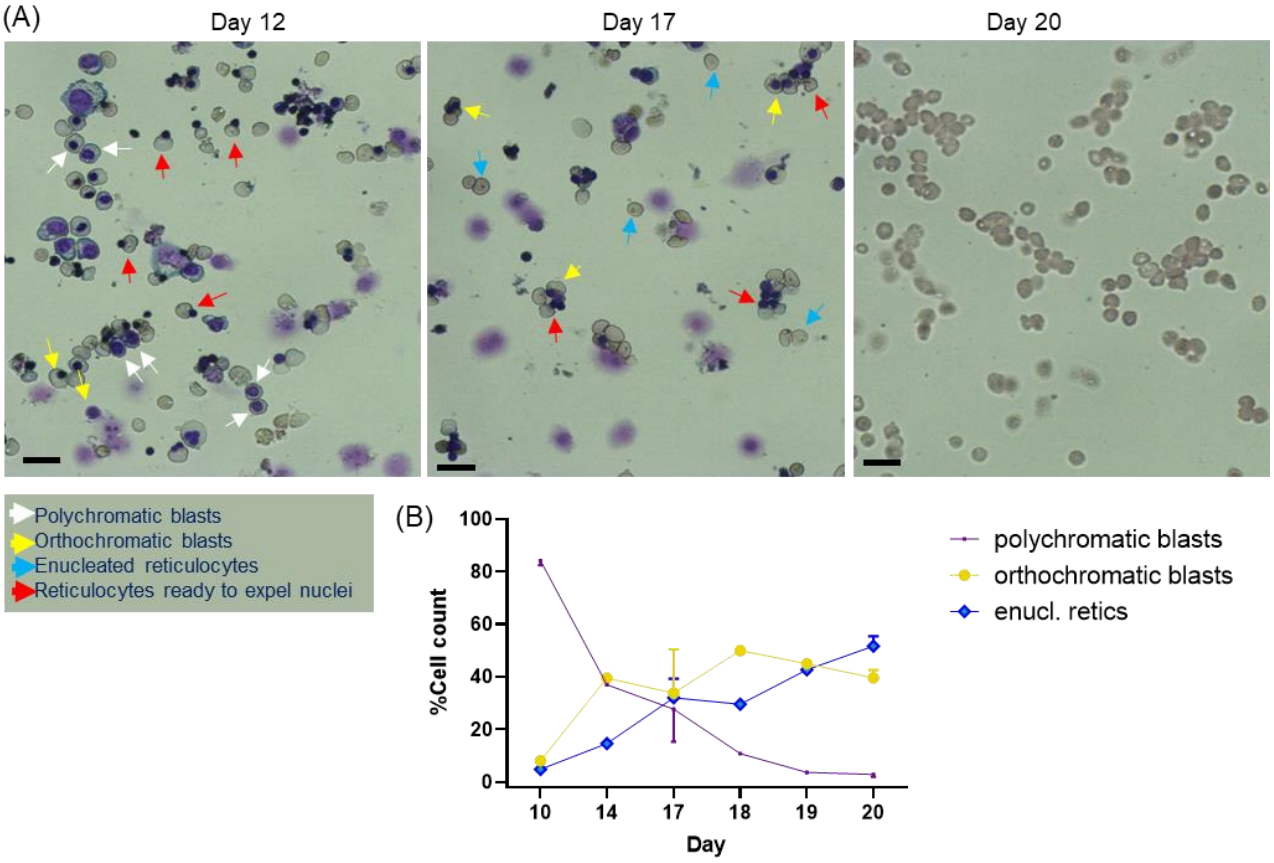

Figure 3.2 Morphology of reticulocytes during their maturation. **(A)** Light microscope images acquired. Reticulocytes appear in grey. At day 12 (left image), immature reticulocytes containing dark round purple nuclei (polychromatic blasts) are shown by white arrows, orthochromatic blasts with smaller size nuclei (in dark blue) are shown by yellow arrows and cells expelling nuclei are shown by red arrows. At day 17 (middle image), most nuclei have reduced in size (orthochromatic blasts showed by yellow arrows). Enucleated reticulocytes can be seen (blue arrows), as well as reticulocytes ready to expel their nuclei (red arrows). At day 20 (right image) after leukocyte filtration, a homogeneous population of enucleated reticulocytes remains. Scale bars indicate 20μm. **(B)** Cell counts of 20 fields per coverslip at different stages in three different cultures. Data represent mean ± SD. Numbers for day 20 are before leukocyte filtration.

3.3 Identification of red cell-derived particles and autophagic vesicles

3.3.1 Optimising flow cytometry analysis

Flow cytometry is routinely used for RCDP detection and has revealed that numbers of RCDP are higher in SCD patients than healthy individuals (255, 269, 332). Usually, an antibody targeting the extracellular (ex.) domain of GPA is used to detect RCDP. Colleagues have demonstrated the extrusion of AV from CR media by confocal microscopy using BRIC163 antibody, which detects a cytoplasmic (cyt.) epitope of GPA. This suggested that such AV have an inside-out orientation of the membrane (123, 127, 334). In order to detect RCDP and AV, different antibodies recognising extracellular and cytoplasmic domains of abundant proteins expressed on RBC (GPC, band 3 and GLUT1) were incubated with PFP from SCD patients or CR media and analysed by flow cytometry.

3.3.1.1 Antibody titration

Typically, antibody titrations using flow cytometry are carried out to determine the antibody concentration that will show the maximum stained population without shifting the negative population into the positive range (see Flow-cytometry in Chapter 2.6), as this indicates non-specific staining. All antibodies used for flow cytometry were titrated in equal volumes of CR media or SCD PFP, as described in the methods (Chapter 2.6). The titrated antibody concentration in the stained samples ranged from 0.156 to 5μg/ml and for most antibodies the optimum concentration was between 0.156-0.625μg/ml. When higher concentrations (10μg/ml) were tested, non-specific staining was observed since most of the populations appeared positive and shifted to the right (see following section), indicating that antibody concentration was too high. During all antibody titrations and flow cytometry experiments, the diluent (PBS buffer) was stained with the same antibody concentration as the sample and any fluorescence observed in the buffer was subtracted from the stained samples.

RCDP from CR media were a homogeneous population and the optimum antibody concentrations were easier to determine. For most antibodies tested, the optimum concentration was 0.625μg/ml, apart from ex. GPA (clone BRIC256), which was 0.312μg/ml. On the other hand, the first experiments in SCD PFP samples, showed many events that were difficult to distinguish in the stained and the unstained subpopulations. Additionally, variability was observed in the scatter characteristics (FSC for size and SSC for granularity) among different patients. In order to get a better defined RDCP population and check the antibody specificity, different conditions were tried: (i) diluting SCD PFP, (ii) use of a negative control and (iii) use of an alternative to an isotype control.

i) Dilution of plasma

SCD plasma was diluted 1:1, 1:2 and 1:5 in PBS buffer (Chapter 2.6) in order to dilute the cellular debris and permit better discrimination. The antibody used for this work recognised the ex. GPA, one of the most abundant proteins in human erythrocytes. The discrimination of positively stained and the negative populations in PFP diluted 1:5 was better than undiluted PFP and all other dilutions tested (Fig. 3.3). The antibody concertation used ranged from 0.156 to 5μg/ml and serial half dilutions of ex. GPA were carried out. The optimum concentration was 1.25μg/ml. Subsequently, SCD PFP was diluted only in 1:5 when used in flow cytometry experiments and all the antibodies were titrated in this plasma dilution. The optimum concentration for each antibody is summarised in Table 3.1, at the end of this subsection.

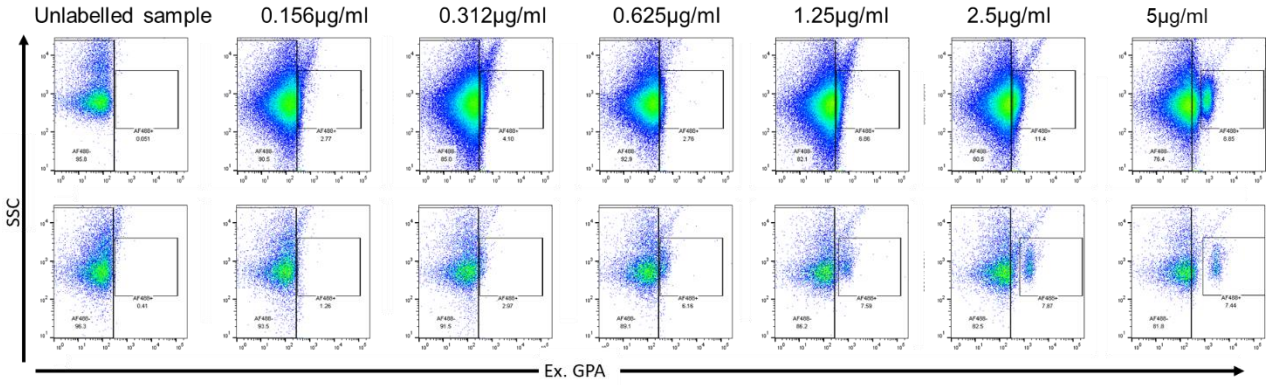

Figure 3.3 Antibody titration in plasma. Ex. anti-GPA-AlexaFluor 488 titrations of undiluted (upper panel) and diluted SCD PFP 1:5 (lower panel) using concentrations 0.156-5μg/ml. Left and right gates in each plot represent the negative and the positive populations, respectively. The gates were set based on unlabelled samples (left column). PFP samples were from the same patient.

ii) Negative control

HL-60 cells were chosen as a negative control because they do not expose RBC proteins, so no positive population was expected. HL-60 cells were analysed under the same experimental conditions as the SCD PFP samples and CR media. The results showed that these cells did not express the examined proteins, confirming the gate for the negative population was appropriately positioned.

(iii) Alternative negative control

Despite having HL-60 cells as a negative control, introducing an isotype control would be beneficial since some of the populations were still not distinct. Isotypes are produced in a similar manner to the antibody of interest but they target a different epitope, showing that the tested antibody is specific. As the antibodies were conjugated to AlexaFluor (AF) 488 or 647 (described in Chapter 2.6), a similar antibody to be used as an isotype control was not available. As an alternative to confirm antibody specificity and that the concentrations used were appropriate, plasma from murine blood was used, mixed in different ratios with SCD PFP and serial half titrations were repeated. Further diluting the human SCD PFP with a known negative cell population should allow the best antibody dilution to be determined, in order to get better discrimination.

Ex. anti-GPA was found to be human specific, since only human RCDP were stained (Fig. 3.4). Also, when human and mouse plasma were used at ratios of 9:1 and 7.5:2.5, the GPA^+ populations were more distinct and better discriminated. Again, non-specific staining was observed upon incubation with higher concentrations of the antibody. The optimum concentration was 0.625µg/ml. These results indicated that better discrimination of the stained populations was obtained in further diluted SCD PFP samples using a negative population, providing confidence that the antibody staining works better with diluted SCD PFP.

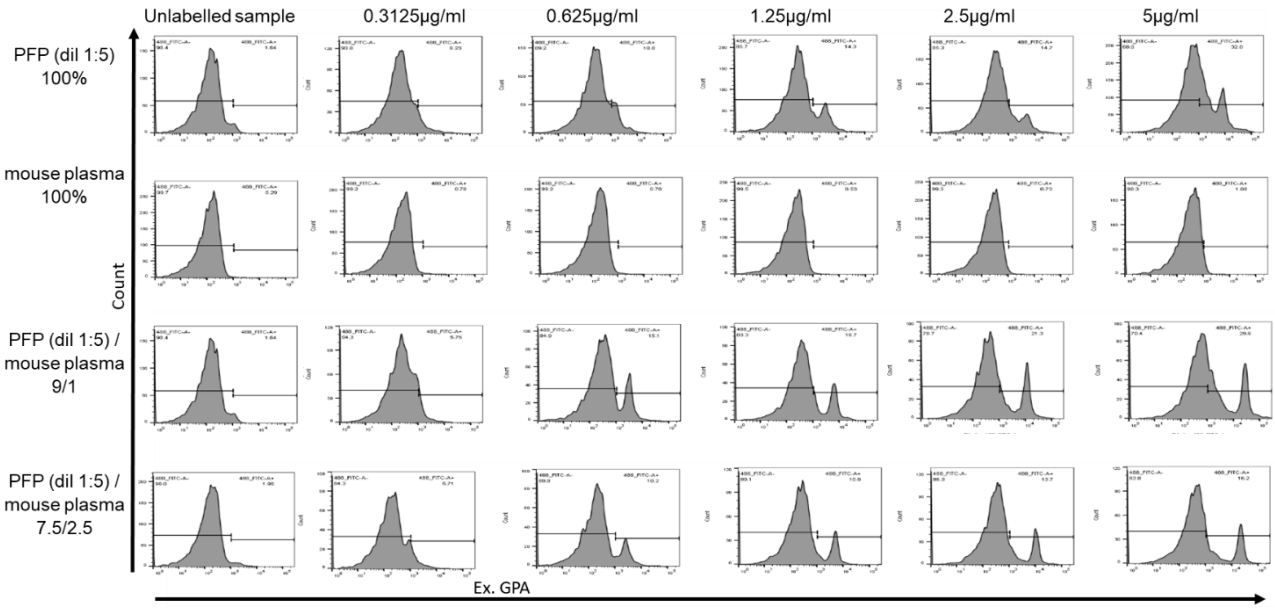

Figure 3.4 Use of mouse plasma as an alternative control in antibody titration, in SCD plasma. Histograms of antibody titrated in pure SCD PFP diluted 1:5 in PBS (upper panel), mouse plasma (middle panel) or PFP mixed with mouse plasma 9/1 and 7.5/2.5. Gates were set based on the unlabelled samples (left column).

At the end of the experiments, 2 ideal concentrations were obtained from each antibody titration using 2 SCD PFP dilution methods: one diluting SCD PFP 1:5 in PBS buffer and a second using murine plasma. The final optimum concentration was defined as the average of both concentration values (Table 3.1). It was determined for all the antibodies available at that time and it was used for all subsequent flow cytometry experiments. The optimum concentration provided maximum labelling whilst avoiding non-specific staining. For all antibodies, except ex./cyt. GPA and GLUT1 (highlighted in Table 3.1), the optimum concentration was the same obtained from both methods, whereas for ex./cyt. GPA and GLUT1 the average of the two concentrations was used. Since both methods showed the same antibody concentrations for most of the antibodies, it was decided that for new antibodies, only antibody titrations in PFP diluted 1:5 would be carried out and the laborious titrations in murine plasma were omitted.

Table 3.1 Optimum antibody concentration calculated from two dilution methods.

Antigen	Clone	Best concentration (µg/ml) in PFP diluted:		Final optimum concentration (µg/ml) (average)
		1:5	murine plasma	
Ex. GPA-AF 488*	BRIC256	1.25	0.625	0.937
Ex. GPA- AF 647*	BRIC256	0.312	0.312	0.312
Cyt. GPA- AF 488	BRIC163	1.25	0.625	0.937
Ex. Band 3- AF 488	BRIC200	2.5	2.5	2.5
Cyt. Band 3- AF 488	BRIC155	1.25	1.25	1.25
Cyt. GPC- AF 488	BGRL100	0.156	0.156	0.156
GLUT1- AF 488	BRAC67	2.5	1.25	1.875

*AF: AlexaFluor

3.3.1.2 Investigation of platelets and HLA cells in plasma

SCD PFP from different patients were found to have populations with different scatter characteristics (see PFP from 1 patient in Fig. 3.5A and 2 patients in Fig. 3.5B). In order to identify the origin of different populations in the SCD PFP, a directly conjugated PAB-PE antibody, which is a specific marker for platelets, was used. A human anti-HLA class I (FITC) marker was also used to detect GPA^+ RCDP from HLA^+ cells in plasma. The rationale behind was that HLA is expressed by nucleated cells (303), thus, RCDP which result from enucleated cells do not expose HLA and could be distinguished from the rest of the PFP components. Both antibodies were used separately, along with anti-GPA antibody. Platelets and HLA cells were detected in 3/3 and 19/19 samples tested respectively (Fig 3.5A and B). GPA^+, PAB^+ and HLA^+ populations were assigned specific colours then FSC and SSC characteristics of all events were examined (GPA red, PAB and HLA orange), to

determine the scatter characteristics. Platelet presence in SCD PFP (Fig. 3.5A) showed that they were not totally removed by centrifugation. As was seen with RCDP, dilution of SCD PFP allowed better detection of platelets compared to undiluted SCD PFP. Furthermore, platelets were found to have comparable scatter characteristics with GPA^+ events, as both populations showed similar FSC and SSC values (Fig. 3.5A). HLA cells were distributed along the whole population and their scatter characteristics differed (Fig. 3.5B). All samples were shown to have a distinct GPA^+ population. CR media from 3 cultures was also examined for HLA^+ events but they could not be detected. This was to be expected, since this media was collected from enucleated reticulocytes only. Following investigation of platelets and HLA^+ cells in SCD PFP, as well as optimising the flow cytometry protocol, GPA^+ events from SCD PFP and CR media were also examined for the presence of other proteins expressed on RBC.

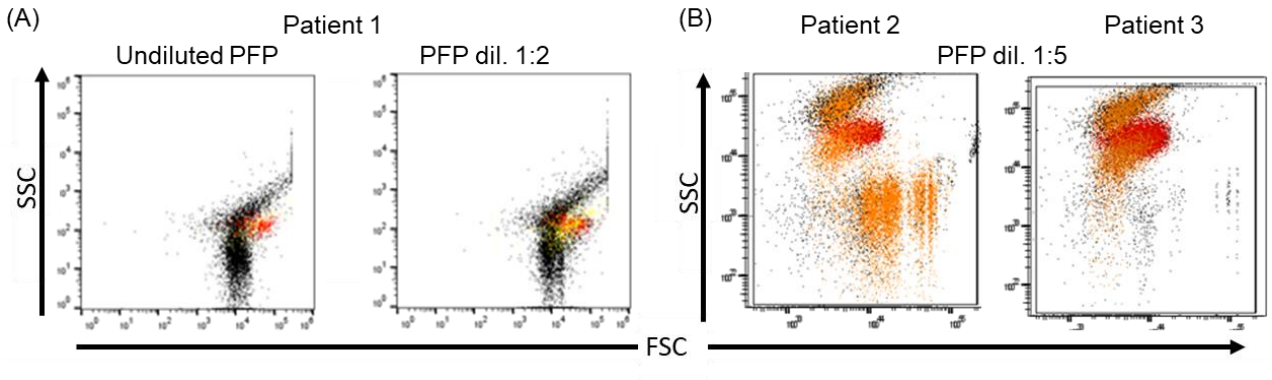

Figure 3.5 Platelet and HLA detection in plasma by flow cytometry. **(A)** FSC and SSC plots from SCD plasma stained with ex. GPA^+ (in red) and PAB (in orange) in undiluted PFP (left) and diluted PFP (right). **(B)** Dot plots showing the distribution of GPA^+ (red) and HLA^+ (orange) in PFP diluted 1:5. Samples are from two different patients and plots are representative of 3 and 19 patients, respectively.

3.3.2 Abundance of red cell proteins

Protein abundance was examined using an antibody panel (GPA, GPC, band 3 and GLUT1, see Table 3.1). Flow cytometry results showed that SCD PFP samples expose all the tested proteins (Fig. 3.6A). The levels of protein exposure on 111 SCD PFP samples were highest for ex. GPA (mean ± SD, 41.92% ± 24.35%) and ex. Band 3 (26.60% ± 25.55%), whereas lower levels of cyt. GPA (3.37% ± 9.88%), cyt. Band 3 (2.58% ± 7.81%), cyt. GPC (0.42% ± 1.06%) and GLUT1 (1.95% ± 5.42%) were detected (Table 3.2). Ex. GPA was significantly higher than all other proteins ($P \leq 0.02$). Similarly, ex. Band 3 expression was also significantly increased compared to the cytoplasmic proteins and GLUT1 ($P<0.0001$), whereas cyt. GPA was only significantly elevated compared to cyt. GPC ($P=0.04$, Table 3.2). Since the presence of extracellular domains of the

proteins corresponds to RCDP and cytoplasmic domains to AV, it was shown that RCDP levels are higher than AV in SCD PFP. With regards to GLUT1, the exact epitope is yet unknown. The manufacturer (PDPU) assumed the antibody detects an intracellular one. This is in line with the low detected levels of GLUT1, which indicated it potentially detects a cytoplasmic epitope of GLUT1.

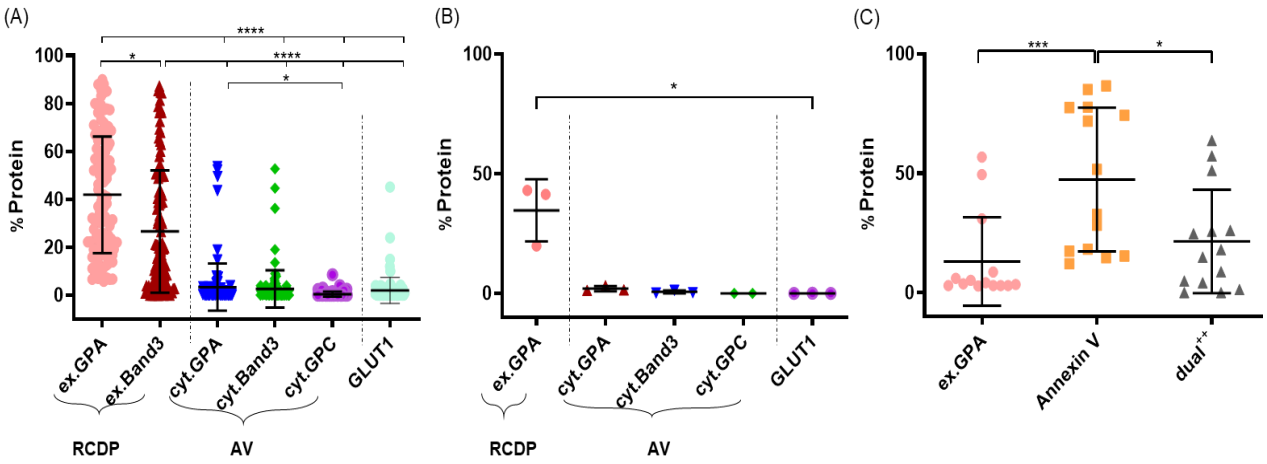

Figure 3.6 Proteins detected in plasma and CR media by flow cytometry. SCD PFP and CR media was stained with a panel of antibodies targeting abundant RBC proteins. Exposure of RBC proteins **(A)** in PFP from 111 patient samples and **(B)** 3 reticulocyte cultures. Dotted lines divide extracellular protein domains associated with RCDP and cytoplasmic domains associated with AV. **(C)** PS exposure in 14 SCD PFP samples. Lines represent mean and standard deviation. Statistical analyses were performed by nonparametric ANOVA using Kruskal-Wallis test (*P<0.05, **P≤0.01, ***P≤0.001).

In CR media (Fig. 3.6B) the levels of ex. GPA exposure were higher than other proteins examined (34.73% ± 12.96%) but only significantly increased compared to GLUT1 (P= 0.04). The extracellular domain of band 3 was not assessed in CR media. Low levels were detected for cyt. GPA (2.01% ± 1.0%), cyt. Band 3 (0.65% ± 0.61%), GPC and GLUT1 (0.03% ± 0.01% and 0.06 ± 0.07% respectively). This indicates that cultured reticulocytes mainly produced RCDP.

SCD PFP was also examined for PS exposure which is an indicator of deformed RBC membrane and RCDP formation (95, 176). Annexin V binds PS and it is widely used for PS detection (335, 336). PFP from 14 SCD patients were stained with ex. GPA and annexin V (Fig. 3.6C). Levels of annexin V^+ events were higher (47.38% ± 30.13%) than ex. GPA^+ (13.07% ± 18.51%, P=0.001) and ex. GPA^+/annexin V^+ (21.48% ± 21.68%, P=0.04).

Table 3.2 Statistical comparison of proteins detected in SCD plasma.

Antigen	Mean	SD	P value				
			ex. Band 3	cyt. GPA	cyt. Band 3	cyt. GPC	GLUT1
ex. GPA	41.92	24.35	**0.02**	**<0.0001**	**<0.0001**	**<0.0001**	**<0.0001**
ex. Band 3	26.60	25.55	-	**<0.0001**	**<0.0001**	**<0.0001**	**<0.0001**
cyt. GPA	3.37	9.88	-	-	>0.999	**0.04**	>0.999
cyt. Band 3	2.58	7.81	-	-	-	0.38	>0.999
cyt. GPC	0.42	1.06	-	-	-	-	0.08
GLUT1	1.95	5.42	-	-	-	-	-

Results of proteins detected in SCD patient samples (n=111) were compared using a nonparametric ANOVA and Kruskal-Wallis test. Bold text indicates significant differences between proteins compared.

3.3.3 Size estimation

The size of the detected RCDP (stained with anti-ex. GPA-AF 488) and AV (stained with anti-cyt. GPA-AF 488) in SCD PFP and CR media was assessed by flow cytometry. Two different populations of known size were selected as controls: (i) SV and (ii) commercially available size beads.

3.3.3.1 Use of known size storage vesicles

During initial flow cytometry experiments, some SV prepared by a colleague were used. Their size was calculated to be 175nm by using the NanoSight LM10 system, as has been previously reported for such vesicles (183). However, these SV were undetectable by flow cytometry, showing that the RCDP and AV detected by flow cytometry were larger than 200nm.

3.3.3.2 Size beads

Commercially available size beads were used ranging in diameter from 0.02µm to 2µm and tested on the flow cytometer. The instrument detected beads of 2µm, 1µm and 0.5µm diameter but it was not sensitive enough to detect the smaller sizes (0.2, 0.1 and 0.02µm). When FSC and SSC of SCD patients (Fig. 3.7 left upper panel) and CR media (left lower panel) were plotted, ex. GPA^+ events (in red) were located close to the 0.5µm size beads (light blue) for both sources. Histograms of abundance of detected populations were also created in order to better discriminate the scatter of each population (Fig 3.7 right). Cyt. GPA^+ AV (green, right upper panel) from SCD PFP were found

to have a similar size to ex. GPA$^+$ RCDP (0.5µm), whereas AV from CR media (green, right lower panel) were found to be smaller and were located below the 0.5µm beads. However, since the instrument could not detect the 0.2µm size beads we can assume that AV in CR media are larger than 0.2µm.

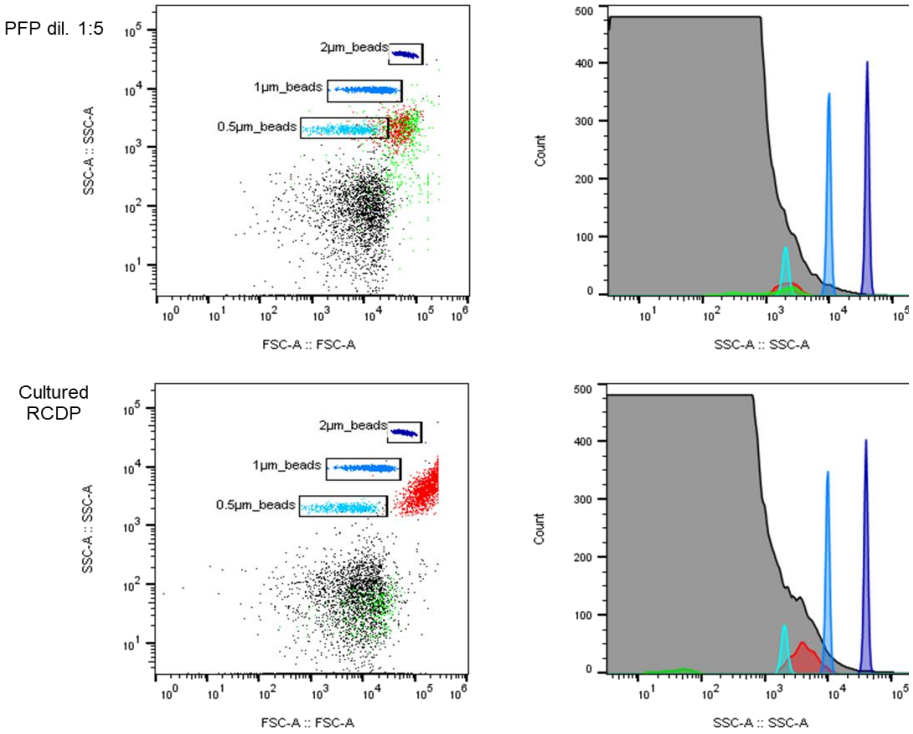

Figure 3.7 GPA$^+$ red cell vesicle size estimation using size beads. Representative samples from 5 SCD PFP (above) and CR media (n=1, below) were stained with anti-ex. GPA-AF 488 (for RCDP) or anti-cyt. GPA-AF 488 (for AV), along with commercial FITC-labelled size beads and examined by flow cytometry. In a plot of SSC versus FSC (left dots plots), the position of the size beads was shown using gates, to illustrate the relationship between events detected on SCD PFP (upper plot, representative of 5 SCD patient samples) and CR media (lower plot) and size. Beads are shown in dark blue, blue and light blue for 2, 1, 0.5µm size, respectively. Ex. GPA$^+$ RCDP is in red, cyt. GPA$^+$ AV in green and the unstained population in black. Histograms of SSC versus event count were also created (right plots) to quantitate the detected events in PFP (upper plot) and CR media (lower plot). The unstained population is shown in grey.

Size estimation for ex. and cyt. Band 3$^+$, cyt. GPC$^+$ and GLUT1$^+$ was also attempted in 2 SCD PFP samples. All these populations had the same scatter characteristics as GPA$^+$ events and AV when examined by flow cytometry and so it was expected that they would have similar sizes. However, all protein domains in both samples were found in particularly low levels and could not be easily discriminated when plotted on FSC vs SSC. Therefore, size assessment for these populations was not possible and additional proteins on RCDP and AV were tested.

3.4 Examination of highly immunogenic proteins on sickle cells

CR media express most of the RBC proteins (unpublished data from collaborators). In an attempt to further characterise the protein content of RCDP and AV, immunogenic proteins that contribute to alloimmunisation in SCD, such as Kell, Kidd and Duffy, were examined on RCDP from SCD PFP, CR media and SV from outdated blood units (day 35). The antibody specificity was tested on SC and on a panel of RBC designed for identification of minor antigens, such as Rh, Fy and Jk, which was used as a positive control (see Table 2.1 for antibodies used). Individual samples from 19 SCD patients and 2 healthy donors were tested and all were found to be strongly positive (mean ± SD, 79.06 ± 7.34% and 69.03 ± 1.13%, respectively) for the Kell protein. However, the results from the antibodies targeting Kidd and Duffy proteins were negative, even for the positive control. This showed that the antibodies were not sensitive enough for this analysis, hence SCD PFP, CR media and SV were not further examined. Instead, RCDP and AV were sorted using FACS, to further assess morphology and investigate whether true microvesicles or cell debris were isolated.

3.5 Isolation of red cell-derived particles and autophagic vesicles using FACS

3.5.1 Optimisation of red cell-derived particle isolation using FACS

In order to isolate adequate numbers of RCDP from SCD PFP, only samples with a high number of RCDP detected by flow cytometry were used. The sample preparation was modified to maximise the sorting yield (Chapter 2.8). For this, some factors should be taken into account and adjusted, like determination of SCD PFP and CR media dilution, antibody dilution and RCDP enrichment using sedimentation.

3.5.1.1 Sample dilution

Due to the small size of the microvesicles, stained RCDP do not sediment using conventional centrifugation and could not be washed, hence stained SCD PFP was further diluted up to twenty times to remove unbound antibody. However, this led to further dilution of GPA^+ events and sorting took several hours, without achieving a sufficient yield for further experiments (< $1x10^4$ events). After testing several SCD PFP and CR media dilutions, it was decided to dilute both sources 1:10.

3.5.1.2 Antibody dilution

Since ex. GPA was highly present among the tested RBC proteins when analysed by flow cytometry, the respective antibody (BRIC256) was chosen for sorting by FACS. For the early sorting experiments, a higher concentration was used than that for flow cytometry (1.25µg/ml), in order to achieve good discrimination of GPA^+ events. CR media was stained in the same way.

3.5.1.3 Pelleting samples

Prior to sorting, some SCD PFP samples were pelleted using ultra-centrifugation (100,000g) and high-speed (20,000g) centrifugation (as described in Chapter 2.5.1) in order to enrich RCDP. Sorted populations were compared with those obtained from non-pelleted SCD PFP. Non pelleted samples from both SCD PFP and CR media were shown to have a distinct GPA^+ population with relatively high SSC (Fig. 3.8A). This population had higher scatter than the main population when plotted against FSC (Fig. 3.8B). Although FSC represents size, SSC, which indicates granularity, is more sensitive for microparticle detection, thus, sorting was based on GPA^+ and SSC characteristics. In terms of the pelleted SCD PFP, the high scatter population was decreased compared to the non-pelleted samples. However, pelleted samples also had a lower scatter GPA^+ population that overlapped with the main population when plotted against FSC. This population is more representative of small RCDP than the higher scatter one, which seem to correspond to large RCDP. In this Chapter, terms "sorted small" and "sorted large" RCDP were used to describe GPA^+ events sorted from the low and high SSC gate, respectively.

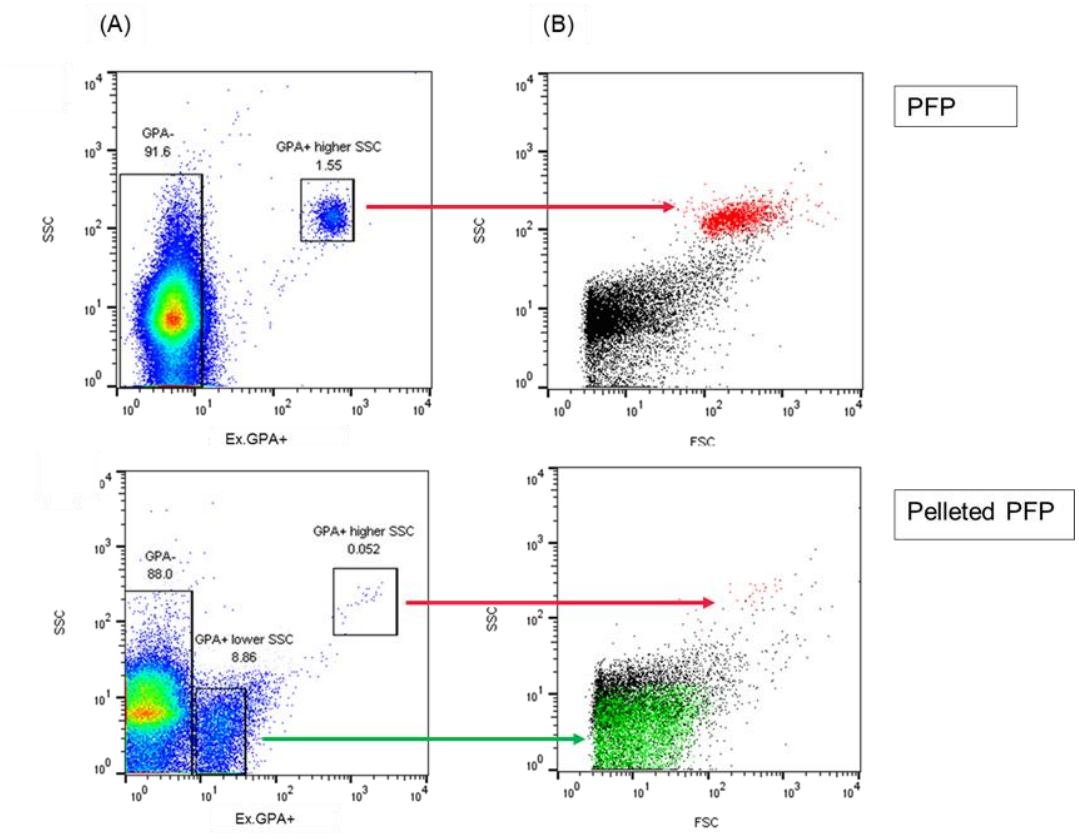

Figure 3.8 Sorting strategy for GPA^+ vesicles from plasma. (A) Non-pelleted PFP (upper dot plot) and pelleted PFP (lower plot), by ultra-centrifugation (100,000g). Samples were stained for ex. GPA and plotted against SSC. **(B)** Forward and side scatter characteristics of samples. Large GPA^+ (higher SCC events) are shown in red, small GPA^+ (lower SSC) from pelleted PFP are green and the GPA negative population is black.

3.5.1.4 Refining plasma pelleting and antibody titrations

The effects of SCD PFP sedimentation using high-speed centrifugation at 20,000g (as described in Chapter 2.5.1), as a less "harsh" method that would not damage the RCDP, was examined in 3 SCD samples. Pelleted RCDP from equal SCD PFP volumes, isolated by ultra- and high-speed centrifugation from the same patient, were compared. Furthermore, pelleted RCDP were stained with 3 different concentrations of ex. GPA (0.312μg/ml, 0.625μg/ml and 1.25μg/ml). Higher antibody concentrations resulted in better discrimination of small GPA$^+$ events, whereas large GPA$^+$ events were found well-discriminated for all concentrations used (Fig. 3.9). Furthermore, sorting of small GPA$^+$ events was only possible from the samples stained with the highest antibody concentration (1.25μg/ml), since the lower concentrations did not succeed to stain a discrete population that could be sorted. Thus, it was confirmed that staining SCD PFP using a GPA concentration of 1.25μg/ml was right, as a good discrimination for sorting is required.

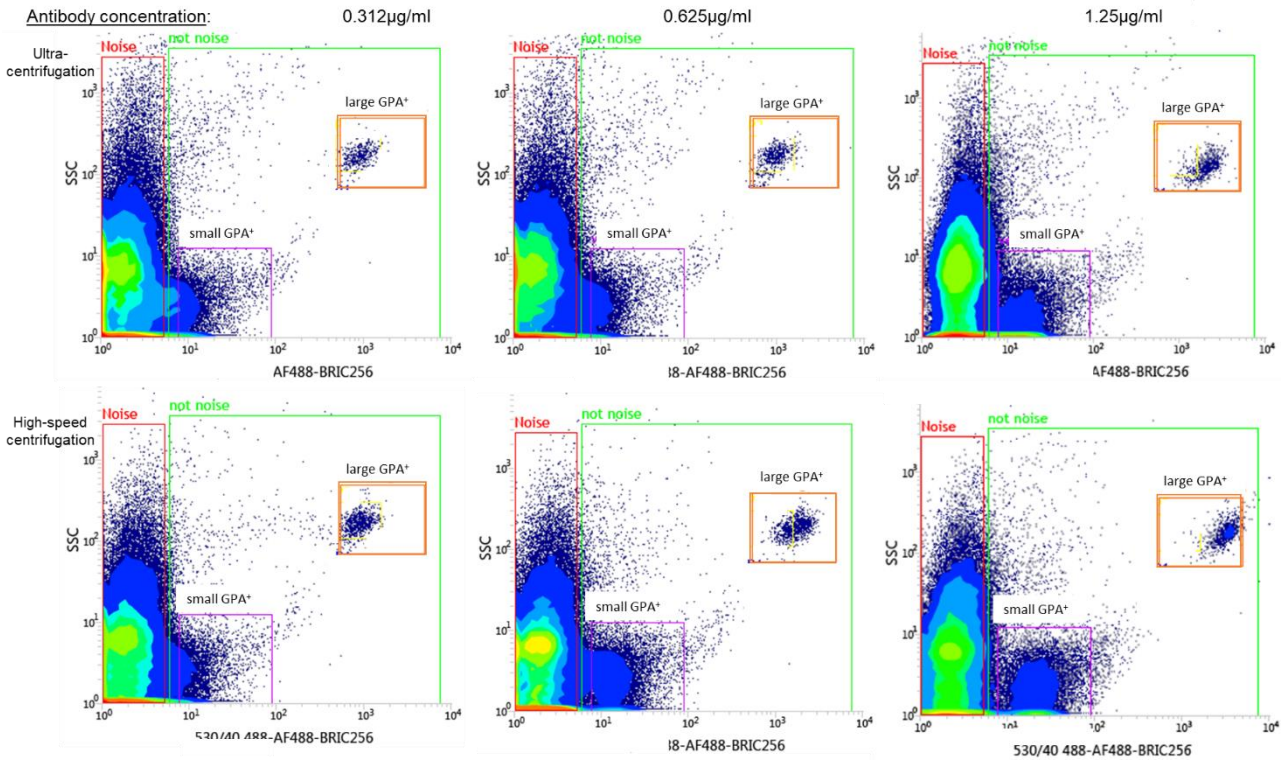

Figure 3.9 Comparison of methods of vesicle sedimentation for isolation by FACS. Representative plots of PFP from SCD patients (n=3). Samples were split and pelleted by ultra-centrifugation at 100,000g (upper panel) or high-speed centrifugation at 20,000g (lower panel). Pellets were stained using 3 different concentrations of ex. GPA (0.312μg/ml, 0.625μg/ml and 1.25μg/ml). Instrument noise and negative events are shown in the red gate. GPA$^+$ events in the green gate were further separated based on higher SCC (large events, orange gate) and lower SSC (small events, purple gate).

Both centrifugation methods did not reveal variability in small and large ex. GPA^+ populations: means of 0.70% ± 0.36% and 0.24 ± 0.30% large GPA^+ events were detected after ultra- and high-speed centrifugation, respectively, while the proportions of small GPA^+ events were 5.32 ± 5.39% and 5.22 ± 7.60%, respectively (Table 3.3). However, variability in small GPA^+ events numbers among different patients was observed. Both methods gave similar numbers of small and large GPA^+ events, which were not found statistically significant and were equally used for sample sedimentation. As populations below 1.5% were too low to be sorted, none of the large GPA^+ events from pelleted PFP could be collected and small GPA^+ events were sorted instead.

Table 3.3 Assessment of sorting potential using the proportions of GPA^+ events in pelleted plasma, by two centrifugation methods.

SCD Patient ID	Ultra-centrifugation		High-speed centrifugation	
	Small GPA^+ (%)	**Large GPA^+ (%)**	**Small GPA^+ (%)**	**Large GPA^+ (%)**
1	11.47	0.78	13.98	0.59
2	3.08	1.01	1.30	0.10
3	1.40	0.30	0.38	0.04
Mean	5.32	0.70	5.22	0.24
SD	5.39	0.36	7.60	0.30

Statistical analysis between small and large GPA^+ events from both methods was carried out using a paired nonparametric t-test ($P>0.999$ and $P=0.25$, respectively).

3.5.1.5 Determination of size limit detection by FACS compared to flow cytometry

SV of known size (175nm) were tested on the cell sorter, as was previously described in section 3.3.3.1 for flow cytometry. Again, the instrument was not sensitive enough to detect these SV. This means that small RCDP detected by FACS had a diameter bigger than 0.2μm, as was shown before for flow cytometry. Small and large sorted GPA^+ from pelleted and non pelleted PFP, respectively, were subsequently analysed using a MACSQuant flow cytometer and only large RCDP could be detected, showing that the sorter was more sensitive for small size particle detection, rather than the flow cytometer.

3.5.2 Yields of sorted red cell-derived particles

When sorting non pelleted SCD PFP from 9 patients was examined, a large variability among different samples was observed; 100µl non-pelleted SCD plasma gave $4x10^3$-$3.6x10^5$ (mean ± SD, $1.33x10^5$ ± $1.20x10^5$ large RCDP (Table 3.4). Variability was also observed in 4 pelleted SCD samples using ultra-centrifugation. Yields for large GPA^+ ranged from $3x10^4$-$3x10^5$ ($1.30x10^5$ ± $1.18x10^5$). Small GPA^+ events were not detected in non pelleted SCD PFP. In the 4 pelleted samples, yields of small RCDP were higher up to $5.6x10^6$, ($19.50x10^5$ ± $25.30x10^5$ GPA^+ events). This showed that ultra-centrifugation assisted in RCDP enrichment, as more GPA^+ events were obtained from a concentrated pellet rather than non pelleted PFP. Large GPA^+ events from all samples and small events from pelleted samples only, were collected for morphology and protein content characterisation. Media from one reticulocyte culture gave $3x10^5$ GPA^+ large events.

Table 3.4 Event number of small and large GPA^+ particles in pelleted and non pelleted plasma.

Non pelleted SCD PFP		**Pelleted SCD PFP**		
SCD Patient	**Large GPA^+ ($x10^5$)**	**SCD Patient**	**Small GPA^+ ($x10^5$)**	**Large GPA^+ ($x10^5$)**
4	0.04	13	0.21	2.00
5	0.42	14	56.45	0.27
6	1.42	15	6.98	0.34
7	1.05	16	14.36	2.60
8	0.44	**Mean**	19.50	1.30
9	1.50	**SD**	25.30	1.18
10	0.59			
11	3.63			
12	2.83			
Mean	1.33			
SD	1.20			

Attempts to isolate AV using FACS

The cytoplasmic domains of GPA and band 3 were used for sorting AV from different SCD PFP samples, along with calcein AM, a marker of intact microvesicles. However, the AV events detected were too low to be sorted.

3.6 Protein determination on sorted red cell-derived particles by Bradford assay

Although the Bradford assay is routinely used to detect total protein in SV preparations, protein detection in sorted GPA^+ events proved extremely challenging. As sorted samples were used in other analyses, only a limited number could be used for the protein assay. Replicate readings from different aliquots of the same sample were always variable and inconsistent. After many unsuccessful attempts using both sorted large and small RCDP from SCD PFP and CR media, it was concluded that the quantity obtained was insufficient for accurate protein detection. The majority of the sorted GPA^+ events were used for size and morphology assessment.

3.7 Size estimation of sorted red cell-derived particles using DLS

Sorted small and large GPA^+ populations from SCD PFP and CR media were examined using DLS, in order to get an estimation of their size. Since small RCDP from CR media could not be sorted, only large RCDP populations were analysed from this source. SV populations from donated blood of known size (185nm on the NanoSight LM10 system) were prepared by a colleague and used as controls. Large and small sorted RCDP were diluted using filtered PBS (as described in Chapter 2.10) and measurements were carried out on a DLS machine. For several large and small sorted RCDP, measurements could not be taken as the samples were too polydisperse. PBS buffer particles were shown to be 8-9nm and SV (n=3) were around 200 nm (Fig. 3.10A), confirming the NanoSight measurement.

Large sorted RCDP from 3 individual SCD patients had peaks at 4-5μm, which was same for large sorted RCDP from one reticulocyte culture. Small sorted RCDP from one SCD patient were found to range between 1-5μm giving a flatter peak at 3-4μm (Fig. 3.10B, magnification of 3.10A). The results were different to those from flow cytometry using size beads, which suggested that GPA^+ events were approximately 0.5μm. However, these data indicate that DLS is accurate for small particles, such as SV, and that the majority of the small sorted RCDP are 1-2μm smaller than the large sorted RCDP from SCD PFP or CR media. These populations were not detected in SV or PBS buffer (Fig. 3.10C). RCDP size and morphology were also assessed by microscopy.

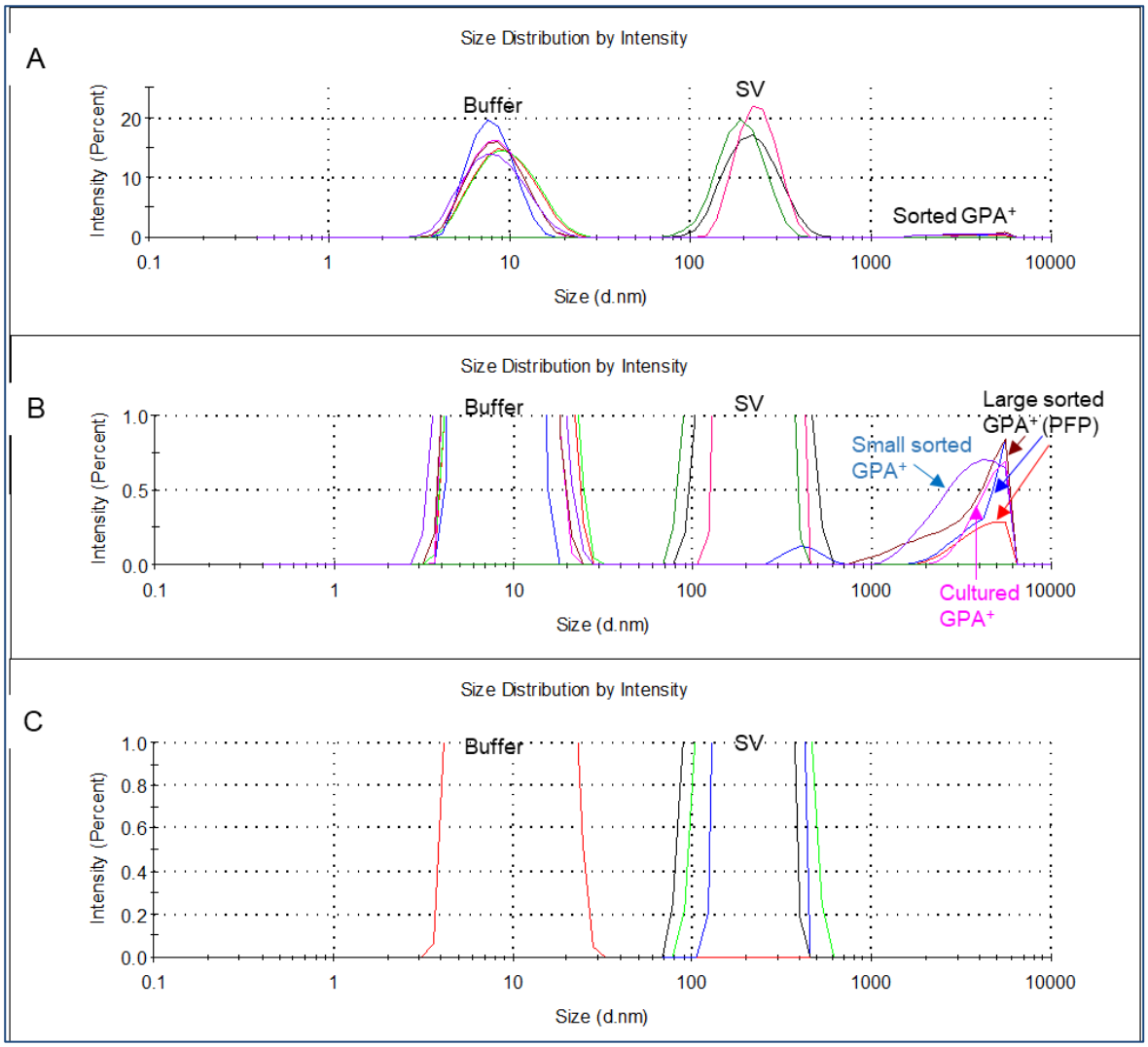

Figure 3.10 Size estimation of sorted GPA⁺ events using DLS. Large and small sorted RCDP from SCD PFP and CR media, diluted in PBS buffer, along with SV of known size (185nm) were analysed by DLS. **(A)** Histogram of the detected populations. **(B)** Magnification of the histogram (A). SV populations (n=3) are shown in pink, green and dark blue. Large sorted RCDP from SCD PFP (n=3, in brown, blue and red) have a similar size to large sorted RCDP from CR media (n=1, in cerise), whereas small sorted RCDP (n=1, in light blue) had a lower size distribution. **(C)** Magnification of a histogram showing the PBS buffer and the SV populations (n=3) demonstrating that no populations larger than 200nm are detected.

3.8 Size estimation of large sorted particles using microscopy

To assess the morphology of sorted large and small RCDP, they were examined by conventional confocal, as well as spinning disk confocal microscopy. Confocal microscopy gave variable results. Tracking small numbers of sorted GPA⁺ events on slides proved to be extremely difficult. Sorted RCDP were shown to form aggregates and clusters in most cases (Fig. 3.11). GPA⁺ events from CR

media could not be detected. Unpublished data from laboratory colleagues using confocal microscopy estimated such RCDP to be smaller than 2μm. Here, these sorted large RCDP from SCD PFP were 1-6μm, which is closer to that of RBC (7-8μm) (50). Images from GPA^+ events larger than 2.5μm were not captured, since they were thought to be remaining RBC/SC. However, considering the multiple centrifugation steps in order to get SCD PFP, these findings suggested the presence of membrane blebs and/ or macrovesicles (MaV), with size similar to RBC ghosts, rather than small RCDP, or that the instrument was not sensitive enough to image GPA^+ events. For these reasons it was decided to step back from conventional confocal microscopy and try other microscopy techniques.

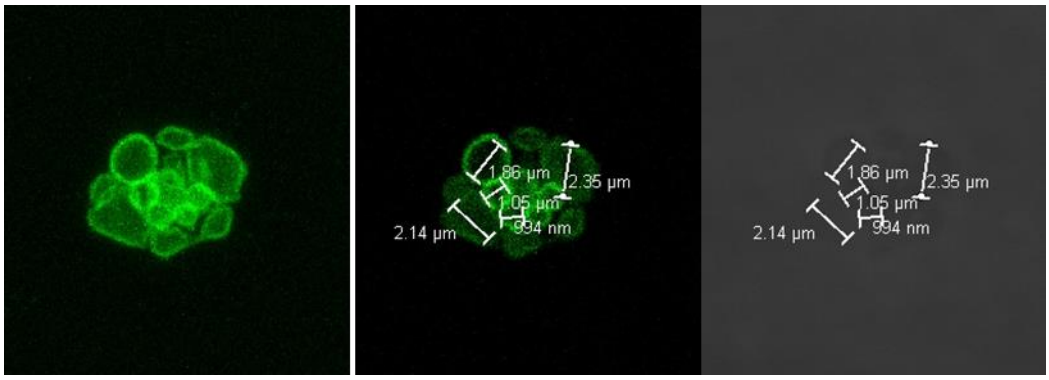

Figure 3.11 Confocal analysis of sorted GPA^+ events from plasma. Sorted large GPA^+ RCDP were examined by confocal microscopy and found to form aggregates (left). Their size was between 1-2.4μm on bright field, estimated by Adobe Photoshop (right). Images are representative from 5 SCD patients and were visualised using 40x magnification.

Images from spinning-disk confocal microscopy showed that sorted populations from SCD and CR media were mainly comprised of round particles (Fig. 3.12A). In order to calculate the size and radial symmetry of these RCDP, the Hough circle transform, a tool selective for round objects which ignores ellipses, was used. Images from 5 individual patients were analysed and were found to have a median size of 7μm (range 6.8-7.8μm, Fig. 3.12B), which is the size of erythrocytes (50). Knowing that all red cells were removed from the SCD PFP by centrifugation, it is possible that these particles are MaV, which have formed in the circulation as a result of repeated sickling events.

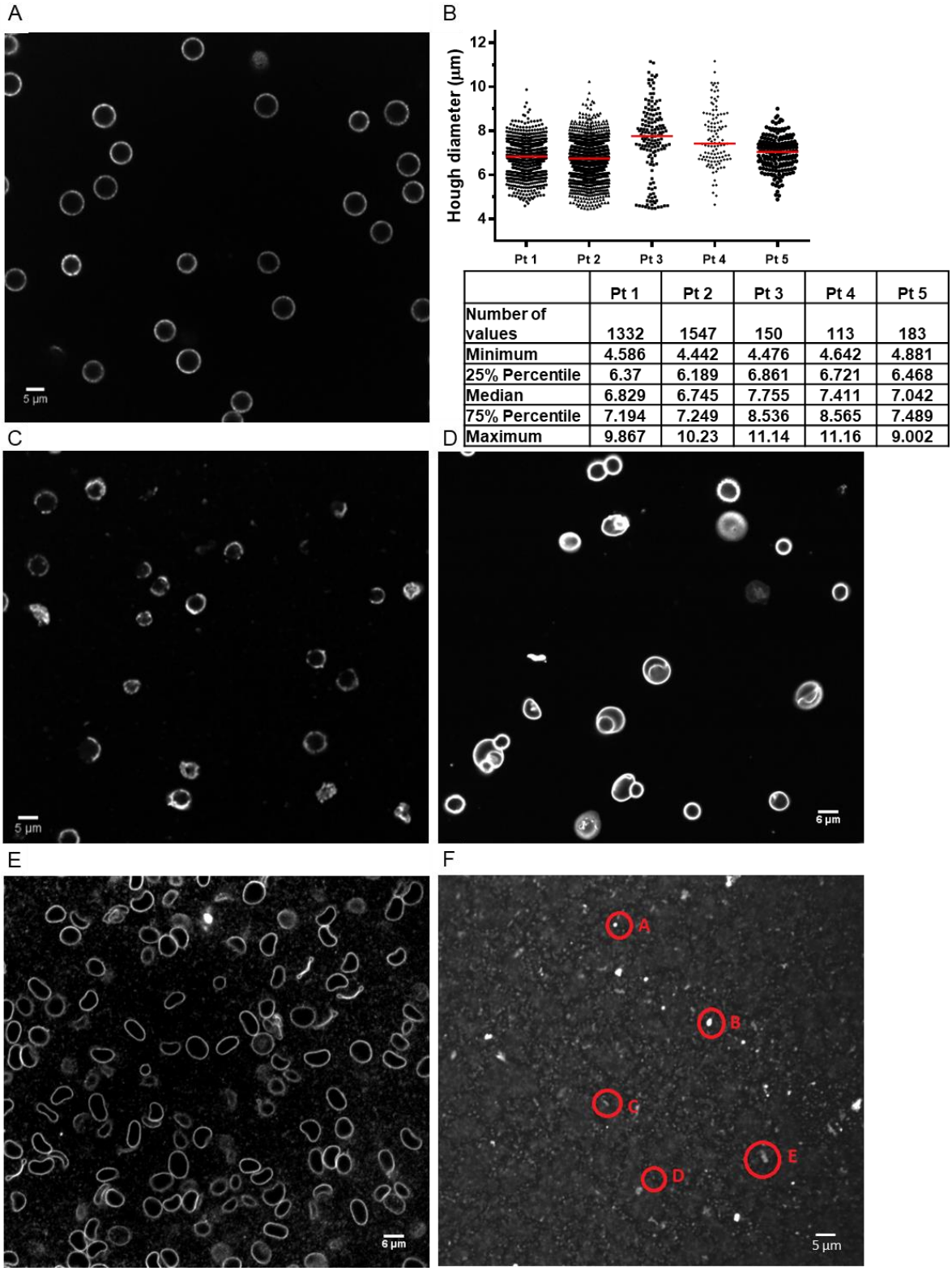

	Pt 1	Pt 2	Pt 3	Pt 4	Pt 5
Number of values	1332	1547	150	113	183
Minimum	4.586	4.442	4.476	4.642	4.881
25% Percentile	6.37	6.189	6.861	6.721	6.468
Median	6.829	6.745	7.755	7.411	7.042
75% Percentile	7.194	7.249	8.536	8.565	7.489
Maximum	9.867	10.23	11.14	11.16	9.002

Figure 3.12 Spinning-disk confocal analyses. Populations were stained using anti-ex. GPA- AF 488 before visualisation. Digital image of: **(A)** large GPA$^+$ sorted events from SCD PFP and **(B)** scatter plot of size of each individual round object detected in samples from 5 SCD patients. Line represents median, raw data are shown in table. **(C)** Digital images of cultured GPA$^+$ sorted RCDP, (**D)** SC, **(E)** media from stored blood units and **(F)** 200nm diameter SV. Red circles (A-E) represent round SV of a size that was close to the instrument diffraction limit. Images were visualised using a 60x (NA 1.2) water-immersion lens.

Images taken of sorted, cultured GPA$^+$ RCDP showed a mixed population of spherical particles along with blebs or broken membrane (Fig. 3.12C), in which it was difficult to determine the size. Morphology of SC, media from stored blood units from which RBC had been removed, as well as 200 nm SV, were also examined for comparison. A mixed population of deformed SC and RBC was detected, as well as smaller round particles (Fig. 3.12D). Storage media revealed the presence of large apoptotic bodies, MaV or even ghost membranes (Fig. 3.12E). The SV population was found to be below the diffraction limit of the instrument, thus, too small to be detected (Fig. 3.12F). Since the morphology of RCDP from CR media, SC, storage media and SV did not reveal round particles, their size could not be detected by the Hough circle transform method. Furthermore, the fluorescent signal in SC which corresponds to GPA abundance, was higher than the signal of GPA$^+$ events from CR media and SV. This suggests that detected RCDP were membrane structures with less integral membrane rather than intact cells. Small sorted GPA$^+$ RCDP could not be detected with either microscope.

3.9 Analysis using imaging flow cytometry (ImageStream)

3.9.1 ImageStream analysis of GPA$^+$ sorted particles from plasma

In addition to microscopy methods, SCD PFP as well as sorted large from non pelleted PFP and small GPA$^+$ from pelleted SCD PFP were analysed using ImageStream, an imaging flow cytometer with high sensitivity and resolution, as well as the ability to visualise each individual event. Scatter intensity vs max pixel scatter were plotted (Fig. 3.13A) and from this, as was described before (Chapter 2.7), 2 main populations were distinguished: one comprised of small, low scatter events and the other contained larger events with high scatter. Large events from non-pelleted SCD PFP were found in low and high scatter areas (Fig. 3.13A left), while the vast majority of pelleted samples, from either ultra-centrifugation or high-speed centrifugation, were located in the low scatter area (Fig 3.13A right). When images from low and high scatter events were viewed by bright field, differences in size and morphology were revealed: GPA$^+$ RCDP and AV, exposing the extracellular or cytoplasmic domain, respectively, were detected in the low scatter area were found to be below 1µm (Fig. 3.13B), which is a similar size to microvesicles (155). Generally, AV were less abundant in SCD PFP and were shown to have a smaller size than RCDP. Large particles, which mainly corresponded to MaV and/or RBC ghosts, were detected in the high scatter area (Fig. 3.13C). In addition, the majority of small sorted GPA$^+$, which could not be detected by conventional flow cytometry previously, were visualised to be as small as microvesicles by imaging flow cytometry (Fig. 3.13B). Presence of ex. GPA$^+$ /cyt. GPA$^+$ events was also observed in both areas, indicating unsealed membrane fragments or large unsealed RBC ghosts (Fig. 3.13Bii and 3.13Cii). Healthy, intact erythrocytes (Fig. 3.13Di) and MaV or ghost membranes (Fig. 3.13Dii and iii) were observed using bright field and they could easily be distinguished, as MaV lacked the integrity of the erythrocyte membrane.

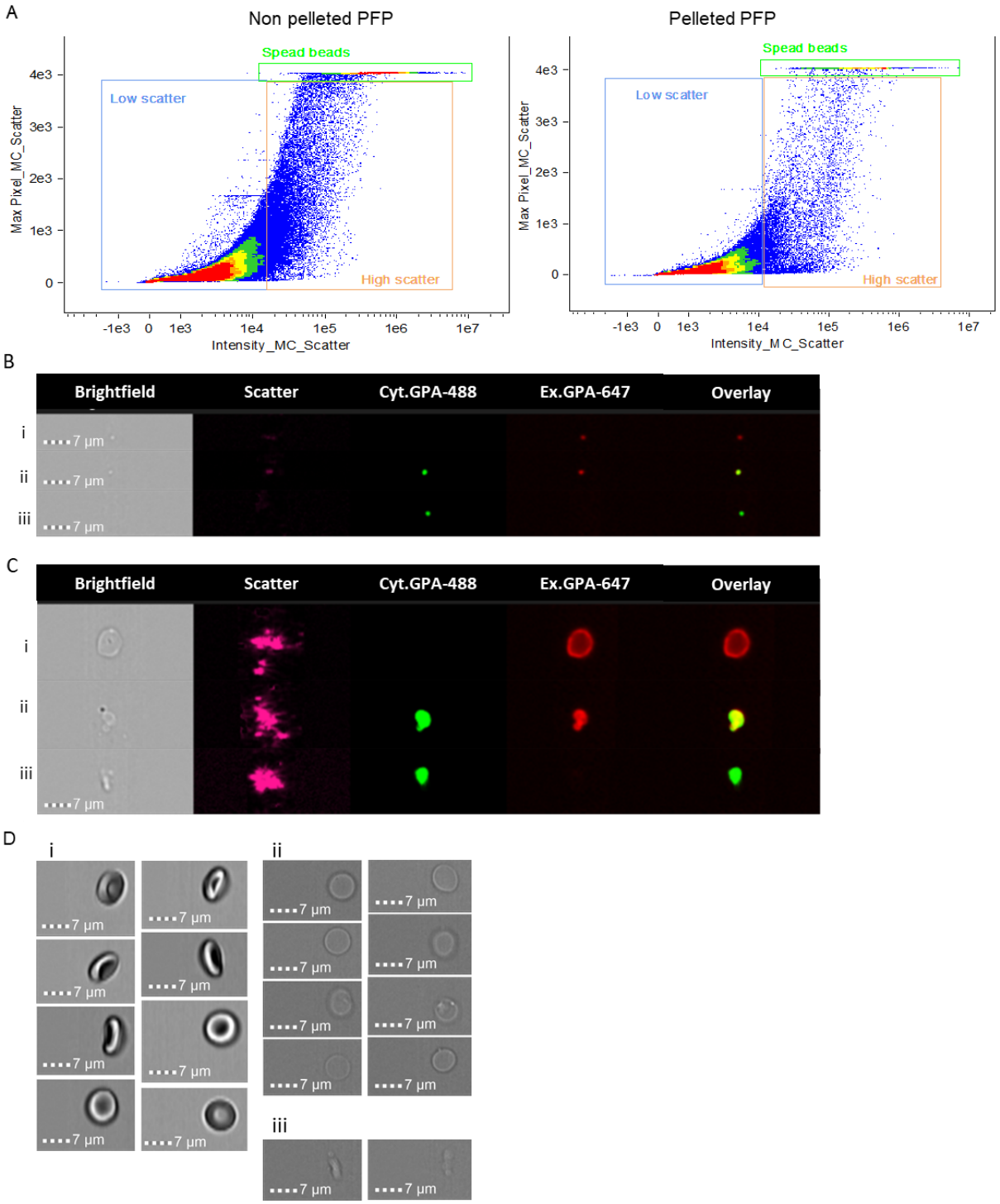

Figure 3.13 Morphology of objects detected by imaging flow cytometry. (A) Scatter intensity vs max pixel scatter of sorted GPA$^+$ events in non-pelleted samples (left panel) and pelleted SCD PFP (right panel). High SSC area containing MaV (in orange) and low SSC area containing small RCDP/AV (blue) were gated as shown. Speed beads had the highest scatter and were excluded (green). **(B)** SCD plasma stained with anti-ex. GPA-AF 488 and anti-cyt. GPA-AF 647. Images of **(B)** low scatter and **(C)** high scatter MaV from SCD PFP (i) ex. GPA, (ii) dual and (iii) cyt. GPA positive. **(D)** Bright field views of (i) RBC from a healthy individual, (ii) MaV from SCD PFP and (iii) side views of MaV from SCD PFP. Figures B, C and D were provided by Dr Tosti Mankelow.

3.9.2 Comparison of imaging flow cytometry with conventional flow cytometry

The above findings revealed that imaging flow cytometry could detect small populations, like small sorted GPA^+ and size beads of 0.2μm, which could not be previously detected by flow cytometry. To compare instrument sensitivities, PFP from 4 SCD patients was stained with the same antibody panel against RBC used for flow cytometry (ex. and cyt. GPA, cyt. GPC, cyt. Band 3 and GLUT1, see Table 3.1). Stained samples were divided into two; one was analysed by flow cytometry (FC) and the other by ImageStream (IS, Fig 3.14A). In this experiment, samples were not separated into low and high scatter but the whole population was gated, in order to include all events in the calculations, and allow comparison with the flow cytometer data. The results showed that levels of 2 out of the 6 protein domains analysed, ex. Band 3 and ex. GPA, were found to be higher by IS than flow cytometry. IS detected mean ± SD, 49.63% ± 29.64% for ex. GPA levels, whereas FC detected only 9.99% ± 11.50%. Ex. Band 3 was also detected at higher levels by IS compared to flow cytometry: 40.95 ± 21.14% to 6.25% ± 7.26%. All cytoplasmic domains of GPA, band 3, GPC and GLUT1 were detected in particularly low levels (<0.5%, Fig 3.14B). Statistical analysis using nonparametric ANOVA was applied to all results and only ex. GPA and ex. Band 3 were significantly higher than GLUT1 (P=0.054 and 0.008, respectively), when detected by IS. The above revealed that the imaging flow cytometry is more sensitive for detecting RCDP exposing ex. Band 3 and ex. GPA. The barely detectable levels of cytoplasmic GPA, band 3, GPC and GLUT1 suggest that SCD patients produce far less AV than RCDP.

In addition, SCD PFP along with size beads and SV 175nm were also analysed, as was previously done by FC (section 3.3.3.2 and Fig 3.7). The imaging flow cytometer was able to detect the SV population (peak in red), as well as the 0.2μm size beads (green) (Fig 3.14C), whereas the conventional flow cytometer could not detect these populations (see Fig. 3.7). Both populations were well discriminated. A colleague, passed some SCD PFP through a 1.2μm filter then analysed by IS. Interestingly, all MaV were removed and the low scatter population remained (purple). This population had the same scatter characteristics as the low scatter population of an unfiltered SCD PFP sample (blue). These two populations were distributed between the SV and the 0.2μm size beads peaks, revealing that the majority of the low scatter events were under 200nm. MaV had a bigger scatter and the peak (white) was just below the peaks of 0.5μm (orange) and 1μm (yellow) beads. However, these findings were different to the large particles observed in bright field (Fig. 3.13C, D). Previously, the flow cytometer was unable to detect not only the SV and the 0.2μm size beads, but also the small sorted RCDP (Fig. 3.7). Flow cytometry showed that detected GPA^+ RCDP and AV for SCD PFP had a size close to 0.5μm (red, green, light blue and blue, respectively on Figure 3.6), whereas the IS showed that such populations correspond to MaV (Fig. 3.13C, D and 3.14C, histogram in white).

A

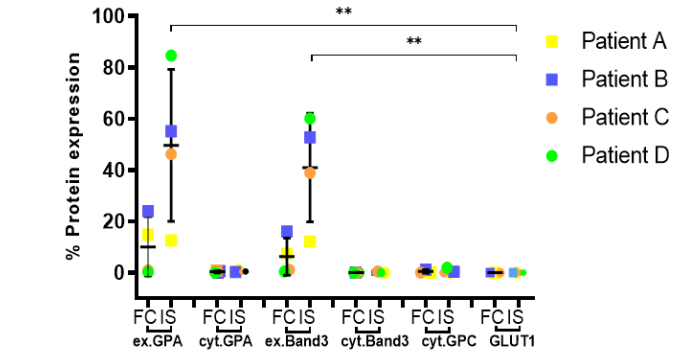

B

Antigen	FC mean%	FC SD%	IS mean%	IS SD%
Ex. GPA	9.99	11.5	49.63	29.64
Cyt. GPA	0.38	0.43	0.54	0.32
Ex. Band 3	6.25	7.26	40.95	21.14
Cyt. Band 3	0.05	0.05	0.12	0.25
Cyt. GPC	0.5	0.66	0.59	0.96
GLUT1	0.05	0.02	0.00	0.00

C

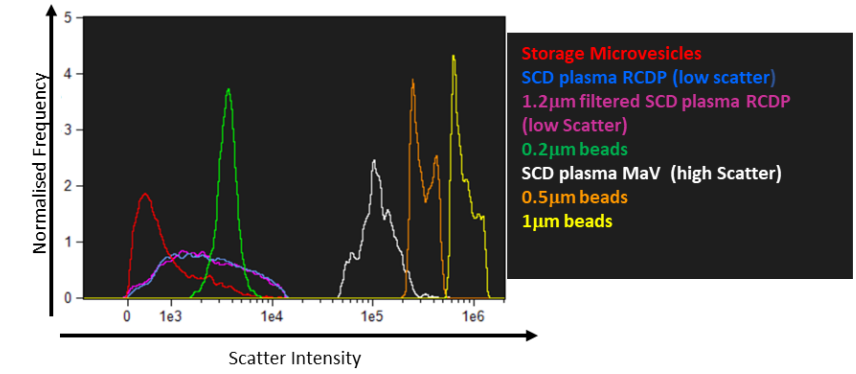

Figure 3.14 Comparison of imaging flow cytometry and conventional flow cytometry.

(A) SCD PFP was stained for 6 RBC proteins and analysed by flow cytometry (FC) and ImageStream (IS). Bars represent mean ± SD from 4 SCD patient samples. Statistical analyses were performed by nonparametric ANOVA using Kruskal-Wallis test (*P<0.05, **P≤0.01, ***P≤0.001). **(B)** Table showing mean ± SD of protein levels detected by FC and IS. **(C)** SCD PFP was analysed by imaging flow cytometry along with size beads. Histogram showing the scatter intensity of different size populations detected by imaging flow cytometry: SV 175nm (red), RCDP from SCD PFP (low scatter, blue), 1.2µm filtered SCD plasma RCDP (low scatter, purple), 0.2µm beads (green), MaV from SCD PFP (high scatter, white), 0.5µm beads (orange) and 1µm beads (yellow). High scatter events (white MaV population) can be removed by filtration through a 1.2µm filter. Figure C was provided by Dr Tosti Mankelow.

3.9.3 Summary of populations identified using different methods

The results of the populations detected by different techniques are summarised in Figure 3.15. RCDP and AV from SCD plasma and CR media were found to expose extracellular and cytoplasmic domains of proteins, respectively, by flow cytometry. Their size was estimated to be 0.5-1µm for RCDP and below 0.5µm for AV by size beads (range 0.2-2µm using SSC feature), whereas 0.2µm beads could not be detected by the flow cytometer. Ex. GPA$^+$ from both sources were prevalent and FACS was used to isolated them. In an attempt to increase the yield of sorted ex. GPA$^+$ events, some SCD samples were pelleted and a population with lower scatter than what was detected in non pelleted plasma was revealed. Hence, three different populations were sorted: large GPA$^+$

events with high scatter from non pelleted SCD PFP and CR media, as well as lower and high scatter populations containing small and large ex. GPA$^+$, respectively, from pelleted SCD PFP. The protein content, morphology and size of these sorted populations were further assessed. Flow cytometry could detect sorted large GPA$^+$ events but not the small ones. Total protein could not be determined for any sorted population by the Bradford assay. Size was found to be 4-5μm for large GPA$^+$ events from SCD PFP and CR media and 3μm for small GPA$^+$ events by using DLS. The size of small GPA$^+$ events and SV 0.2μm, used as a control, could not be estimated by spinning-disk confocal analysis either. However, large GPA$^+$ events from SCD PFP were 7μm, which is the size of RBC. This is in line with the findings from conventional confocal, whereas the other 2 populations could not be detected.

Assuming that large sorted events from SCD PFP correspond to MaV, imaging flow cytometry was used to identify protein content and morphology of small and large GPA$^+$ events from SCD PFP, as well as unsorted plasma. Sorted small GPA$^+$ events, SV and size beads of 0.2μm were visualised for first time using this technology. Size estimation showed that small GPA$^+$ events were approximately 0.2μm, whereas MaV were larger than this, <0.5μm. When using bright field, detected populations revealed a size range starting from below 1μm, which corresponds to true microvesicles or AV and reaching to larger MaV of 7μm. Imaging flow cytometry proved more sensitive than conventional flow cytometry for small particle detection.

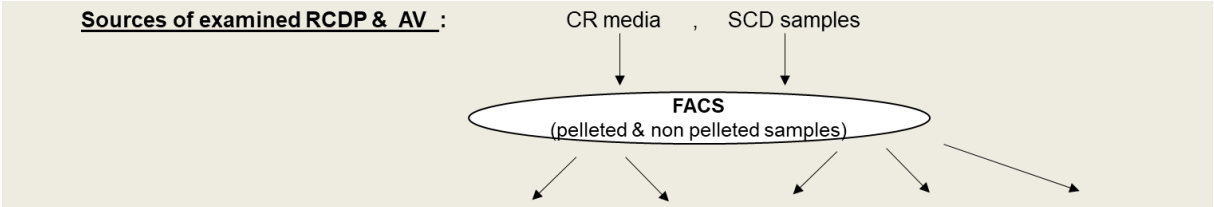

Analytical methods	Control		CR media		SCD PFP		
	Beads (0.2μm)	SV (0.2μm)	unsorted	sorted large GPA$^+$	unsorted	sorted small GPA$^+$	sorted large GPA$^+$
Flow cytometry	Not detected	Not detected	RCDP: 0.5-1μm	-	RCDP: ~0.5μm AV: <0.5μm	Not detected	detected
Bradford assay	-	-	-	Did not work	-	Did not work	Did not work
DLS	-	0.2μm	-	4-5μm	-	3μm	4-5μm
Confocal microscopy	-	-	-	Not detected	-	Not detected	1-7μm
Spin-disk confocal microscopy	-	Not detected	-	detected	-	Not detected	7μm
Imaging flow cytometry	detected	detected	-	-	detected	SSC: 0.2μm BF: <1μm	SSC: <0.5μm BF: ~6μm

Figure 3.15 Schematic of populations detected by different methods. Isolated sorted GPA$^+$ and unsorted RCDP from CR media and SCD PFP, as well as controls used and the methods investigated for analysis are shown. Hyphens indicate that the population was not examined by the method. Where applicable, size estimation is stated. BF - bright field.

3.10 Discussion

Defective SC and low reticulocyte maturation due to splenic dysfunction lead to release of free Hb and RCDP into the circulation (255). RCDP are thought to form during RBC maturation by membrane blebbing, resulting in right side-out microvesicles that expose PS (267, 269, 337). A number of studies have measured the presence of RCDP in SCD patients and healthy individuals and they have been reported to be more abundant in SCD patients, probably because of their inefficient clearance by patients' dysfunctional spleens (179, 180, 255, 269). Our colleagues have previously identified AV on the surface of maturing reticulocytes with an inside-out orientation, exposing PS and the cytoplasmic domains of RBC membrane proteins (127).

Identification and characterisation of RCDP in the plasma of SCD patients has generally been done by conventional flow cytometry, using antibodies targeting extracellular protein domains (267-269, 337). Here, we aimed to characterise RCDP and AV from cultured reticulocytes using a well-established protocol (123, 334), as well as SCD plasma. $CD34^+$ cells were isolated from aphaeresis cones and differentiated into enucleated reticulocytes, then, they were isolated and cultured to produce microvesicles. CR media was assessed by flow-cytometry and showed higher levels of ex. GPA^+ than the other cytoplasmic protein domains. This indicates that cultured reticulocytes mainly produce RCDP. The presence of membrane parts from reticulocytes along with intact RCDP is also possible. Despite of low AV levels detected in CR media, their presence was confirmed by the cytoplasmic RBC proteins using flow cytometry. This is in line with our collaborators' findings, detecting cytoplasmic protein domains of AV on the surface of cultured reticulocytes by microscopy (127). In our study, reticulocytes were removed from analysed CR media. It is probable that the low AV levels could indicate that these AV were attached on the reticulocyte surface and more time was needed so that AV can be released in the media. In this case, most AV were removed along with the cells during the centrifugation step and eventually, CR media contained less quantity of them.

Protein abundance on SCD PFP was found to be very heterogenous, as populations were difficult to discriminate by flow cytometry. For this, different PFP dilutions were tested in order to dilute the cellular debris. Plasma diluted 1:5 showed better discrimination than undiluted plasma and other dilutions tested. Furthermore, to overcome the difficulty of indistinct populations, as there was no appropriate isotype control available, human plasma was diluted with murine plasma and antibody titrations were carried out. Titrations were also carried out in SCD PFP diluted 1:5. These experiments confirmed that the antibodies used were human specific and did not stain murine cells. The heterogenous PFP population was also found to contain platelet remnants, remaining from the centrifugation step during PFP separation from RBC in blood. HLA class I cells, were also detected, since the plasma contains numerous types of nucleated cells that express HLA (303), such as T-cells, macrophages, dendritic cells and granulocytes.

Detection of the proteins that are important in alloimmunisation, such as Kell, Kidd and Duffy (120) by flow cytometry, was attempted. Routinely, such phenotyping is carried out by detecting haemagglutination by serology, using RBC from the donor and plasma from the patient (338, 339). RCDP would be expected to agglutinate since they are part of the RBC membrane, however, there is no evidence in the literature. Additionally, potential agglutination of RCDP would require large amounts in order clumping to be visualised. Thus, it was attempted to establish a protocol using flow cytometry, in order to be able to examine both RBC and plasma. Initially, SC were assessed and patients expressed the Kell protein highly. This indicates that these patients require matched Kell blood units to prevent development of alloantibodies that will haemolyse donor RBC post transfusion (322, 340). However, results for Kidd and Duffy indicated that the antibodies used were not suitable for flow cytometry analysis. Thus, further analysis of these proteins in SCD PFP was not carried out.

FACS was used to isolate RCDP from SCD PFP and CR media for further characterisation. Additionally, SCD plasma was pelleted by ultra-centrifugation (100,000g) to enrich RCDP, as a common method for exosome isolation (341, 342). Pelleted SCD PFP showed a low SSC population, whereas non pelleted plasma and CR media showed a higher SSC population. Ultra-centrifugation was also compared to high-speed centrifugation (20,000g) regarding number of low SSC RCDP and both provided similar results of low SSC events. Low scatter RCDP were hypothesised to correspond to microvesicles but they could not be visualised by conventional or spinning-disk confocal microscopy, neither conventional flow cytometry, so this could not be confirmed. High SSC RCDP corresponded to what was described as small microvesicles by others, using flow cytometry (179, 180, 255, 269). This population had a similar size to RBC when analysed by conventional and spinning-disk confocal microscopy. However, high SSC RCDP had a less integral membrane than that of RBC/SC, indicating that less bright populations correspond to defective membrane structures rather than intact cells and probably correspond to ghosts and MaV. Ghosts come from RBC haemolysis and contain RBC membrane but lack haemoglobin. *In vitro*, ghost membranes can be prepared by RBC hypotonic lysis and have been studied to understand the properties of RBC membranes (343). We recently showed that particles exposing both the extracellular and cytoplasmic domains of GPA or band 3 in SCD samples probably correspond to ghosts, indicating that the cytoplasmic domains were exposed during membrane sealing, after the release of Hb (Smith *et. al*, manuscript submitted).

Protein content of low and high sorted populations, from non-pelleted and pelleted SCD samples, was assessed using the Bradford assay. Although this protocol works fine for assessing protein in ghost membrane preparations and SV, we never managed to get reproducible results. This may be due to the limited number of sorted events used, as sorted populations were examined by different methods. Another reason might be the high level of glycosylation of these populations. As the Bradford dye binds amino acid residues (mainly arginine, lysine, tryptophan, phenylalanine and tyrosine) under acidic conditions (344), post-translational modifications like glycosylation, was found

to under-estimate the protein content measured by Bradford, when compared to unmodified proteins (345). This indicated that Bradford may not be a suitable protein assay for these glycosylated sorted populations.

Plasma from SCD patients was found to express all the RBC proteins tested by flow-cytometry: ex./cyt. GPA, ex./cyt. Band 3, cyt. GPC and GLUT1. Levels of extracellular GPA and band 3 were significantly higher than all the cytoplasmic domains tested. This showed that RCDP levels are higher than AV in SCD PFP. However, the flow cytometer failed to detect SV and size beads of 0.2μm, suggesting that it is not sensitive for small populations. Although that RCDP exhibiting extracellular RBC proteins have been detected by others using flow cytometry (268, 269, 337, 346, 347), our results indicated that small RCDP could not be detected. SCD PFP was also examined for PS exposure, as other groups have reported that RCDP were PS decorated (268, 269, 337, 346, 347). PS is usually found on the inner part of the RBC membrane and it is a known “eat me” signal for phagocytic cells (94). Its translocation on surface indicates disturbance in RBC symmetry, followed by RCDP formation and budding (95, 176). Furthermore, it is well known to cause hypercoagulation in SCD (333). PS levels were significantly elevated than ex. GPA, as well as GPA/PS decorated RCDP, which is in line to what was previously detected by flow cytometry in RCDP in SCD, associated with raping aging of SC (268, 269, 337, 346, 347). Since it was shown that AV also expose PS during their formation through membrane endocytosis (127), part of the PS^{+} RCDP detected by flow cytometry, could correspond to AV.

SCD PFP examination by imaging flow cytometry revealed a wide range of population sizes, from MaV and fragments of red cell membrane to small microvesicles, RCDP and AV. Similarly, when sorted pelleted and non pelleted SCD PFP were viewed by bright field imaging, it was found that high scatter particles mainly correspond to MaV and/or RBC ghosts and low scatter to small RCDP, probably exported by cellular blebbing during repeated cellular sickling and recovery (255). This demonstrates that circulating RCDP consist of different sizes rather than a single homogenous population, previously reported by flow cytometry (179, 180, 255, 269). Comparison of the results from imaging flow cytometry with those from conventional flow cytometry leads us to conclude that RCDP detected by many conventional flow cytometers are in fact not microvesicles but larger MaV. This could be attributed to differences in the light scattering intensity between biological particles and polystyrene sized beads (232).

Recently, we showed that RCDP are much more abundant in SCD PFP than AV (Smith *et. al*, manuscript submitted). Furthermore, similarly to previous studies using conventional flow cytometry (346, 347), there are significant differences in the numbers of RCDP present in the plasma of healthy individuals and SCD patients. Also, SCD patients in crisis exhibited significantly elevated numbers of right side-out RCDP and membrane fragments in plasma exposing both domains of GPA, likely formed by the sickling process (Smith *et. al*, manuscript submitted). The majority of MaV were

strongly PS positive. When this population was removed from SCD PFP, the plasma clotting time was increased more than 3-fold, whereas removal of all RCDP and MaV led to a 7-fold increase. These data indicate that removal of MaV and RCDP exposing PS could contribute to a novel therapy for hypercoagulation in SCD (Smith *et. al*, manuscript submitted).

DLS was used to get a size estimation of sorted samples. SV of known size 0.2μm, measured using nanoparticle tracking analysis by a colleague, gave similar readings to those obtained from DLS were in line with measurements. Low and high SSC RCDP were shown to be 3μm and 4-5μm, respectively. From the results of spinning-disk confocal analysis and imaging flow cytometry, size of high SSC RCDP seems to be under-estimated by DLS. However, all findings agree that sorted high SSC RCDP, which are the events detected by a conventional flow cytometer, mainly correspond to MaV. We conclude that DLS could be used for a rough estimation of RCDP size but not for accurate measurements. It could give accurate reading for small particles like SV though, as it has been reported to be accurate for monodisperse populations (224). For accurate results, other methods should be explored. Use of NTA was avoided in this study, as the estimated average particle size of the analysed population is required for instrument calibration, which was not the case for our samples.

In summary, we showed for the first time the heterogeneity of RCDP in SCD plasma, using imaging flow cytometry. Small microvesicles and AV were visualised and it was found that they substantially differ from RCDP detected by others using flow cytometry, as they were found to correspond to MaV and RBC ghosts. Imaging flow cytometry was more sensitive than flow cytometry for small particle detection. Knowing that removal of RCDP and MaV exposing PS reduces plasma clotting time, further characterisation of RCDP and AV in SCD PFP and healthy individuals is needed, as it may examine their role in pathology and health, or even reveal new biomarkers for SCD.

Chapter 4 Characterisation of red cell-derived, autophagic and storage vesicles

4.1 Introduction

Vaso-occlusion is a common feature in SCD, caused by blockage of blood vessels due to abnormal SC. The spleen, which is responsible for clearance of senescent and damaged cells, gets frequently damaged by SC too (52, 56). It is hypothesised that a dysfunctional spleen causes elevated numbers of RCDP and AV, as has been reported using flow cytometry (179, 180, 255, 269), since they can't be removed efficiently. In healthy individuals, RCDP are thought to be formed during reticulocyte maturation. In SCD however, repeated RBC sickling events probably lead to increased RCDP, contributing to higher RCDP levels.

Whereas RCDP are considered to have a right-side out orientation exposing PS (267, 269, 337), AV, as reported by our colleagues, are hypothesised to have an inside-out formation but exhibited PS as well (Fig. 4.1) (127). In the previous Chapter, we attempted to examine the role of RCDP and AV in SCD and concluded that what others have identified as RCDP in SCD by flow cytometry (179, 180, 255, 269) were probably MaV and RBC ghosts. Imaging flow cytometry revealed the differences in scatter between biological samples and size beads that others have used to determine RCDP size and indicated less accurate estimation in the light scattering intensity detected by flow cytometry (232). We have recently found that RCDP levels were increased in SCD patients in crisis compared to those in steady state. Additionally, removal of MaV was shown to decrease the blood clotting times, which suggested that their removal could reduce vaso-occlusive episodes in SCD (Smith *et. al*, manuscript submitted). However, the role of RCDP and AV has not yet been explored. Isolation and further characterisation of enriched RCDP and AV in healthy individuals and SCD, as well as exploring the differences in the proteome, could reveal potential biomarkers to predict painful vaso-occlusive episodes in patients.

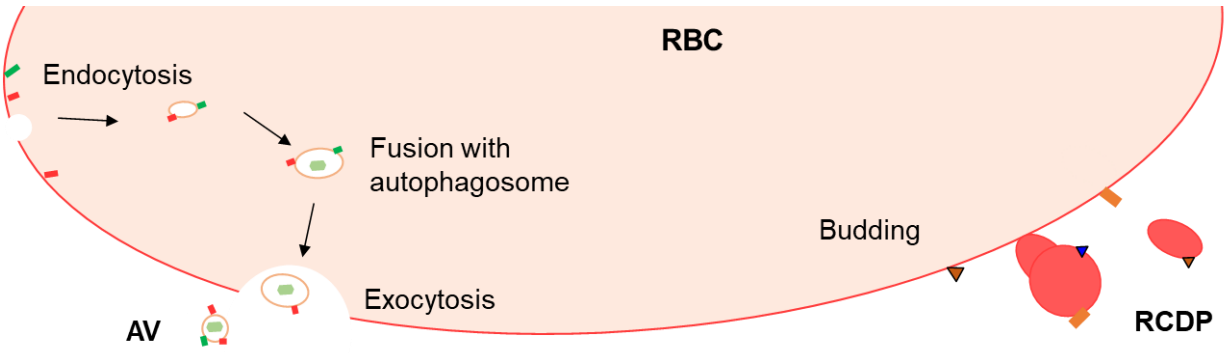

Figure 4.1 Hypothetical mechanism of autophagic vesicle and red cell-derived particle formation. AV are formed via the RBC membrane internalisation by endocytosis and fusion with an autophagosome. A large particle is formed, then AV are released extracellularly and exposing the cytoplasmic components of the RBC. RCDP are formed by membrane budding and expose the extracellular components.

Microvesicle isolation usually takes place using sequential or ultra-centrifugation (348). In this Chapter, the quality of isolated RCDP and AV from SCD and healthy plasma was compared using FACS in pelleted and non pelleted samples, as well as immunomagnetic separation as an alternative to pelleting. Potential MaV presence in enriched RCDP was examined by microscopy. TEM was used to assess the morphology of enriched RCDP and AV, while DLS provided size estimation of the isolated populations. Imaging flow cytometry was used to assess RBC protein exposure on enriched RCDP and AV along with calcein AM, a marker for intact MP (349). Annexin V that detects PS exposure, indicating apoptosis, (335, 336) was also used. Finally, differences in the proteome among enriched RCDP and AV from SCD and healthy plasma were investigated. In most experiments, SV from outdated blood units (day 35) were examined as a comparison to RCDP.

RESULTS

4.2 Red cell-derived particle, autophagic and storage vesicle isolation and characterisation

4.2.1 Optimisation of particle enrichment in plasma using immunomagnetic beads

4.2.1.1 Comparison of isolation methods and morphology examination

In experiments to date, isolation of RCDP and AV was carried out by FACS of samples pelleted by either ultra- (100,000g) or high-speed (20,000g) centrifugation (Chapter 2.5.1). The morphology of these ex. GPA^+ sorted populations was examined by TEM, in order to identify whether these sorted RCDP were true microvesicles or membrane fragments. However, during early TEM experiments, visualising sorted pelleted GPA^+RCDP was not possible. Instead, only membrane fragments were observed (Fig. 4.2A). Hence, instead of RCDP it was decided to use controls, such as SV (used in Chapters 3.3.3.1 and 3.5.1.5), which were expected to have similar morphology to RCDP, since both particle types originate from RBC. SV were shown to be round, enclosed by a lipid bilayer (Fig. 4.2B). Also, RCDP enriched by magnetic beads coupled to anti-ex. GPA (see Chapter 2.5.2), were tested. It was hypothesised that as these beads would surround RCDP, they may improve detection by TEM. Indeed, these beads were observed even to cover pelleted RCDP in some cases (Fig. 4.2C). At higher magnifications, magnetic beads appeared as roundish, grey structures on RCDP. Round and tubular RCDP structures were also observed in pelleted and non pelleted samples (Fig. 4.2D). Low RCDP levels, initially detected in sorted pelleted SCD PFP by TEM, led us to question the efficiency of the isolation method. Ultra-centrifugation sediments small size particles (348) but practically the sedimentation of all small particles is impossible. Additionally, the sorter could not sort particles below 0.2μm (see Chapter 3.5.1.5), hence small PFP particles could not be isolated. Furthermore, despite the fact that centrifugation at high velocities is a common method for MP isolation (341, 342), the potential damage to RCDP and AV due to the high speed was a concern. The morphology of enriched RCDP by both methods was further examined by TEM, in order to identify if isolated particles were MP or RBC membrane fragments.

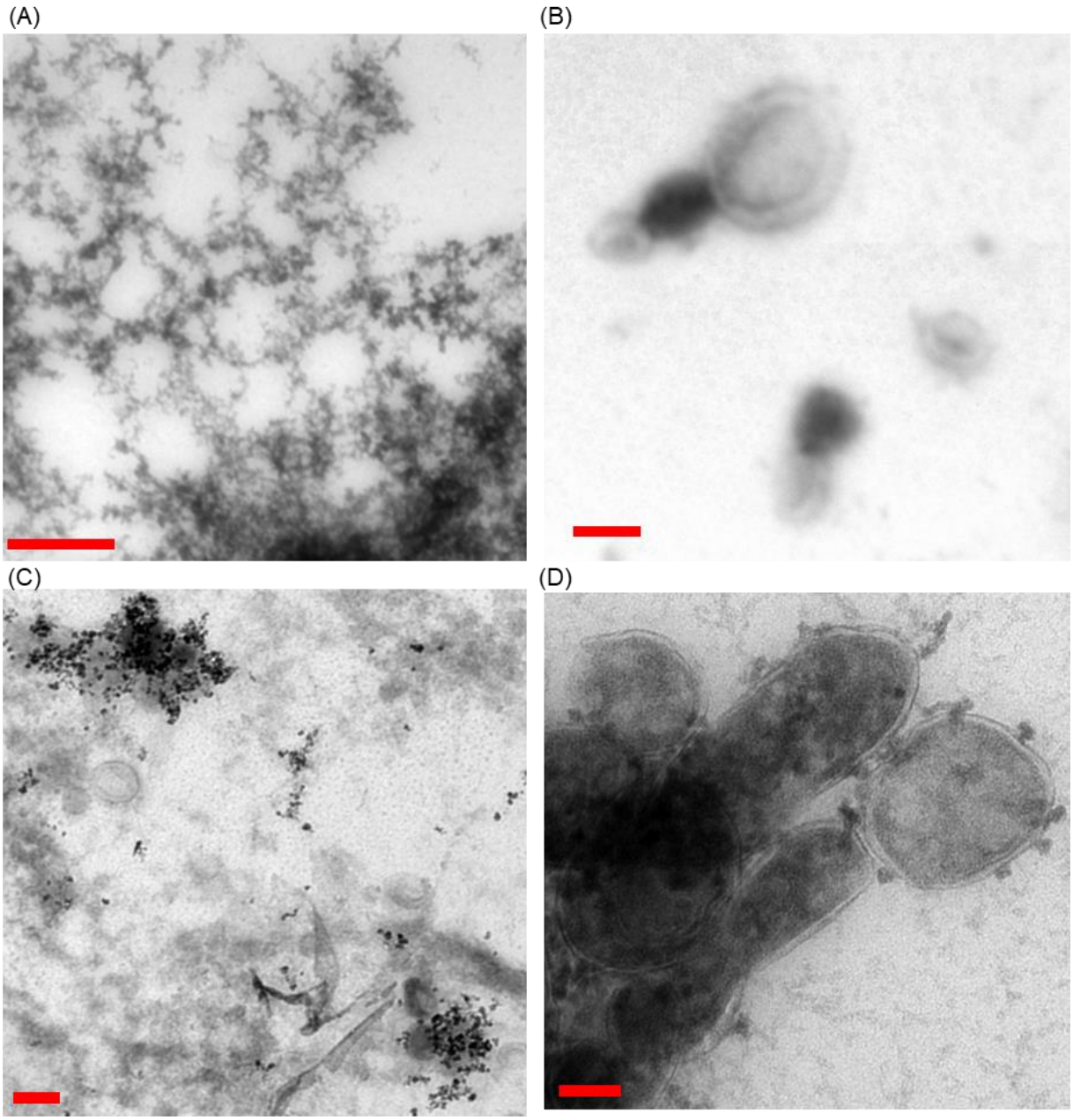

Figure 4.2 Morphology examination of enriched red cell-derived particles by two different methods on TEM. (A) Small sorted pelleted RCDP were mainly comprised of membrane fragments rather than round particles. Image is representative of 15 samples. **(B)** Round SV from 1 blood unit. **(C)** RCDP isolated from pelleted and **(D)** non pelleted SCD PFP. Magnetic beads (~50nm) appeared as roundish, dark structures surrounding circular and tubular RCDP. Scale bars indicate (i) 0.5μm (ii-iii) 0.2μm and (iv) 0.1μm.

4.2.1.2 Examination of macrovesicles present in enriched particles from filtered plasma

Prior to magnetic isolation, PFP was filtered (3μm) to remove MaV and ghosts. RCDP, enriched from SCD PFP using beads, were stained with anti-ex. GPA and then examined by confocal microscopy (Chapter 2.9.1), using a newer microscope (Leica SP8 Inverted Confocal Microscope System) than what was previously used in Chapter 3.8. The results showed that detected particles close to 5μm in size were probably MaV and ghosts and were not retained by the filter (Fig. 4.3Ai). This was also confirmed in several RCDP preparations by TEM (Fig. 4.3Bi). Interestingly, in all cases, detected MaV were shown to "contain" RCDP (Fig. 4.3Aii, Bii). Furthermore, it was revealed that immunomagnetic separation could isolate RCDP below 0.2mm (Fig.4.3Bii), whereas FACS failed.

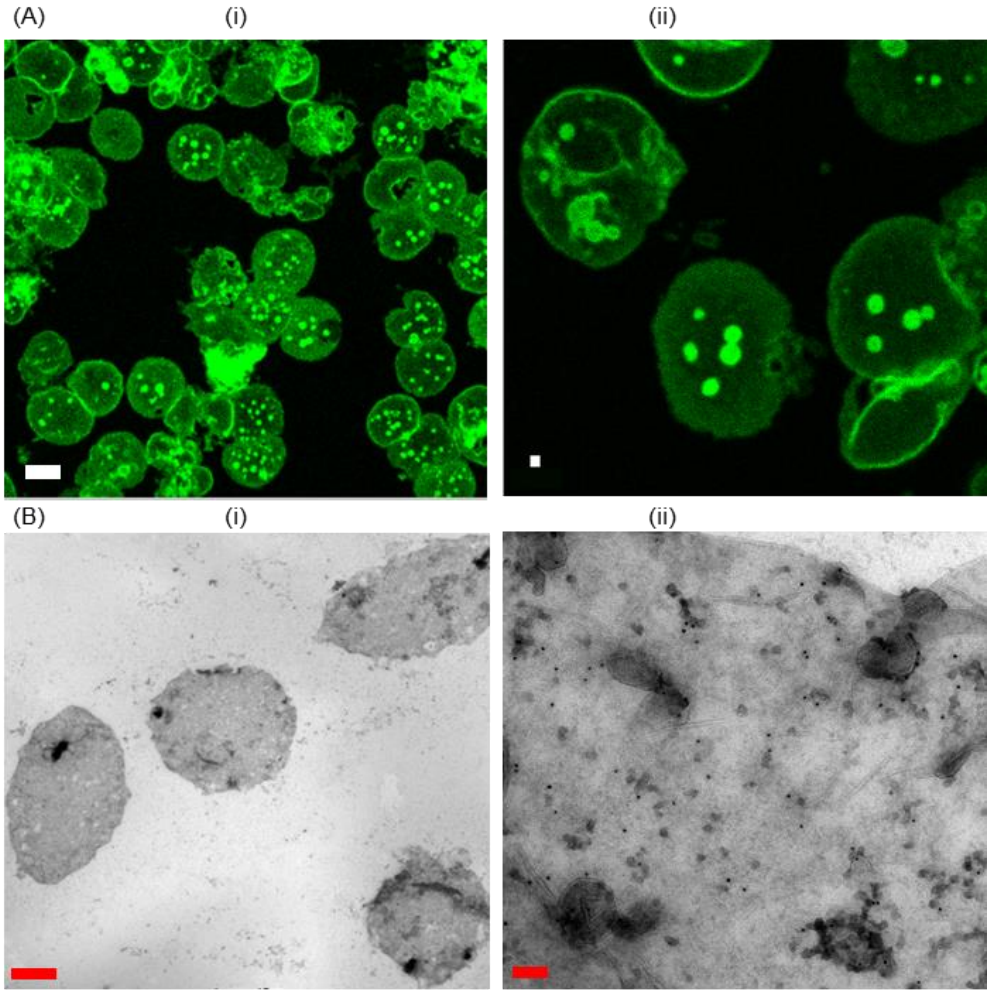

Figure 4.3 Examination of enriched red cell particles from 3μm filtered plasma. **(A)** Confocal analysis of enriched RCDP stained with anti-ex. GPA-FITC. Round MaV larger than 5μm were observed (i). Green dots represent RCDP bonded to MaV. Enlarged image of the same sample (ii). Images were from 1 experiment and visualised using 400X magnification. Scale bars indicate 5μm (i) and 0.5μm (ii). **(B)** TEM images of MaV present in isolated RCDP, representative from 10 samples. (i). Magnified section of an MaV, where small RCDP are present, probably bonded by beads (ii). Scale bars correspond to 2μm (i) and 0.1μm (ii).

The presence of RCDP inside or on MaV could be due to bonding, either during initiation of coagulation by PS or by the magnetic beads used for isolation (Fig. 4.4Ai and ii). To remove MaV from RCDP preparations, PFP was filtered (1.2μm), then filtered samples were imaged by TEM (Fig. 4.4Bi and ii respectively). Similar to what was previously observed by imaging flow cytometry, MaV were retained by such a filter (Fig. 4.4 and Chapter 3.9.2). It should be mentioned though that when PFP was passed through a 3μm filter by gravity instead of using a plunger, no MaV were found.

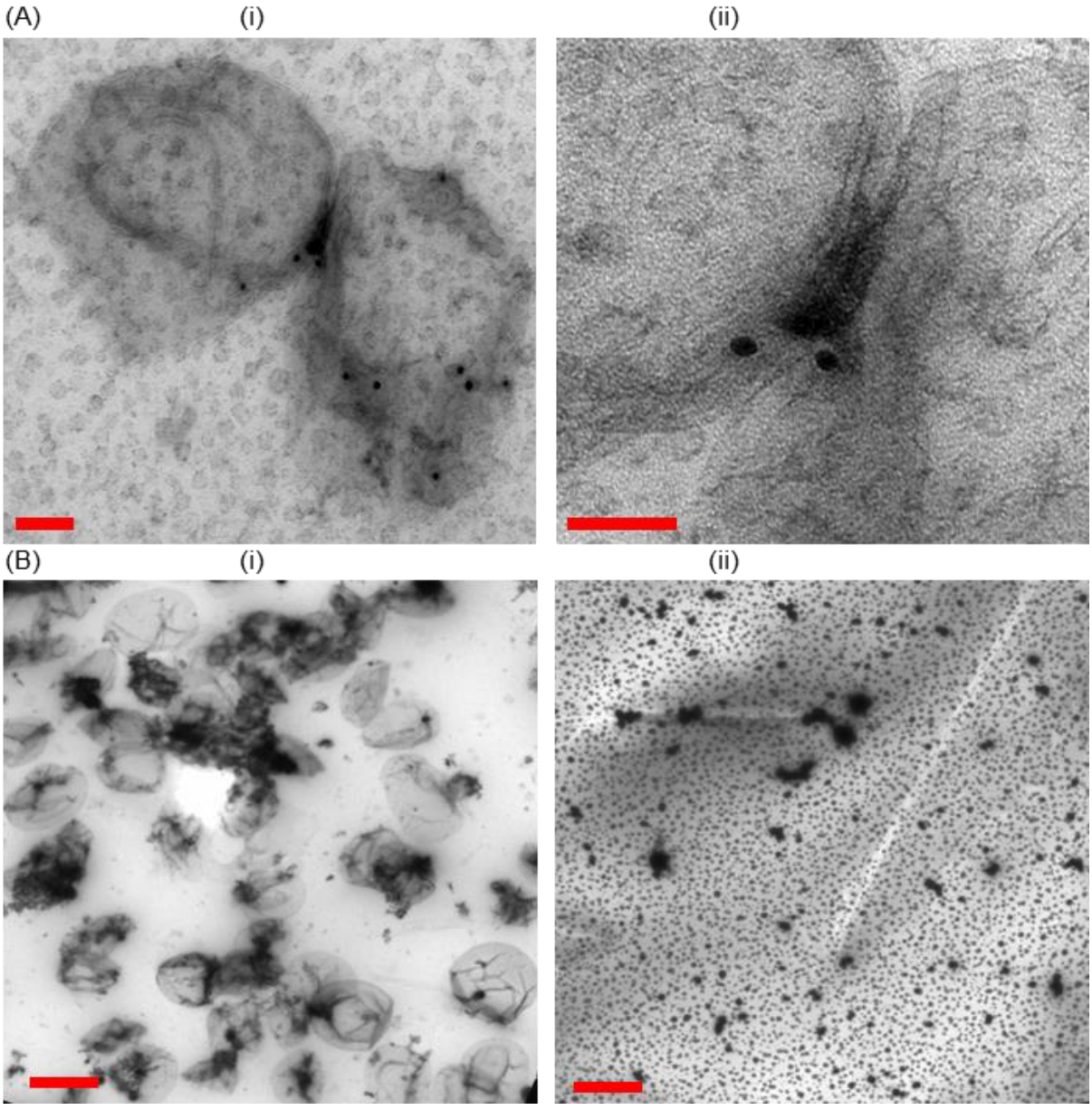

Figure 4.4 Examination of different filters in macrovesicle removal from enriched particles. (A) TEM image of two MaV bonded with immunomagnetic beads (i). Magnification of the bonding site. The beads (~50nm) appear in the middle as a dark blob. Scale bars indicate 100nm (i) and 50nm (ii). TEM images are representative from 20 SCD samples tested. **(B)** RCDP enriched from 3μm (i) and 1.2μm (ii) filtered SCD PFP. Black spots are stained by immunolabelling. Scale bars indicate 5μm.

4.2.1.3 Antibody contribution to the total protein.

So far, the examined populations were isolated using either FACS or magnetic beads. Both methods, however, included the use of an anti-GPA antibody, which targeted the RCDP. In order to be able to carry out any protein determination, like protein assays or proteomic profile analysis, the contribution to the total protein content of the antibody used for sorting (BRIC256), as well as the immunomagnetic beads, was examined by SDS-PAGE and Coomassie blue staining, to visualise the total protein in each lane.

Samples analysed were:
1) sorted small GPA^+ from pelleted (100,000g) SCD plasma (patient 17)
2) sorted small GPA^+ from pelleted (100,000g) SCD plasma (patient 18)
3) isolated RCDP using anti-ex.GPA beads from pelleted (100,000g) SCD plasma (patient 18)
4) isolated RCDP using anti-ex.GPA beads from pelleted (100,000g) SCD plasma (patient 19)
5) isolated RCDP using anti-ex.GPA beads from pelleted (20,000g) SCD plasma (patient 19)
6) 1/5 the quantity of (4)
7) 1/5 the quantity of (5)

Using the above samples, total protein was compared in RCDP isolated from FACS and magnetic beads in samples pelleted by ultra-centrifugation (Fig. 4.5, lanes 1-3). Ultra- and high-speed centrifugation were compared in enriched samples using anti-ex. GPA beads (lanes 4-7). Since there was no information in the literature regarding running sorted RCDP on a gel, 3 sample volumes were tested: 1x quantity for sorted populations (1-2) which were relatively pure, as they comprised of sorted GPA^+ events only. For GPA^+ events enriched using beads, samples were eluted in MACS buffer in the end of the isolation step (see Chapter 2.5.2) and therefore were diluted. For comparison, patient plasma used for sorting in lane (2) was also used for RCDP enriched using beads in lane 3. In lanes 6-7 double the quantity of plasma was used compared to 1-3. Lanes 4-5 contained the same samples as 6-7 but a 5x RCDP quantity was used (10x compared to lanes 1-3), in case these samples had a very low protein content. Despite the different RCDP quantities used, final sample volumes loaded in the lanes were all the same, topped up with sample buffer (see Chapter 2.11.5).

The results showed that RCDP enriched by ex. GPA beads (lanes 3-7) contained more protein than RCDP sorted by FACS, especially between 50-80kDa (Fig. 4.5). This was obvious among samples 1-3, which all had the same RCDP quantity and sample 3 revealed stacked protein bands not observed in 1 and 2. The highest protein content was observed in samples 4 and 5 that had the highest RCDP quantity of all samples tested. Other protein bands below and above 50-80kDa were observed, especially for samples 4-7 (Fig. 4.5 indicated with dots). As the molecular weight of GPA detected on a gel ranges from 50-100kDa (~98kDa for dimer, ~60kDa for GPA/GPB and 30kDa for the monomer) (350, 351), the results from lanes 3-6 indicated that the immunomagnetic beads used in lane 3 contributed more to the total protein than the antibody used for sorting (lanes 1-2) but this

would need to be confirmed. As beads could be used in non pelleted PFP, RCDP damage due to high velocity in pelleted plasma would be avoided. Also, TEM imaging showed that immunomagnetic separation could isolate smaller RCDP than FACS (part ii). Hence, it was decided that RCDP enrichment would only be carried out using magnetic beads.

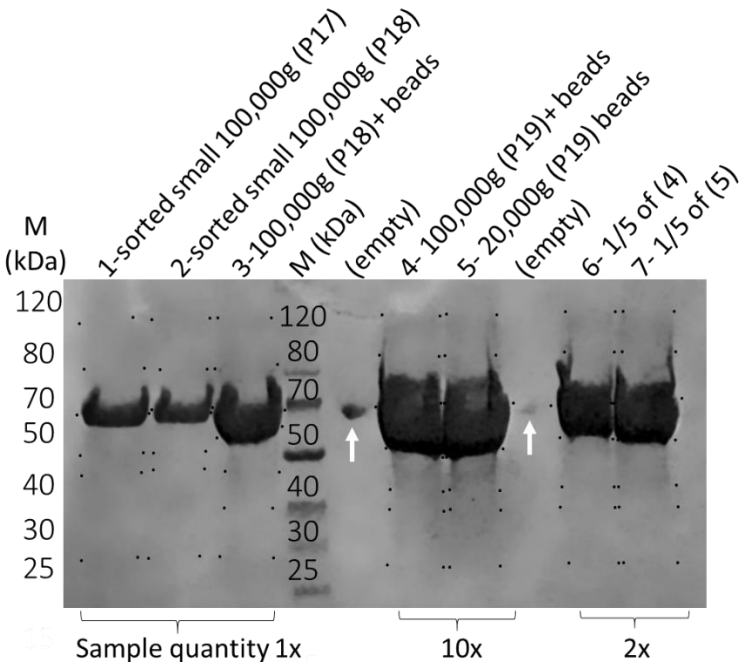

Figure 4.5 Comparison of total protein in samples enriched by FACS and magnetic beads. RCDP from 3 SCD patients' plasma (P17-19), enriched using ultra- (100,000g) and high-speed (20,000g) by FACS (low SSC events, lanes 1-2), or immunomagnetic beads (3) were run on a gel code blue stained SDS-PAGE. RCDP from non pelleted plasma, enriched using beads were also examined (lanes 4-7) to determine protein content. Different RCDP quantities are indicated. Molecular weight markers (M) indicated in kDa. Detected protein bands on the samples are indicated by dotted lines. White arrows indicate sample spillage in empty lanes from the nearby samples. Image is representative from one experiment.

4.2.1.4 Extent of antibody contribution to protein content.

To examine the contribution of the magnetic beads to the total protein content, beads along with anti-ex. GPA (BRIC256) antibody were run on a Coomassie blue stained gel. The antibody was used to indicate the apparent molecular weight of GPA, as the theoretical molecular weight of the dimer is 39kD. In parallel, RCDP from a SCD patient (P20) were isolated using 3 different bead concentrations (3, 1.5 and 0.75%(v/v)) . Half of the samples were non pelleted (Np.A, Np.B, Np.C) and the other half were pelleted (p.A, p.B, p.C, Fig 4.6A). The rationale behind this was that unbound beads would pellet and enriched RCDP would remain in the supernatant. Pellets and supernatants (supern.) were run separately, to identify whether pelleted magnetic beads contributed to the total

protein content. Detected bands from the antibody indicated by black arrows, showed that the apparent molecular weights were 69kDa for the GPA dimer, 52kDa GPA/GPB and 27kDa the monomer (Fig 4.6B). Similar bands to the first two were observed in all PFP samples, apart from the pellets and the samples that contained beads only. Other protein bands were also observed (indicated by horizontal yellow arrows). Bands detected in the pellets revealed far less protein than supernatants. Visual examination of protein isolated using bead concentrations 3-1.5%(v/v) did not show differences in the enriched protein, whereas 0.75%(v/v) isolated lower amounts. Protein bands were not quantified though.

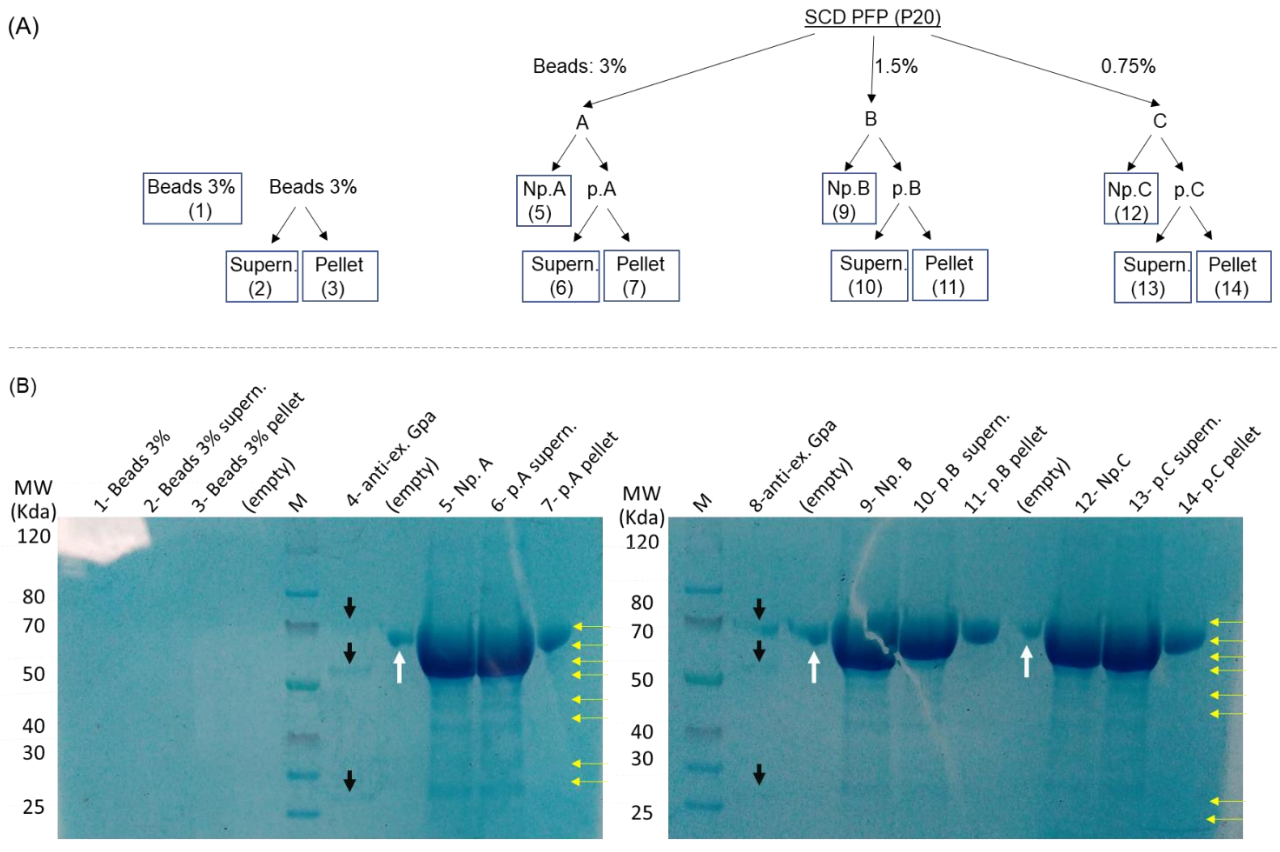

Figure 4.6 Assessment of beads contribution to the total protein. (A) Schematic of the sample processing. Immunomagnetic beads and non pelleted SCD PFP from one patient (P20) were isolated using 3 different bead concentrations: 3,1.5 and 0.75%(v/v) (Np.A, Np.B, Np.C). Half of these samples were pelleted (p.A, p.B, p.C) and pellets and supernatant (supern.) were analysed separately. Squares indicate tested samples and number corresponds to the lane indicated on the gels below. **(B)** Coomassie blue stained gels of protein identified in pelleted and non pelleted samples: immunomagnetic beads (wells 1-3), anti-ex. GPA (wells 4,8), Np.A-C (5,9,12) and p.A-C (6-7, 10-11, 13-14 for PFP). Bright area on top left was caused by light reflection during imaging. Molecular weight markers (M) indicated in kDa. Black vertical arrows indicate bands of the antibody and white vertical arrows sample spillage in empty lanes from the nearby samples. Horizontal yellow arrows indicate protein bands observed.

In order to identify which protein corresponded to band of approx. 69-70kDa weight, which was present in all samples in the experiments above, the band from lane 1 of gel in Figure 4.5 was cut and sent for mass spectrometry (see Chapter 2.12.1). Results showed that this protein corresponded to BSA, which was present in both enriched samples. Sorted samples were collected in PBS, however, BSA was present in the buffer during the staining step before FACS (see Chapter 2.8). In samples enriched using immunomagnetic beads, BSA was present in the PBS eluting buffer (see Chapter 2.5.2). For all future experiments using magnetic beads, albumin was not added to the elution buffer after communication with the manufacturer. However, most importantly, the appearance of bands different to GPA (yellow arrows in Fig. 4.6) showed the presence of other proteins at adequate levels to be detected by a Coomassie blue staining.

4.2.1.5 Bead concentration optimisation for red cell-derived particle and autophagic vesicle isolation

The findings from assessing different bead concentrations led us to consider which would be the best to isolate most RCDP from SCD PFP without saturating the sample. At the same time, optimisation for AV isolation was carried out. Commercial beads detecting extracellular GPA were available at the time of the experiments but not against cytoplasmic GPA. For this reason, it was decided to use one of the antibodies detecting cyt. GPA (BRIC163) or band 3 (BRIC155 or BRIC132) conjugated to AF647, as described in Chapter 2.3. Then, commercial beads against AF647 were used and AV were eluted similarly to RCDP (Chapter 2.5.2). In most cases, SCD plasma was split into 2 parts, each to be enriched for RCDP or AV.

Initially, our colleagues suggested 10-4%(v/v) anti-ex. GPA beads for RCDP enrichment. This was based on observations by imaging flow cytometry, where using these concentrations GPA RCDP could not be detected in the flow through buffer used to wash RCDP and beads, therefore they were retained by the magnet (see Chapter 2.5.2). No information was available for the anti-AF 647 beads. To determine the recovery of enriched RCDP and AV, samples enriched from 4 SCD samples using 4%(v/v) beads targeting ex. GPA^+ and cyt. GPA^+ respectively, were analysed by imaging flow cytometry. Then, absolute counts were identified in plasma and enriched populations. Results were variable, with recoveries ranging 8-33% for RCDP and 4-43% for AV (see Table 4.1) and conclusions could not be made.

Table 4.1 Purity calculation before and after vesicle enrichment from plasma using 4% beads.

SCD PFP	RCDP/ml in plasma (pre) x10^6	RCDP/ml (post) x10^6	%RCDP recovery	AV/ml in plasma (pre) x10^6	AV/ml (post) x10^6	% AV recovery
21	5.03	1.67	33.27	39.55	1.61	4.06
22	76.89	11.03	14.35	6.10	2.24	36.68
23	86.23	6.85	7.94	18.50	1.34	7.23
24	12.64	1.16	9.20	2.77	1.18	42.76
Mean	45.20	5.18	16.19	16.73	1.59	22.68
SD	42.27	4.67	11.72	16.65	4.65	19.87

To further investigate the bead concentration, different patient samples enriched by different bead concentrations starting from 4% were assessed by TEM, in order to identify potential saturation with beads in samples. From this, it was revealed that even 1%(v/v) anti-ex. GPA beads was saturating the sample (Fig. 4.7, left). After assessing the morphology of different bead concentrations, the optimum one was found to be 0.35%(v/v) for RCDP and 0.12%(v/v) for AV (Fig. 4.7). Tubular and round RCDP were also observed.

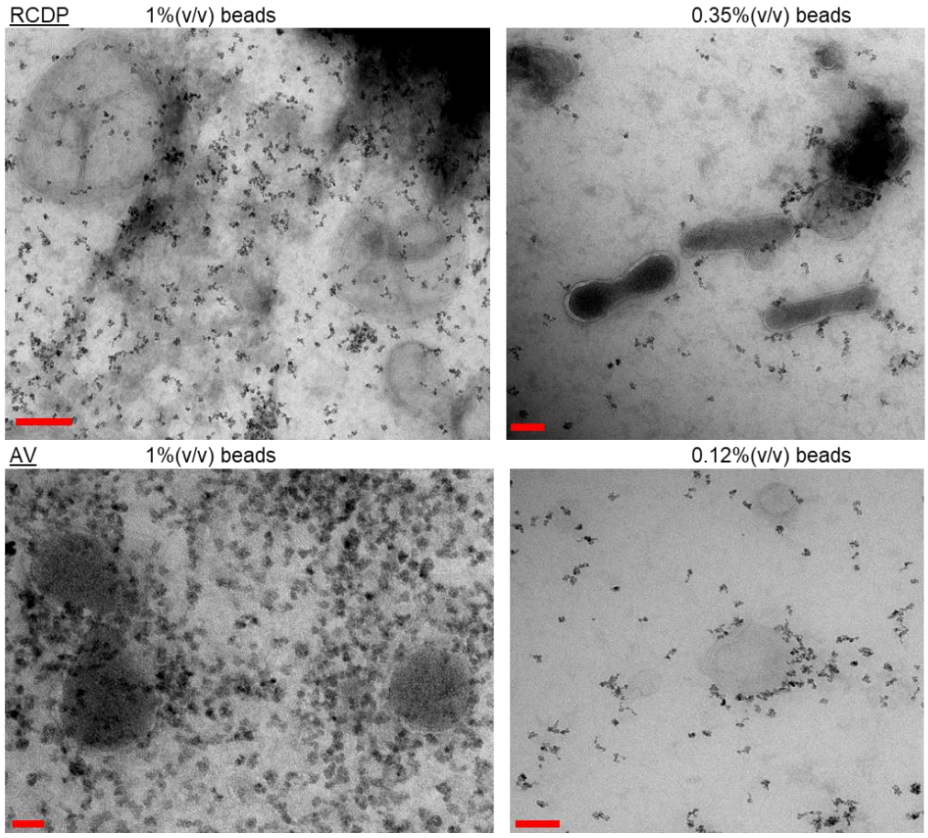

Figure 4.7 Examination of bead saturation by TEM. Enriched RCDP (above) using immunomagnetic beads 1%(v/v) (left) and 0.35%(v/v) (right) were examined by TEM, enriched AV (below) using 1%(v/v) (left) and 0.12%(v/v) (right) beads. Scale bars indicate 200nm (top left), 50nm (bottom left) and 100nm (right column). Images are representative from at least 3 samples tested.

4.3 Morphology of enriched populations in health and sickle cell disease

4.3.1 Red cell-derived particles and autophagic vesicles

In order to ensure isolation of true MP rather than membrane fragments, RCDP and AV were examined by TEM. The presence of extracellular (for RCDP) and cytoplasmic (for AV) domains of GPA and band 3 was confirmed by immunogold staining (Chapter 2.9.3). RCDP detected were larger and more abundant compared to AV. Despite the unavoidable presence of membrane fragments due to sickling, both types were mainly found as round particles with an external lipid bilayer (Fig. 4.8A for RCDP and B for AV). AV were not found to form rod structures, in contrast to tubular RCDP shown before (Fig. 4.2 and 4.7). This is probably due to their formation through endocytosis. Magnetic beads appeared as circular, grey structures (blue arrows) and gold particles (~10nm) as black dots (yellow arrows). Enriched RCDP were stained with anti- ex. GPA or band 3 (BRIC256 or BRIC200, respectively). Isolated AV were already stained with cyt. GPA- or band 3-AF 647, as part of the isolation protocol (Chapter 2.5.2). As previously observed by imaging flow cytometry (Chapter 3.9.2), there was a great diversity in size amongst RCDP found in the plasma of SCD patients (Fig. 4.8Ci). Moreover, the TEM results showed that RCDP and AV (stained only against extracellular or cytoplasmic proteins domains, not both) are structures with an intact plasma membrane (Fig. 4.7, and Fig. 4.8). CR media from 1 culture (discussed in Chapter 3.2) was examined by TEM, however, no MP were detected. RCDP and AV from healthy donors were also isolated using magnetic beads 48h from blood collection. After immunogold labelling, round and tubular RCDP were detected in different sizes (Fig. 4.8Ci), as was found for SCD RCDP. Detection of AV was also possible and round structures with a lipid bilayer were detected (Fig. 4.8Cii). Comparison of the morphology of RCDP and AV from healthy and SCD plasma did not reveal differences.

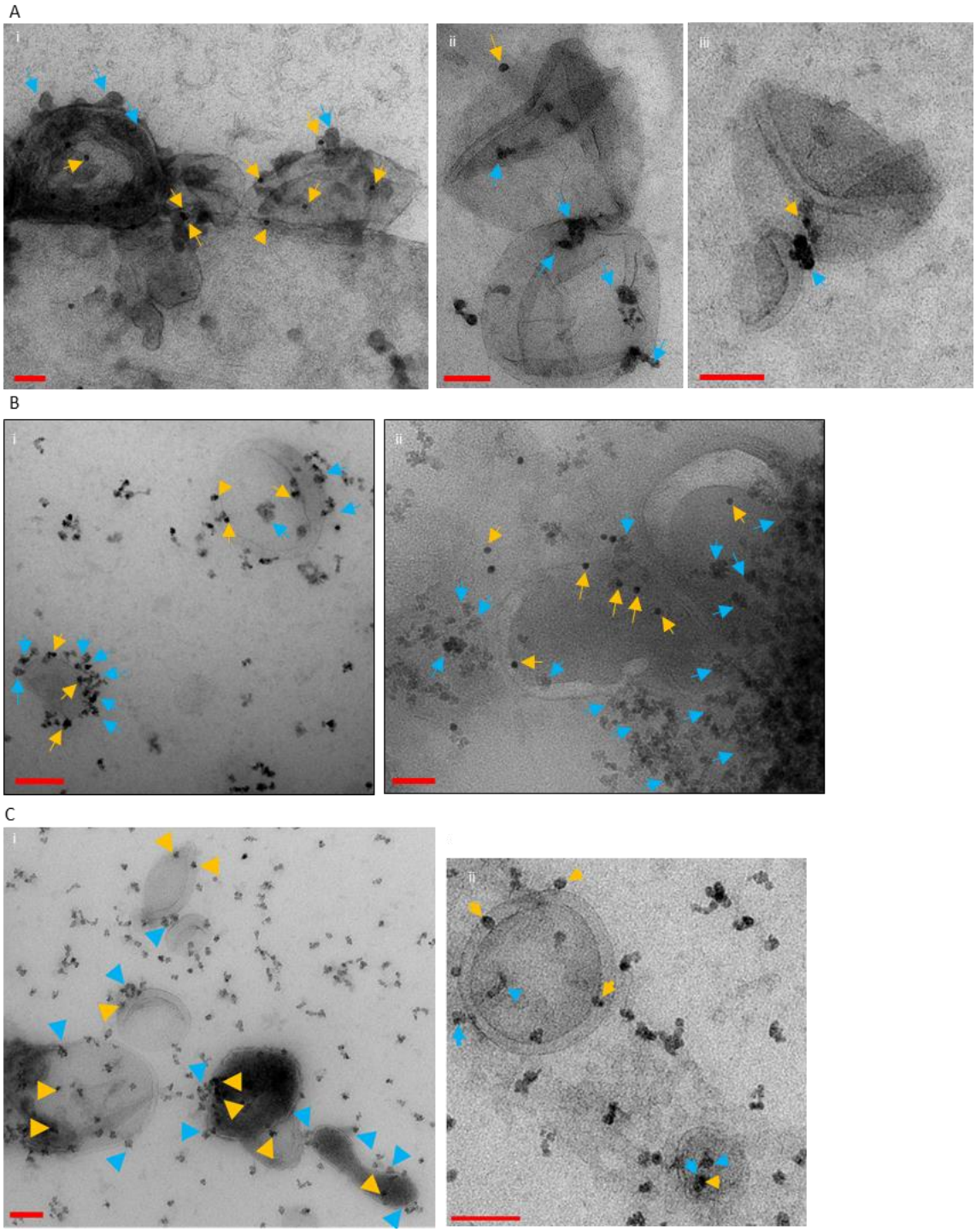

Figure 4.8 TEM of enriched red cell-derived particles and autophagic vesicles. (A) Isolated RCDP from SCD PFP were stained using (i) immunogold labelled ex. GPA (R10) or (ii) & (iii) ex. Band 3 (BRIC200). Red scale bars indicate 50nm (i) or 100nm (ii and iii). **(B)** AV from SCD PFP either (i) cyt. Band 3 (BRIC155) positive were stained with gold cyt. Band 3 (BRAC66) or (ii) cyt. GPA (BRIC163) positive were stained using gold cyt. Band 3 (BRAC66). Red scale bars indicate 100nm (i) or 50nm (ii). **(C)** Isolated RCDP were stained using gold ex. GPA (R10) (i) and AV stained with cyt. GPA (BRIC163) (ii) from healthy PFP. Scale bars indicate 100nm (i) & (ii). Yellow arrows indicate immunogold particles and blue magnetic beads. All images are representative from at least 3 samples.

4.3.2 Storage vesicles and storage effects

Apart from RCDP and AV, the morphology of 3 SV preparations was examined. These SV were formed by RBC budding during storage (165, 352) and were isolated from outdated blood units (day 35) by centrifugation (Chapter 2.2.3) then immunogold labelling followed. SV were found to form round and tubular structures surrounded by lipid membranes (Fig. 4.9A). Gold particles detecting ex. GPA were also observed (yellow arrows). In addition, old SV isolated 49 days after blood collection from one blood unit were also examined (Fig. 4.9B). Despite the presence of gold particles detecting ex. GPA on several SV, their shape had changed remarkably, probably because of biochemical alterations during storage, forming irregular structures. Generally, SV lost their round shape and less ex. GPA could be seen.

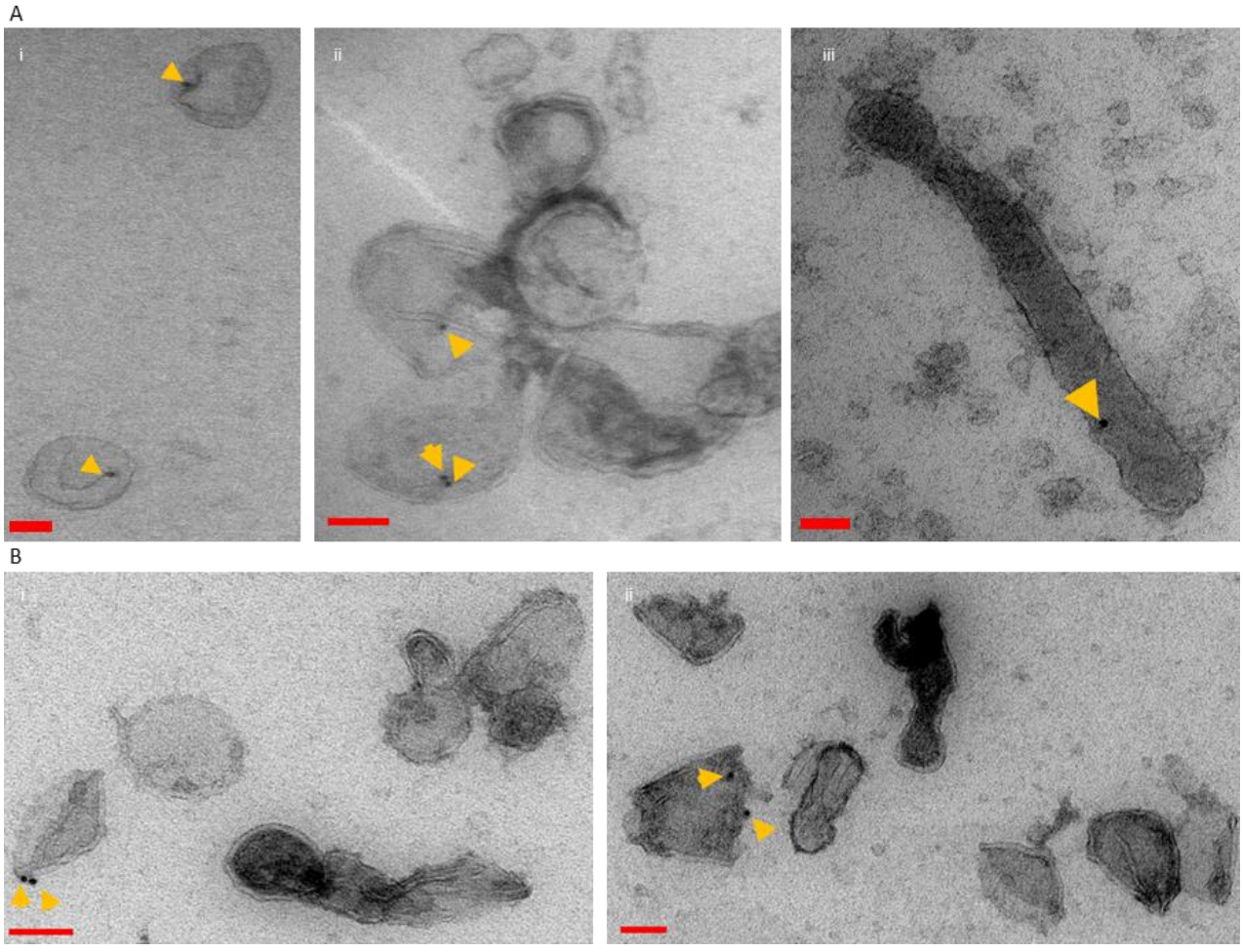

Figure 4.9 TEM of storage vesicles. (A) SV were isolated on day 35 by centrifugation, then stained using immunogold labelling against ex. Band 3 (i) or ex. GPA (ii & iii). Red scale bars indicate 100nm (ii & iii) or 50nm (iii). **(B)** SV isolated on day 49 and stained for ex GPA. Red scale bars indicate 100nm (ii & iii). Yellow arrows indicate immunogold particles. Images in (A) are representative of 3 SV preparations and images in B of 1.

4.3.3 Imaging storage vesicles by super resolution microscopy

So far, confocal microscopy could detect RCDP close to 1μm but it was not found sensitive enough to detect smaller RCDP, as they were close to instrument's diffraction limit. For this, super resolution microscopy was carried out on SV preparations (day 35), as it was easier to enrich high numbers due to the isolation method used (Chapter 2.2.3). Then, SV were stained with anti-ex. GPA or anti-ex. Band 3 (Fig. 4.10 left and right, respectively). For first time, it was possible to detect particles below 1μm, as observed above on a confocal microscope (see Fig. 4.3A). This indicated that visualisation of enriched RCDP and AV by confocal microscopy was possible. However, it was not carried out due to lack of time.

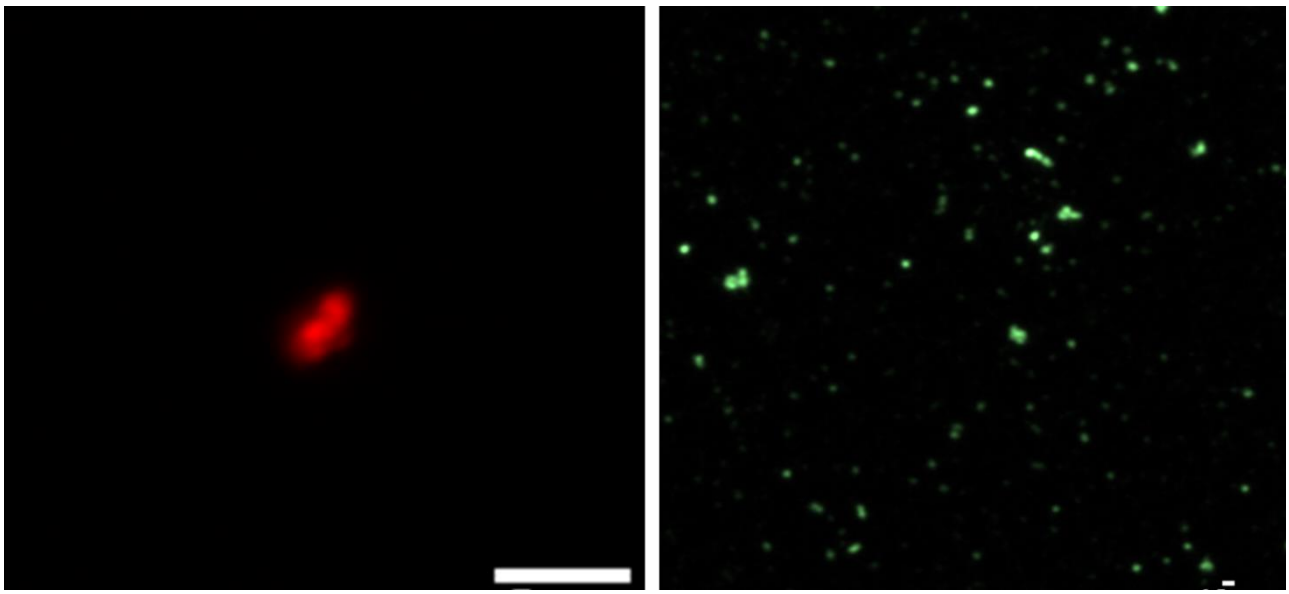

Figure 4.10 Protein detection in storage vesicles. Images from 2 SV preparations were stained with anti-ex GPA-AF 647 (left) or anti-ex. Band 3-AF 488 (right). White bars represent 5μm (left) or 0.5μm (right). Image was captured using 1000X magnification.

4.4 Size determination of enriched red cell particles, autophagic and storage vesicles by DLS

The size of RCDP and AV from SCD and healthy PFP isolated using immunomagnetic beads, as well as SV (day 35) preparations was estimated using DLS. Since RCDP and AV contained magnetic beads (50nm), the instrument could have miscalculated the size by up to 100nm, in cases where 2 beads were bonded on anti-diametric positions on the MP. As described in Chapter 3.7, DLS failed to read polydisperse samples and so enriched RCDP and AV from only 3/10 plasma samples, could be measured by the instrument. First peak (PK1 on the table) at 6-9nm corresponded to buffer particles and it was observed in all experiments. RCDP, readings from 1 SCD sample (P21) and 1 healthy (H1) showed 2 peaks around 60 and 480nm, suggesting similar RCDP sizes between SCD and healthy individuals. However, a second sample from a healthy individual (H2), revealed one

peak at 193nm, demonstrating size variability between healthy samples. A small peak at approx. 5.5µm was detected (Fig. 4.11A, not shown on the table), which probably corresponds to large membrane fragments. It should be considered that since all these particles are bonded with magnetic beads, the reading of 50nm probably corresponds to unbound beads and therefore RCDP detected ranged from 150-420nm.

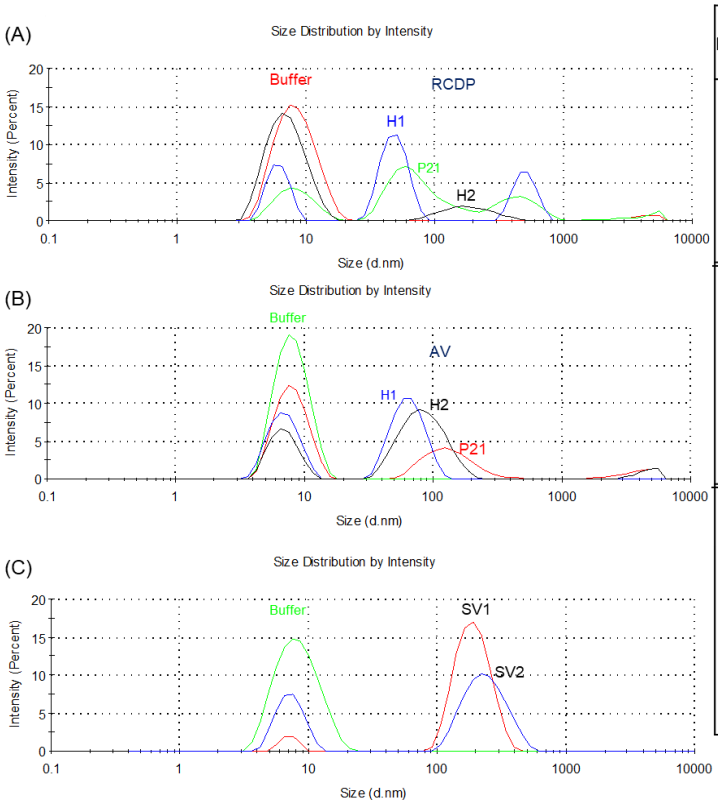

MP	Sample Name	Pk 1 Mean Int (d.nm)	Pk 1 Area Int %	Pk 2 Mean Int (d.nm)	Pk 2 Area Int %	Pk 3 Mean Int (d.nm)	Pk 3 Area Int %
RCDP	Buffer	8.645	96.8	4097	3.2	0	0
	P21	8.476	24.8	78.91	50.5	454.2	20.4
	H1	6.142	26.9	49.22	49.2	505.5	23.9
	H2	7.267	85.4	193.2	14.6	0	0
AV	Buffer	8.205	100	0	0	0	0
	P21	8.131	63.5	141.5	30	4057	6.6
	H1	7.059	43.8	65.22	56.2	0	0
	H2	7.023	30.4	87.66	65.2	4624	4.4
SV	Buffer	8.586	100	0	0	0	0
	SV1	7.173	5.8	195.4	94.2	0	0
	SV2	7.357	33	245	67	0	0

Figure 4.11 Size estimation of enriched plasma vesicles and storage vesicles by DLS. On the left: RCDP **(A)** and AV **(B)** were enriched from 1 SCD PFP sample (SCD1) and 2 healthy (H1, H2) PFP sample and their size, along with diluent buffer used (red for (A) and green for (B)), was estimated using DLS. **(C)** Size estimations from 2 SV (day 35) preparations in red and blue. Buffer is shown in green. In the table, the mean intensity of detected MP diameter (d. nm) and the area intensity (%) of each peak (PK) are presented.

AV enriched using cyt. GPA from the same samples used above, were found to be less diverse in size, approx. 65nm for healthy AV and 142nm for AV from SCD plasma (Fig. 4.11B). Similar to the RCDP results, the peak detected at 4-4.6µm was probably composed of large membrane fragments. Considering that readings in healthy samples corresponded to unbound beads, it was estimated that larger AV from SCD samples could reach up to 100nm. On the other hand, results from 2 SV preparations were close to 200nm (Fig. 4.11C), which is the reported size for such SV (183).

4.5 Detection of red cell proteins, calcein AM and PS on enriched and storage vesicles

Protein abundance was examined by imaging flow cytometry, as was previously shown to be a more sensitive method for protein detection than flow cytometry (Chapter 3.9-10). RCDP and AV were stained against RBC proteins (ex./cyt. GPA, ex./cyt. Band 3, cyt. GPC and GLUT1), along with calcein AM, an intact marker for MP (349). Calcein AM was only used along with anti-ex or cyt. GPA (dual staining) in order to detect intact RCDP or AV, respectively. RCDP from 6 SCD PFP showed that despite being enriched for ex. GPA, ex. Band 3 was the most abundant protein ($7.72x10^6 \pm 1.01x10^7$ RCDP/ml) (Fig. 4.12A and Table 4.2). Ex. GPA was detected in $2.57x10^6 \pm 2.43x10^6$ RCDP/ml, whereas all cytoplasmic proteins tested (GPA, band 3 and GPC) as well calcein AM^+/ ex. GPA^+ RCDP were found at lower levels below $6.6x10^5$ events/ml. Ex. Band 3 was significantly higher than cyt. Band 3 (P=0.02), as well as GLUT1 (P=0.04) (Table 4.2, indicated in bold). The higher levels detected for the extracellular protein domains confirmed that detected RCDP were indeed right-side out, exposing extracellular RBC protein domains as parts of RBC membrane.

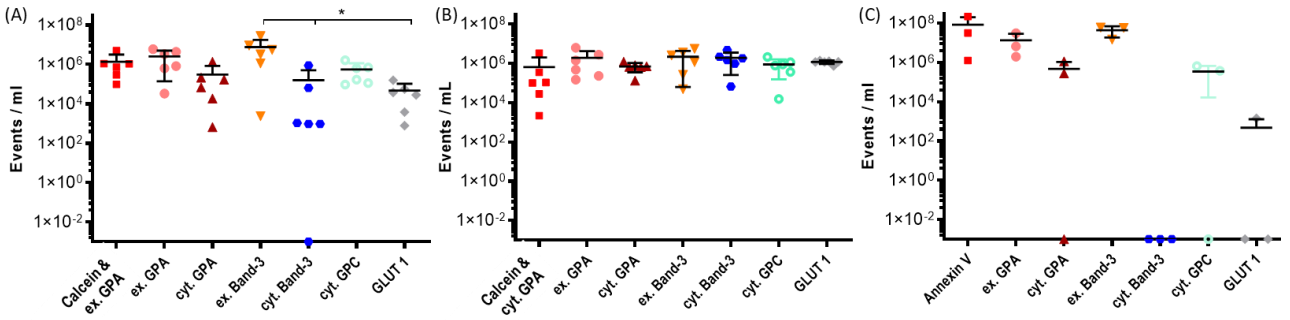

Figure 4.12 Protein abundance of enriched plasma and storage vesicles. Isolated RCDP **(A)** and AV **(B)** using immunomagnetic separation from 6 SCD PFP were stained against RBC proteins (ex./cyt. GPA, ex./cyt. Band 3, cyt. GPC and GLUT1) and calcein AM, then analysed by imaging flow cytometry. **(C)** SV (day 35) (n=3) were stained with the same antibody panel and annexin V. Lines represent mean ± SD.

Interestingly, in AV isolated from 6 patients using an anti- cyt. GPA, ex. and cyt. Band 3 were also the most prevalent proteins ($2.18x10^6$/ml ± $2.12x10^6$ and $2.08x10^6$/ml ± $1.76x10^6$, respectively) (Fig. 4.12B and Table 4.2). AV exposing ex GPA^+ were found at concentrations of $1.89x10^6 \pm 2.38x10^6$/ml and $GLUT1^+$at $1.08x10^6 \pm 2.27x10^5$/ml. Cyt. GPA, cyt GPC and calcein/cyt. GPA dual positive AV numbers were below $1x10^6$ /ml (Table 4.2). There was no significant difference in the number of AV expressing these different proteins. Because of the similar levels of ex and cyt. Band 3 as well as ex. GPA (appr. $2x10^6$) exposed on AV, despite the fact that the enrichment was based on cyt. GPA, it was hypothesised that presence of extracellular and cytoplasmic domains probably corresponds to membrane fragments rather than AV. Furthermore, increased levels of GLUT1 on AV compared

to RCDP (Table 4.2), suggest that the antibody detects a cytoplasmic epitope, which is in line with what was shown before in Chapter 3.9.2, where GLUT1 levels, as well as all cytoplasmic domains were found to be less exposed than extracellular domains in SCD PFP. Despite cyt. Band 3 and GLUT1 positive events being higher in AV than RCDP, no statistical significance was revealed. Interestingly, Calcein AM/ ex. or cyt GPA dual positive events were similar (approx. $6x10^5$ events/ml), which means that numbers of isolated intact RCDP and AV were the same in plasma. However, the total number of RCDP ($1.2x10^7$ /ml) was 9-fold higher than AV ($9.2x10^6$ /ml).

Three SV preparations from outdated blood (day 35) were also examined for the presence of the above RBC proteins, as well as annexin V, an apoptotic marker that targets PS (Fig. 4.12C) (335, 336). The number of annexin V^+ events were higher ($8.28x10^7 \pm 1.16x10^8$/ml) along with ex. Band ($4.39x10^7 \pm 2.54x10^7$/ml). Slightly lower numbers of ex. GPA^+ ($1.32x10^7 \pm 1.56x10^7$/ml) were found, whereas rest of the proteins were present on low numbers of SV (< $5x10^5$/ml) but the differences were not statistically significant.

Table 4.2 Absolute protein counts in particles detected by imaging flow cytometry

Events/ ml	PS $x10^7$	Calcein/ GPA $x10^5$	ex.GPA $x10^5$	cyt.GPA $x10^5$	ex.Band3 $x10^5$	cyt.Band3 $x10^5$	cyt.GPC $x10^5$	GLUT1 $x10^5$	Total events/ ml $x10^5$
RCDP Mean	-	6.19	25.71	3.10	**77.17***	1.58	5.62	0.47	119.84
RCDP SD	-	3.93	24.31	5.34	101.20	3.55	5.90	0.58	-
AV Mean	-	6.57	18.95	6.98	21.80	20.83	6.38	10.77	92.28
AV SD	-	13.2	23.79	3.93	21.18	17.57	4.47	2.27	-
SV Mean	8.28	-	131.69	4.69	438.69	0	3.40	0.005	140.64
SV SD	11.61	-	55.66	5.91	253.90	0	3.24	0.008	-

Results of proteins detected in enriched RCDP, AV from SCD plasma (both n=6) and SV (n=2) were compared using a nonparametric ANOVA and Kruskal-Wallis test. * P≤0.04 compared to cyt. Band3 and GLUT1.

4.6 Optimising a protein quantification protocol on enriched vesicles

Further protein characterisation of RCDP and AV from SCD and healthy PFP was attempted by proteomic analysis using mass spectrometry, in order to identify any differences between these populations. For this type of analysis, protein concentrations tested should be the same for all sample types, so meaningful comparisons can be drawn. All the different methods and conditions tested are summarised in Table 4.3.

i) Bradford assay and different red cell hypotonic lysis buffers

Initially, protein quantification was attempted using the Bradford method, which was used successfully for ghost membrane and SV preparations. All results obtained for RCDP and AV by this method were either too low to be detected or did not provide reproducible results. A commercial hypotonic RBC lysis buffer was also used, as well RIPA buffer (Chapter 2.11.1), unsuccessfully. Despite concentrating the enriched population using centrifugal filters, protein levels were always undetectable. It was assumed that enriched RCDP and AV numbers were low, hence, higher PFP volumes for enrichment were used. RCDP and AV from SCD and healthy PFP were isolated from appr. 25ml, rather than 1ml, which was the usual PFP volume.

Table 4.3 Protein assays and conditions tested for red cell ghosts, storage and enriched vesicles.

Protein assay	Conditions	RBC ghosts	SV	RCDP/AV
i) Bradford (plate reader)	Protocol used for ghosts/ SV	Y	Y	N
	Change lysis buffer	-	-	N
	Concentration by filter	-	-	N
	Higher PFP volume	-	-	N
ii) BCA (plate reader)	RIPA 1:1	-	Y	N
	RIPA 1:2	-	Y	N
	RIPA 1:4	-	N	N
iii) Bradford (Nanodrop)	Nanodrop (↓volume)	N	N	N
	Protein precipitation	Y	Y	Y

	Concentration (µg/ml)		
Sonication+ spin	428.33	138.33	81.67
Mechanical force+spin	378.33	508.33	75.00
Spin only	215.00	108.33	55.00

*Detection limit : 250-100µg/ml

Details of the BCA assay (encircled in blue) are presented on the right. Y-assay worked, N-assay did not work. Hyphen - not examined. Entries in red indicate readings below the test sensitivity.

ii) Assessment of protein dissociation in protein quantification

Another reason for undetectable protein levels could be the incomplete lysis, due to inadequate mixing of the sample in lysis buffer and the formation of protein aggregates. The effects of dissociating protein by sonication, mechanical forcing by passing samples through a syringe, or just mixing thoroughly, were assessed. RIPA buffer was added to SV preparations at 1:1, 1:2 and 1:4 volume ratios and samples were either mixed using a vortex, sonicated or forced through a syringe (Chapter 2.11.1). A centrifugation step followed, to pellet insoluble proteins and debris, then supernatants were collected and tested using a commercial BCA kit (Chapter 2.11.3). Results showed that both dissociation methods gave similar protein content compared to mixing, which always produced the lowest protein concentration. It was decided to use mechanical force, which was more gentle for the sample than sonication. However, when enriched RCDP and AV were tested, the protein concentrations were either too low to be detected, or readings were inconsistent. One thought was that protein levels in enriched RCDP and AV were undetectable because they were eluted in PBS buffer, just after the enrichment stage (see Chapter 2.5.2 and Fig. 2.1). Lysis buffers are usually added to a cell pellet, which was not the case here, as enriched RCDP and AV were in solution. Thus, RIPA buffer 10x was used at a final 1x concentration on enriched RCDP and AV. However, again, this did not work for RCDP and AV.

iii) Protein precipitation

Since a relatively large volume of sample was required for readings using a plate reader (20-100µl), the Nanodrop was used instead, which requires only a few microlitres of the sample. However, RIPA buffer was shown to interfere with the Nanodrop. Thus, protein precipitation using acetone was carried out, in order to remove the lysis buffer and precipitate the protein. The readings from the Nanodrop indicated that protein concentrations in enriched RCDP from both SCD and healthy PFP ranged from 67-85mg/ml, whereas AV from both sources ranged from 74-94mg/ml (Table 4.4). As controls, beads for each type were included and protein concentration was found to be 63mg/ml for the RCDP control and 73mg/ml for the AV. RBC ghosts and SV lysates, which had previously had protein concentration determined by Bradford assay (Chapter 2.11.2), were also quantified using the Nanodrop and same readings were obtained. The readings from the Nanodrop were used to examine protein presence in lysates and controls by immunoblotting.

Table 4.4 Protein detected in controls and lysates using Nanodrop.

Controls	Protein (mg/ml)	Lysates	Prot $_{RCDP}$ (mg/ml)	Prot $_{AV}$ (mg/ml)
RCDP (anti-GPA beads)	63.35	H3	72.00	74.39
AV (anti-cyt GPA+ beads)	72.87	H4	75.92	76.64
RBC ghosts	5.66	H5	84.77	82.87
SV	1.34	P21	77.71	74.74
		P22	74.39	76.50
		P23	69.82	93.88
		P24	66.73	76.13

Prot - protein detected in RCDP or AV lysates.

iv) Investigation of protein levels by immunoblotting

Before lysates were sent for mass spectrometry, an additional validation was carried out. This was to confirm that proteins originated from RBC by immunoblotting against band 3 (Chapter 2.11.6). Initially, protein was loaded at 20µg/well and RBG ghost membranes were used as a positive control. Samples were probed for band 3, as well as stomatin, which is widely exposed by SV and RBC membranes (183, 216). Both proteins were detected in the positive controls but not in the samples (Fig. 4.13). Band 3 was detected as a smear at appr. 90-100kDa and apparent molecular weight of stomatin was appr. 30-32kDa. Blotting experiments were repeated several times, increasing the sample concentrations up to 150µg/well and no bands were detected for band 3.

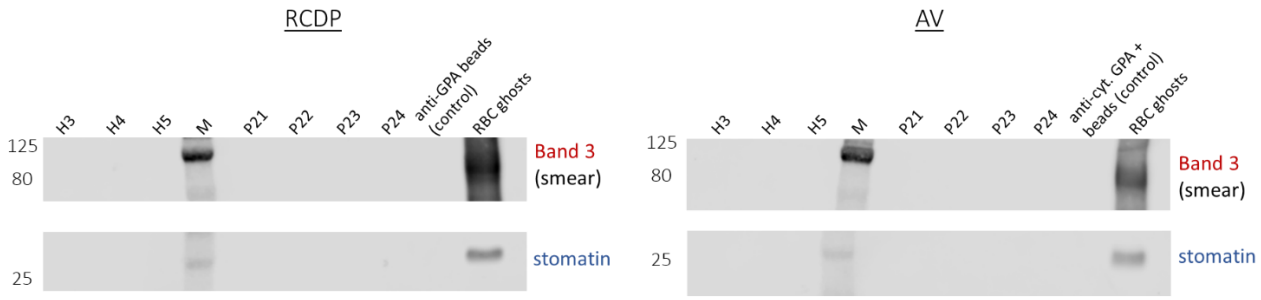

Figure 4.13 Investigation of band 3 and stomatin on SDS-PAGE gels and blots. Lysates of RCDP (left) and AV (right) from 3 healthy (H) and 4 SCD (P) PFP samples were analysed for band 3 (BRIC170) and stomatin, using RBC ghosts as a positive control. Molecular weight marker (M) indicated in kDa. Representative result from 6 experiments.

v) Protein identification using mass spectrometry

Finally, a quick mass spectrometry test (Chapter 2.12.2) was carried out in 2 lysates, one from RCDP and one from AV, both enriched from SCD samples. Results revealed that samples were enriched in keratin and other contaminants but no RBC proteins were present. This was in line with the results from immunoblot analysis (see Fig. 4.13).

4.7 Discussion

In SCD patients, destruction of abnormal cells as well as incomplete reticulocyte maturation, due to splenic sequestration, results in increased RCDP levels compared to healthy individuals (179, 180, 255, 269). It is suggested that RCDP are formed by membrane blebbing, resulting in right side-out microvesicles which expose PS (267, 269, 337). Our colleagues have previously reported the presence of AV on maturing reticulocytes, as well as sickle cells. AV were found to expose PS, as well as the cytoplasmic domains of RBC membrane proteins, having therefore an inside-out orientation (127, 182). It was suggested that these AV are removed by splenic passage during reticulocyte maturation and phagocytosed by splenic macrophages. In SCD patients, a damaged spleen would cause AV to be released directly into plasma, resulting in elevated AV numbers in such patients (127).

Some commonly reported methods for MP isolation are sequential or differential centrifugation and size exclusion chromatography, which can isolate small particle sizes (348). Since our interest was focused on RBC particles only, the above methods were not applicable, as MP from other types of blood cells would be collected. FACS was assessed for RCDP and AV isolation from non pelleted and pelleted SCD plasma, targeting ex. or cyt. GPA, respectively. However, FACS failed to detect small particles below 200nm in size. Furthermore, high velocity centrifugation used to pellet PFP could damage RCDP and AV, or even lead to formation of artificial MP (348, 353, 354). As RCDP would ideally be isolated from plasma without centrifugation (353), immunomagnetic separation using commercial beads that target either ex. GPA directly for RCDP isolation, or cyt. GPA, indirectly for AV identification, was a more gentle and efficient way of enrichment. This was the first demonstration of RCDP and AV enrichment from SCD and healthy plasma. From observations by collaborators using imaging flow cytometry, all RCDP and AV could be removed by using 4-10%(v/v) of these beads in plasma, as they could not be detected in the flow through before elution. However, TEM revealed that such concentrations were saturating the sample with beads and so lower bead concentrations were tested. Saturation with beads could potentially contribute to the total protein content, especially in AV where the anti-cyt. GPA was used. However, this was not found to be the case, when protein content was analysed. The optimum concentration was found to be 0.35%(v/v) for beads targeting RCDP and 0.12%(v/v) for AV.

Due to the immunomagnetic beads bound to enriched RCDP and AV, DLS and nanotracking analysis, which are widely used for size estimation, could not be used to detect size (353). Both methods calculate size according to their Brownian motion and beads on MP would be considered to be a single particle. However, since RCDP and AV were analysed under the same protocol, DLS provided a rough size estimate for the most abundant large populations. RCDP from SCD and healthy plasma were approx. 150-420nm, whereas AV from SCD were approx. 100nm. Readings of AV from healthy plasma corresponded to unbound beads (~50nm), indicating that AV are cleared by the spleen in healthy individuals (127). As the above estimations were from 2 samples from

healthy individuals and 1 from SCD plasma, more samples need to be examined. However, this suggested that RCDP are larger than AV. This is in line with our findings from imaging flow cytometry, where detected AV were much smaller than RCDP and were far less abundant than them (Smith *et. al*, manuscript submitted). These findings were also confirmed by TEM, as RCDP were found to be larger and more abundant than AV. Additionally, sizes detected by DLS, as well as observations by TEM, are in the range suggested for microvesicles (up to 1μm) and exosomes (up to 150nm) (155), which further supports the categorisation of RCDP and AV as microvesicles and exosomes, respectively.

Recently, we demonstrated that RCDP and AV from SCD PFP can be visualised using imaging flow cytometry (Smith *et. al*, manuscript submitted). However, it was assumed that small membrane aggregates and tiny membrane fragments could be regarded as small, round particles by the instrument. TEM allowed us to distinguish intact round RCDP and AV from membrane structures and prove that the morphology of isolated RCDP and AV from SCD and healthy PFP corresponded to true microvesicles, rather than membrane fragments. The morphology of RCDP and MaV is in agreement to what was first observed in healthy individuals, by cryo-electron microscopy (355). However, this is the first demonstration of RCDP in SCD plasma, as well as AV in both plasma sources.

Imaging flow cytometry showed that RCDP from healthy and SCD plasma expose the extracellular domains of GPA and band 3, which further supports the concept that RCDP are formed by membrane budding. On the other hand, similar levels of extracellular and cytoplasmic protein domains on AV indicated the existence of inside-out AV, along with unsealed membrane blebs. GLUT1 expression was 10-fold higher on AV than RCDP. This supported the manufacturer's (PDPU) assumption that the antibody recognises an intracellular epitope, as well as our hypothesis about AV formation through autophagy. Recently we showed that numbers of RCDP and AV were 5-fold and 3-fold higher in SCD plasma than in healthy individuals respectively, while RCDP were significantly increased in crisis patients than in healthy plasma (Smith *et. al*, manuscript submitted), suggesting they may play a role in vaso-occlusion in these patients. More research in this field may reveal useful biomarkers for vaso-occlusive crisis in SCD. While significantly higher RCDP numbers in SCD patients than healthy individuals have been previously reported by others using flow cytometry (333, 346), here we confirm that previous findings corresponded to RBC ghosts and MaV rather than microvesicles.

Intact RCDP and AV were identified by staining with calcein AM, along with ex. GPA or cyt. GPA, respectively. Calcein AM can easily permeate intact cells and is hydrolysed by intracellular esterases, producing a fluorescent product (356, 357). RCDP and AV, which expressed calcein AM, were found to be similar but relatively low compared to other proteins examined, such as GPA and band 3. This might indicate that due to their small size, some RCDP and AV may lack esterases. It could also be that calcein AM binding to small RCDP and AV is prevented by their high curvature.

However, as only GPA was used along with calcein AM in order to identify intact vesicles from RBC, it would be interesting to repeat this experiment replacing GPA with band 3, which was found in higher levels than GPA. Analysis of SV by imaging flow cytometry revealed mainly ex. Band 3 and PS exposure. The last finding is not surprising due to increasing PS levels on senescent RBC during RBC aging (191, 217, 358). Band 3 is one of the most abundant proteins on RBC, along with GPA (90). Despite the fact that it undergoes aggregation or degradation during storage, band 3 remains abundant in stored RBC (day 42) and SV (218), which is in line with our findings. Our findings that SV change shape to less round particles during storage, can be attributed to storage conditions and band 3 clustering, as irregular RBC morphology have also been reported for stored RBC (358, 359).

Our finding that RCDP levels were higher in SCD patients in crisis than in steady state lead us to hypothesise that removal of large RCDP and MaV may alleviate vaso-occlusive episodes in SCD (Smith *et. al*, manuscript submitted). Exploring the differences in proteome between RCDP and AV in healthy individuals and SCD patients could potentially reveal useful biomarkers of vaso-occlusion, as well as the severity of the disease. A considerable amount of time was devoted to optimisation of a protocol that could quantify proteins in enriched RCDP and AV. Initially, it was attempted to minimise manipulation of RCDP and AV samples. However, difficulties in protein quantification led to the addition of multiple steps in the protocol, such as protein dissociation and precipitation. Although the initial experiments by Coomassie stained SDS-PAGE gels revealed that protein could be identified in RCDP and AV samples, the updated protocol used for lysate preparation did not allow us to identify the major RBC membrane proteins like band 3, probably due to denaturation. Taking this work forward, protein loading of enriched RCDP and AV could be calibrated by matching the sample loading using immunoblotting (360). Despite the fact that protein quantification would be only semi-quantitated, sample manipulation and protein denaturation will be prevented. Furthermore, this would provide an estimation of relative protein abundance amongst samples, allowing protein examination by comparative proteomics analysis.

In β-thalassaemia, the proteome of RCDP has been explored in patients and compared with that in healthy individuals by Kittivorapart *et. al*, 2018. Protein exposure for antioxidants, iron sequestering proteins and chaperones was higher in patients than controls, whereas haptoglobin and hemopexin, which remove free haemoglobin and heme respectively, were found to be significantly reduced, 7.1-to 20-fold for haptoglobin and 12.5-to 25-fold for hemopexin (361). Similar reductions in the last two proteins was also reported in paediatric SCD patients, which suggested that these proteins could be used as biomarkers for the severity of both diseases (362). However, in that study, RCDP were isolated by ultra-centrifugation and sedimented particles could originate not only from RBC but from any cell type. Presumably, this is the reason that pelleted protein from 1ml plasma was more than enough for tandem mass tag labelling mass spectrometry and immunoblotting in the β-thalassaemia study.

In another study examining the proteome of band 3 complexes in RBC and SV during ageing, analysed protein gel bands were used. The findings suggested adenylosuccinate lyase, α-adducin and flotillin-2 as potential markers for RBC ageing during storage (218). Despite the efficiency of this method, in our study it was attempted to identify the whole proteome of RCDP and AV, including the low protein levels which would not be picked up by a Coomassie-based stain on a gel.

In conclusion, immunomagnetic separation proved to be a better method for RCDP and AV isolation of all sizes, without damaging the plasma. This is the first demonstration of small RCDP and AV in SCD and healthy samples. AV from both sources were found to expose the cytoplasmic domains of GPA, band 3, GPC, GLUT1 and PS, whereas RCDP exhibited the extracellular domains along with PS. RCDP were found to be larger and more abundant than AV. Further research on their proteome may identify differences in healthy and SCD samples and reveal new biomarkers for vaso-occlusive episodes.

Chapter 5 Inducing tolerance to red cell antigens in a murine model

5.1 Introduction

SCD patients undergoing frequent blood transfusions in order to increase the numbers of healthy RBC, can develop alloimmunisation, which is a major complication as it can lead to life-threatening haemolytic reactions and haemolysis (310, 311). This is caused by genetical and racial differences between patients with African ethnicity and white donors (363, 364). Alloimmunisation has been found to depend on the patient's immune system, as well as the age of first transfusion. It has been shown that children who received their first transfusion before age 3 had significantly lower alloimmunisation levels compared to those transfused later, probably due to their undeveloped immune system (322-326).

Different mechanisms have been suggested to explain alloimmunisation but the exact mechanism is yet unknown (120). A proposed model described decreased levels of immune suppressive IL-10, which enable APC to recognise the antigen on the transfused RBC and proceed to antigen presentation and alloantibody production (365). A study in alloimmunised and non alloimmunised chronically transfused 22 SCD and 8 β-thalassemia major patients showed suppressed peripheral Tregs and increased Th1 responses to Th2 along with higher levels of circulating IFN-γ and lower IL-10 levels in alloimmunised patients compared to those without alloantibody present (317). Furthermore, B regulatory cells (Bregs), that were previously shown to control Treg and Th differentiation (366, 367), were also found to produce lower levels of IL-10 in alloimmunised patients and failed to inhibit TNF-α production by monocytes efficiently, suggesting implication of IL-10, IFN-γ and TNF-α in alloimmunisation (368).

Since 1911, it is known that the regular exposure to an antigen can enable the immune system to become tolerant to it (369). In some cases of allergic diseases, it has been shown that tolerance can be achieved by specific allergen immunotherapy, via antigen delivery in increased doses in order to cause desensitisation (370). For example, immunotherapy against house dust mites and pollen in allergic rhinitis can result in remission in up to 80% of cases (371). Billingham *et. al,* in 1953 were the first to induce tolerance to transplanted tissue by administration of allogeneic BM and splenocytes into neonatal mice. Once the animals had reached adulthood, they were successfully given skin allografts from the same source as the BM and splenocytes without immunosuppression (372). Later in 1969 induced tolerance to sheep RBC was demonstrated in mice by inoculating the sensitiser once or twice (373). In some other studies, patients received a blood transfusion before kidney transplantation from the donor and revealed less rejection than patients who haven't been previously transfused (374-376). Conjugation of the antigen to cellular components is known to promote antigen uptake by dendritic cells (377, 378). This can trigger the differentiation of IL-10 producing Tregs and further promote tolerance (379, 380). RCDP and SV are recognised by immune cells (179, 180). Here, we explored the possibility of inducing tolerance to different blood groups, by exposing immune competent mice to low levels of RBC antigens exposed on RBC ghost

preparations and SV. The immunogenicity of ghost from SCD and healthy donor samples, 22 days after blood collection, was also examined. Responses were assessed using serology, as well as a commercial cytokine assay.

RESULTS

5.2 Experimental design

5.2.1 Developing an appropriate haemagglutination test for mouse plasma

To investigate whether inducing tolerance to RBC antigens is possible, ghosts preparations (Chapter 2.2.2) were used as natural RBC antigen carriers (381). To assess the immune responses *in vivo* after inoculations (Chapter 2.13.1), a respective test had to be developed. Serology is commonly used to assess RBC compatibility prior to blood transfusion (338, 339). Here, we modified a commercial haemagglutination assay used for detection of paroxysmal nocturnal haemoglobinuria. This assay was selected because the microtubes used for the test contain rabbit anti-mouse antibody within the gel matrix, which means that it can bind mouse antibodies in the plasma (Fig. 5.1Ai). Our hypothesis was that if the mouse plasma contains antibodies against human RBC, then those antibodies will bind to the cells during incubation (Fig. 5.1Aii) and haemagglutination will occur. Next, anti-mouse secondary antibodies in the gel will bind the heavy chain of mouse antibodies linked to agglutinated RBC, retaining the cell clump on the top of the tube and indicating a positive result (Fig. 5.1Aiii and 5.1B left). If no anti-human antibodies are generated by the mouse, then RBC would sediment in the bottom of the microtube (negative, Fig. 5.1Aiv and 5.1B right).

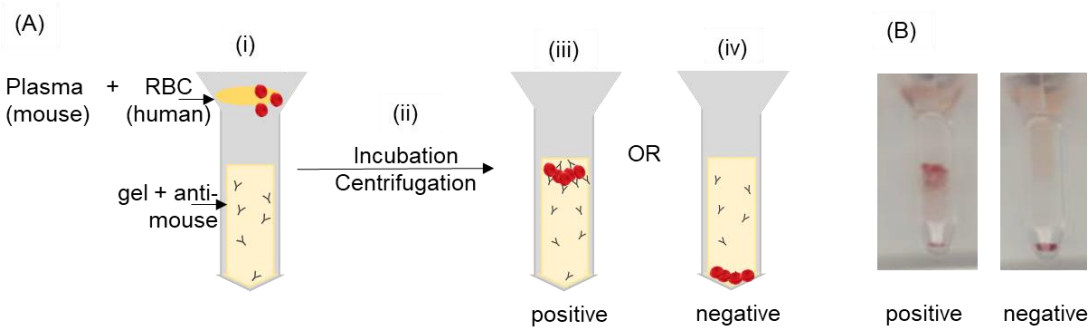

Figure 5.1 Assessment of mouse anti-human antibody production using a gel card. (A) Schematic of the experimental process. Mouse plasma was mixed with human or mouse RBC on the top of the tube (i), then incubated and centrifuged (ii). In a positive reaction, anti-human antibody in mouse plasma coated RBC and caused haemagglutination. Coated RBC were retained by anti-mouse antibody in gel (iii). In absence of mouse anti-human antibody, RBC sank to the bottom of the tube (iv). **(B)** Actual positive (left) and negative results (right) observed on a gel card at the end of the experiment.

Apart from the actual test, which was intact human RBC from the same donor that the ghosts were prepared from (Fig. 5.2A 4th tube), both positive and negative controls were included. Murine RBC (m-RBC) and plasma from the same mouse were used as a negative control, as the plasma would not contain antibodies against its own RBC (Fig. 5.2A 5th tube). As a positive control, a mouse anti-human Lutheran (Lu) antibody was used (see Table 2.1) which caused haemagglutination when mixed with human reference RBC of known phenotype, exposing Lu (Chapter 2.13.4) (Fig. 5.2A 6th tube). Three separate human reference RBC were incubated with mouse plasma (Fig. 5.2A tubes 1-3) and served as alternative positive controls. Initial tests showed that our hypothesis was correct. Apart from the negative and positive results for all the controls (Fig 5.2A and B), in some cases the antibody was specific to the donor cells (Fig 5.2C). A mixed result was obtained sometimes, indicating that the anti-human antibody concentration in mouse plasma was too low to cause haemagglutination of RBC (Fig 5.2D and E). In these cases, the test was repeated a week later and usually by this time the antibody concentration had increased enough to cause haemagglutination.

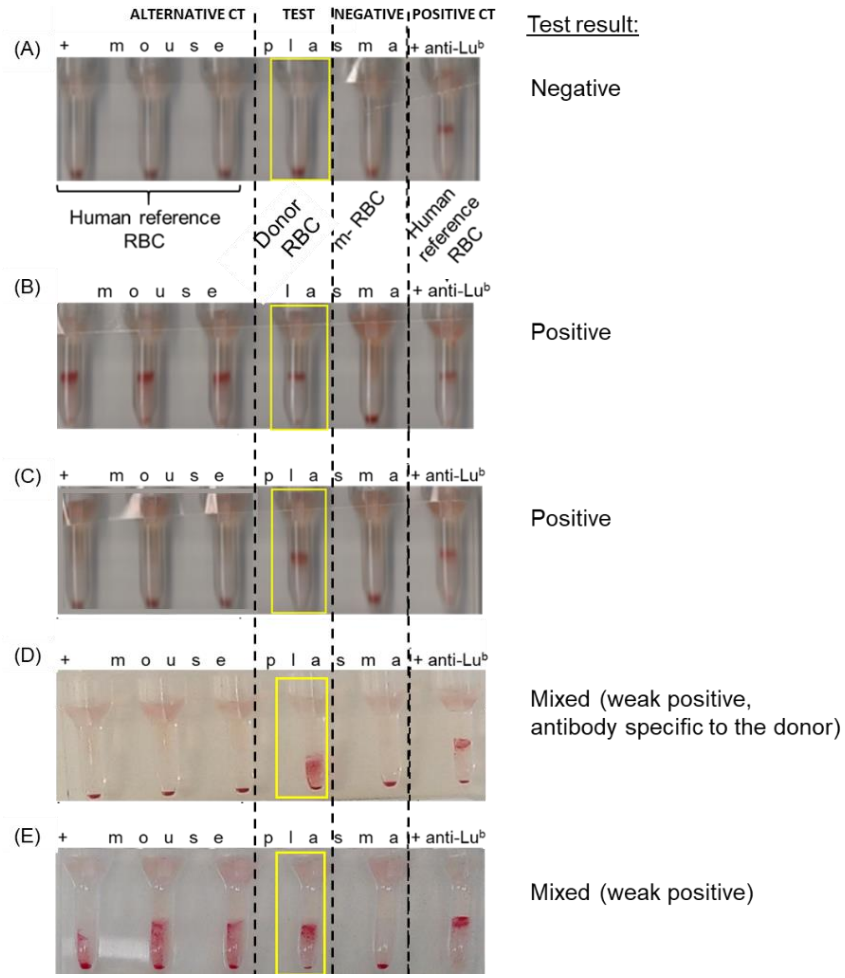

Figure 5.2 Detected results on a gel card. Human reference cells (tubes 1-3 and 6, alternative and positive controls, respectively)**,** donor RBC (4th tube in yellow box, actual test) and m-RBC (5th tube, negative control) (all 0.8%) were mixed with mouse plasma (tubes 1-5) or mouse-anti human Lu (6th tube). **(A)** Negative and **(B)** positive reactions. **(C)** Positive reaction specific to the donor. **(D)** Mixed result, indicated a weak positive reaction specific to the donor. **(E)** Mixed, weak positive result. CT-control.

5.2.2 Setting up an appropriate experimental model

This study had to be designed, validated and optimised from the beginning. Immune competent BALB/c mice were used, since this strain is widely used for assessing immune responses (373, 382). In the early phase of the experiments, the immunogenicity of ghost preparations was examined, due to the fact that Hb remnants during their preparation from RBC could potentially trigger haemolysis, as well as the fact that they carry RBC antigens, such as Kell (381). Ghosts are larger than SV (7μm to 200nm, see Chapters 3.8 and 4.4, respectively) meaning they could contain more antigens on their membrane than smaller SV. Hence, induction of an immune response using ghosts could potentially be stronger. Also, ghosts were chosen for the first experiments as a more accessible source than SV, since they can be counted on a conventional flow cytometer. Use of SV on the other hand, required accurate readings that could be taken by an imaging flow cytometer outside of Bristol (Chapter 2.7), as their size was previously found to be below the detection limit of the flow cytometer (Chapter 3.3.3.1). In order to reproduce biochemical changes on transfused RBC caused by storage, such as PS exposure (221), ghosts were prepared from RBC 22 days after blood collection (Chapter 2.2.2). PS exposure is of great importance as it is a well-known “eat me” signal for phagocytic cells (94), it would therefore stimulate these cells leading to an immune response. The quality of ghost preparations was examined by GPA and band 3 levels, as well as PS by flow cytometry (Chapter 2.6), in order to ensure that these proteins remained intact after preparation. Additionally, ghost preparations from 2 blood units were examined for the presence of calcein AM, in order to identify how well sealed they were. Both preparations found positive for calcein AM (65.6 and 71.4% respectively), which indicates that they were well resealed after RBC lysis (Fig. 5.3). This showed that the protocol selected for ghost preparation, generated resealed ghosts, representing a sealed population like cells or MP, rather than large membrane fragments.

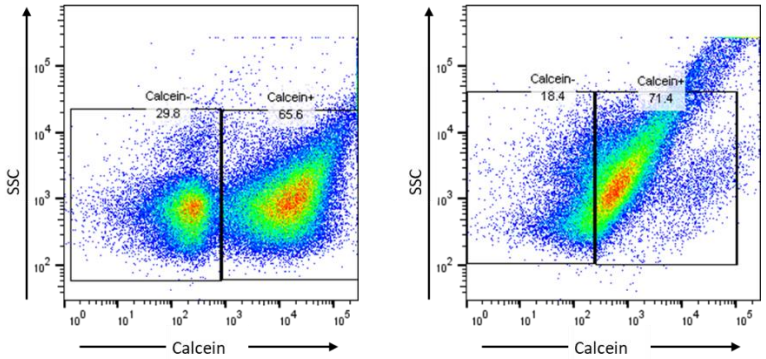

Figure 5.3 Examination of red cell ghost preparations. Ghosts were prepared from RBC using hypotonic lysis, from 2 blood units 22 days after collection. Ghosts were stained with calcein AM to examine sealing after RBC lysis. Flow plots from both units are shown.

One limiting factor was the volume of blood obtained after bleeding the mice: each haemagglutination test required 125µl of plasma (5 tubes x25µl), which corresponded to approx. 250µl blood. However, the test was validated to work with half the volume of plasma/ RBC by our colleagues at NHSBT. This means that at least 125µl of blood needed to be aspirated, which is a relatively large volume for venepunctures, requiring time to collect. Use of serum instead of plasma by leaving blood to clot was not an option, as RBC were needed for serology. Instead, blood was collected in Alsever's whereby both RBC and plasma could be used.

In order to examine the sensitivity of the haemagglutination test on a gel card in diluted plasma, half serial dilutions were carried out using plasma samples from 3 mice which previously showed haemagglutination on termination. The detection limit of the gel card was shown to be very low. Mixed positive results indicating semi-haemagglutination and a reduction in antibody levels, was detected even when plasma was diluted more than 1,280 times (Fig 5.4). Thus, it was decided that it was only necessary to aspirate 5-10µl of blood, corresponding to 2.5-5µl plasma for these tests and dilute in 100µl Alsever's. The dilution factor (DF) was calculated as a ratio of final volume to the initial volume and ranged from 22-42 (110-105µl total volume of blood in Alsever's / 5-2.5µl plasma). For this reason, capillaries used to aspirate the venepunctures were marked to indicate 2.5, 5 and 10µl of volume.

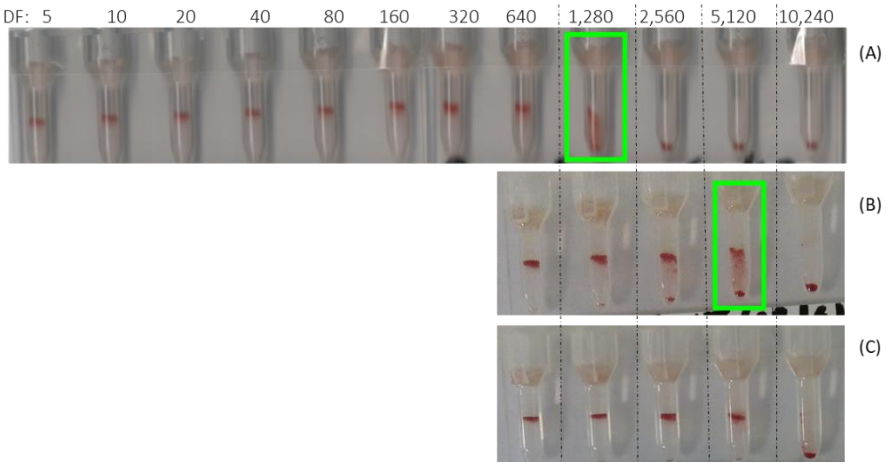

<u>Figure 5.4</u> Assessing the gel card sensitivity by antibody titres. Three mice (A-C) were injected with $5x10^5$ ghosts (day 0), challenged with RBC from the same donor 22 days later and exsanguinated on day 36. Half dilutions from murine plasma diluted in Alsever's. Green boxes indicate mixed haemagglutination. In sample C a mixed reaction was not observed using the dilution factors indicated. DF - dilution factor.

Another restrictive factor was the method of cardiac blood collection on termination. During the first experiments, blood was collected by inserting the needle from the top of the mouse heart (Fig. 5.5i). While competent users applying the procedure can collect up to 1ml, here, blood collections ranged from few microlitres up to 700µl. In later experiments, cardiac puncture was performed from the bottom of the heart which usually provided appr. 1ml of cardiac blood (Fig. 5.5ii).

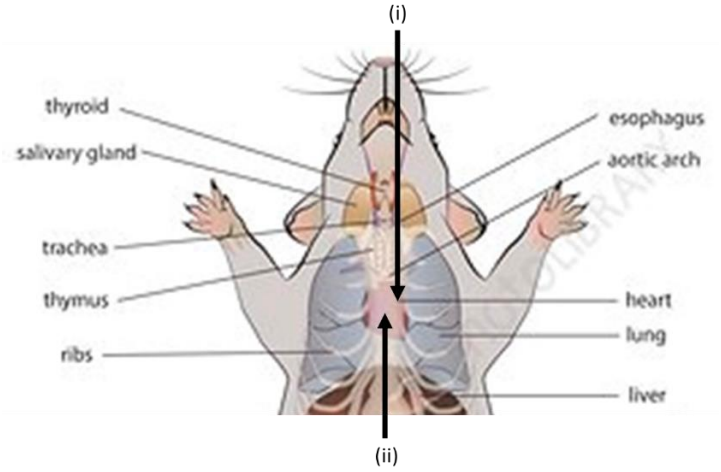

Figure 5.5 Syringe position for cardiac puncture. Mice were anaesthetised with isoflurane and cardiac puncture was performed either from the top (i) or the bottom (ii) of the sternum. In both cases, needles were positioned horizontally, as the arrows indicated. Image was reproduced from (383).

5.3 Investigating immune responses induced by ghost preparations

Choosing the dose to induce tolerance was the most challenging part of the experimental design. It was decided to start with $1x10^5$ ghosts, as such doses were reported to enhance T-cell differentiation to Th1, rather than Th2, in mice, when using sheep RBC (384). Ghosts were emulsified with CFA, a suspension of inactive mycobacteria in oil that induces immune responses (385), then injected subcutaneously. The early experiments lasted 9-15 days and aimed to assess immune responses and differences in cytokine levels between mice receiving HBSS in CFA (controls) and mice inoculated with ghosts/CFA (Fig. 5.6A). Immune responses were further assessed by serology and a commercial cytokine assay that can test up to 40 different cytokines (Chapter 2.13.5).

In the first experiment, 3 mice were inoculated with $1x10^5$ ghosts from an A^+ blood donor, which was the lowest dose reported to induce Th1 responses (384) and 3 mice were given HBSS (controls). It was not known whether ghosts may induce a rapid and severe immune response, so mice were culled after 9 days, without being exposed to RBC (Fig. 5.6A). Serology tests showed positive immune reactions to ghosts (Fig. 5.6B). Proinflammatory cytokines and chemoattractants, such as B lymphocyte chemoattractant (BLC) (386), tissue inhibitor of metalloproteinase-1 (TIMP-1) (387, 388), soluble intercellular adhesion molecule (sICAM-1) (389), complement component 5a (C5/C5a) (390), stromal cell-derived factor 1 (SDF-1 or CXCL12) (391) and macrophage colony-stimulating factor (M-CSF) (392) were the most abundant detected by the cytokine assay, although most of them were at very low levels. However, this assay does not provide quantitative information, instead it allows comparisons of different cytokines (Fig. 5.6C). To determine the predominant cytokines detected, pixel values obtained from primed and control mice were transformed to $\log_{10}$ (Fig. 5.6D). Then, the mean pixel densities of pro-inflammatory cytokines expressed at higher levels (>1.4 in D) are shown (Fig. 5.6E). Log>1.4 was chosen to present overexpressed cytokines by excluding

corresponding pixel intensities which were detected in very low levels. Anti-inflammatory IL-1ra and pro-inflammatory TNF-α are also presented, as molecules of interest. IL-1ra has been reported to control inflammation (393), while TNF-α is implicated in inflammation (394) and has also has been reported in alloimmunised patients (368). IL-1ra and TNF-α were detected at low levels in the controls but were absent in mice inoculated with ghosts.

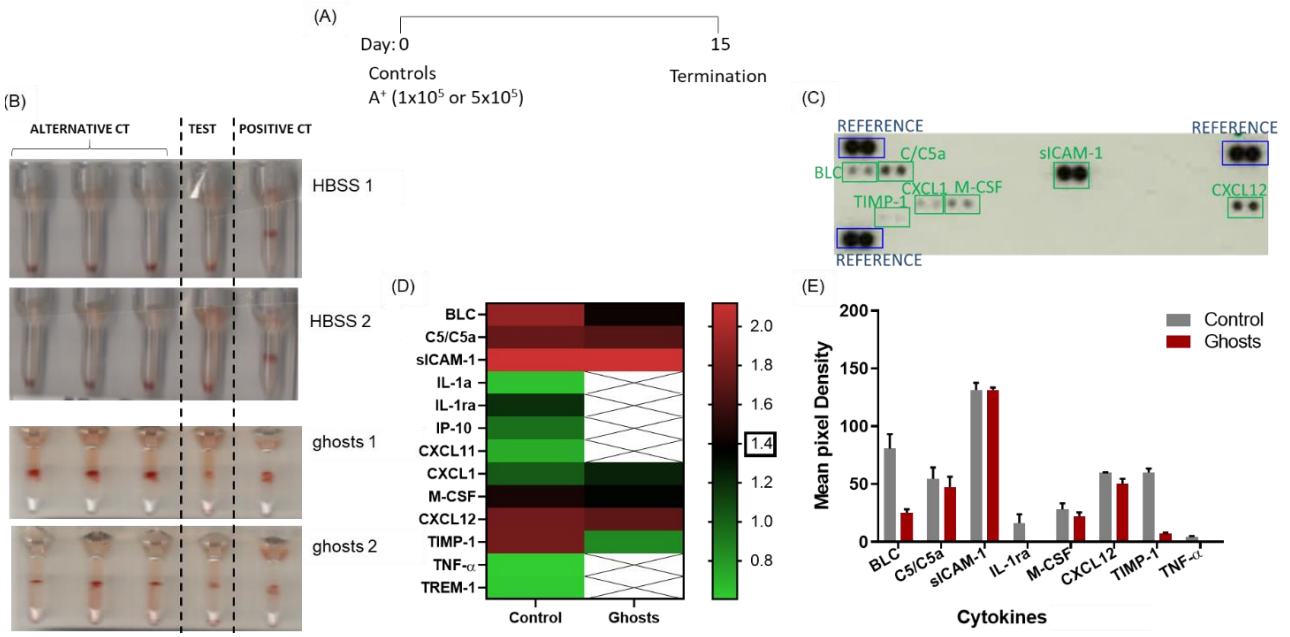

Figure 5.6 Responses following inoculation of ghosts. Mice were given HBSS (controls, n=3) or 1x10^5 RBC ghosts in CFA (n=3) and left for 15 days. Peripheral blood was collected from 2 mice per group and plasma was used for analysis. **(A)** Schematic of the experimental process. **(B)** Haemagglutination results of the controls (negative result) and mice given ghosts (positive). Alternative haemagglutination controls (3 human reference RBC incubated with mouse plasma), actual test (donor's cells with mouse plasma) and positive controls (1 human reference RBC with mouse-anti human antibody) are indicated. CT -control. **(C)** Blot from commercial cytokine assay from one mouse given ghosts. Reference spots (blue) showed that the membrane was incubated with the secondary antibody before exposure. Duplicates of detected cytokines are boxed in green. **(D)** Log10 transformation of mean pixel intensity of all cytokines detected in blots, after background was subtracted from control (n=2) and mice exposed to ghosts (n=2). Undetectable cytokines are indicated with a crossed box. **(E)** Mean pixel intensity of cytokines in (C) with expression >1.4 and cytokines of interest. Data shown as mean ± SD.

BLC as well as TIMP-1 were expressed at higher levels in the controls than the primed mice. Similar levels of sICAM-1, indicating inflammation (389), C5/C5a, a chemoattractant for macrophages and neutrophils (390) and CXCL12, which induces chemotaxis for lymphocytes and macrophages, were found in controls and ghost primed animals (391). M-CSF that activates macrophages during

inflammation (392) and chemokine CXCL1 which activates neutrophils at the inflammatory site (395) were detected in lower levels among the dominant cytokines. Cytokine levels between both groups could not be statistically examined due to the limited number of replicates (n=2). The same results were obtained when the experiment was repeated using higher ghost inocula of $5x10^5$. The results from these 2 experiments showed that the chosen concentrations of ghosts were capable of inducing an immune response. In addition, ghosts may dampen immune responses, as most of the cytokines were decreased or undetectable when compared to the controls.

In subsequent experiments the dose of RBC ghosts was increased to $1x10^6$. Haemagglutination was detected in all six primed mice (ghosts x1) 15 days after inoculation (Fig. 5.7A). In order to investigate whether cytokine production could be further induced, a boost of the same dose of ghosts as the initial inoculum (ghosts x2) was given to 3/6 primed mice. The experiment was terminated on day 24 and haemagglutination was detected in all tested mice.

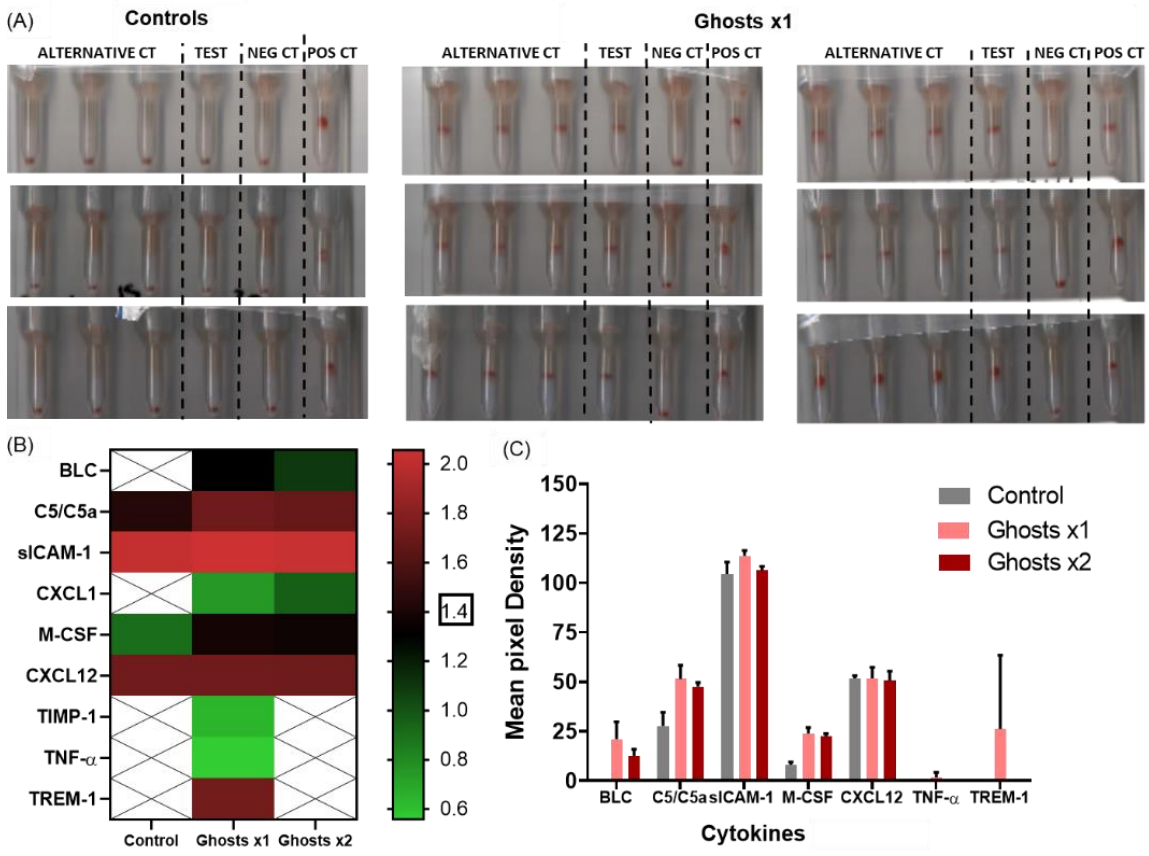

Figure 5.7 Assessing immune responses after a boost of red cell ghosts. Mice were given HBSS (control, n=3) or 10^6 RBC ghosts in CFA (n=6). **(A)** Haemagglutination assessment of all mice on day 15, before the boost. Tests, as well as alternative, negative (NEG) and positive (POS) controls (CT) are indicated. **(B)** Log10 transformation of mean pixel intensity of all cytokines detected in control, primed mice (ghosts x1, n=2) or boosted (ghosts x2, n=2), to show cytokine expression. Undetectable cytokines are indicated with a crossed box. **(C)** Mean pixel intensity of higher detected cytokines in (B) (log_{10}>1.4) and cytokines of interest. Data shown as mean ± SD.

Anti-inflammatory IL-1ra was absent and only pro-inflammatory cytokines were detected (Fig. 5.7B), although TNF-α was only found in primed mice, at very low levels. The dominant cytokines detected from highest to lowest were sICAM-1, CXCL12, C5/C5a, M-CSF and BLC (Fig. 5.7C), as was shown in previous experiments. There were no differences in CXCL12 and sICAM-1 levels among the three groups, whereas BLC was absent in control and slightly higher in primed mice. Increased levels of M-CSF were also detected in both ghost groups (Fig. 5.7 and C). It was also the first time that TREM-1, which is expressed on neutrophils, some monocytes and macrophages (396) was found at higher levels in primed mice. However, statistical analysis could not be performed between groups due to the small number of replicates (n=2). Levels of M-CSF, BLC and TREM-1 were found to be higher in primed mice than in controls. This suggested that higher doses of ghosts can induce different cytokine levels.

5.4 Assessing effects of exposure to red cell antigens

Next, it was investigated whether tolerance could be induced after challenging mice with human RBC. For the following experiments, ghosts and RBC from the same donor with A^+ blood were used, in order to avoid antibody generation against RBC antigens from different donors. To prevent potential detrimental effects on the mice, the dose used was lower ($5x10^5$) (Fig. 5.8A). Haemagglutination was showed for 6/6 tested mice on day 14 (Fig. 5.8B) and they were split into 3 groups (n=2 per group) to be challenged with different RBC doses: $2.5x10^5$ RBC, $5x10^5$ or no RBC. Control mice, which were not primed with ghosts, were given $2.5x10^6$ RBC. The final groups were formed as stated below:

1. $2.5x10^5$ RBC (controls, n=3), referred to as RBC (1)
2. $5x10^5$ ghosts, $2.5x10^5$ RBC (n=2), referred to as ghosts +RBC (2)
3. $5x10^5$ ghosts, $5x10^5$ RBC (n=2), referred to as ghosts +RBC (3)
4. $5x10^5$ ghosts, no RBC (n=2), referred to as ghosts

Mice were left for 2 weeks and then culled (day 35 from start of experiment). Haemagglutination was observed in all mice but all controls showed positive reactions only to the donor and not for the reference cells, suggesting that the antibody response is specific (Fig 5.8C). This also implied that ghosts are more immunogenic than RBC, as positive reactions were observed with the reference cells. Ghost immunogenicity may be attributed to potentially more exposed antigens resulting from hypotonic lysis of RBC during their preparation. Since the donor had blood group A^+ and the reference cells were always O^+, it was questioned whether the generated immune response was an anti-A antibody. Cytokine assessment revealed the presence of pro-inflammatory cytokines only (Fig 5.8D and E), while prevalent cytokines found were sICAM-1, CXCL12, C5/C5a, M-CSF and BLC, which is similar to what was found in the previous experiments above. Although sICAM-1 levels were

similar for all groups, levels of C5/C5a, M-CSF and CXCL12 were found to be lower in mice primed with ghosts and challenged with RBC (3).

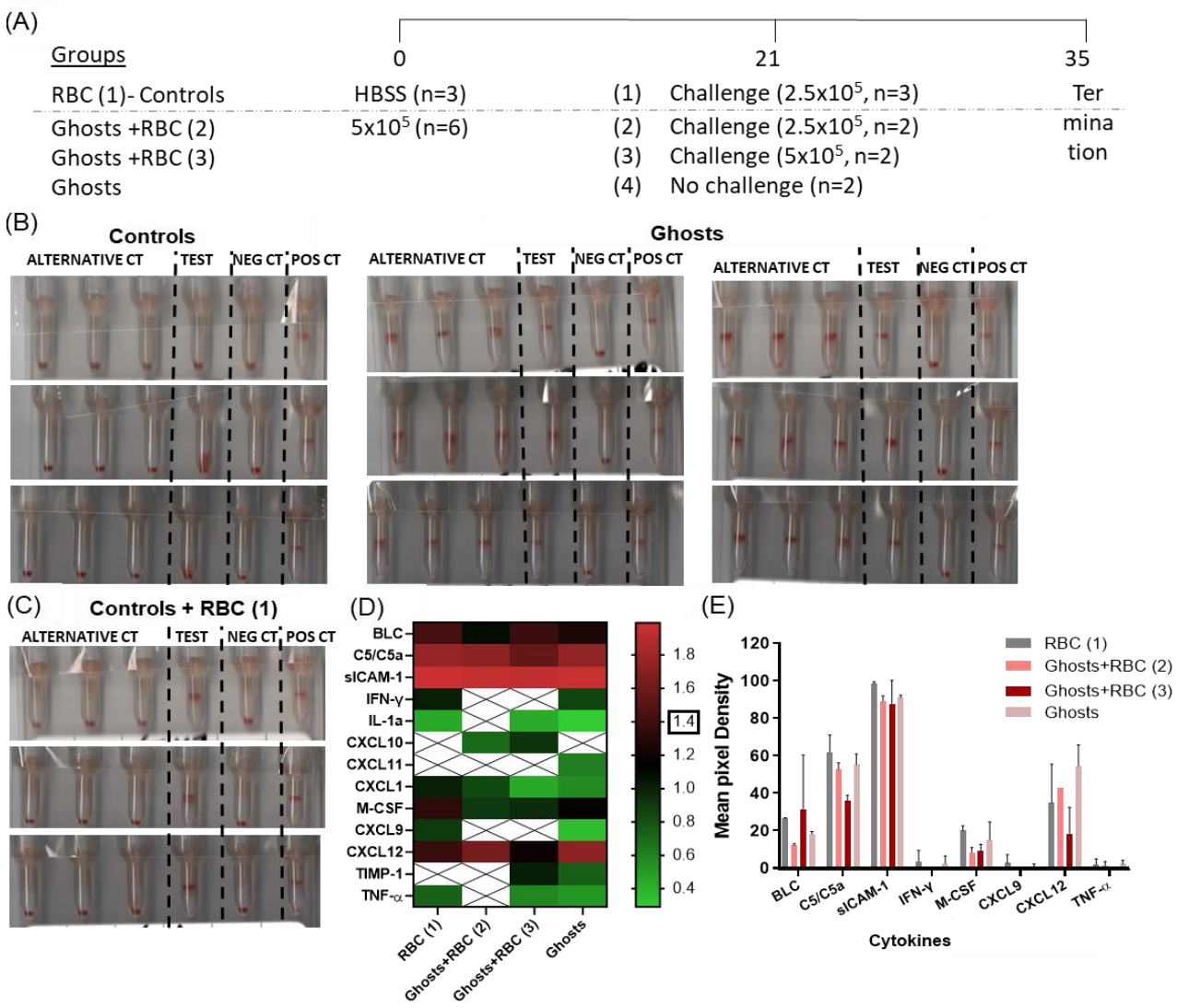

Figure 5.8 Examination of immune responses post red cell challenge. Mice were given HBSS (n=3) or 5x10^5 RBC ghosts (n=6) and left for 20 days. Then, all mice apart from 2 mice primed with ghosts, were challenged with 2.5x10^5 RBC (1) or 5x10^5 RBC (2). **(A)** Schematic of the experiment. **(B)** Haemagglutination examination of all mice on day 15. Tests, as well as alternative, negative (NEG) and positive (POS) controls (CT) are indicated. **(C)** Positive results and antigen specificity (haemagglutination against donor RBC only) were observed in controls after termination (day 35). **(D)** Log10 transformation of mean pixel intensity of all cytokines detected in mice to show log-fold cytokine expression. Undetectable cytokines were indicated with crossed box. **(E)** Mean pixel intensity of higher detected cytokines (log10>1.4) and cytokines of interest. Data shown as mean ± SD.

The most abundant cytokines detected were C5/C5a, sICAM, M-CSF and CXCL12. Their levels were similar in controls -RBC (1) and ghost groups, although slightly reduced in mice challenged with higher number of RBC (group 3). BLC levels were higher in group 3, while mice challenged with the lower RBC dose (group 2) had lower BLC than other groups and the lowest M-CSF levels. Additionally, IFN-γ and TNF-α, which were previously reported in alloimmunised SCD patients (368), as well as chemokine ligand 9 (CXCL9), which was found to be overexpressed in β-thalassemia major patients (397) were found at low levels in control and ghost groups but were reduced or undetectable in primed mice challenged with RBC. Anti-inflammatory IL-1ra was not detected. Again, limited replicates for all groups of primed mice (n=2) did not allow statistical analyses.

5.5 Comparisons of responses to O and A blood groups

In order to investigate whether the response observed above was to anti-A antigens, ABO O^+ blood was examined as a source of ghosts and RBC. Furthermore, ghosts were replaced with SV from outdated ABO O^+ and A^+ blood (day 35), in order to investigate and compare their immunogenicity with what was observed above using ghosts. These SV naturally originate from the RBC membrane, exposing membrane antigens (218). Groups of 3 mice were primed with $5x10^5$ A^+ SV per mouse, or with O^+ SV at 3 different doses: $1x10^5$, $5x10^5$ and $1x10^6$ (Fig 5.9A). Most of the mice did not show an immune response 15 days after inoculation. Thus, a boost of the same initial inoculum, was given to all mice. Ten days later, all mice given O^+ SV showed positive haemagglutination results, whereas 1/3 of mice given A^+ SV was positive and one showed mixed results. Therefore, control and O^+ SV mice were challenged with $5x10^5$ O^+ RBC on day 32. Mice given A^+ SV delayed in showing haemagglutination reactions and were challenged with $5x10^5$ A^+ RBC on day 49. In order to investigate if some cytokines need more time to be produced, only 2/3 mice in each group exposed to O^+ RBC, along with 2/3 controls, were terminated 2 weeks after being challenged, on day 47. The remaining O^+ mice were terminated with A^+ RBC challenged mice 2 weeks post A^+ RBC challenge (day 67), in order to compare findings (Fig 5.9A). The groups examined are stated as below:

1. $5x10^5$ O^+ RBC only on day 32 (control)
2. $5x10^5$ A^+ SV + $5x10^5$ A^+ RBC on day 49, referred to as A^+
3. $1x10^5$ O^+ SV x2 + $5x10^5$ O^+ RBC on day 32, referred to as O^+ (1)
4. $5x10^5$ O^+ SV x2 + $5x10^5$ O^+ RBC on day 32, referred to as O^+ (2)
5. $1x10^6$ O^+ SV x2 + $5x10^5$ O^+ RBC on day 32, referred to as O^+ (3)

Post termination of the experiment, revealed positive haemagglutination for all mice, showing that 1-$5x10^5$ SV from both ABO groups were capable of inducing an immune response. Data on cytokine levels in SV primed mice were normalised to controls from the same time interval, in order to compare cytokine expression, 20 days after RBC challenge (Fig. 5.9B).

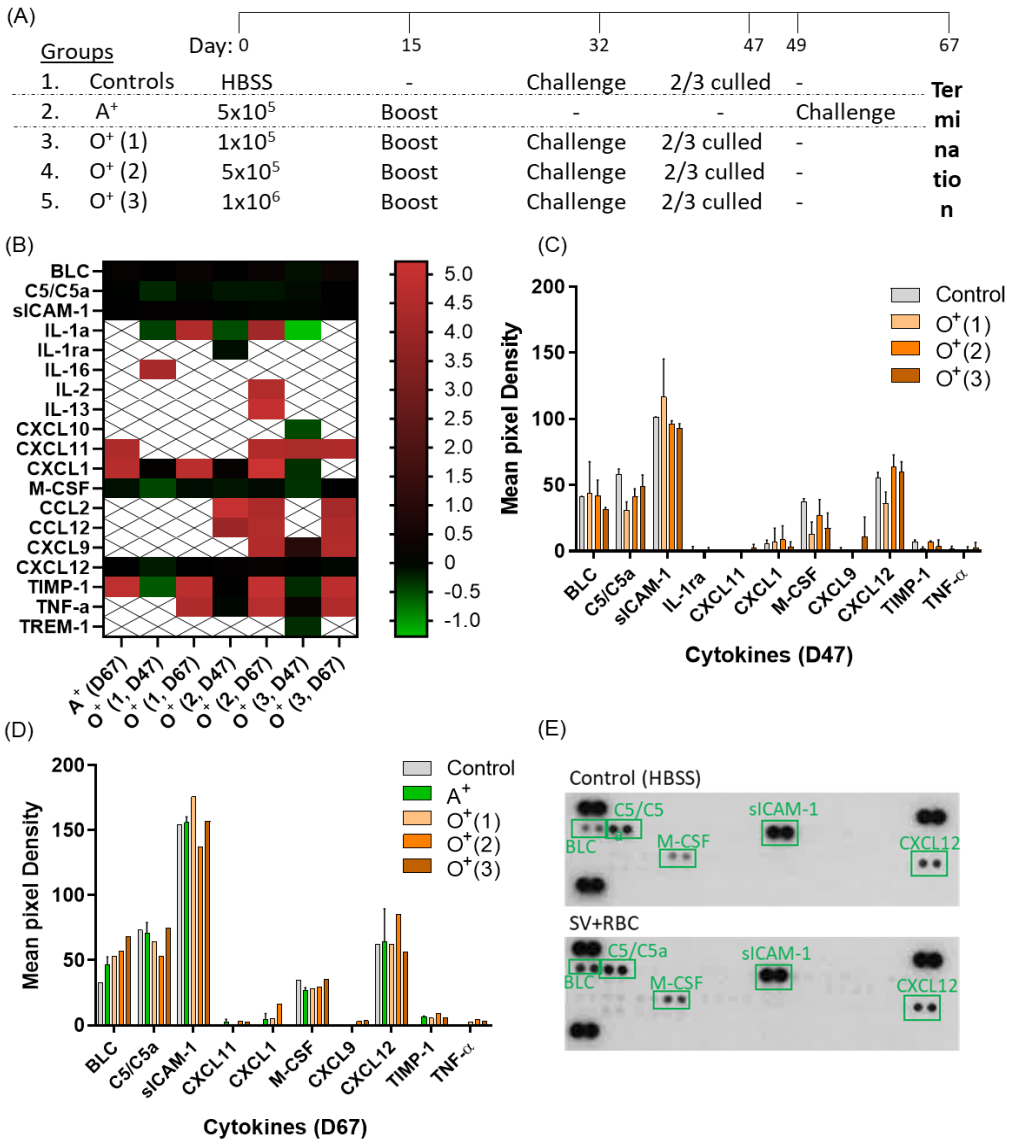

Figure 5.9 Comparison of immune responses post A^+ and O^+ red cell challenge. Fifteen mice were given HBSS (n=3) or $5x10^5$ A^+ SV (A^+, n=3) or three different doses of O^+ SV: $1x10^5$ (O^+ (1), n=3), $5x10^5$ (O^+ (2), n=3) and $1x10^6$ (O^+ (3), n=3). A boost same as the initial inoculum was given on day 15. All mice given O^+ SV had a positive immune reaction on day 32 and were challenged with O^+ RBC from the same donor, along with controls. Two weeks later, 2/3 mice given O^+ SV along with 2/3 controls were culled. A^+ SV mice were challenged with A^+ SV from the same donor on day 49. All remaining mice were culled 2 weeks later. **(A)** Schematic of the experimental procedure. **(B)** Cytokine levels were normalised to respective controls (day 47 or 67) and log10 transformed to show log-fold difference of mean pixel intensity of all cytokines detected in the different experimental groups. Undetectable cytokines are indicated with a crossed box. **(C)** Mean pixel intensity of log-fold difference (>4) detected cytokines and cytokines of interest in mice inoculated with O^+ blood, culled on day 47 and **(D)** in mice inoculated with A^+ and O^+ blood terminated on day 47. Data shown as mean ± SD. **(E)** Blots from 1 control (HBSS) and 1 mouse that was primed with SV and boosted (day 0 & 15) and challenged (day 30), were taken down 14 days after the challenge (day 44 from start of the experiment).

Cytokines with high log-fold difference (>4 in B) for most samples like CXCL11, CXCL1 and TIMP 1 are presented for both timepoints (Fig. 5.9C for day 47 and Fig.5.9D for day 67, respectively). IL-1ra, TNF-α, and CXCL9 were also included as cytokines of interest. An increase in the levels of TNF-α, CXCL1 and CXCL11 were also observed at day 67 compared to day 47 in all groups, although again their levels were very low compared other cytokines detected. Anti-inflammatory IL-1ra was detected only in O^+ (2) mice on day 47. The levels of the inflammation attenuator TIMP-1 were elevated compared to controls, particularly at day 67, albeit at low levels. Also, M-CSF and C5/C5a levels were found to be lower for all samples on day 47 than day 67. However, cytokine pixel values for each interval showed that both TIMP-1 and IL-1ra were particularly low, compared to the elevated levels of sICAM-1, CXCL12, C5/C5a, M-CSF and BLC for both time points.

As differences in cytokine levels did not differ substantially from the pattern observed previously, meaning that dominant cytokines were always the same in every experiment performed, a final investigation into cytokine expression took place. One mouse was given HBSS (control) and another SV, then the primed mouse was given a boost on day 15 and challenged with RBC 15 days later, on day 30. Both mice were culled 2 weeks later (day 44 from start of the experiment) and tested for cytokine expression. As blots showed no differences in cytokine levels between control and test (Fig. 5.9E), it was decided that the commercial cytokine assay was not sensitive enough and was not used further. The above experiments demonstrated that SV from ABO O^+ and A^+ were capable of inducing tolerance in this model. Therefore, in an attempt to imitate the frequent blood transfusions SCD patients receive, a second RBC challenge was introduced in subsequent experiments.

5.6 Sequential challenge with red cells

Alloimmunisation is developed due to exposure to antigens after multiple blood transfusions (363, 364). Therefore, immune responses after a second RBC challenge along with a higher SV dose were examined. Mice were given HBSS or $1x10^6$ O^+ SV. Since primed mice produced an immune response at different time points in all previous experiments, it was decided that mice would be grouped according to the time of their response. Haemagglutination was examined after 15 days and only 3/8 primed mice showed positive or mixed reactions. Thus, 5 mice were given a boost of the same initial inoculum. Two weeks later 5/8 mice showed haemagglutination and were challenged with $1x10^6$ O^+ RBC along with 4 controls, on day 30. All responders received a second RBC challenge, 29 days after the first and were left for 2 weeks, before they were terminated. At the end of the experiment, there were 7 groups of mice:

1. No SV, RBC x2 (controls, n=4)
2. SV x1, RBC x1 (n=1)
3. SV x1, RBC x2 (n=2)

4. SV x2, no RBC (n=3)
5. SV x2, RBC x1 (n=1)
6. SV x2, RBC x2 (n=1)
7. no SV or RBC (n=3)

In order to examine how strong the immune response was, mouse antibody levels were examined by serology, through antibody titres in serial dilutions of plasma. Low dilution factors would mean that the antibody levels were low, whereas high dilution factors would indicate high levels of the antibody, suggesting strong responses. Results indicated that mice that were primed before being challenged with RBC had lower immune responses (dilution factors ≤808), whereas mice that were given RBC without priming (RBC x2 only), showed stronger immune responses and higher antibody levels (1,464.5 ± 1,313 Table 5.1). This was over 10-fold higher than in mice primed with SV but not challenged (134.7 ± 58.3). Mice, which were not exposed to SV nor RBC, did not agglutinate. This was a first indication that tolerance to foreign blood antigens can be induced when using SV.

Table 5.1 Antibody titres in plasma.

Mouse	Dilution Factors						
	No SV or RBC	**No SV, RBC x2**	**SV x1, RBC x1**	**SV x1, RBC x2**	**SV x2, no RBC**	**SV x2, RBC x1**	**SV x2, RBC x2**
1	0	808	101	808	202	808	808
2	0	3,232	-	808	101	-	-
3	0	1,616	-	-	101	-	-
4	-	202	-	-	-	-	-
Mean	0	1,464.5	101	808	134.7	808	808
SD	0	1,313.0	-	0	58.3	-	-

Serial half dilutions of murine plasma to detect antibodies using serology. Dilution factors that showed mixed haemagglutination responses were determined.

The same experiment was repeated using a larger number of mice. Six mice were used as controls receiving HBSS and 12 mice were given $1x10^6$ O^+ SV, from a different donor than the previous study. Here, 3 categories were examined:

1. RBC x2 only (controls, n=6)
2. SV x1, no RBC (n=6)
3. SV x 1, RBC x2 (n=6)

On day 20, 6/12 mice tested positive for haemagglutination, 1 showed a mixed result and 5 were negative. However, due to time restraints with potential forthcoming building closures, all mice along with controls were not boosted but challenged with RBC on day 21. A second challenge took place

28 days later, on day 49 and the experiment was terminated 15 days later. Statistical analyses of data, using a nonparametric ANOVA and Kruskal-Wallis, showed that primed and not boosted mice which were challenged twice (SV x1, RBC x2) were found to have significantly higher levels (912.9 ± 441.8) than controls which did not receive SV (RBC x2 only, 376.00 ± 244.3) and mice primed with SV but not challenged (SV x1, no RBC, 300± 285.7, P≤0.02, Table 5.2).

Table 5.2 Plasma dilution factors detecting mixed agglutination.

Mouse	Dilution Factors		
	RBC x2 only	**SV x1, no RBC**	**SV x1, RBC x2**
1	600	80	720
2	240	720	800
3	200	200	350
4	160	700	1800
5	680	200	800
6	-	-	960
7	-	-	960
Mean	376.0	300.0	**912.9***
SD	244.3	285.7	441.8

Antibody titres were determined in murine plasma post termination, using serology. Results among tested groups were compared using a nonparametric ANOVA and Kruskal-Wallis test. *Significantly higher compared to RBC x2 only and SV x1, no RBC (P≤0.02).

Taking results from the two latest experiments together, it was shown that mice, that had been primed, boosted and challenged twice (Fig. 5.10A), showed similar antibody titres to non-primed controls (SV x1, RBC x2 and RBC only), which were 889.6 ± 385.4 and 859.8 ± 1,003, respectively (Fig. 5.10B). However, there was a large variation in antibody titres detected in mice that had not been primed with SV. The antibody levels of primed and twice challenged mice (SVx1, RBC x2) were higher than primed, non-challenged mice, particularly the group that were primed, then boosted (P=0.03). Non-challenged mice primed and boosted (SV x2, no RBC) showed lower dilution factors than those primed once: 134.7 ± 58.31 vs 380.0 ± 305.3.

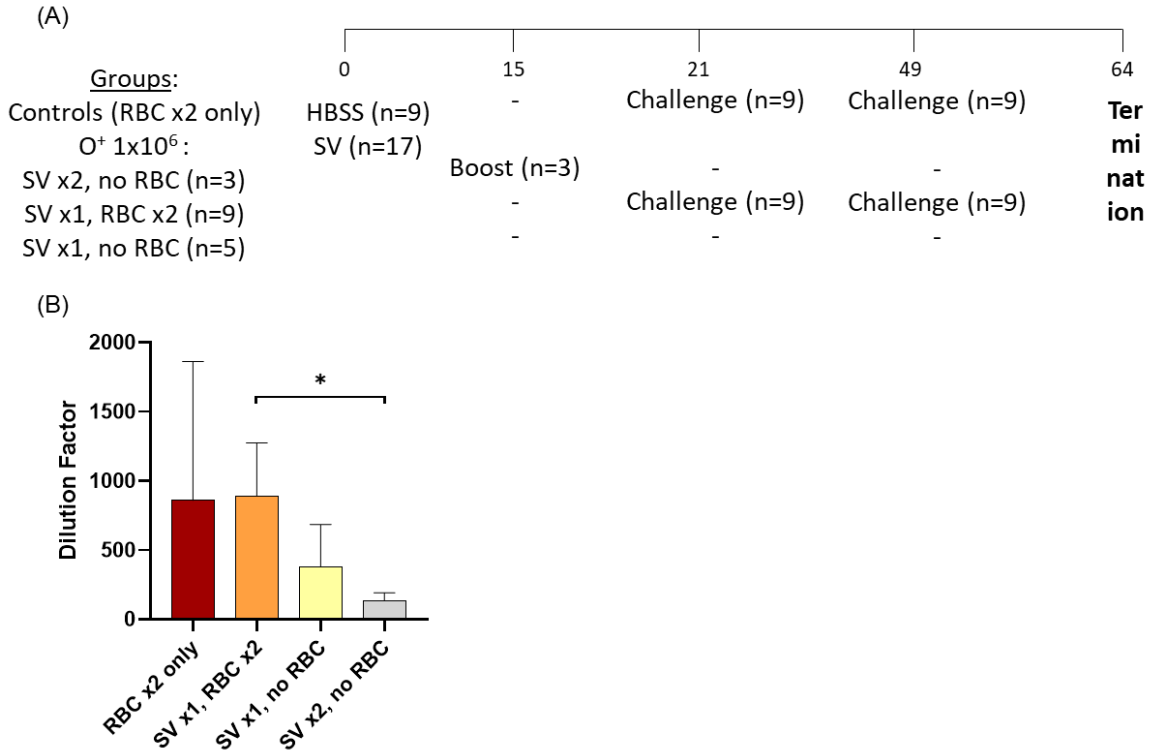

Figure 5.10 Investigation of tolerance induction. **(A)** Schematic of the experimental design. Mice were given HBSS (controls, n=9) or 10^6 RBC SV ABO O^+ (SV x1, n=17). On day 15, 3 tested mice that did not show immune response by serology were given a boost (SVx2, no RBC). On day 21, the controls and primed mice that showed immune reaction but were not given a boost previously, were challenged with 10^6 O^+ RBC (n=9). On day 49, the same mice were challenged for second time (SVx1, RBC x2). The remaining five mice with a negative haemagglutination result at day 15 were not challenged (SVx1, no RBC). The experiment was terminated at day 64. **(B)** Antibody titres in the combined studies. Data shown as mean ± SD.

5.7 Examination of sickle cell ghost immunogenicity

It was questioned whether SCD ghosts, which are known to expose PS (123, 127, 334), were more immunogenic than ghosts prepared from normal healthy blood. Separate groups of mice were inoculated with $1.7x10^5$ A^+ ghosts either sorted from SCD PFP using anti ex. GPA- AF 647 or with ghosts prepared from a day 22 A^+ blood unit. PS expression was estimated by flow cytometry to be 63.7% for SCD ghosts and 78.7% for A^+ healthy ghosts (Fig. 5.11A). Both groups of mice did not show haemagglutination throughout this period, upon examination in plasma diluted 100 times. At the end of the experiment (day 36), serology was performed in pure plasma and haemagglutination was detected in all tests, revealing that plasma examined at several time points during the experiment was too dilute. Subsequently, antibody titres in half serial dilutions were calculated and

they were found to be similar for both ghost groups: 23.8 ± 2.5 detected in SCD ghosts and 25 ± 4.1 for healthy ghosts (Fig. 5.11B), which were not statistically different when examined by an unpaired non parametric t-test (P>0.99). The results showed that ghosts from SCD PFP or from healthy donors, exposing similar PS levels, induce similar antibody production in mice.

(A)

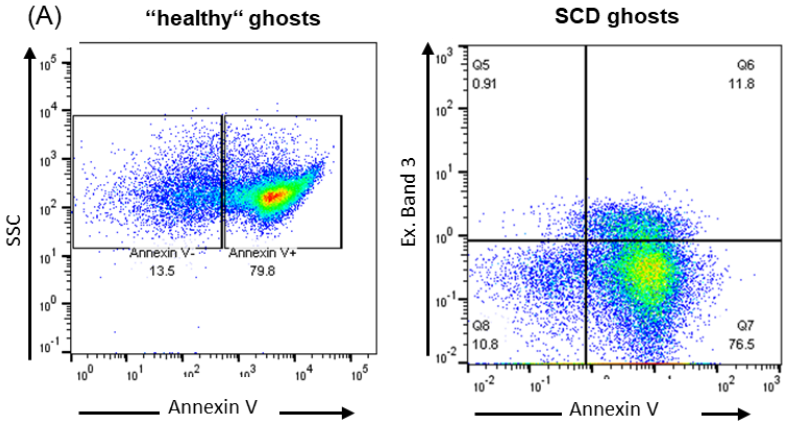

(B)

Number	Dilution Factors	
	SCD ghosts	Healthy ghosts
1	20	25
2	25	30
3	25	25
4	25	20
Mean	23.8	25.0
SD	2.5	4.1

Figure 5.11 Comparison of ghosts from sickle cell patients and healthy donors. Mice were given 1.7x10^5 A^+ ghosts from SCD plasma or day 22 A^+ healthy blood. On termination (day 36), the immune response was determined by serology and antibody titres determined. **(A)** PS levels determined by flow cytometry before the inoculations, using annexin V (FITC) and anti- ex. Band 3-AF 647 (for SCD ghosts only). **(C)** Plasma dilution factors after termination.

5.8 Discussion

Alloimmunisation in frequently transfused SCD patients can lead to dangerous haemolytic reactions and haemolysis (310, 311). It has been shown to depend on the patient's immune state, as well as the age of first transfusion (322-326). The most common highly immunogenic antigens that have been found are RhC, RhD and RhE, K in the Kell system, Jk^b in Kidd system, S in the MNS system and Fy^a and Fy^b in Duffy system (120, 312). Alloimmunisation cannot be prevented by using phenotypically matched blood because of the great diversity of the *RH* gene in individuals of African origin (314) and because RhC, Fy^a, Fy^b, Jk^b and S are rare in most SCD patients unlike in prevalent white donors (315).

Generally, induction of tolerance depends on various factors, such as the dose, the delivery method and the type of APC targeted (398). While $CD4^+$ Th1 subset is mainly responsible for cell-mediated responses, usually through cytokine secretions such as IFN-γ, humoral immune responses (Th2) usually produce IL-4 and IL-5 to activate B cells and trigger antibody production (399, 400). Antigen affinity with MHCII has also been found to enhance Th1 or Th2 responses, as strong MHC affinity favours Th1 and low affinity promotes Th2 (401). In tolerance studies, prevention of antibody production and B-cell stimulation is desired, thus, experimental design targets enhanced Th1 production rather than Th2 and induction of anti-inflammatory humoral responses (384, 402).

Protein replacement therapies are used to elevate levels in patients with protein deficiency, such as haemophilia (403). To reduce immune responses to the protein, drug administration usually takes place either with soluble proteins and peptides or through their conjugation to apoptotic cells or MP and this was reported to induce immunological tolerance (378, 404, 405). RBC have been investigated as delivery vehicles for therapeutic peptides and erythrocyte-binding antigens (398, 406, 407). They were shown to induce tolerance to proteins in a model of autoimmune type 1 diabetes (408, 409). Another study explored the potential of a K peptide from the Kell blood group to be used for specific immunotherapy for K negative mothers after incompatible pregnancy with a K-positive foetus. K is known to cause haemolytic disease of the newborn when delivered from a K positive mother during pregnancy (410, 411). The K peptide was found to induce tolerance *in vitro* in Th-cells isolated by alloimmunised K-negative individuals, when compared to those without anti-K alloantibody presence. Also, the peptide induced immune suppression in HLA-transgenic mice, suggesting its beneficial use in specific immunotherapy (139). More recently the dose of RBC used was shown to affect the immune response. Priming mice with a low ($1x10^5$) or high ($1x10^9$) dose of sheep RBC intravenously, has been reported to induce Th1 cells and Th2 cells, respectively, when examined by cytokine mRNA expression (384). Inflammation status has also been reported to affect alloantibody production in murine models after transfusion. It was shown to increase alloimmunisation magnitude in mice with inflammation, than those transfused in the absence of inflammation (412-415). Additionally, tolerance after transfusion to RBC expressing transgenic human GPA or membrane-bound hen egg lysozyme antigen, was reported in mice in the absence

of inflammation in another study. These mice produced undetectable antibody levels in contrast to transfused mice that had inflammation (416). However, as far as we are aware the potential of using ghosts or SV to induce tolerance to human RBC antigens in immune competent mice and particularly the highly immunogenic antigens in alloimmunisation has not been investigated.

Due to the novelty of this project, the experimental procedures needed to be designed from the beginning. Additionally, the tests to examine the immune reactions had to be developed. Serology is commonly used to assess RBC compatibility prior to blood transfusion through RBC haemagglutination (338, 339). However, despite such tests being relatively easy to set up and perform, in this case it would be laborious and time-consuming to establish due to the novelty of this work. As a base, commercial gel cards containing anti-mouse antibody were used along with human reference RBC of known phenotype. As a positive control, a mouse anti-human Lu antibody was used that caused haemagglutination when mixed with cells known to expose this antigen. Mouse RBC with plasma from the same mouse, which were not expected to agglutinate, were used as negative controls. The assay was found to be very sensitive, as it could detect immune reactions upon dilution up to 8,000-fold in some cases. In terms of the delivery method, intravenous inoculation of low ($1x10^5$) and high ($1x10^9$) doses of sheep RBC was suggested to induce tolerance to the inoculum (373, 384). Subcutaneous administration of the sensitiser in pollen allergies was also shown to decrease sensitivity to the allergen either by Th2 downregulation, or Th1 upregulation (417, 418). Here, we used subcutaneous delivery of the inocula, as it is a common delivery method for adjuvants, in order to induce inflammation by CFA (385).

Human RBC ghost preparations, as well as SV were investigated for their ability to induce tolerance to human RBC antigens in mice. Ghosts preparations and SV have been shown to be natural RBC antigen carriers (218, 381), hence, they could be used to expose the immune cells to these antigens. A range of doses, previously showed to induce tolerance were tested, starting from the lowest reported one ($1x10^5$) and reaching up to $1x10^6$ were tested. All doses within that range showed haemagglutination. However, immune responses between ghosts and SV were developed at different timepoints, ranging from 1-6 weeks, regardless the dose used. RBC ghosts were shown to be more immunogenic than the same dose of SV, as immune reactions in mice, detected by serology, were always achieved by day 15. This may be explained from differences in size and consequently length of membrane surface exposing antigens, as ghosts were previously found to be close to 7μm and SV 200nm. For the latest experiments $1x10^6$ SV per mouse was used. The optimum dose would be one which induced an immune response, decrease inflammatory cytokines in challenged mice and increase anti-inflammatory ones. However, this needs to be further investigated.

The immune reactions detected were not found to be dependent on ABO groups, as ghosts and SV from both A^+ and O^+ units were found to be capable of inducing haemagglutination. Serology results showed that mouse antibody developed against the human inocula was specific to donor RBC ghost

preparations in a few cases and not to human alternative controls used, as haemagglutination in those controls was not observed. Knowing that PS, an “eat me” signal for phagocytes (94) is increased in RBC during storage (106, 107) it was questioned whether SCD ghosts, which expose PS (123, 127, 334) were more immunogenic than ghosts from blood units. These ghosts were prepared 22 days after blood collection, in order to increase PS levels and imitate PS exposure on stored RBC. The same doses for both ghosts were inoculated, and antibody titres were similar on termination, indicating comparable immunogenicity. This may be explained by the similar PS levels both ghost groups showed.

A study in alloimmunised and non alloimmunised chronically transfused SCD (n=22) and β-thalassemia major patients (n=8), revealed suppressed peripheral Tregs and decreased Th1 along with higher levels of IFN-γ and lower IL-10 levels in alloimmunised patients than patients without alloantibody present. Half of the alloimmunised patients had higher levels of intracellular IL-4 in their $CD4^+$ than non alloimmunised patients, suggesting an increased Th2 humoral immune response in the alloantibody responders. All patients exhibited increased levels of Th17, indicating inflammation (317). Furthermore, Bregs in alloimmunised patients were also found to produce lower levels of IL-10 and they failed to inhibit TNF-α production by monocytes efficiently implying participation of IL-10, IFN-γ and TNF-α in alloimmunisation (368). Our results showed undetectable levels of circulating IL-10 in all mice. Reduced levels in challenged mice were found for IFN-γ and TNF-α, which were previously reported in alloimmunised SCD patients (368), as well as for CXCL9, which was found to be overexpressed in β-thalassemia major patients (397) and decreased in maternal RhD alloimmunisation (419). Decreased levels of the above inflammatory molecules in challenged mice indicate a reduction in inflammatory response. On the other hand, anti-inflammatory IL-1ra, which inhibits pro-inflammatory IL-1 controlling inflammatory response (393), was elevated in challenged groups in a few cases but was found to be decreased in other. However, it should be mentioned that detected levels of IFN-γ, TNF-α, IL-1ra and CXCL9 were particularly low.

The majority of the circulating cytokines detected across all the experiments were pro-inflammatory and chemoattractants, such as BLC, sICAM-1, C5/C5a, CXCL12 and in some cases, M-CSF and TIMP-1, as a response to foreign RBC antigens. Anaphylatoxin C5a is produced after activation of complement (420). In a study comparing responses after transfusion of RBC from a donor or from the same patient collected several weeks before operation, C5a was found significantly decreased 1 day after operation in both groups and reached the pre transfusion levels 4-5 days later (421). ICAM has been found at increased levels 48 hours after a blood transfusion in preterm infants, along with IL-1β, IL-6, IL-8, IFN-γ, TNF-α, IL-17 and monocyte chemoattractant protein-1 (422). Additionally, exposure of stored RBC to isolated T-cells *in vitro* led to decreased T-cell proliferation, as well as reduced levels of IL-10, IL-17α, IFN-γ, TNF-α and GM-CSF, suggesting RBC involvement in immunosuppression observed post transfusion (423). The presence of BLC, CXCL12 and M-CSF indicated chemotaxis and activation of lymphocytes (BLC, CXCL12) and macrophages (CXCL12,

M-CSF), as a response to inflammation caused by human RBC antigens (386, 391, 392). Here, differences in prevalent molecules between samples and controls were subtle and furthermore, many cytokines are produced in very low amounts *in vivo* (384). Thus, it was decided that the particular cytokine assay is not sensitive enough for such analyses.

Antibody titres were subsequently used to compare murine anti-human antibody levels in plasma among tested animals. Low titre values indicated low antibody levels, which means lower immune responses that may imply induction of tolerance. On the other hand, high titres suggested higher antibody levels and stronger immune responses that could lead to inflammation and haemolysis of donor RBC. The first attempt to induce tolerance to sequential RBC challenges showed promising results, in which mice primed with SV or primed and boosted, exhibited lower antibody levels than non-primed animals, although the number of mice were limiting. Combining these data with results from a second experiment revealed similar titres for primed and non-primed mice, although there was greater variation in control (non primed) animals. Primed mice, as well as primed and boosted that had not been challenged, showed the lower antibody titres. In particular, antibody levels in primed and boosted mice were significantly decreased compared to mice primed once and challenged twice. This finding could indicate that double exposure of the animals to the antigen may be a better approach. However, due to the developing situation with SARS CoV2 it was not possible to transfuse the mice that had been primed and boosted to investigate whether or not this would be the case. Studies using synthetic peptides have shown that multiple doses were required to induce tolerance, whilst a single dose favoured priming for potential vaccination (424).

In conclusion, we developed an experimental *in vivo* model to investigate responses to RBC antigens together with a reliable, sensitive haemagglutination assay for assessing immune responses. Further research would have included functional comparison of T cell proliferation responses between treated mice and controls. However, this was not possible in the time frame and the cessation of all research activity due to the ongoing pandemic.

Chapter 6 Discussion

In normal physiology, RCDP are thought to be produced during the maturation of the RBC and along with senescent cells are cleared by the spleen. However, deformed SC frequently damage the spleen and this results in significantly higher numbers of RCDP in the plasma of SCD patients than healthy individuals (179, 180, 255, 269). RCDP are thought to have a right side-out orientation due to their formation by membrane shedding, exposing extracellular domains of RBC membrane proteins. On the other hand, AV, a type of autophagic exosome, are thought to have an inside-out orientation, exposing cytoplasmic protein domains. It was suggested that these AV are removed by splenic passage in healthy individuals. In SCD patients however, a damaged spleen would cause AV to be released directly into plasma, exhibiting elevated numbers of both AV and RCDP in these cases (127). This project aimed to characterise RCDP and AV in SCD patients, healthy individuals and in cultured reticulocyte (CR) media and compare the findings with SV from out of date blood units.

6.1 Summary of the key findings in the thesis and suggestions to take the project forward.

Chapter 3	Chapter 4	Chapter 5
Presence of RBC ghosts and large MaV along with small RCDP in plasma from healthy individuals and SCD patients. Demonstrated that previous reports on RCDP probably correspond to ghosts: Imaging flow cytometry was an accurate method for small RCDP and AV analysis.	Intact, enriched RCDP and AV were isolated and characterised for first time. RCDP expose extracellular RBC membrane protein domains and AV cytoplasmic. Both expose PS. SV expose extracellular RBC proteins and PS. RCDP are larger and more abundant than AV in healthy and SCD plasma.	Tolerance induction to RBC antigens using RBC ghosts and SV: a suitable experimental model was developed and a robust serology assay to assess immune responses was set up. Serial antibody dilutions indicated that tolerance may be induced in some cases. SCD ghosts and ghosts from normal blood expose similar PS levels and showed similar immunogenicity.
Future work	**Future work**	**Future work**
Continuation of this work was carried out in Chapter 4.	Examination of RCDP and AV presence in CR media using TEM and imaging flow cytometry. Proteomic profiling to explore differences in RCDP and AV from SCD and healthy plasma. Biomarkers for vaso-occlusive crisis in SCD may be revealed. Development of a removal device for MaV and ghosts to reduce vaso-occlusion in SCD. Investigation of RCDP, AV and SV as vehicles for therapeutic drugs or peptides.	Examine whether tolerance can be achieved by increased exposure to antigens. Assessment of T-cell proliferation between control and treated mice. If successful, use of a humanised mouse model to investigate if tolerance can be induced in a more relevant system.

Until now, identification and characterisation of RCDP in the plasma of SCD patients have generally taken place using conventional flow cytometry, targeting extracellular RBC protein domains (267-269, 337). Here, we aimed to characterise RCDP and AV from SCD plasma, as well as from CR media. The cultured reticulocytes were generated using a well-established protocol (123, 334). Flow cytometry performed on SCD PFP and CR media revealed the presence of the extracellular domains of abundant RBC proteins, like GPA and band 3. The presence of PS, an apoptotic marker previously reported on senescent RBC (106, 107) and RCDP (179, 180, 255, 269), was also confirmed, as was previously shown in SCD PFP by others, using flow cytometry. Cytoplasmic domains of GPA, band 3, GPC and GLUT1 were also detected at lower levels, suggesting AV were also present in SCD plasma and CR media. When particles from SCD and healthy plasma, exposing extracellular GPA, were isolated using FACS, different microscopy methods, such as TEM and spinning-disc confocal, showed that the particles detected by flow cytometry were too large to be considered small MP. Furthermore, imaging flow cytometry along with TEM revealed that SCD and healthy plasma consisted of heterogenous populations composed of microvesicles (0.05-1μm diameter), large RBC ghosts (approx.6-7μm) and MaV (1-6μm). This suggested that previous reports on RCDP (267-269, 337), using size beads, had probably detected ghost membranes rather than small RCDP. This may be attributed to differences in the light scattering intensity between biological samples and size beads (232). Structures positive for both extracellular and cytoplasmic domains of GPA and band 3 or PS, detected by flow cytometry, were shown to correspond to RBC ghosts and MaV when analysed on an imaging flow cytometer. Smaller structures positive for both domains of GPA and band 3 were also revealed. It is possible that these small and large double positive structures in SCD were caused by repeated polymerisation, as well as sealing of the membrane after RBC haemolysis, which is characteristic of SCD (178, 255, 332). Ghost numbers varied among different SCD patients, probably due to the level of haemolysis and RBC fragility. Due to lack of time, it was not possible to examine CR media for the presence of RCDP and AV by TEM or imaging flow cytometry.

Imaging flow cytometry and TEM revealed the presence of RCDP, ghosts and MaV, as well as AV, in SCD and healthy plasma. Most importantly, these data suggest that previously reported RCDP in SCD plasma using flow cytometry (267-269, 337) corresponded to large ghosts rather than small RCDP. Imaging flow cytometry was proven to be an accurate method for imaging and protein characterisation of small MP. It also revealed that RCDP were more abundant than AV in SCD and healthy plasma. Both MP types were found in increased levels in SCD plasma compared to that from healthy donors.

In Chapter 4, isolation of RCDP and AV from SCD plasma for further analysis was investigated using various methods: FACS failed to detect particles smaller than 200nm and pelleting samples by ultra- or high-speed centrifugation (100,000g and 20,000g, respectively) was found to generate artificial MP by destroying cells, or even damaging existing RCDP and AV, as observed by examination using TEM. Size exclusion chromatography or differential centrifugation, both widely used for MP isolation,

could not be used, as isolation by these methods is based on particle size (348). This is to say that MP from all blood cell types would be enriched rather than just RCDP. Eventually, immunomagnetic separation was chosen in order to gently isolate RCDP and AV of all sizes from SCD and healthy plasma. RCDP were targeted by immunomagnetic beads against extracellular GPA directly, whereas an indirect approach was applied for AV, as no commercial beads detecting cytoplasmic GPA were available. This took place by targeting the AlexaFluor 647 fluorochrome the antibody used against cytoplasmic GPA was conjugated to. TEM and immunogold staining confirmed that enriched populations were intact, round RCDP and AV, enclosed by an external lipid bilayer, similar to what has been previously shown for RCDP in healthy individuals, using cryo-electron microscopy (355). SV from of out of date blood units were used as a comparison, since they are formed RBC by membrane budding. Both tubular and round RCDP were detected in healthy and SCD plasma, whereas only round AV were found in each source. Round SV were also detected and found to lose their membrane integrity and circular shape in aged blood units probably due to storage lesions (191). This is the first visual evidence of RCDP in SCD plasma, as well as AV in both plasma sources. CR media was not examined by imaging flow cytometry and TEM due to lack of time.

Analyses using imaging flow cytometry revealed the prevalence of extracellular domains on RCDP from healthy and SCD plasma, as well as SV, confirming that they were right-side out and they were probably formed by membrane budding. AV exhibited similar levels of extracellular and cytoplasmic domains, indicating that membrane blebs, exposing extracellular and cytoplasmic domains, were also isolated. This revealed limitations in the isolation method, which enriched not only AV but also membrane fragments. This was also confirmed by TEM. Furthermore, the presence of intact RCDP and AV was confirmed by staining, using calcein AM, which is a widely used marker for intact cells. Calcein AM can permeate the membrane, then become hydrolysed by intracellular esterases and produce fluorescence in intact cells (356, 357). RCDP were found to be larger and more abundant than AV in both SCD and healthy PFP, on bright field of imaging flow cytometry, as well as TEM and DLS. Altogether these findings indicate the presence of right-side out RCDP and inside-out AV in healthy and SCD plasma for first time. In addition, the use of imaging flow cytometry and TEM suggested that RCDP detected by flow cytometry in previous studies (179, 180, 255, 269), were probably RBC ghosts and MaV. Knowing that MP transfer cellular material from parental cells (152), further investigation of their composition may reveal information on their relevance in normal healthy individuals and those with SCD.

We have recently shown that the numbers of RCDP and AV were 5-fold and 3-fold higher in SCD plasma than in healthy individuals, respectively, using imaging flow cytometry. Also, RCDP were significantly increased in SCD patients with acute pain (crisis) compared to those in steady state and healthy individuals. This is probably due to impaired splenic function. Furthermore, removal of MaV and RBC ghosts from SCD plasma was shown to decrease the blood clotting times. Therefore, it

may be possible to diminish vaso-occlusion in SCD cases by removing MaV and ghosts by developing a removal device (Smith *et. al*, manuscript submitted).

Alloimmunisation is another complication in SCD patients, caused by frequent blood transfusions between genetical and racial differences in patients with African origin and white donors. Auto-and alloantibody development can cause life-threatening haemolytic reactions and haemolysis (363, 364). Alloimmunisation has been found to depend on the patient's immune system and the age of first transfusion (322-326). The most common immunogenic antigens in alloimmunised SCD patients have been reported to be RhC, RhD and RhE, K in the Kell system, Jk^b in Kidd system, S in the MNS system and Fy^a and Fy^b in Duffy system (120, 312). Although the exact mechanism of alloimmunisation is unknown (425), in Chapter 5 we investigated a potential approach to alleviate alloimmunisation. Knowing that the regular exposure to an antigen can tolerise the immune system to it (378, 380, 426), we thought that RBC ghosts and SV from blood units may be used as natural carriers to induce tolerance to immunogenic antigens in a murine model. Our data had shown that ghost and SV expose RBC antigens by imaging flow cytometry (discussed above) confirming proteomic analyses of SV (218). Prior to *in vivo* inoculation, RBC ghosts and SV were examined by flow cytometry and imaging flow cytometry, respectively, and were shown to expose the extracellular domains of RBC membrane proteins, like GPA and band 3. They were are also found to expose PS, which has been found on senescent RBC in blood units prior to transfusion (123, 127, 334). In addition, PS is a known signal for phagocytosis by professional cells (94) which would enhance immune responses. Ghosts and SV were both found intact after staining with calcein AM (349), showing that particularly ghosts were well re-sealed after RBC lysis.

Tolerance was previously shown to be induced against sheep RBC in mice by inoculating the cells once or twice (373). Additionally, inoculation with a low or high dose of sheep RBC has been reported to increase Th1 responses compared to Th2 in mice, thereby preventing B cell stimulation as well as antibody production and potentially promoting tolerance (384). Due to the novelty of this project using human red-cell-derived components, the animal model and experimental process had to be set up from the beginning. Initially, RBC ghost preparations from day 22 blood bags were used, as natural carriers of RBC antigens (218). It was hypothesised that they would be a better source to induce tolerance to these antigens than RBC, as they have lost Hb during preparation, which could exaggerate potential haemolysis. The administered dose ($1x10^5$) was based on the lowest sheep RBC dose reported to increase Th1 response compared to Th2 (384). This was shown to induce an immune response, indicated by haemagglutination when assessed by serology. Importantly, there were no adverse effects on the mice which meant that increased doses could be tested in subsequent experiments. At all doses of ghosts from healthy donors investigated (max $1x10^6$), antibody generation was detected by 2 weeks from inoculation and administration of a boost was not needed.

Subsequently, ghost preparations from healthy donors were compared to sorted ghosts from SCD plasma in this model. Ghost from both sources exposed similar levels of PS that should induce recruitment of phagocytic cells. On termination the antibody levels were similar in mice exposed to both sources, indicating that SCD ghosts were as effective as ghost from healthy donors, potentially because of the comparable PS levels which might induce similar B cell activity.

When SV were investigated for their ability to induce an immune reaction, a longer response time (1-4 weeks more) than ghosts was observed. In many cases a boost of SV was required before a positive haemagglutination reaction was observed. Therefore, SV are potentially less immunogenic than healthy ghost membrane preparations. Immune responses were found to be ABO unrelated, as both O^+ and A^+ samples induced an immune response. While an early experiment suggested that priming with SV may induce tolerance, as assessed by serology, this was not confirmed in subsequent experiments. On the other hand, mice that had been primed and boosted exhibited lower antibody levels, indicating that multiple exposure to SV may be a better approach. However, it was not possible to investigate this further due to closure of the University facilities in response to the SARS-Cov-2 outbreak.

Our approach using intact biological material, such as SV, was different to other studies exploring specific immunotherapy to RBC antigens, using peptides to induce tolerance to Kell blood group. K is the most immunogenic antigen of the Kell system and in cases of a K-negative mother and a K-positive foetus in pregnancy, it can lead to haemolytic disease of the newborn. A K peptide (1M) exhibiting K polymorphism at the C terminus was shown to induce tolerance to a carrier conjugated to synthetic Kell protein residues in a humanised mouse model (139). In other studies, the presence of inflammation was reported to increase alloantibody production in murine models after transfusion (412-415). However, a separate study demonstrated that tolerance to RBC expressing transgenic human GPA or membrane-bound hen egg lysozyme antigen could be achieved in the absence of inflammation (416). The above underlie the importance of inflammatory status and indicate that despite the fact that immune responses were induced in the work described here using an inflammatory adjuvant as a vehicle (CFA), it may be worth exploring immune responses excluding its use. Cytokine assessment using a commercial cytokine assay panel did not reveal differences in cytokines between controls and challenged mice. This may be due to lack of sensitivity in the assay or very low levels of cytokines that can be detected *in vivo* (384).

6.2 Further Work

Taking this project forward, it would be worth examining in CR media for the presence of RCDP and AV. Potential differences amongst RCDP and AV from healthy individuals, SCD patients, CR media as well as differences with SV, could be determined by proteomic analysis. CR media may be a more accessible source of RCDP, as it is a by-product from reticulocyte cultures and may be donated from colleagues growing these cells. In this case, a simple centrifugation step to remove cultured reticulocytes will be performed, rather than expensive and time-consuming immunomagnetic separation for large plasma volumes. Also, comparison of the proteome of RCDP, AV and RBC ghosts between healthy individuals and SCD patients and CR media, may reveal receptors for cell communication, biomarkers for vaso-occlusive crisis and severity of the disease, as could lead to further investigation of their role in health and pathology. Knowing the thrombotic properties of RBC ghosts and MaV, the development of a removal device targeting extracellular GPA or band 3 from SCD patient plasma may be beneficial in preventing vaso-occlusion in SCD.

From a different angle, the role of RCDP in normal physiological conditions could be further explored. While it has been suggested that RCDP are phagocytosed by splenic and liver macrophages, communication with other cell types is yet unknown. Knowing that MP transfer cellular cargo during cell communication (152), RCDP from a mouse could be isolated and labelled using a fluorescent dye, such as PKH26. This dye has been successfully used to label induced red-cell vesicles using *in vivo* imaging systems (427). Labelled RCDP could be then re-introduced back to the donor mouse. Tracking may help us explore and understand the interactions of RCDP with other cells. There may be potential to use therapeutic peptide or drug loaded RCDP to target pathological conditions like cancer. Although SV can be easily obtained from blood units, RCDP may be a better source of MP, as they expose lower levels of the apoptotic marker PS and they can avoid phagocytosis. Also, loaded RCDP from the same donor are likely to be less immunogenic than foreign vehicles like SV.

In terms of the immunological part of the project, more experiments including sequential challenge of primed, boosted and non primed mice are required, to determine the optimal conditions to induce tolerance. With regards to the inoculum, a direct comparison of SV and ghost from the same donors could determine if ghosts are better than SV in stimulation of immune responses, when examined by serology. Also, other experiments could determine immune responses with or without the inflammatory adjuvant (CFA) by serology, exploring its contribution to inflammation. For this, incomplete Freund's adjuvant could be used, or even pure ghosts/SV in HBSS. For consistency, inoculate will be given subcutaneously in the early experiments. However, intravenous injections would be investigated later, since this is a simple delivery method of therapeutic material, such as vaccines, to animals and humans.

Apart from serology, T-cell proliferation assays using splenocytes from primed and non primed, challenged mice groups, will provide an indication of T cell activation. Use of CD3, CD4, CD8, CD25, CD27 and CD45RA markers along with cell trace violet by flow cytometry, will indicate the proliferation of different T cell subsets including naïve T cells, Tregs, effector and memory T cells. Proliferation upon stimulation with RBC will indicate response to the inoculum, whereas unresponsive cells will imply anergy and potential tolerance. Cytokine detection could be performed using different available commercial assays than the one used previously, to investigate whether there is a more sensitive assay for this work.

Finally, if tolerance is induced, experiments in a humanised mouse model would be essential to investigate responses in a system imitating the human system. This would involve exposing neonatal humanised mice to SV or ghosts then challenging them with RBC as a proof of principle of inducing tolerance in young (<3 years) SCD patients. Hence, it may be easier to decrease alloimmunisation in adult patients, by exposure to RBC antigens in early childhood.

6.3 Conclusion

While RCDP in healthy individuals have been visualised previously, we managed to demonstrate for first time the morphological characteristics and protein content of RCDP in SCD patients. The imaging flow cytometry and TEM data suggests that previous reports of RCDP in SCD actually correspond to RBC ghosts. Also, this study is the first demonstration of AV in SCD patients and healthy individuals. RCDP and AV numbers were significantly higher in SCD than in healthy plasma suggesting they may be indicators of disease severity. Furthermore, SV and RBC ghosts could be used to induce tolerance to RBC antigens and revealed a potential approach to alleviate alloimmunisation in SCD patients.

REFERENCES

1. Galloway JL, Zon LI. Ontogeny of hematopoiesis: examining the emergence of hematopoietic cells in the vertebrate embryo. Curr Top Dev Biol. 2003;53:139-58.
2. Palis J, Yoder MC. Yolk-sac hematopoiesis: the first blood cells of mouse and man. Exp Hematol. 2001;29(8):927-36.
3. Paik EJ, Zon LI. Hematopoietic development in the zebrafish. Int J Dev Biol. 2010;54(6-7):1127-37.
4. Moore MA, Owen JJ. Chromosome marker studies on the development of the haemopoietic system in the chick embryo. Nature. 1965;208(5014):956 passim.
5. Kiecker C, Bates T, Bell E. Molecular specification of germ layers in vertebrate embryos. Cell Mol Life Sci. 2016;73(5):923-47.
6. Detrich HW, Kieran MW, Chan FY, Barone LM, Yee K, Rundstadler JA, et al. Intraembryonic hematopoietic cell migration during vertebrate development. Proc Natl Acad Sci U S A. 1995;92(23):10713-7.
7. Palis J. Primitive and definitive erythropoiesis in mammals. Front Physiol. 2014;5:3.
8. McGrath KE, Frame JM, Fromm GJ, Koniski AD, Kingsley PD, Little J, et al. A transient definitive erythroid lineage with unique regulation of the β-globin locus in the mammalian embryo. Blood. 2011;117(17):4600-8.
9. Bertrand JY, Kim AD, Violette EP, Stachura DL, Cisson JL, Traver D. Definitive hematopoiesis initiates through a committed erythromyeloid progenitor in the zebrafish embryo. Development. 2007;134(23):4147-56.
10. Lacaud G, Kouskoff V. Hemangioblast, hemogenic endothelium, and primitive versus definitive hematopoiesis. Exp Hematol. 2017;49:19-24.
11. Yoshimoto M, Porayette P, Glosson NL, Conway SJ, Carlesso N, Cardoso AA, et al. Autonomous murine T-cell progenitor production in the extra-embryonic yolk sac before HSC emergence. Blood. 2012;119(24):5706-14.
12. Pinho S, Frenette PS. Haematopoietic stem cell activity and interactions with the niche. Nat Rev Mol Cell Biol. 2019;20(5):303-20.
13. Medvinsky A, Dzierzak E. Definitive hematopoiesis is autonomously initiated by the AGM region. Cell. 1996;86(6):897-906.
14. de Bruijn MF, Ma X, Robin C, Ottersbach K, Sanchez MJ, Dzierzak E. Hematopoietic stem cells localize to the endothelial cell layer in the midgestation mouse aorta. Immunity. 2002;16(5):673-83.
15. Cumano A, Godin I. Ontogeny of the hematopoietic system. Annu Rev Immunol. 2007;25:745-85.
16. Palis J. Ontogeny of erythropoiesis. Curr Opin Hematol. 2008;15(3):155-61.
17. Schofield R. The relationship between the spleen colony-forming cell and the haemopoietic stem cell. Blood Cells. 1978;4(1-2):7-25.
18. Akashi K, Traver D, Miyamoto T, Weissman IL. A clonogenic common myeloid progenitor that gives rise to all myeloid lineages. Nature. 2000;404(6774):193-7.
19. Doulatov S, Notta F, Eppert K, Nguyen LT, Ohashi PS, Dick JE. Revised map of the human progenitor hierarchy shows the origin of macrophages and dendritic cells in early lymphoid development. Nat Immunol. 2010;11(7):585-93.
20. Månsson R, Hultquist A, Luc S, Yang L, Anderson K, Kharazi S, et al. Molecular evidence for hierarchical transcriptional lineage priming in fetal and adult stem cells and multipotent progenitors. Immunity. 2007;26(4):407-19.
21. Sanjuan-Pla A, Macaulay IC, Jensen CT, Woll PS, Luis TC, Mead A, et al. Platelet-biased stem cells reside at the apex of the haematopoietic stem-cell hierarchy. Nature. 2013;502(7470):232-6.
22. Yamamoto R, Morita Y, Ooehara J, Hamanaka S, Onodera M, Rudolph KL, et al. Clonal analysis unveils self-renewing lineage-restricted progenitors generated directly from hematopoietic stem cells. Cell. 2013;154(5):1112-26.
23. Dykstra B, Kent D, Bowie M, McCaffrey L, Hamilton M, Lyons K, et al. Long-term propagation of distinct hematopoietic differentiation programs in vivo. Cell Stem Cell. 2007;1(2):218-29.

24. Benveniste P, Frelin C, Janmohamed S, Barbara M, Herrington R, Hyam D, et al. Intermediate-term hematopoietic stem cells with extended but time-limited reconstitution potential. Cell Stem Cell. 2010;6(1):48-58.
25. Wilson A, Laurenti E, Oser G, van der Wath RC, Blanco-Bose W, Jaworski M, et al. Hematopoietic stem cells reversibly switch from dormancy to self-renewal during homeostasis and repair. Cell. 2008;135(6):1118-29.
26. Foudi A, Hochedlinger K, Van Buren D, Schindler JW, Jaenisch R, Carey V, et al. Analysis of histone 2B-GFP retention reveals slowly cycling hematopoietic stem cells. Nat Biotechnol. 2009;27(1):84-90.
27. Laurenti E, Göttgens B. From haematopoietic stem cells to complex differentiation landscapes. Nature. 2018;553(7689):418-26.
28. Hamey FK, Göttgens B. Demystifying blood stem cell fates. Nat Cell Biol. 2017;19(4):261-3.
29. Velten L, Haas SF, Raffel S, Blaszkiewicz S, Islam S, Hennig BP, et al. Human haematopoietic stem cell lineage commitment is a continuous process. Nat Cell Biol. 2017;19(4):271-81.
30. Notta F, Zandi S, Takayama N, Dobson S, Gan OI, Wilson G, et al. Distinct routes of lineage development reshape the human blood hierarchy across ontogeny. Science. 2016;351(6269):aab2116.
31. Scott EW, Simon MC, Anastasi J, Singh H. Requirement of transcription factor PU.1 in the development of multiple hematopoietic lineages. Science. 1994;265(5178):1573-7.
32. Cantor AB, Orkin SH. Transcriptional regulation of erythropoiesis: an affair involving multiple partners. Oncogene. 2002;21(21):3368-76.
33. Thompson MA, Ransom DG, Pratt SJ, MacLennan H, Kieran MW, Detrich HW, et al. The cloche and spadetail genes differentially affect hematopoiesis and vasculogenesis. Dev Biol. 1998;197(2):248-69.
34. Sumanas S, Jorniak T, Lin S. Identification of novel vascular endothelial-specific genes by the microarray analysis of the zebrafish cloche mutants. Blood. 2005;106(2):534-41.
35. Liao EC, Paw BH, Oates AC, Pratt SJ, Postlethwait JH, Zon LI. SCL/Tal-1 transcription factor acts downstream of cloche to specify hematopoietic and vascular progenitors in zebrafish. Genes Dev. 1998;12(5):621-6.
36. Pham VN, Lawson ND, Mugford JW, Dye L, Castranova D, Lo B, et al. Combinatorial function of ETS transcription factors in the developing vasculature. Dev Biol. 2007;303(2):772-83.
37. Narula J, Smith AM, Gottgens B, Igoshin OA. Modeling reveals bistability and low-pass filtering in the network module determining blood stem cell fate. PLoS Comput Biol. 2010;6(5):e1000771.
38. Pimanda JE, Ottersbach K, Knezevic K, Kinston S, Chan WY, Wilson NK, et al. Gata2, Fli1, and Scl form a recursively wired gene-regulatory circuit during early hematopoietic development. Proc Natl Acad Sci U S A. 2007;104(45):17692-7.
39. Tsai FY, Keller G, Kuo FC, Weiss M, Chen J, Rosenblatt M, et al. An early haematopoietic defect in mice lacking the transcription factor GATA-2. Nature. 1994;371(6494):221-6.
40. Shivdasani RA, Mayer EL, Orkin SH. Absence of blood formation in mice lacking the T-cell leukaemia oncoprotein tal-1/SCL. Nature. 1995;373(6513):432-4.
41. Zhu H, Traver D, Davidson AJ, Dibiase A, Thisse C, Thisse B, et al. Regulation of the lmo2 promoter during hematopoietic and vascular development in zebrafish. Dev Biol. 2005;281(2):256-69.
42. Sumanas S, Gomez G, Zhao Y, Park C, Choi K, Lin S. Interplay among Etsrp/ER71, Scl, and Alk8 signaling controls endothelial and myeloid cell formation. Blood. 2008;111(9):4500-10.
43. Jagannathan-Bogdan M, Zon LI. Hematopoiesis. Development. 2013;140(12):2463-7.
44. Visnjic D, Kalajzic Z, Rowe DW, Katavic V, Lorenzo J, Aguila HL. Hematopoiesis is severely altered in mice with an induced osteoblast deficiency. Blood. 2004;103(9):3258-64.
45. Frenette PS, Pinho S, Lucas D, Scheiermann C. Mesenchymal stem cell: keystone of the hematopoietic stem cell niche and a stepping-stone for regenerative medicine. Annu Rev Immunol. 2013;31:285-316.
46. Kricun ME. Red-yellow marrow conversion: its effect on the location of some solitary bone lesions. Skeletal Radiol. 1985;14(1):10-9.

47. Milner LA, Kopan R, Martin DI, Bernstein ID. A human homologue of the Drosophila developmental gene, Notch, is expressed in CD34+ hematopoietic precursors. Blood. 1994;83(8):2057-62.
48. Calvi LM, Adams GB, Weibrecht KW, Weber JM, Olson DP, Knight MC, et al. Osteoblastic cells regulate the haematopoietic stem cell niche. Nature. 2003;425(6960):841-6.
49. Bianconi E, Piovesan A, Facchin F, Beraudi A, Casadei R, Frabetti F, et al. An estimation of the number of cells in the human body. Ann Hum Biol. 2013;40(6):463-71.
50. Rand RP, Burton AC. Mechanical properties of the red cell membrane. I. Membrane stiffness and intracellular pressure. Biophys J. 1964;4:115-35.
51. Mohandas N, Gallagher PG. Red cell membrane: past, present, and future. Blood. 2008;112(10):3939-48.
52. Weatherall DJ. Towards molecular medicine; reminiscences of the haemoglobin field, 1960-2000. Br J Haematol. 2001;115(4):729-38.
53. Bot FJ, van Eijk L, Schipper P, Löwenberg B. Human granulocyte-macrophage colony-stimulating factor (GM-CSF) stimulates immature marrow precursors but no CFU-GM, CFU-G, or CFU-M. Exp Hematol. 1989;17(3):292-5.
54. Hattangadi SM, Wong P, Zhang L, Flygare J, Lodish HF. From stem cell to red cell: regulation of erythropoiesis at multiple levels by multiple proteins, RNAs, and chromatin modifications. Blood. 2011;118(24):6258-68.
55. Chasis JA, Mohandas N. Erythroblastic islands: niches for erythropoiesis. Blood. 2008;112(3):470-8.
56. Anstee DJ. Production of erythroid cells from human embryonic stem cells (hESC) and human induced pluripotent stem cells (hiPS). Transfus Clin Biol. 2010;17(3):104-9.
57. Mel HC, Prenant M, Mohandas N. Reticulocyte motility and form: studies on maturation and classification. Blood. 1977;49(6):1001-9.
58. Chasis JA, Prenant M, Leung A, Mohandas N. Membrane assembly and remodeling during reticulocyte maturation. Blood. 1989;74(3):1112-20.
59. Kim HO. In-vitro stem cell derived red blood cells for transfusion: are we there yet? Yonsei medical journal. 2014;55(2):304-9.
60. Prchal JT, Gregg XT. Red cell enzymes. Hematology Am Soc Hematol Educ Program. 2005:19-23.
61. Romano AH, Conway T. Evolution of carbohydrate metabolic pathways. Res Microbiol. 1996;147(6-7):448-55.
62. Kruger NJ, von Schaewen A. The oxidative pentose phosphate pathway: structure and organisation. Curr Opin Plant Biol. 2003;6(3):236-46.
63. Betz T, Lenz M, Joanny JF, Sykes C. ATP-dependent mechanics of red blood cells. Proc Natl Acad Sci U S A. 2009;106(36):15320-5.
64. Daleke DL. Regulation of phospholipid asymmetry in the erythrocyte membrane. Curr Opin Hematol. 2008;15(3):191-5.
65. van Wijk R, van Solinge WW. The energy-less red blood cell is lost: erythrocyte enzyme abnormalities of glycolysis. Blood. 2005;106(13):4034-42.
66. Benesch R, Benesch RE. Intracellular organic phosphates as regulators of oxygen release by haemoglobin. Nature. 1969;221(5181):618-22.
67. McMullin MF. The molecular basis of disorders of red cell enzymes. J Clin Pathol. 1999;52(4):241-4.
68. PerutZ MF, Rossmann MG, CULLIS AF, MUIRHEAD H, WILL G, NORTH AC. Structure of haemoglobin: a three-dimensional Fourier synthesis at 5.5-A. resolution, obtained by X-ray analysis. Nature. 1960;185(4711):416-22.
69. Kozberg M, Hillman E. Chapter 10 - Neurovascular coupling and energy metabolism in the developing brain. Masamoto K, Hirase H, Yamada K, editors: Elsevier; 2016. 213-42 p.
70. Hardison RC. A brief history of hemoglobins: plant, animal, protist, and bacteria. Proc Natl Acad Sci U S A. 1996;93(12):5675-9.
71. Wu T, Wang X, Cohen B, Ge H. Molecular Modeling of Normal and Sickle Hemoglobins. International Journal for Multiscale Computational Engineering - INT J MULTISCALE COMPUT ENG. 2010;8:237-44.
72. Monod J, Wyman J, Changeux JP. On the nature of allosteric transitions: a plausible model. J Mol Biol. 1965;12:88-118.

73. Kilmartin JV, Rossi-Bernardi L. Inhibition of CO2 Combination and Reduction of the Bohr Effect in Haemoglobin chemically modified at its α-Amino Groups. Nature. 1969;222(5200):1243-6.
74. Lundin D, Berggren G, Logan DT, Sjöberg BM. The origin and evolution of ribonucleotide reduction. Life (Basel). 2015;5(1):604-36.
75. White C, Yuan X, Schmidt PJ, Bresciani E, Samuel TK, Campagna D, et al. HRG1 is essential for heme transport from the phagolysosome of macrophages during erythrophagocytosis. Cell Metab. 2013;17(2):261-70.
76. Docherty JC, Firneisz GD, Schacter BA. Methene bridge carbon atom elimination in oxidative heme degradation catalyzed by heme oxygenase and NADPH-cytochrome P-450 reductase. Arch Biochem Biophys. 1984;235(2):657-64.
77. Frimat M, Boudhabhay I, Roumenina LT. Hemolysis Derived Products Toxicity and Endothelium: Model of the Second Hit. Toxins (Basel). 2019;11(11).
78. Balla J, Jacob HS, Balla G, Nath K, Eaton JW, Vercellotti GM. Endothelial-cell heme uptake from heme proteins: induction of sensitization and desensitization to oxidant damage. Proc Natl Acad Sci U S A. 1993;90(20):9285-9.
79. Kiefer CR, Snyder LM. Oxidation and erythrocyte senescence. Curr Opin Hematol. 2000;7(2):113-6.
80. Matarrese P, Straface E, Pietraforte D, Gambardella L, Vona R, Maccaglia A, et al. Peroxynitrite induces senescence and apoptosis of red blood cells through the activation of aspartyl and cysteinyl proteases. FASEB J. 2005;19(3):416-8.
81. Reid ME, Mohandas N. Red blood cell blood group antigens: structure and function. Semin Hematol. 2004;41(2):93-117.
82. Speicher DW, DeSilva TM, Speicher KD, Ursitti JA, Hembach P, Weglarz L. Location of the human red cell spectrin tetramer binding site and detection of a related "closed" hairpin loop dimer using proteolytic footprinting. J Biol Chem. 1993;268(6):4227-35.
83. Ungewickell E, Bennett PM, Calvert R, Ohanian V, Gratzer WB. In vitro formation of a complex between cytoskeletal proteins of the human erythrocyte. Nature. 1979;280(5725):811-4.
84. Karinch AM, Zimmer WE, Goodman SR. The identification and sequence of the actin-binding domain of human red blood cell beta-spectrin. J Biol Chem. 1990;265(20):11833-40.
85. Bennett V. Proteins involved in membrane--cytoskeleton association in human erythrocytes: spectrin, ankyrin, and band 3. Methods Enzymol. 1983;96:313-24.
86. Narla J, Mohandas N. Red cell membrane disorders. Int J Lab Hematol. 2017;39 Suppl 1:47-52.
87. Anstee DJ. The relationship between blood groups and disease. Blood. 2010;115(23):4635-43.
88. Thomas SL, Bouyer G, Cueff A, Egée S, Glogowska E, Ollivaux C. Ion channels in human red blood cell membrane: actors or relics? Blood Cells Mol Dis. 2011;46(4):261-5.
89. Reid ME, Westhoff CM. Chapter 8 - Other Blood Group Antigens and Antibodies. In: Hillyer CD, Silberstein LE, Ness PM, Anderson KC, Roback JD, editors. Blood Banking and Transfusion Medicine (Second Edition). Philadelphia: Churchill Livingstone; 2007. p. 96-111.
90. Anstee DJ. Blood group-active surface molecules of the human red blood cell. Vox Sang. 1990;58(1):1-20.
91. Rahuel C, London J, d'Auriol L, Mattei MG, Tournamille C, Skrzynia C, et al. Characterization of cDNA clones for human glycophorin A. Use for gene localization and for analysis of normal of glycophorin-A-deficient (Finnish type) genomic DNA. Eur J Biochem. 1988;172(1):147-53.
92. Chasis JA, Mohandas N. Red blood cell glycophorins. Blood. 1992;80(8):1869-79.
93. Zwaal RF, Schroit AJ. Pathophysiologic implications of membrane phospholipid asymmetry in blood cells. Blood. 1997;89(4):1121-32.
94. Ravichandran KS. Beginnings of a good apoptotic meal: the find-me and eat-me signaling pathways. Immunity. 2011;35(4):445-55.
95. Graham TR. Flippases and vesicle-mediated protein transport. Trends Cell Biol. 2004;14(12):670-7.
96. Lee SH, Meng XW, Flatten KS, Loegering DA, Kaufmann SH. Phosphatidylserine exposure during apoptosis reflects bidirectional trafficking between plasma membrane and cytoplasm. Cell Death Differ. 2013;20(1):64-76.

97. Bevers EM, Comfurius P, Dekkers DW, Zwaal RF. Lipid translocation across the plasma membrane of mammalian cells. Biochim Biophys Acta. 1999;1439(3):317-30.
98. Kobayashi T, Menon AK. Transbilayer lipid asymmetry. Curr Biol. 2018;28(8):R386-R91.
99. Bitbol M, Fellmann P, Zachowski A, Devaux PF. Ion regulation of phosphatidylserine and phosphatidylethanolamine outside-inside translocation in human erythrocytes. Biochim Biophys Acta. 1987;904(2):268-82.
100. Bevers EM, Williamson PL. Phospholipid scramblase: an update. FEBS Lett. 2010;584(13):2724-30.
101. Kamp D, Sieberg T, Haest CW. Inhibition and stimulation of phospholipid scrambling activity. Consequences for lipid asymmetry, echinocytosis, and microvesiculation of erythrocytes. Biochemistry. 2001;40(31):9438-46.
102. Lew VL, Bookchin RM. Ion transport pathology in the mechanism of sickle cell dehydration. Physiol Rev. 2005;85(1):179-200.
103. Etzion Z, Tiffert T, Bookchin RM, Lew VL. Effects of deoxygenation on active and passive Ca2+ transport and on the cytoplasmic Ca2+ levels of sickle cell anemia red cells. J Clin Invest. 1993;92(5):2489-98.
104. Joiner CH. Cation transport and volume regulation in sickle red blood cells. Am J Physiol. 1993;264(2 Pt 1):C251-70.
105. Morel O, Jesel L, Freyssinet JM, Toti F. Cellular mechanisms underlying the formation of circulating microparticles. Arterioscler Thromb Vasc Biol. 2011;31(1):15-26.
106. Aiken NR, Galey WR, Satterlee JD. A peroxidative model of human erythrocyte intracellular Ca2+ changes with in vivo cell aging: measurement by 19F-NMR spectroscopy. Biochim Biophys Acta. 1995;1270(1):52-7.
107. Woon LA, Holland JW, Kable EP, Roufogalis BD. Ca2+ sensitivity of phospholipid scrambling in human red cell ghosts. Cell Calcium. 1999;25(4):313-20.
108. Landsteiner K. Ueber agglutinationserscheinurgen normalen menschilchen blutes. Vien: Wien Klin Wschr; 1901.
109. Watkins WM, Morgan WTJ. Some observations on the O and H characters of human blood and secretions. Vox Sang. 1955;5:1-14.
110. Landsteiner K, Wiener AS. An Agglutinable Factor in Human Blood Recognized by Immune Sera for Rhesus Blood. Proceedings of the Society for Experimental Biology and Medicine. 1940;43(1):223-.
111. Nicholson LB. The immune system. Essays Biochem. 2016;60(3):275-301.
112. Springer GF, Horton RE. Blood group isoantibody stimulation in man by feeding blood group-active bacteria. J Clin Invest. 1969;48(7):1280-91.
113. Wuttke NJ, Macardle PJ, Zola H. Blood group antibodies are made by CD5+ and by CD5- B cells. Immunol Cell Biol. 1997;75(5):478-83.
114. Thomaidis T, Fouskaris G, Matsaniotis N. Isohemagglutinin activity in the first day of life. Am J Dis Child. 1967;113(6):654-7.
115. Branch DR. Anti-A and anti-B: what are they and where do they come from? Transfusion. 2015;55 Suppl 2:S74-9.
116. Quraishy N, Sapatnekar S. Chapter Six - Advances in Blood Typing. In: Makowski GS, editor. Advances in Clinical Chemistry. 77: Elsevier; 2016. p. 221-69.
117. International Society of Blood Transfusion (ISBT). Red Cell Immunogenetics and Blood Group Terminology 2019 [Available from: https://**www.isbtweb.org/working-parties/red-cell-immunogenetics-and-blood-group-terminology/**].
118. Dean L. Blood Groups and Red Cell Antigens- Chapter 2, Blood group antigens are surface markers on the red blood cell membrane. Bethesda (MD): National Center for Biotechnology Information (US); 2005 [Available from: https://**www.ncbi.nlm.nih.gov/books/NBK2264/**].
119. Kimura A, Uda T, Nakashima S, Ikeda H, Yasuda S, Osawa M, et al. ABO blood grouping of bloodstains by sandwich ELISA using monoclonal antibody specific for human red cell band 3. Int J Legal Med. 1993;105(4):209-12.
120. Yazdanbakhsh K, Ware RE, Noizat-Pirenne F. Red blood cell alloimmunization in sickle cell disease: pathophysiology, risk factors, and transfusion management. Blood. 2012;120(3):528-37.
121. Anstee DJ, Gampel A, Toye AM. Ex-vivo generation of human red cells for transfusion. Curr Opin Hematol. 2012;19(3):163-9.

122. Dias J, Gumenyuk M, Kang H, Vodyanik M, Yu J, Thomson JA, et al. Generation of red blood cells from human induced pluripotent stem cells. Stem Cells Dev. 2011;20(9):1639-47.
123. Griffiths RE, Kupzig S, Cogan N, Mankelow TJ, Betin VM, Trakarnsanga K, et al. Maturing reticulocytes internalize plasma membrane in glycophorin A-containing vesicles that fuse with autophagosomes before exocytosis. Blood. 2012;119(26):6296-306.
124. Trakarnsanga K, Wilson MC, Griffiths RE, Toye AM, Carpenter L, Heesom KJ, et al. Qualitative and quantitative comparison of the proteome of erythroid cells differentiated from human iPSCs and adult erythroid cells by multiplex TMT labelling and nanoLC-MS/MS. PLoS One. 2014;9(7):e100874.
125. Trakarnsanga K, Griffiths RE, Wilson MC, Blair A, Satchwell TJ, Meinders M, et al. An immortalized adult human erythroid line facilitates sustainable and scalable generation of functional red cells. Nat Commun. 2017;8:14750.
126. Kupzig S, Parsons SF, Curnow E, Anstee DJ, Blair A. Superior survival of ex vivo cultured human reticulocytes following transfusion into mice. Haematologica. 2017;102(3):476-83.
127. Mankelow TJ, Griffiths RE, Trompeter S, Flatt JF, Cogan NM, Massey EJ, et al. Autophagic vesicles on mature human reticulocytes explain phosphatidylserine-positive red cells in sickle cell disease. Blood. 2015;126(15):1831-4.
128. Beutler B, Du X, Xia Y. Precis on forward genetics in mice. Nat Immunol. 2007;8(7):659-64.
129. Rongvaux A, Takizawa H, Strowig T, Willinger T, Eynon EE, Flavell RA, et al. Human hemato-lymphoid system mice: current use and future potential for medicine. Annual review of immunology. 2013;31:635-74.
130. Yurino A, Takenaka K, Yamauchi T, Nunomura T, Uehara Y, Jinnouchi F, et al. Enhanced Reconstitution of Human Erythropoiesis and Thrombopoiesis in an Immunodeficient Mouse Model with Kit(Wv) Mutations. Stem cell reports. 2016;7(3):425-38.
131. Mosier DE, Gulizia RJ, Baird SM, Wilson DB. Transfer of a functional human immune system to mice with severe combined immunodeficiency. Nature. 1988;335(6187):256-9.
132. Lapidot T, Pflumio F, Doedens M, Murdoch B, Williams DE, Dick JE. Cytokine stimulation of multilineage hematopoiesis from immature human cells engrafted in SCID mice. Science. 1992;255(5048):1137-41.
133. Bosma GC, Custer RP, Bosma MJ. A severe combined immunodeficiency mutation in the mouse. Nature. 1983;301(5900):527-30.
134. Legrand N, Ploss A, Balling R, Becker PD, Borsotti C, Brezillon N, et al. Humanized mice for modeling human infectious disease: challenges, progress, and outlook. Cell Host Microbe. 2009;6(1):5-9.
135. Brehm MA, Cuthbert A, Yang C, Miller DM, DiIorio P, Laning J, et al. Parameters for establishing humanized mouse models to study human immunity: analysis of human hematopoietic stem cell engraftment in three immunodeficient strains of mice bearing the IL2rgamma(null) mutation. Clinical immunology (Orlando, Fla). 2010;135(1):84-98.
136. Hu Z, Van Rooijen N, Yang Y-G. Macrophages prevent human red blood cell reconstitution in immunodeficient mice. Blood. 2011;118(22):5938-46.
137. Cox CV, Diamanti P, Moppett JP, Blair A. Investigating CD99 Expression in Leukemia Propagating Cells in Childhood T Cell Acute Lymphoblastic Leukemia. PLOS ONE. 2016;11(10):e0165210.
138. Diamanti P, Cox CV, Moppett JP, Blair A. Dual targeting of Hsp90 in childhood acute lymphoblastic leukaemia. Br J Haematol. 2018;180(1):147-9.
139. Stephen J, Cairns LS, Pickford WJ, Vickers MA, Urbaniak SJ, Barker RN. Identification, immunomodulatory activity, and immunogenicity of the major helper T-cell epitope on the K blood group antigen. Blood. 2012;119(23):5563-74.
140. Smith NH, Henry KL, Cadwell CM, Bennett A, Hendrickson JE, Frame T, et al. Generation of transgenic mice with antithetical KEL1 and KEL2 human blood group antigens on red blood cells. Transfusion. 2012;52(12):2620-30.
141. Shinde P, Howie HL, Stegmann TC, Hay AM, Waterman HR, Szittner Z, et al. IgG Subclass Determines Suppression Versus Enhancement of Humoral Alloimmunity to Kell RBC Antigens in Mice. Frontiers in immunology. 2020;11:1516-.
142. Faes C, Ilich A, Sotiaux A, Sparkenbaugh EM, Henderson MW, Buczek L, et al. Red blood cells modulate structure and dynamics of venous clot formation in sickle cell disease. Blood. 2019;133(23):2529-41.

143. Moras M, Lefevre SD, Ostuni MA. From Erythroblasts to Mature Red Blood Cells: Organelle Clearance in Mammals. Front Physiol. 2017;8:1076.
144. Ji P, Murata-Hori M, Lodish HF. Formation of mammalian erythrocytes: chromatin condensation and enucleation. Trends Cell Biol. 2011;21(7):409-15.
145. Anderson HL, Brodsky IE, Mangalmurti NS. The Evolving Erythrocyte: Red Blood Cells as Modulators of Innate Immunity. J Immunol. 2018;201(5):1343-51.
146. Abugo OO, Rifkind JM. Oxidation of hemoglobin and the enhancement produced by nitroblue tetrazolium. J Biol Chem. 1994;269(40):24845-53.
147. Balagopalakrishna C, Manoharan PT, Abugo OO, Rifkind JM. Production of superoxide from hemoglobin-bound oxygen under hypoxic conditions. Biochemistry. 1996;35(20):6393-8.
148. Zhang ZW, Cheng J, Xu F, Chen YE, Du JB, Yuan M, et al. Red blood cell extrudes nucleus and mitochondria against oxidative stress. IUBMB Life. 2011;63(7):560-5.
149. Barodka VM, Nagababu E, Mohanty JG, Nyhan D, Berkowitz DE, Rifkind JM, et al. New insights provided by a comparison of impaired deformability with erythrocyte oxidative stress for sickle cell disease. Blood Cells Mol Dis. 2014;52(4):230-5.
150. Kalra H, Simpson RJ, Ji H, Aikawa E, Altevogt P, Askenase P, et al. Vesiclepedia: a compendium for extracellular vesicles with continuous community annotation. PLoS Biol. 2012;10(12):e1001450.
151. Wolf P. The nature and significance of platelet products in human plasma. Br J Haematol. 1967;13(3):269-88.
152. EL Andaloussi S, Mäger I, Breakefield XO, Wood MJ. Extracellular vesicles: biology and emerging therapeutic opportunities. Nat Rev Drug Discov. 2013;12(5):347-57.
153. McVey MJ, Maishan M, Blokland KEC, Bartlett N, Kuebler WM. Extracellular vesicles in lung health, disease, and therapy. Am J Physiol Lung Cell Mol Physiol. 2019;316(6):L977-L89.
154. Li A, Zhang T, Zheng M, Liu Y, Chen Z. Exosomal proteins as potential markers of tumor diagnosis. J Hematol Oncol. 2017;10(1):175.
155. Théry C, Ostrowski M, Segura E. Membrane vesicles as conveyors of immune responses. Nat Rev Immunol. 2009;9(8):581-93.
156. Cocucci E, Racchetti G, Meldolesi J. Shedding microvesicles: artefacts no more. Trends Cell Biol. 2009;19(2):43-51.
157. Théry C, Boussac M, Véron P, Ricciardi-Castagnoli P, Raposo G, Garin J, et al. Proteomic analysis of dendritic cell-derived exosomes: a secreted subcellular compartment distinct from apoptotic vesicles. J Immunol. 2001;166(12):7309-18.
158. Simpson RJ, Lim JW, Moritz RL, Mathivanan S. Exosomes: proteomic insights and diagnostic potential. Expert Rev Proteomics. 2009;6(3):267-83.
159. Escola JM, Kleijmeer MJ, Stoorvogel W, Griffith JM, Yoshie O, Geuze HJ. Selective enrichment of tetraspan proteins on the internal vesicles of multivesicular endosomes and on exosomes secreted by human B-lymphocytes. J Biol Chem. 1998;273(32):20121-7.
160. Bard MP, Hegmans JP, Hemmes A, Luider TM, Willemsen R, Severijnen LA, et al. Proteomic analysis of exosomes isolated from human malignant pleural effusions. Am J Respir Cell Mol Biol. 2004;31(1):114-21.
161. Gustafson D, Veitch S, Fish JE. Extracellular Vesicles as Protagonists of Diabetic Cardiovascular Pathology. Front Cardiovasc Med. 2017;4:71.
162. Harding C, Heuser J, Stahl P. Receptor-mediated endocytosis of transferrin and recycling of the transferrin receptor in rat reticulocytes. J Cell Biol. 1983;97(2):329-39.
163. Pan BT, Johnstone RM. Fate of the transferrin receptor during maturation of sheep reticulocytes in vitro: selective externalization of the receptor. Cell. 1983;33(3):967-78.
164. Werre JM, Willekens FL, Bosch FH, de Haans LD, van der Vegt SG, van den Bos AG, et al. The red cell revisited--matters of life and death. Cell Mol Biol (Noisy-le-grand). 2004;50(2):139-45.
165. Gov N, Cluitmans J, Sens P, Bosman GJCGM. Chapter 4 Cytoskeletal Control of Red Blood Cell Shape: Theory and Practice of Vesicle Formation. Advances in Planar Lipid Bilayers and Liposomes. 10: Academic Press; 2009. p. 95-119.
166. Sadallah S, Eken C, Schifferli JA. Erythrocyte-derived ectosomes have immunosuppressive properties. J Leukoc Biol. 2008;84(5):1316-25.
167. Fourcade O, Simon MF, Viodé C, Rugani N, Leballe F, Ragab A, et al. Secretory phospholipase A2 generates the novel lipid mediator lysophosphatidic acid in membrane microvesicles shed from activated cells. Cell. 1995;80(6):919-27.

168. Donadee C, Raat NJ, Kanias T, Tejero J, Lee JS, Kelley EE, et al. Nitric oxide scavenging by red blood cell microparticles and cell-free hemoglobin as a mechanism for the red cell storage lesion. Circulation. 2011;124(4):465-76.
169. Kapil V, Weitzberg E, Lundberg JO, Ahluwalia A. Clinical evidence demonstrating the utility of inorganic nitrate in cardiovascular health. Nitric Oxide. 2014;38:45-57.
170. Münzel T, Daiber A. Inorganic nitrite and nitrate in cardiovascular therapy: A better alternative to organic nitrates as nitric oxide donors? Vascul Pharmacol. 2018;102:1-10.
171. Liu C, Zhao W, Christ GJ, Gladwin MT, Kim-Shapiro DB. Nitric oxide scavenging by red cell microparticles. Free Radic Biol Med. 2013;65:1164-73.
172. Barteneva NS, Fasler-Kan E, Bernimoulin M, Stern JN, Ponomarev ED, Duckett L, et al. Circulating microparticles: square the circle. BMC Cell Biol. 2013;14:23.
173. Elsayh KI, Zahran AM, El-Abaseri TB, Mohamed AO, El-Metwally TH. Hypoxia biomarkers, oxidative stress, and circulating microparticles in pediatric patients with thalassemia in Upper Egypt. Clin Appl Thromb Hemost. 2014;20(5):536-45.
174. De Franceschi L, Bertoldi M, Matte A, Santos Franco S, Pantaleo A, Ferru E, et al. Oxidative stress and β-thalassemic erythroid cells behind the molecular defect. Oxid Med Cell Longev. 2013;2013:985210.
175. Alaarg A, Schiffelers RM, van Solinge WW, van Wijk R. Red blood cell vesiculation in hereditary hemolytic anemia. Front Physiol. 2013;4:365.
176. Lentz BR. Exposure of platelet membrane phosphatidylserine regulates blood coagulation. Prog Lipid Res. 2003;42(5):423-38.
177. Biró E, Sturk-Maquelin KN, Vogel GM, Meuleman DG, Smit MJ, Hack CE, et al. Human cell-derived microparticles promote thrombus formation in vivo in a tissue factor-dependent manner. J Thromb Haemost. 2003;1(12):2561-8.
178. Camus SM, De Moraes JA, Bonnin P, Abbyad P, Le Jeune S, Lionnet F, et al. Circulating cell membrane microparticles transfer heme to endothelial cells and trigger vasoocclusions in sickle cell disease. Blood. 2015;125(24):3805-14.
179. Liu RM, Adam M, Hammond JR, Orr L, Turbide C. Vesicle formation during reticulocyte maturation. Association of plasma membrane activities with released vesicles (exosomes). J Biol Chem. 1987;262(19):9412-20.
180. Ney PA. Normal and disordered reticulocyte maturation. Curr Opin Hematol. 2011;18(3):152-7.
181. Razi M, Chan EY, Tooze SA. Early endosomes and endosomal coatomer are required for autophagy. J Cell Biol. 2009;185(2):305-21.
182. Mankelow TJ, Griffiths RE, Trompeter S, Flatt JF, Cogan NM, Massey EJ, et al. The ins and outs of reticulocyte maturation revisited: The role of autophagy in sickle cell disease. Autophagy. 2016;12(3):590-1.
183. Rubin O, Crettaz D, Canellini G, Tissot JD, Lion N. Microparticles in stored red blood cells: an approach using flow cytometry and proteomic tools. Vox Sang. 2008;95(4):288-97.
184. Rumsby MG, Trotter J, Allan D, Michell RH. Recovery of membrane micro-vesicles from human erythrocytes stored for transfusion: a mechanism for the erythrocyte discocyte-to-spherocyte shape transformation. Biochem Soc Trans. 1977;5(1):126-8.
185. Sharma S, Sharma P, Tyler LN. Transfusion of blood and blood products: indications and complications. Am Fam Physician. 2011;83(6):719-24.
186. Wannez A, Devalet B, Chatelain B, Chatelain C, Dogné JM, Mullier F. Extracellular Vesicles in Red Blood Cell Concentrates: An Overview. Transfus Med Rev. 2019;33(2):125-30.
187. JPAC- Joint United Kingdom Blood Transfusion Services Professional Advisory Committe. Handbook of Transfusion Medicine, 3.3. Blood products, 3.3.2.3. Specifications of blood components. United Kingdom Blood Services: TSO; 2013.
188. Westerman M, Porter JB. Red blood cell-derived microparticles: An overview. Blood Cells Mol Dis. 2016;59:134-9.
189. Kor DJ, Van Buskirk CM, Gajic O. Red blood cell storage lesion. Bosn J Basic Med Sci. 2009;9 Suppl 1:21-7.
190. D'Alessandro A, Liumbruno G, Grazzini G, Zolla L. Red blood cell storage: the story so far. Blood Transfus. 2010;8(2):82-8.

191. D'Alessandro A, Kriebardis AG, Rinalducci S, Antonelou MH, Hansen KC, Papassideri IS, et al. An update on red blood cell storage lesions, as gleaned through biochemistry and omics technologies. Transfusion. 2015;55(1):205-19.
192. Bosman GJ, Lasonder E, Luten M, Roerdinkholder-Stoelwinder B, Novotný VM, Bos H, et al. The proteome of red cell membranes and vesicles during storage in blood bank conditions. Transfusion. 2008;48(5):827-35.
193. Gevi F, D'Alessandro A, Rinalducci S, Zolla L. Alterations of red blood cell metabolome during cold liquid storage of erythrocyte concentrates in CPD-SAGM. J Proteomics. 2012;76 Spec No.:168-80.
194. Zimrin AB, Hess JR. Current issues relating to the transfusion of stored red blood cells. Vox Sang. 2009;96(2):93-103.
195. Nemkov T, Hansen KC, Dumont LJ, D'Alessandro A. Metabolomics in transfusion medicine. Transfusion. 2016;56(4):980-93.
196. Tzounakas VL, Georgatzakou HT, Kriebardis AG, Voulgaridou AI, Stamoulis KE, Foudoulaki-Paparizos LE, et al. Donor variation effect on red blood cell storage lesion: a multivariable, yet consistent, story. Transfusion. 2016;56(6):1274-86.
197. Tzounakas VL, Georgatzakou HT, Kriebardis AG, Papageorgiou EG, Stamoulis KE, Foudoulaki-Paparizos LE, et al. Uric acid variation among regular blood donors is indicative of red blood cell susceptibility to storage lesion markers: A new hypothesis tested. Transfusion. 2015;55(11):2659-71.
198. Antonelou MH, Kriebardis AG, Stamoulis KE, Economou-Petersen E, Margaritis LH, Papassideri IS. Red blood cell aging markers during storage in citrate-phosphate-dextrose-saline-adenine-glucose-mannitol. Transfusion. 2010;50(2):376-89.
199. Bicalho B, Pereira AS, Acker JP. Buffy coat (top/bottom)- and whole-blood filtration (top/top)-produced red cell concentrates differ in size of extracellular vesicles. Vox Sang. 2015;109(3):214-20.
200. Almizraq RJ, Holovati JL, Acker JP. Characteristics of Extracellular Vesicles in Red Blood Concentrates Change with Storage Time and Blood Manufacturing Method. Transfus Med Hemother. 2018;45(3):185-93.
201. Jy W, Horstman LL, Ahn YS. Microparticle size and its relation to composition, functional activity, and clinical significance. Semin Thromb Hemost. 2010;36(8):876-80.
202. Pertinhez TA, Casali E, Baroni F, Berni P, Baricchi R, Spisni A. A Comparative Study of the Effect of Leukoreduction and Pre-storage Leukodepletion on Red Blood Cells during Storage. Front Mol Biosci. 2016;3:13.
203. García-Roa M, Del Carmen Vicente-Ayuso M, Bobes AM, Pedraza AC, González-Fernández A, Martín MP, et al. Red blood cell storage time and transfusion: current practice, concerns and future perspectives. Blood Transfus. 2017;15(3):222-31.
204. Högman CF, Hedlund K, Sahleström Y. Red cell preservation in protein-poor media. III. Protection against in vitro hemolysis. Vox Sang. 1981;41(5-6):274-81.
205. Tissot JD, Bardyn M, Sonego G, Abonnenc M, Prudent M. The storage lesions: From past to future. Transfus Clin Biol. 2017;24(3):277-84.
206. Kriebardis AG, Antonelou MH, Stamoulis KE, Economou-Petersen E, Margaritis LH, Papassideri IS. RBC-derived vesicles during storage: ultrastructure, protein composition, oxidation, and signaling components. Transfusion. 2008;48(9):1943-53.
207. D'Alessandro A, Reisz JA, Culp-Hill R, Korsten H, van Bruggen R, de Korte D. Metabolic effect of alkaline additives and guanosine/gluconate in storage solutions for red blood cells. Transfusion. 2018;58(8):1992-2002.
208. Rolfsson Ó, Sigurjonsson Ó, Magnusdottir M, Johannsson F, Paglia G, Guðmundsson S, et al. Metabolomics comparison of red cells stored in four additive solutions reveals differences in citrate anticoagulant permeability and metabolism. Vox Sang. 2017;112(4):326-35.
209. Wiley JS, McCulloch KE, Bowden DS. Increased calcium permeability of cold-stored erythrocytes. Blood. 1982;60(1):92-8.
210. D'Amici GM, Rinalducci S, Zolla L. Proteomic analysis of RBC membrane protein degradation during blood storage. J Proteome Res. 2007;6(8):3242-55.
211. Rinalducci S, Ferru E, Blasi B, Turrini F, Zolla L. Oxidative stress and caspase-mediated fragmentation of cytoplasmic domain of erythrocyte band 3 during blood storage. Blood Transfus. 2012;10 Suppl 2:s55-62.

212. Wolfe LC, Byrne AM, Lux SE. Molecular defect in the membrane skeleton of blood bank-stored red cells. Abnormal spectrin-protein 4.1-actin complex formation. J Clin Invest. 1986;78(6):1681-6.
213. Ralser M, Wamelink MM, Kowald A, Gerisch B, Heeren G, Struys EA, et al. Dynamic rerouting of the carbohydrate flux is key to counteracting oxidative stress. J Biol. 2007;6(4):10.
214. Rinalducci S, Marrocco C, Zolla L. Thiol-based regulation of glyceraldehyde-3-phosphate dehydrogenase in blood bank-stored red blood cells: a strategy to counteract oxidative stress. Transfusion. 2015;55(3):499-506.
215. Reisz JA, Wither MJ, Dzieciatkowska M, Nemkov T, Issaian A, Yoshida T, et al. Oxidative modifications of glyceraldehyde 3-phosphate dehydrogenase regulate metabolic reprogramming of stored red blood cells. Blood. 2016;128(12):e32-42.
216. Wither M, Dzieciatkowska M, Nemkov T, Strop P, D'Alessandro A, Hansen KC. Hemoglobin oxidation at functional amino acid residues during routine storage of red blood cells. Transfusion. 2016;56(2):421-6.
217. Prudent M, Crettaz D, Delobel J, Seghatchian J, Tissot JD, Lion N. Differences between calcium-stimulated and storage-induced erythrocyte-derived microvesicles. Transfus Apher Sci. 2015;53(2):153-8.
218. Prudent M, Delobel J, Hübner A, Benay C, Lion N, Tissot JD. Proteomics of Stored Red Blood Cell Membrane and Storage-Induced Microvesicles Reveals the Association of Flotillin-2 With Band 3 Complexes. Front Physiol. 2018;9:421.
219. Salzer U, Zhu R, Luten M, Isobe H, Pastushenko V, Perkmann T, et al. Vesicles generated during storage of red cells are rich in the lipid raft marker stomatin. Transfusion. 2008;48(3):451-62.
220. Salzer U, Ahorn H, Prohaska R. Identification of the phosphorylation site on human erythrocyte band 7 integral membrane protein: implications for a monotopic protein structure. Biochim Biophys Acta. 1993;1151(2):149-52.
221. Verhoeven AJ, Hilarius PM, Dekkers DW, Lagerberg JW, de Korte D. Prolonged storage of red blood cells affects aminophospholipid translocase activity. Vox Sang. 2006;91(3):244-51.
222. Kestens V, Bozatzidis V, De Temmerman PJ, Ramaye Y, Roebben G. Validation of a particle tracking analysis method for the size determination of nano- and microparticles. J Nanopart Res. 2017;19(8):271.
223. Gross J, Sayle S, Karow AR, Bakowsky U, Garidel P. Nanoparticle tracking analysis of particle size and concentration detection in suspensions of polymer and protein samples: Influence of experimental and data evaluation parameters. Eur J Pharm Biopharm. 2016;104:30-41.
224. Witwer KW, Buzás EI, Bemis LT, Bora A, Lässer C, Lötvall J, et al. Standardization of sample collection, isolation and analysis methods in extracellular vesicle research. J Extracell Vesicles. 2013;2.
225. Parisse P, Rago I, Ulloa Severino L, Perissinotto F, Ambrosetti E, Paoletti P, et al. Atomic force microscopy analysis of extracellular vesicles. Eur Biophys J. 2017;46(8):813-20.
226. Lutz HU, Liu SC, Palek J. Release of spectrin-free vesicles from human erythrocytes during ATP depletion. I. Characterization of spectrin-free vesicles. J Cell Biol. 1977;73(3):548-60.
227. Antonelou MH, Seghatchian J. Update on extracellular vesicles inside red blood cell storage units: Adjust the sails closer to the new wind. Transfus Apher Sci. 2016;55(1):92-104.
228. Poncelet P, Robert S, Bailly N, Garnache-Ottou F, Bouriche T, Devalet B, et al. Tips and tricks for flow cytometry-based analysis and counting of microparticles. Transfus Apher Sci. 2015;53(2):110-26.
229. Lacroix R, Robert S, Poncelet P, Kasthuri RS, Key NS, Dignat-George F, et al. Standardization of platelet-derived microparticle enumeration by flow cytometry with calibrated beads: results of the International Society on Thrombosis and Haemostasis SSC Collaborative workshop. J Thromb Haemost. 2010;8(11):2571-4.
230. van der Pol E, Sturk A, van Leeuwen T, Nieuwland R, Coumans F, group I-S-VW. Standardization of extracellular vesicle measurements by flow cytometry through vesicle diameter approximation. J Thromb Haemost. 2018;16(6):1236-45.
231. van der Pol E, Coumans FA, Grootemaat AE, Gardiner C, Sargent IL, Harrison P, et al. Particle size distribution of exosomes and microvesicles determined by transmission electron microscopy, flow cytometry, nanoparticle tracking analysis, and resistive pulse sensing. J Thromb Haemost. 2014;12(7):1182-92.

232. Lannigan J, Erdbruegger U. Imaging flow cytometry for the characterization of extracellular vesicles. Methods. 2017;112:55-67.
233. Headland SE, Jones HR, D'Sa AS, Perretti M, Norling LV. Cutting-edge analysis of extracellular microparticles using ImageStream(X) imaging flow cytometry. Sci Rep. 2014;4:5237.
234. Görgens A, Bremer M, Ferrer-Tur R, Murke F, Tertel T, Horn PA, et al. Optimisation of imaging flow cytometry for the analysis of single extracellular vesicles by using fluorescence-tagged vesicles as biological reference material. J Extracell Vesicles. 2019;8(1):1587567.
235. Aleshnick M, Foley JH, Keating FK, Butenas S. Procoagulant activity in stored units of red blood cells. Biochem Biophys Res Commun. 2016;474(4):680-5.
236. Lu C, Shi J, Yu H, Hou J, Zhou J. Procoagulant activity of long-term stored red blood cells due to phosphatidylserine exposure. Transfus Med. 2011;21(3):150-7.
237. Fischer D, Büssow J, Meybohm P, Weber CF, Zacharowski K, Urbschat A, et al. Microparticles from stored red blood cells enhance procoagulant and proinflammatory activity. Transfusion. 2017;57(11):2701-11.
238. El-Benna J, Dang PM, Gougerot-Pocidalo MA. Priming of the neutrophil NADPH oxidase activation: role of p47phox phosphorylation and NOX2 mobilization to the plasma membrane. Semin Immunopathol. 2008;30(3):279-89.
239. Cardo LJ, Wilder D, Salata J. Neutrophil priming, caused by cell membranes and microvesicles in packed red blood cell units, is abrogated by leukocyte depletion at collection. Transfus Apher Sci. 2008;38(2):117-25.
240. Belizaire RM, Prakash PS, Richter JR, Robinson BR, Edwards MJ, Caldwell CC, et al. Microparticles from stored red blood cells activate neutrophils and cause lung injury after hemorrhage and resuscitation. J Am Coll Surg. 2012;214(4):648-55; discussion 56-7.
241. Organisation W-WH. Anaemia: World Health Organisation; [Available from: https://**www.who.int/health-topics/anaemia#tab=tab_1** [Accessed.
242. JPAC- Joint United Kingdom Blood Transfusion Services Professional Advisory Committee. Transfusion Handbook, 8. Effective transfusion in medical patients, 8.6. Haemoglobinopathies [Available from: https://**www.transfusionguidelines.org/transfusion-handbook/8-effective-transfusion-in-medical-patients/8-6-haemoglobinopathies**].
243. T N, LF G-M, DT L. Beta Thalassemia. Treasure Island (FL): StatPearls Publishing; 2020.
244. Committee J-JUKUBTaTTSPA. Handbook of Transfusion Medicine, 8. Effective transfusion in medical patients, 8.6. Haemoglobinopathies. 5 ed. Committee JUKUBTaTTSPA, editor. United Kingdom Blood Services: TSO; 2013.
245. Ingram VM. A specific chemical difference between the globins of normal human and sickle-cell anaemia haemoglobin. Nature. 1956;178(4537):792-4.
246. McGann PT, Hernandez AG, Ware RE. Sickle cell anemia in sub-Saharan Africa: advancing the clinical paradigm through partnerships and research. Blood. 2017;129(2):155-61.
247. Dormandy E, James J, Inusa B, Rees D. How many people have sickle cell disease in the UK? J Public Health (Oxf). 2018;40(3):e291-e5.
248. Dykes G, Crepeau RH, Edelstein SJ. Three-dimensional reconstruction of the fibres of sickle cell haemoglobin. Nature. 1978;272(5653):506-10.
249. Carragher B, Bluemke DA, Gabriel B, Potel MJ, Josephs R. Structural analysis of polymers of sickle cell hemoglobin. I. Sickle hemoglobin fibers. J Mol Biol. 1988;199(2):315-31.
250. Wishner BC, Ward KB, Lattman EE, Love WE. Crystal structure of sickle-cell deoxyhemoglobin at 5 A resolution. J Mol Biol. 1975;98(1):179-94.
251. Fronticelli C, Gold R. Conformational relevance of the beta6Glu replaced by Val mutation in the beta subunits and in the beta(1-55) and beta(1-30) peptides of hemoglobin S. J Biol Chem. 1976;251(16):4968-72.
252. Brunson A, Lei A, Rosenberg AS, White RH, Keegan T, Wun T. Increased incidence of VTE in sickle cell disease patients: risk factors, recurrence and impact on mortality. Br J Haematol. 2017;178(2):319-26.
253. Odièvre MH, Verger E, Silva-Pinto AC, Elion J. Pathophysiological insights in sickle cell disease. Indian J Med Res. 2011;134:532-7.
254. Edelstein SJ, Telford JN, Crepeau RH. Structure of fibers of sickle cell hemoglobin. Proc Natl Acad Sci U S A. 1973;70(4):1104-7.
255. Allan D, Limbrick AR, Thomas P, Westerman MP. Release of spectrin-free spicules on reoxygenation of sickled erythrocytes. Nature. 1982;295(5850):612-3.

256. Hannemann A, Cytlak UMC, Gbotosho OT, Rees DC, Tewari S, Gibson JS. Effects of o-vanillin on K+ transport of red blood cells from patients with sickle cell disease. Blood Cells, Molecules, and Diseases. 2014;53(1):21-6.
257. Welbourn EM, Wilson MT, Yusof A, Metodiev MV, Cooper CE. The mechanism of formation, structure and physiological relevance of covalent hemoglobin attachment to the erythrocyte membrane. Free Radic Biol Med. 2017;103:95-106.
258. Waugh SM, Low PS. Hemichrome binding to band 3: nucleation of Heinz bodies on the erythrocyte membrane. Biochemistry. 1985;24(1):34-9.
259. Kaushal M, Byrnes C, Khademian Z, Duncan N, Luban NL, Miller JL, et al. Examination of Reticulocytosis among Chronically Transfused Children with Sickle Cell Anemia. PLoS One. 2016;11(4):e0153244.
260. Hebbel RP. Adhesion of sickle red cells to endothelium: myths and future directions. Transfus Clin Biol. 2008;15(1-2):14-8.
261. El Nemer W, Colin Y, Le Van Kim C. Role of Lu/BCAM glycoproteins in red cell diseases. Transfus Clin Biol. 2010;17(3):143-7.
262. Kaul DK, Hebbel RP. Hypoxia/reoxygenation causes inflammatory response in transgenic sickle mice but not in normal mice. J Clin Invest. 2000;106(3):411-20.
263. Hebbel RP, Osarogiagbon R, Kaul D. The endothelial biology of sickle cell disease: inflammation and a chronic vasculopathy. Microcirculation. 2004;11(2):129-51.
264. Pauling L, Itano HA. Sickle cell anemia a molecular disease. Science. 1949;110(2865):543-8.
265. Morris CR, Kato GJ, Poljakovic M, Wang X, Blackwelder WC, Sachdev V, et al. Dysregulated arginine metabolism, hemolysis-associated pulmonary hypertension, and mortality in sickle cell disease. JAMA. 2005;294(1):81-90.
266. Pinto VM, Balocco M, Quintino S, Forni GL. Sickle cell disease: a review for the internist. Internal and Emergency Medicine. 2019;14(7):1051-64.
267. Shet AS, Aras O, Gupta K, Hass MJ, Rausch DJ, Saba N, et al. Sickle blood contains tissue factor-positive microparticles derived from endothelial cells and monocytes. Blood. 2003;102(7):2678-83.
268. van Beers EJ, Schaap MC, Berckmans RJ, Nieuwland R, Sturk A, van Doormaal FF, et al. Circulating erythrocyte-derived microparticles are associated with coagulation activation in sickle cell disease. Haematologica. 2009;94(11):1513-9.
269. Westerman M, Pizzey A, Hirschman J, Cerino M, Weil-Weiner Y, Ramotar P, et al. Microvesicles in haemoglobinopathies offer insights into mechanisms of hypercoagulability, haemolysis and the effects of therapy. British journal of haematology. 2008;142(1):126-35.
270. Platt OS, Thorington BD, Brambilla DJ, Milner PF, Rosse WF, Vichinsky E, et al. Pain in sickle cell disease. Rates and risk factors. N Engl J Med. 1991;325(1):11-6.
271. Bunn HF. Pathogenesis and treatment of sickle cell disease. N Engl J Med. 1997;337(11):762-9.
272. Ohene-Frempong K, Weiner SJ, Sleeper LA, Miller ST, Embury S, Moohr JW, et al. Cerebrovascular accidents in sickle cell disease: rates and risk factors. Blood. 1998;91(1):288-94.
273. Topley JM, Rogers DW, Stevens MC, Serjeant GR. Acute splenic sequestration and hypersplenism in the first five years in homozygous sickle cell disease. Arch Dis Child. 1981;56(10):765-9.
274. Powell RW, Levine GL, Yang YM, Mankad VN. Acute splenic sequestration crisis in sickle cell disease: early detection and treatment. J Pediatr Surg. 1992;27(2):215-8; discussion 8-9.
275. Bohnsack JF, Brown EJ. The role of the spleen in resistance to infection. Annu Rev Med. 1986;37:49-59.
276. William BM, Corazza GR. Hyposplenism: a comprehensive review. Part I: basic concepts and causes. Hematology. 2007;12(1):1-13.
277. Cameron PU, Jones P, Gorniak M, Dunster K, Paul E, Lewin S, et al. Splenectomy associated changes in IgM memory B cells in an adult spleen registry cohort. PLoS One. 2011;6(8):e23164.
278. Ochocinski D, Dalal M, Black LV, Carr S, Lew J, Sullivan K, et al. Life-Threatening Infectious Complications in Sickle Cell Disease: A Concise Narrative Review. Front Pediatr. 2020;8:38.

279. Hojyo S, Fukada T. Roles of Zinc Signaling in the Immune System. J Immunol Res. 2016;2016:6762343.
280. Dunkelberger JR, Song WC. Complement and its role in innate and adaptive immune responses. Cell Res. 2010;20(1):34-50.
281. Pearson HA, Spencer RP, Cornelius EA. Functional asplenia in sickle-cell anemia. N Engl J Med. 1969;281(17):923-6.
282. Crosby WH. Hyposplenism: an inquiry into normal functions of the spleen. Annu Rev Med. 1963;14:349-70.
283. Brown AK, Sleeper LA, Miller ST, Pegelow CH, Gill FM, Waclawiw MA. Reference values and hematologic changes from birth to 5 years in patients with sickle cell disease. Cooperative Study of Sickle Cell Disease. Arch Pediatr Adolesc Med. 1994;148(8):796-804.
284. Ballester OF, Abdallah JM, Prasad AS. Impaired IgM antibody responses to an influenza virus vaccine in adults with sickle cell anemia. Am J Hematol. 1985;20(4):409-12.
285. Koffi KG, Sawadogo D, Meite M, Nanho DC, Tanoh ES, Attia AK, et al. Reduced levels of T-cell subsets CD4+ and CD8+ in homozygous sickle cell anaemia patients with splenic defects. Hematol J. 2003;4(5):363-5.
286. Romagnani S. T-cell subsets (Th1 versus Th2). Ann Allergy Asthma Immunol. 2000;85(1):9-18; quiz , 21.
287. Rogers DW, Clarke JM, Cupidore L, Ramlal AM, Sparke BR, Serjeant GR. Early deaths in Jamaican children with sickle cell disease. Br Med J. 1978;1(6126):1515-6.
288. Rees DC, Olujohungbe AD, Parker NE, Stephens AD, Telfer P, Wright J, et al. Guidelines for the management of the acute painful crisis in sickle cell disease. Br J Haematol. 2003;120(5):744-52.
289. Griffin TC, McIntire D, Buchanan GR. High-dose intravenous methylprednisolone therapy for pain in children and adolescents with sickle cell disease. N Engl J Med. 1994;330(11):733-7.
290. Raphael JL, Kamdar A, Wang T, Liu H, Mahoney DH, Mueller BU. Day hospital versus inpatient management of uncomplicated vaso-occlusive crises in children with sickle cell disease. Pediatr Blood Cancer. 2008;51(3):398-401.
291. Davis BA, Allard S, Qureshi A, Porter JB, Pancham S, Win N, et al. Guidelines on red cell transfusion in sickle cell disease. Part I: principles and laboratory aspects. Br J Haematol. 2017;176(2):179-91.
292. Agrawal RK, Patel RK, Shah V, Nainiwal L, Trivedi B. Hydroxyurea in sickle cell disease: drug review. Indian J Hematol Blood Transfus. 2014;30(2):91-6.
293. Odièvre MH, Bony V, Benkerrou M, Lapouméroulie C, Alberti C, Ducrocq R, et al. Modulation of erythroid adhesion receptor expression by hydroxyurea in children with sickle cell disease. Haematologica. 2008;93(4):502-10.
294. Leonard A, Tisdale J, Abraham A. Curative options for sickle cell disease: haploidentical stem cell transplantation or gene therapy? British Journal of Haematology. 2020;189(3):408-23.
295. NHS. Sickle cell disease- Treatment 2019 [Available from: https://**www.nhs.uk/conditions/sickle-cell-disease/treatment/**].
296. Sickle cell disease news. Approved treatments 2019 [Available from: https://sicklecellanemianews.com/approved-treatments/ [Accessed.
297. Niihara Y, Smith WR, Stark CW. A Phase 3 Trial of l-Glutamine in Sickle Cell Disease. N Engl J Med. 2018;379(19):1880.
298. Matsui NM, Borsig L, Rosen SD, Yaghmai M, Varki A, Embury SH. P-selectin mediates the adhesion of sickle erythrocytes to the endothelium. Blood. 2001;98(6):1955-62.
299. Riley TR, Riley TT. Profile of crizanlizumab and its potential in the prevention of pain crises in sickle cell disease: evidence to date. J Blood Med. 2019;10:307-11.
300. Vichinsky E, Hoppe CC, Ataga KI, Ware RE, Nduba V, El-Beshlawy A, et al. A Phase 3 Randomized Trial of Voxelotor in Sickle Cell Disease. N Engl J Med. 2019;381(6):509-19.
301. Netea MG, Schlitzer A, Placek K, Joosten LAB, Schultze JL. Innate and Adaptive Immune Memory: an Evolutionary Continuum in the Host's Response to Pathogens. Cell Host Microbe. 2019;25(1):13-26.
302. Dean L. Blood Groups and Red Cell Antigens - Chapter 3, Blood transfusions and the immune system. Bethesda (MD): National Center for Biotechnology Information (US); 2005 [Available from: https://**www.ncbi.nlm.nih.gov/books/NBK2265**].

303. McDevitt H. The discovery of linkage between the MHC and genetic control of the immune response. Immunol Rev. 2002;185:78-85.
304. Trowsdale J, Knight JC. Major histocompatibility complex genomics and human disease. Annu Rev Genomics Hum Genet. 2013;14:301-23.
305. Brown CJ, Navarrete CV. Clinical relevance of the HLA system in blood transfusion. Vox Sang. 2011;101(2):93-105.
306. Wooldridge L, Ekeruche-Makinde J, van den Berg HA, Skowera A, Miles JJ, Tan MP, et al. A single autoimmune T cell receptor recognizes more than a million different peptides. J Biol Chem. 2012;287(2):1168-77.
307. Parslow T, Stites D, Terr A, Imboden J. Imunologia Médica. 10th ed. Rio de Janeiro: Guanabara Koogan; 2004.
308. Mincheff MS, Meryman HT, Kapoor V, Alsop P, Wötzel M. Blood transfusion and immunomodulation: a possible mechanism. Vox Sang. 1993;65(1):18-24.
309. Zimring JC, Welniak L, Semple JW, Ness PM, Slichter SJ, Spitalnik SL, et al. Current problems and future directions of transfusion-induced alloimmunization: summary of an NHLBI working group. Transfusion. 2011;51(2):435-41.
310. Habibi A, Mekontso-Dessap A, Guillaud C, Michel M, Razazi K, Khellaf M, et al. Delayed hemolytic transfusion reaction in adult sickle-cell disease: presentations, outcomes, and treatments of 99 referral center episodes. Am J Hematol. 2016;91(10):989-94.
311. Noizat-Pirenne F, Bachir D, Chadebech P, Michel M, Plonquet A, Lecron JC, et al. Rituximab for prevention of delayed hemolytic transfusion reaction in sickle cell disease. Haematologica. 2007;92(12):e132-5.
312. Campbell-Lee SA, Kittles RA. Red blood cell alloimmunization in sickle cell disease: listen to your ancestors. Transfus Med Hemother. 2014;41(6):431-5.
313. Nickel RS, Hendrickson JE, Fasano RM, Meyer EK, Winkler AM, Yee MM, et al. Impact of red blood cell alloimmunization on sickle cell disease mortality: a case series. Transfusion. 2016;56(1):107-14.
314. Pirenne F, Yazdanbakhsh K. How I safely transfuse patients with sickle-cell disease and manage delayed hemolytic transfusion reactions. Blood. 2018;131(25):2773-81.
315. Pandey H, Das SS, Chaudhary R. Red cell alloimmunization in transfused patients: A silent epidemic revisited. Asian J Transfus Sci. 2014;8(2):75-7.
316. Yazdanbakhsh K. Mechanisms of sickle cell alloimmunization. Transfus Clin Biol. 2015;22(3):178-81.
317. Bao W, Zhong H, Li X, Lee MT, Schwartz J, Sheth S, et al. Immune regulation in chronically transfused allo-antibody responder and nonresponder patients with sickle cell disease and β-thalassemia major. Am J Hematol. 2011;86(12):1001-6.
318. Platt OS. Sickle cell anemia as an inflammatory disease. J Clin Invest. 2000;106(3):337-8.
319. Iikuni N, Lourenço EV, Hahn BH, La Cava A. Cutting edge: Regulatory T cells directly suppress B cells in systemic lupus erythematosus. J Immunol. 2009;183(3):1518-22.
320. Lim HW, Hillsamer P, Banham AH, Kim CH. Cutting edge: direct suppression of B cells by CD4+ CD25+ regulatory T cells. J Immunol. 2005;175(7):4180-3.
321. Wing JB, Sakaguchi S. Multiple treg suppressive modules and their adaptability. Front Immunol. 2012;3:178.
322. Strauss RG, Levy GJ, Sotelo-Avila C, Albanese MA, Hume H, Schloz L, et al. National survey of neonatal transfusion practices: II. Blood component therapy. Pediatrics. 1993;91(3):530-6.
323. Floss AM, Strauss RG, Goeken N, Knox L. Multiple transfusion fail to provoke antibodies against blood cell antigens in human infants. Transfusion. 1986;26(5):419-22.
324. Diamond LK, Allen DM, Magill FB. Congenital (erythroid) hypoplastic anemia. A 25-year study. Am J Dis Child. 1961;102:403-15.
325. Spanos T, Karageorga M, Ladis V, Peristeri J, Hatziliami A, Kattamis C. Red cell alloantibodies in patients with thalassemia. Vox Sang. 1990;58(1):50-5.
326. Michail-Merianou V, Pamphili-Panousopoulou L, Piperi-Lowes L, Pelegrinis E, Karaklis A. Alloimmunization to red cell antigens in thalassemia: comparative study of usual versus better-match transfusion programmes. Vox Sang. 1987;52(1-2):95-8.
327. Calabro S, Gallman A, Gowthaman U, Liu D, Chen P, Liu J, et al. Bridging channel dendritic cells induce immunity to transfused red blood cells. J Exp Med. 2016;213(6):887-96.

328. Sun CM, Fiette L, Tanguy M, Leclerc C, Lo-Man R. Ontogeny and innate properties of neonatal dendritic cells. Blood. 2003;102(2):585-91.
329. Dakic A, Shao QX, D'Amico A, O'Keeffe M, Chen WF, Shortman K, et al. Development of the dendritic cell system during mouse ontogeny. J Immunol. 2004;172(2):1018-27.
330. Wubbolts R, Leckie RS, Veenhuizen PTM, Schwarzmann G, Möbius W, Hoernschemeyer J, et al. Proteomic and Biochemical Analyses of Human B Cell-derived Exosomes: potential implications for their function and multivesicular body formation. Journal of Biological Chemistry. 2003;278(13):10963-72.
331. Hristov M, Erl W, Linder S, Weber PC. Apoptotic bodies from endothelial cells enhance the number and initiate the differentiation of human endothelial progenitor cells in vitro. Blood. 2004;104(9):2761-6.
332. Camus SM, Gausserès B, Bonnin P, Loufrani L, Grimaud L, Charue D, et al. Erythrocyte microparticles can induce kidney vaso-occlusions in a murine model of sickle cell disease. Blood. 2012;120(25):5050-8.
333. Chiu D, Lubin B, Roelofsen B, van Deenen LL. Sickled erythrocytes accelerate clotting in vitro: an effect of abnormal membrane lipid asymmetry. Blood. 1981;58(2):398-401.
334. Griffiths RE, Kupzig S, Cogan N, Mankelow TJ, Betin VM, Trakarnsanga K, et al. The ins and outs of human reticulocyte maturation: autophagy and the endosome/exosome pathway. Autophagy. 2012;8(7):1150-1.
335. Vermes I, Haanen C, Steffens-Nakken H, Reutelingsperger C. A novel assay for apoptosis. Flow cytometric detection of phosphatidylserine expression on early apoptotic cells using fluorescein labelled Annexin V. J Immunol Methods. 1995;184(1):39-51.
336. Koopman G, Reutelingsperger CP, Kuijten GA, Keehnen RM, Pals ST, van Oers MH. Annexin V for flow cytometric detection of phosphatidylserine expression on B cells undergoing apoptosis. Blood. 1994;84(5):1415-20.
337. Simak J, Holada K, Risitano AM, Zivny JH, Young NS, Vostal JG. Elevated circulating endothelial membrane microparticles in paroxysmal nocturnal haemoglobinuria. Br J Haematol. 2004;125(6):804-13.
338. Quirino MG, Colli CM, Macedo LC, Sell AM, Visentainer JEL. Methods for blood group antigens detection: cost-effectiveness analysis of phenotyping and genotyping. Hematol Transfus Cell Ther. 2019;41(1):44-9.
339. Beiboer SH, Wieringa-Jelsma T, Maaskant-Van Wijk PA, van der Schoot CE, van Zwieten R, Roos D, et al. Rapid genotyping of blood group antigens by multiplex polymerase chain reaction and DNA microarray hybridization. Transfusion. 2005;45(5):667-79.
340. Rosse WF, Gallagher D, Kinney TR, Castro O, Dosik H, Moohr J, et al. Transfusion and alloimmunization in sickle cell disease. The Cooperative Study of Sickle Cell Disease. Blood. 1990;76(7):1431-7.
341. Konoshenko MY, Lekchnov EA, Vlassov AV, Laktionov PP. Isolation of Extracellular Vesicles: General Methodologies and Latest Trends. Biomed Res Int. 2018;2018:8545347.
342. An M, Wu J, Zhu J, Lubman DM. Comparison of an Optimized Ultracentrifugation Method versus Size-Exclusion Chromatography for Isolation of Exosomes from Human Serum. J Proteome Res. 2018;17(10):3599-605.
343. Schwoch G, Passow H. Preparation and properties of human erythrocyte ghosts. Mol Cell Biochem. 1973;2(2):197-218.
344. de Moreno MR, Smith JF, Smith RV. Mechanism studies of coomassie blue and silver staining of proteins. J Pharm Sci. 1986;75(9):907-11.
345. Fountoulakis M, Juranville JF, Manneberg M. Comparison of the Coomassie brilliant blue, bicinchoninic acid and Lowry quantitation assays, using non-glycosylated and glycosylated proteins. J Biochem Biophys Methods. 1992;24(3-4):265-74.
346. van Tits LJ, van Heerde WL, Landburg PP, Boderie MJ, Muskiet FA, Jacobs N, et al. Plasma annexin A5 and microparticle phosphatidylserine levels are elevated in sickle cell disease and increase further during painful crisis. Biochem Biophys Res Commun. 2009;390(1):161-4.
347. Kasar M, Boğa C, Yeral M, Asma S, Kozanoglu I, Ozdogu H. Clinical significance of circulating blood and endothelial cell microparticles in sickle-cell disease. J Thromb Thrombolysis. 2014;38(2):167-75.
348. Yuana Y, Bertina RM, Osanto S. Pre-analsunytical and analytical issues in the analysis of blood microparticles. Thromb Haemost. 2011;105(3):396-408.

349. Gray WD, Mitchell AJ, Searles CD. An accurate, precise method for general labeling of extracellular vesicles. MethodsX. 2015;2:360-7.
350. Dohnal JC, Potempa LA, Garvin JE. The molecular weights of three forms of glycophorin A in sodium dodecyl sulfate solution. Biochim Biophys Acta. 1980;621(2):255-64.
351. Påhlsson P, Blackall DP, Ugorski M, Czerwinski M, Spitalnik SL. Biochemical characterization of the O-glycans on recombinant glycophorin A expressed in Chinese hamster ovary cells. Glycoconj J. 1994;11(1):43-50.
352. Sens P, Gov N. Force balance and membrane shedding at the red-blood-cell surface. Phys Rev Lett. 2007;98(1):018102.
353. Erdbrügger U, Lannigan J. Analytical challenges of extracellular vesicle detection: A comparison of different techniques. Cytometry A. 2016;89(2):123-34.
354. Dey-Hazra E, Hertel B, Kirsch T, Woywodt A, Lovric S, Haller H, et al. Detection of circulating microparticles by flow cytometry: influence of centrifugation, filtration of buffer, and freezing. Vasc Health Risk Manag. 2010;6:1125-33.
355. Arraud N, Linares R, Tan S, Gounou C, Pasquet JM, Mornet S, et al. Extracellular vesicles from blood plasma: determination of their morphology, size, phenotype and concentration. J Thromb Haemost. 2014;12(5):614-27.
356. Tsao YS, Huang L. Sendai virus induced leakage of liposomes containing gangliosides. Biochemistry. 1985;24(5):1092-8.
357. Maherani B, Arab-Tehrany E, Kheirolomoom A, Geny D, Linder M. Calcein release behavior from liposomal bilayer; influence of physicochemical/mechanical/structural properties of lipids. Biochimie. 2013;95(11):2018-33.
358. Bardyn M, Rappaz B, Jaferzadeh K, Crettaz D, Tissot JD, Moon I, et al. Red blood cells ageing markers: a multi-parametric analysis. Blood Transfus. 2017;15(3):239-48.
359. Roussel C, Dussiot M, Marin M, Morel A, Ndour PA, Duez J, et al. Spherocytic shift of red blood cells during storage provides a quantitative whole cell-based marker of the storage lesion. Transfusion. 2017;57(4):1007-18.
360. McDonough AA, Veiras LC, Minas JN, Ralph DL. Considerations when quantitating protein abundance by immunoblot. Am J Physiol Cell Physiol. 2015;308(6):C426-33.
361. Kittivorapart J, Crew VK, Wilson MC, Heesom KJ, Siritanaratkul N, Toye AM. Quantitative proteomics of plasma vesicles identify novel biomarkers for hemoglobin E/β-thalassemic patients. Blood Adv. 2018;2(2):95-104.
362. Santiago RP, Guarda CC, Figueiredo CVB, Fiuza LM, Aleluia MM, Adanho CSA, et al. Serum haptoglobin and hemopexin levels are depleted in pediatric sickle cell disease patients. Blood Cells Mol Dis. 2018;72:34-6.
363. Vichinsky EP, Earles A, Johnson RA, Hoag MS, Williams A, Lubin B. Alloimmunization in sickle cell anemia and transfusion of racially unmatched blood. N Engl J Med. 1990;322(23):1617-21.
364. Tsao ST, Jackson T, Vege S, Smith-Whitley K, Friedman DF, Westhoff CM. High prevalence of red blood cell alloimmunization in sickle cell disease despite transfusion from Rh-matched minority donors. Blood. 2013;122(6):1062-71.
365. Brantley SG, Ramsey G. Red cell alloimmunization in multitransfused HLA-typed patients. Transfusion. 1988;28(5):463-6.
366. Amu S, Saunders SP, Kronenberg M, Mangan NE, Atzberger A, Fallon PG. Regulatory B cells prevent and reverse allergic airway inflammation via FoxP3-positive T regulatory cells in a murine model. J Allergy Clin Immunol. 2010;125(5):1114-24.e8.
367. Carter NA, Vasconcellos R, Rosser EC, Tulone C, Muñoz-Suano A, Kamanaka M, et al. Mice lacking endogenous IL-10-producing regulatory B cells develop exacerbated disease and present with an increased frequency of Th1/Th17 but a decrease in regulatory T cells. J Immunol. 2011;186(10):5569-79.
368. Bao W, Zhong H, Manwani D, Vasovic L, Uehlinger J, Lee MT, et al. Regulatory B-cell compartment in transfused alloimmunized and non-alloimmunized patients with sickle cell disease. Am J Hematol. 2013;88(9):736-40.
369. Noon L. Prophylactic inoculation against hay fever (historical document). Ann Allergy. 1955;13(6):713-6; passim.
370. Alvarez-Cuesta E, Bousquet J, Canonica GW, Durham SR, Malling HJ, Valovirta E. Standards for practical allergen-specific immunotherapy. Allergy. 2006;61 Suppl 82:1-20.

371. Lee JH, Kim SC, Choi H, Jung CG, Ban GY, Shin YS, et al. A Retrospective Study of Clinical Response Predictors in Subcutaneous Allergen Immunotherapy With House Dust Mites for Allergic Rhinitis. Allergy, asthma & immunology research. 2018;10(1):18-24.
372. Billingham RE, Brent L, Medawar PB. Actively acquired tolerance of foreign cells. Nature. 1953;172(4379):603-6.
373. Playfair JHL. Specific Tolerance to Sheep Erythrocytes in Mouse Bone Marrow Cells. Nature. 1969;222(5196):882-3.
374. Dossetor JB, Mackinnon KJ, Gault MH, Maclean LD. CADAVER KIDNEY TRANSPLANTS. Transplantation. 1967;5(4).
375. Morris PJ, Ting A, Stocker J. Leukocyte antigens in renal transplantation. 1. The paradox of blood transfusions in renal transplantation. Med J Aust. 1968;2(24):1088-90.
376. Opelz G, Sengar DP, Mickey MR, Terasaki PI. Effect of blood transfusions on subsequent kidney transplants. Transplant Proc. 1973;5(1):253-9.
377. Li D, Romain G, Flamar AL, Duluc D, Dullaers M, Li XH, et al. Targeting self- and foreign antigens to dendritic cells via DC-ASGPR generates IL-10-producing suppressive CD4+ T cells. J Exp Med. 2012;209(1):109-21.
378. Sabatos-Peyton CA, Verhagen J, Wraith DC. Antigen-specific immunotherapy of autoimmune and allergic diseases. Curr Opin Immunol. 2010;22(5):609-15.
379. Getts DR, McCarthy DP, Miller SD. Exploiting apoptosis for therapeutic tolerance induction. J Immunol. 2013;191(11):5341-6.
380. Burton BR, Britton GJ, Fang H, Verhagen J, Smithers B, Sabatos-Peyton CA, et al. Sequential transcriptional changes dictate safe and effective antigen-specific immunotherapy of autoimmune disease. Immunology. 2013;140:205-.
381. Bryk AH, Wiśniewski JR. Quantitative Analysis of Human Red Blood Cell Proteome. J Proteome Res. 2017;16(8):2752-61.
382. Lorentz KM, Kontos S, Diaceri G, Henry H, Hubbell JA. Engineered binding to erythrocytes induces immunological tolerance to E. coli asparaginase. Science Advances. 2015;1(6):e1500112.
383. SCIENCEphotoLIBRARY; [Available from: **https://www.sciencephoto.com/media/1046327/view/mouse-anatomy-illustration**].
384. Stamm C, Barthelmann J, Kunz N, Toellner KM, Westermann J, Kalies K. Dose-dependent induction of murine Th1/Th2 responses to sheep red blood cells occurs in two steps: antigen presentation during second encounter is decisive. PLoS One. 2013;8(6):e67746.
385. Stils HF, Jr. Adjuvants and Antibody Production: Dispelling the Myths Associated with Freund's Complete and Other Adjuvants. ILAR Journal. 2005;46(3):280-93.
386. Gunn MD, Ngo VN, Ansel KM, Ekland EH, Cyster JG, Williams LT. A B-cell-homing chemokine made in lymphoid follicles activates Burkitt's lymphoma receptor-1. Nature. 1998;391(6669):799-803.
387. Ries C. Cytokine functions of TIMP-1. Cellular and Molecular Life Sciences. 2014;71(4):659-72.
388. Huang B, Zhao X, Zheng LB, Zhang L, Ni B, Wang YW. Different expression of tissue inhibitor of metalloproteinase family members in rat dorsal root ganglia and their changes after peripheral nerve injury. Neuroscience. 2011;193:421-8.
389. Dzikowska-Diduch O, Domienik-Karłowicz J, Górska E, Demkow U, Pruszczyk P, Kostrubiec M. E-selectin and sICAM-1, biomarkers of endothelial function, predict recurrence of venous thromboembolism. Thrombosis Research. 2017;157:173-80.
390. Ricklin D, Lambris JD. Complement in immune and inflammatory disorders: pathophysiological mechanisms. Journal of immunology (Baltimore, Md : 1950). 2013;190(8):3831-8.
391. Guyon A. CXCL12 chemokine and its receptors as major players in the interactions between immune and nervous systems. Frontiers in Cellular Neuroscience. 2014;8:65.
392. Chitu V, Stanley ER. Colony-stimulating factor-1 in immunity and inflammation. Curr Opin Immunol. 2006;18(1):39-48.
393. Seckinger P, Lowenthal JW, Williamson K, Dayer JM, MacDonald HR. A urine inhibitor of interleukin 1 activity that blocks ligand binding. J Immunol. 1987;139(5):1546-9.

394. Woolf CJ, Allchorne A, Safieh-Garabedian B, Poole S. Cytokines, nerve growth factor and inflammatory hyperalgesia: the contribution of tumour necrosis factor alpha. Br J Pharmacol. 1997;121(3):417-24.
395. Sawant KV, Poluri KM, Dutta AK, Sepuru KM, Troshkina A, Garofalo RP, et al. Chemokine CXCL1 mediated neutrophil recruitment: Role of glycosaminoglycan interactions. Scientific Reports. 2016;6(1):33123.
396. Bouchon A, Dietrich J, Colonna M. Cutting edge: inflammatory responses can be triggered by TREM-1, a novel receptor expressed on neutrophils and monocytes. J Immunol. 2000;164(10):4991-5.
397. Najmaddini H, Hassanshahi G, Ostadebrahimi H, Barkhordari H, Mashayekhi H, Nazari M, et al. Overproduction of CXC chemokines CXCL1, CXCL9, CXCL10 and CXCL12 in β-thalassemia major or patients. Annals of Saudi medicine. 2014;34(2):122-7.
398. Cremel M, Guerin N, Horand F, Banz A, Godfrin Y. Red blood cells as innovative antigen carrier to induce specific immune tolerance. International journal of pharmaceutics. 2013;443(1-2):39-49.
399. Nakayama T, Yamashita M. The TCR-mediated signaling pathways that control the direction of helper T cell differentiation. Semin Immunol. 2010;22(5):303-9.
400. Toellner KM, Luther SA, Sze DM, Choy RK, Taylor DR, MacLennan IC, et al. T helper 1 (Th1) and Th2 characteristics start to develop during T cell priming and are associated with an immediate ability to induce immunoglobulin class switching. J Exp Med. 1998;187(8):1193-204.
401. Corse E, Gottschalk RA, Allison JP. Strength of TCR-peptide/MHC interactions and in vivo T cell responses. J Immunol. 2011;186(9):5039-45.
402. Larché M, Wraith DC. Peptide-based therapeutic vaccines for allergic and autoimmune diseases. Nature Medicine. 2005;11(4):S69-S76.
403. De Groot AS, Scott DW. Immunogenicity of protein therapeutics. Trends Immunol. 2007;28(11):482-90.
404. Liblau RS, Tisch R, Shokat K, Yang X, Dumont N, Goodnow CC, et al. Intravenous injection of soluble antigen induces thymic and peripheral T-cells apoptosis. Proceedings of the National Academy of Sciences of the United States of America. 1996;93(7):3031-6.
405. Lutterotti A, Yousef S, Sputtek A, Stürner KH, Stellmann JP, Breiden P, et al. Antigen-specific tolerance by autologous myelin peptide-coupled cells: a phase 1 trial in multiple sclerosis. Sci Transl Med. 2013;5(188):188ra75.
406. Yan J, Yu J, Wang C, Gu Z. Red Blood Cells for Drug Delivery. Small Methods. 2017;1(12):1700270.
407. Grimm AJ, Kontos S, Diaceri G, Quaglia-Thermes X, Hubbell JA. Memory of tolerance and induction of regulatory T cells by erythrocyte-targeted antigens. Scientific Reports. 2015;5(1):15907.
408. Kontos S, Kourtis IC, Dane KY, Hubbell JA. Engineering antigens for in situ erythrocyte binding induces T-cell deletion. Proceedings of the National Academy of Sciences. 2013;110(1):E60.
409. Pishesha N, Bilate AM, Wibowo MC, Huang N-J, Li Z, Deshycka R, et al. Engineered erythrocytes covalently linked to antigenic peptides can protect against autoimmune disease. Proceedings of the National Academy of Sciences of the United States of America. 2017;114(12):3157-62.
410. Vaughan JI, Manning M, Warwick RM, Letsky EA, Murray NA, Roberts IAG. Inhibition of Erythroid Progenitor Cells by Anti-Kell Antibodies in Fetal Alloimmune Anemia. New England Journal of Medicine. 1998;338(12):798-803.
411. Poole J, Daniels G. Blood group antibodies and their significance in transfusion medicine. Transfus Med Rev. 2007;21(1):58-71.
412. Hendrickson JE, Desmarets M, Deshpande SS, Chadwick TE, Hillyer CD, Roback JD, et al. Recipient inflammation affects the frequency and magnitude of immunization to transfused red blood cells. Transfusion. 2006;46(9):1526-36.
413. Hendrickson JE, Chadwick TE, Roback JD, Hillyer CD, Zimring JC. Inflammation enhances consumption and presentation of transfused RBC antigens by dendritic cells. Blood. 2007;110(7):2736-43.
414. Yu J, Heck S, Yazdanbakhsh K. Prevention of red cell alloimmunization by CD25 regulatory T cells in mouse models. American journal of hematology. 2007;82(8):691-6.

415. Bao W, Yu J, Heck S, Yazdanbakhsh K. Regulatory T-cell status in red cell alloimmunized responder and nonresponder mice. Blood. 2009;113(22):5624-7.
416. Smith NH, Hod EA, Spitalnik SL, Zimring JC, Hendrickson JE. Transfusion in the absence of inflammation induces antigen-specific tolerance to murine RBCs. Blood. 2012;119(6):1566-9.
417. Ebner C, Siemann U, Bohle B, Willheim M, Wiedermann U, Schenk S, et al. Immunological changes during specific immunotherapy of grass pollen allergy: reduced lymphoproliferative responses to allergen and shift from TH2 to TH1 in T-cell clones specific for Phl p 1, a major grass pollen allergen. Clin Exp Allergy. 1997;27(9):1007-15.
418. Wachholz PA, Nouri-Aria KT, Wilson DR, Walker SM, Verhoef A, Till SJ, et al. Grass pollen immunotherapy for hayfever is associated with increases in local nasal but not peripheral Th1:Th2 cytokine ratios. Immunology. 2002;105(1):56-62.
419. Schettini JAdC, Gomes TV, Santos Barreto AK, da Silva Júnior CD, da Matta M, Coutinho ICN, et al. High Levels of CXCL8 and Low Levels of CXCL9 and CXCL10 in Women with Maternal RhD Alloimmunization. Frontiers in Immunology. 2017;8:700.
420. Ciurana CLF, Zwart B, van Mierlo G, Hack CE. Complement activation by necrotic cells in normal plasma environment compares to that by late apoptotic cells and involves predominantly IgM. European Journal of Immunology. 2004;34(9):2609-19.
421. Avall AMD, Hyllner MMD, Bengtson JPMDP, Carlsson LMDP, Bengtsson AMDP. Postoperative Inflammatory Response after Autologous and Allogeneic Blood Transfusion. Anesthesiology: The Journal of the American Society of Anesthesiologists. 1997;87(3):511-6.
422. Dani C, Poggi C, Gozzini E, Leonardi V, Sereni A, Abbate R, et al. Red blood cell transfusions can induce proinflammatory cytokines in preterm infants. Transfusion. 2017;57(5):1304-10.
423. Long K, Woodward J, Procter L, Ward M, Meier C, Williams D, et al. In vitro transfusion of red blood cells results in decreased cytokine production by human T cells. The journal of trauma and acute care surgery. 2014;77(2):198-201.
424. Aichele P, Brduscha-Riem K, Zinkernagel RM, Hengartner H, Pircher H. T cell priming versus T cell tolerance induced by synthetic peptides. J Exp Med. 1995;182(1):261-6.
425. Hudson KE, Fasano RM, Karafin MS, Hendrickson JE, Francis RO. Mechanisms of alloimmunization in sickle cell disease. Current Opinion in Hematology. 2019;26(6).
426. Sohn MH. Efficacy and Safety of Subcutaneous Allergen Immunotherapy for Allergic Rhinitis. Allergy, asthma & immunology research. 2018;10(1):1-3.
427. Usman WM, Pham TC, Kwok YY, Vu LT, Ma V, Peng B, et al. Efficient RNA drug delivery using red blood cell extracellular vesicles. Nature Communications. 2018;9(1):2359.